

Synthesis of α -keto acids and nitriles by enzyme catalysis

Dissertation

zur Erlangung des Doktorgrades der
Naturwissenschaften (Dr. rer. nat.)

Keiko Oike, M. Eng.

aus Toyama, Japan

Bielefeld

Mai 2020

Erstgutachter: Prof. Dr. Harald Gröger

Zweitgutachter: Prof. Dr. Norbert Sewald

Termin der Disputation: 26. Juni 2020

Die vorliegende Arbeit wurde von April 2016 bis Mai 2020 an der Universität Bielefeld im Fachbereich Chemie und Biochemie in der Arbeitsgruppe „Industrielle Organische Chemie und Biotechnologie“ sowie im Laboratory of Enzyme Chemistry des Biotechnology Research Center der Toyama Prefectural University, Toyama, Japan unter Leitung von Herr Prof. Dr. Yasuhisa Asano von November 2018 bis Dezember 2018 angefertigt. Die Betreuung der Arbeit erfolgte durch Herrn Prof. Dr. Harald Gröger über den gesamten Bearbeitungszeitraum.

Hiermit versichere ich, dass ich die vorliegende Dissertation selbständig und nur mit den angegebenen Hilfsmitteln und Quellen angefertigt habe. Die Dissertation hat weder in aktueller noch anderer Fassung einer anderen Fakultät oder Hochschule vorgelegen.

Bielefeld, den 15. Mai 2020



Keiko Oike

Publications as part of this thesis

Articles in peer reviewed journals:

[1] T. Betke, P. Rommelmann, **K. Oike**, Y. Asano, H. Gröger, Cyanide-Free and Broadly Applicable Enantioselective Synthetic Platform for Chiral Nitriles through a Biocatalytic Approach, *Angew. Chem. Int. Ed.* **2017**, *56*, 12361-12366.

[2] T. Betke, P. Rommelmann, **K. Oike**, Y. Asano, H. Gröger, Back-Cover Picture of the *Angew. Chem. Int. Ed.* Issue 40/2017, *Angew. Chem. Int. Ed.* **2017**, *56*, 12374; *Angew. Chem.* **2017**, *129*, 12546.

[3] T. Betke, J. Higuchi, P. Rommelmann, **K. Oike**, T. Nomura, Y. Kato, Y. Asano, H. Gröger, Biocatalytic Synthesis of Nitriles through Dehydration of Aldoximes: The Substrate Scope of Aldoxime Dehydratases, *ChemBioChem* **2018**, *19*, 768-779.

[4] T. Betke, J. Higuchi, P. Rommelmann, **K. Oike**, T. Nomura, Y. Kato, Y. Asano, H. Gröger, Cover Picture of *ChemBioChem* Issue 8/2018, *ChemBioChem* **2018**, *19*, 766.

[5] C. Plass, A. Hinzmann, M. Terhorst, W. Brauer, **K. Oike**, H. Yavuzer, Y. Asano, A. J. Vorholt, T. Betke, H. Gröger, Approaching Bulk Chemical Nitriles from Alkenes: A Hydrogen Cyanide Free Approach through a Combination of Hydroformylation and Biocatalysis, *ACS Catal.* **2019**, *9*, 5198-5203.

[6] A. Hinzmann, M. Stricker, J. Busch, S. Glinski, **K. Oike**, H. Gröger, Selective TEMPO-Oxidation of Alcohols to Aldehydes in Alternative Organic Solvents, *Eur. J. Org. Chem.* **2020**, *16*, 2399-2408.

Book chapter:

[1] S. Wedde, M. Biermann, J. E. Choi, **K. Oike**, N. Zumbärgel, H. Gröger, "The Recent Developments of Enzymatic Oxidation" in *Green Oxidation in Organic Synthesis* (Eds.: N. Jiao, S. S. Stahl), Wiley & Sons Ltd., Hoboken, **2019**.

Oral presentation:

[1] **K. Oike**, H. Gröger, Cyanide-free synthesis of chiral nitriles through catalysis with aldoxime dehydratases, Plenary lecture, *3rd CeBitec Retreat* in Bielefeld, 29. – 30.08.2016.

Poster presentations:

[1] **K. Oike**, T. Betke, P. Rommelmann, Y. Asano, H. Gröger, Cyanide-free synthesis of chiral aryl-substituted nitriles via enzymatic dehydration of aldoximes, *Biotrans 2017* in Budapest, Hungary, 09. – 13.07.2017.

[2] **K. Oike**, T. Betke, P. Rommelmann, Y. Asano, H. Gröger, Cyanide-free access to nitriles via aldoxime dehydratases: Enzyme optimization and stereoselective synthesis, *ICRC 2018 – 8th International CeBiTec Research-Conference Bielefeld* in Bielefeld, 09. – 11.04.2018.

[3] **K. Oike**, T. Betke, P. Rommelmann, A. A. Ingram, Y. Asano, J. M. Risse, K. Friehs, H. Gröger, Cyanide-free access to nitriles via aldoxime dehydratases: Enzyme optimization and stereoselective synthesis, *The 20th Biocatalysis Symposium of Japan* in Yokohama, Japan, 12. – 13.11.2018.

Danksagung

Mein herzlicher Dank gilt meinem Doktorvater Herrn Prof. Dr. Harald Gröger für die Einladung hier nach Bielefeld zur Promotion und die Bereitstellung des spannenden Themas, auf dem ich forschen konnte. Ich möchte mich für die ausgezeichnete Betreuung während der gesamten Zeit bedanken. Dies gilt auch für die Zeit während des Forschungsaufenthaltes in meinem Masterstudium. Ich verdanke ihm die Möglichkeit, hier einen weitreichenden Einblick in die Organische Chemie und die neuen Arbeitsweisen in Deutschland erlangen zu können. Ich werde diese Zeit gerne in Erinnerung behalten.

Weiterhin möchte ich Herrn Prof. Dr. Norbert Sewald für die freundliche Übernahme des Zweitgutachtens vielmals danken.

Ein besonderer Dank gilt meinem frühen Förderer Herrn Prof. Dr. Yasuhisa Asano. Ihm verdanke ich den sehr guten Einstieg in die Welt der Biotechnologie, wodurch ich ausgezeichnet auf die Promotion in Bielefeld vorbereitet war. Ebenfalls möchte ich mich für die Ermöglichung eines erneuten Forschungsaufenthaltes an der Toyama Prefectural University bedanken. Mein Dank gilt ebenfalls Herrn Dr. Daisuke Matsui für die Unterstützung und Ideen auf dem Protein Engineering Projekt, dass ich in Toyama begonnen habe. Weiterhin möchte ich mich noch bei Aem Nuylert sowie dem gesamten „Laboratory of Enzyme Chemistry“ für die schöne OZeit in meiner Heimat bedanken.

Außerdem möchte ich mich bei Frau Prof. Gabriele Fischer von Mollard aus der Biochemie III für die erfolgreiche Kooperation auf dem Forschungsprojekt der α -Ketosäuresynthese bedanken. Mein Dank hier gilt auch Svenja Bloess und Tobias Beuel.

Ferner gilt mein Dank Herren Prof. Dr. Karl Friehs und Dr. Joe-Max Risse aus der Fermentationstechnik für die gute Zusammenarbeit auf dem Fermentationsprojekt. Ebenfalls möchte ich Herrn Thomas Schäffler sowie den zahlreichen Studenten danken, die dieses Projekt tatkräftig unterstützt haben.

Für die finanzielle Unterstützung meiner Arbeit möchte ich mich bei der Fachagentur Nachwachsende Rohstoffe sowie bei dem DAAD, hier im Zusammenhang mit der Finanzierung meines Forschungsaufenthaltes in Toyama, bedanken.

Ich möchte mich vor allem bei den Mitgliedern der „alten“ OC1 bedanken. Insbesondere danke ich euch, Dr. Tobias Betke, Dr. Philipp Rommelmann, Dr. Nadine Zumbrägel und Dr. Daniel Bakonyi, für den super Start hier in Deutschland. Ihr habt mir viel über das Land und die Leute beigebracht. Die fruchtbare Zusammenarbeit auf dem Nitrilprojekt mit euch, Tobias und Philipp, hat mir wirklich eine große Freude bereitet. Nadine, du hast mir vor allem am Anfang

die wichtigsten Worte in Deutsch beigebracht und ich habe mich immer darüber gefreut, zwischendurch mit dir plaudern zu können.

Was wäre eine Arbeitsgruppe ohne die permanenten Mitarbeiter. Angelika Bendick, du hast mir von Anfang an bei Allem geholfen und warst eine super Stütze für meinen Alltag in der Universität. Du hast mir immer zugehört und einen Rat für mich parat gehabt. Ebenfalls danke ich den Technischen Angestellten Thomas Geisler und Anika Hegemann für die Unterstützung und eure freundliche Art. Herrn Prof. Dr. Dietmar Kuck danke ich für die vielen spannenden Unterhaltungen. Herrn Dr. Jens Sproß möchte ich für die Messung der Proteinmassen sowie die Revision dieses Teils meiner Dissertation herzlich danken. Auch Alina Nastke und Niklas Adebar gebührt mein Dank für das Korrekturlesen von Teilen dieser Arbeit. Weiterhin danke ich allen weiteren aktuellen sowie ehemaligen festen Mitarbeitern der IOCB sowie den weiteren Mitgliedern der Arbeitsgruppe für die gemeinsame Zeit.

Ebenfalls möchte ich den zahlreichen japanischen Gaststudenten, die in der Arbeitsgruppe geforscht haben, für die schöne Zeit und die willkommene Gelegenheit auf Japanisch zu sprechen vielmals danken. Dank euch habe ich mich immer an meine Heimat erinnert gefühlt. Auch danke ich Bastian Altemeier. Du hast mir mit deinem Lächeln, wenn wir uns im Labor oder in der Universität gesehen haben, immer eine Freude bereitet.

Darüber hinaus gilt mein Dank Frau Dr. Masako Gröger-Suzuki. Die Unterstützung bei vielen alltäglichen Problemen war wirklich großartig. Die gemeinsamen Mittagessen waren mir immer eine Freude. Ebenfalls möchte ich der Deutsch-Japanischen Gesellschaft Bielefeld e. V. für die Verleihung des Hajime-Hoshi-Preises meinen Dank aussprechen. Ebenfalls möchte ich mich für die zahlreichen netten Stammtischabende sowie den weiteren Veranstaltungen mit Bezug zu meinem Heimatland danken. Insbesondere möchte ich mich bei der Präsidentin Gesa Neuert bedanken. Hier möchte ich auch den vielen Japanischen Gaststudenten aller Fachrichtungen, den hier wohnenden Japanern sowie den Leuten, die sich sehr für mein Heimatland interessieren, herzlich für die gemeinsam verbrachte Freizeit danken.

Ein besonderer Dank gilt meinen Freunden in Japan, die mich aus der Ferne dauerhaft unterstützt sowie mich mit Videotelefonaten immer wieder aufgeheitert haben. Dankeschön Yoshiko und Shingo!

Weiterhin möchte ich noch Andrea Ingram, Manuel Hartmann, Ilse Thomas sowie Jeffrey Ingram und Julian Beer herzlich dafür danken, dass sie mich in Ihre Familie aufgenommen und wie ihre eigene Tochter behandelt haben. Ihr habt mich wirklich sehr gut unterstützt in dieser Zeit.

私の両親に心より感謝致します。どんな時も私の味方で、挫けそうな時は励ましてくれ、遠い日本からいつも応援してくれました。私の両親が居なければ、ドイツ行きの決意も、ドイツで博士号を取得することも成し遂げられなかったでしょう。二人が私の両親であることを誇りに思い、これまで育ててきてくれたことに深く感謝し、これから二人に恩返しをしていきたいと思います。

(Meinen Eltern möchte ich von ganzem Herzen danken. Ihr habt mich auch in sehr schwierigen Situationen immer aufgemuntert und mich, so gut wie es irgend möglich ist, aus dem fernen Japan unterstützt. Wenn ihr nicht gewesen wärt, hätte ich weder die Entscheidung nach Deutschland zu kommen zustande gebracht noch hätte ich meine Doktorarbeit erfolgreich beenden können. Ich bin wirklich stolz darauf, Eltern wie euch zu haben. Ich möchte euch dafür, dass ihr mich aufgezogen habt meinen tiefsten Dank aussprechen. Dieses Gefühl möchte ich Euch eines Tages wieder zurückgeben.)

そして最も感謝したい人は、アーロン・イングラムです。私の一番の理解者であり、常に苦楽を共にしてきた人です。両親同様、彼の支えがなければ、今の私は存在しないでしょう。

(Zuletzt möchte ich noch der Person danken, die mich am besten versteht und sowohl Freud als auch Leid über die gesamte Zeit mit mir gemeinsam durchgestanden hat, Aaron Ingram. Wenn Du und meine Eltern nicht gewesen wärt, wäre ich heute nicht da wo ich stehe.)

Abstract

Novel biocatalytic approaches targeting alternative synthesis routes for compound classes of importance in organic synthesis were explored. An L-amino acid oxidase from the fungus *Hebeloma cylindrosporum* was utilized for the oxidation of L-phenylalanine to the α -keto acid phenylpyruvate with air as oxidant. Process properties for the α -keto acid synthesis with this model substrate such as byproduct formation, host cell for expression and purity of the enzyme, inhibitory effects and catalyst loading were evaluated. 20 mM of substrate could be converted quantitatively with this enzyme. Mainly, a cyanide-free biocatalytic access to nitriles was developed utilizing aldoxime dehydratases, a class of heme b dependent lyases. The scope of the dehydration of chiral arylaliphatic aldoximes was investigated with five recombinant enzymes. Aldoxime dehydratases showed an enantioselective reaction progress especially for halogen-substituted derivatives of 2-phenylpropionaldoxime. A “privileged substrate structure”, featuring a stereocenter in α -position to the aldoxime moiety, strong size differentiation and specific rotational flexibility of the substituents in this position, could be proposed. This structure was proved by enlarging the size of the methyl group. A unique feature in enzyme catalysis was observed for this reaction. Enzymatic transformations are rarely suitable to produce both enantiomers of a product with the same enzyme. In most cases, the (*S*)-nitrile was preferably formed from the isomerically pure *E*-aldoxime, while the (*R*)-nitrile is obtained in transformations of the *Z*-aldoxime with all aldoxime dehydratases. These enzymes were also utilized in a reaction sequence targeting the synthesis of fatty nitriles from biorenewable sources. All steps of this sequence such as alcohol oxidation, aldoxime formation by a condensation reaction and biocatalytic aldoxime dehydration were investigated initially. Furthermore, the fermentative production of the aldoxime dehydratase from *Bacillus* sp. OxB-1, as a bottleneck for industrial application, was investigated. Important parameters for a high cell-density fermentation protocol were evaluated. Although the produced whole-cell catalyst did not reach very high activity compared to expression in shaking flask cultures, an insight into limiting factors of a bioprocess was obtained. Crucial parameters such as the effect of the oxygen saturation in the culture, insufficient plasmid stability and insoluble protein expression were identified. The incorporation of the heme cofactor into aldoxime dehydratases is required for soluble protein expression. In order to address this issue, a mutant library of the same enzyme was constructed utilizing the program INTMSAlign_HiSol. The rationally introduced mutations were designed based on comparison of sequence data and hydrophathy of amino acid regions. By this approach, a higher heme incorporation during protein expression close to 100 % was achieved. The improved cofactor incorporation correlated to a higher specific enzymatic activity. The best rationally designed single mutant showed a specific activity improved by 74 % compared to the wild-type enzyme. This approach represents the first protein engineering-based method for improving heme incorporation.

Table of Contents

1 Biocatalysis as a tool in organic synthesis: Achievements, scope and limitations	1
2 State of the art.....	11
2.1 Synthetic methods for the synthesis of α -keto acids and nitriles.....	11
2.1.1 Enantiomerically pure amino acids and α -keto acids	11
2.1.2 Nitriles	19
2.2 Oxidative transformations with amino acid oxidases and amine oxidases	27
2.2.1 Flavoenzymes: An overview	27
2.2.2 Amino acid oxidases: A variable biocatalyst	28
2.2.2.1 General information and catalytic function.....	28
2.2.2.2 Synthetic pathways with amino acid oxidases	29
2.2.2.3 L-Amino acid oxidases	30
2.2.2.4 D-Amino acid oxidases.....	33
2.2.3 Amine oxidases: Another enzyme for the resolution of amines	37
2.3 Aldoxime dehydratases: Special nitrile producing lyases	41
2.3.1 Isolation and expression of aldoxime degrading enzymes	41
2.3.2 Properties of aldoxime dehydratases.....	42
2.3.2.1 Properties and structure.....	42
2.3.2.2 Catalytic mechanism of aldoxime dehydratases.....	45
2.3.2.3 Other reactions catalyzed by aldoxime dehydratases.....	46
2.3.3 Synthesis of nitriles with aldoxime dehydratases	47
2.3.3.1 Arylaliphatic aldoximes.....	48
2.3.3.2 Aromatic and heteroaromatic aldoximes	51
2.3.3.3 Linear and branched aliphatic aldoximes	53
3 Biocatalytic synthesis of phenylpyruvate with an L-amino acid oxidase	56
3.1 Recent developments regarding fungal L-amino acid oxidases	56
3.2 Motivation	58
3.3 Process properties of the L-phenylalanine oxidation with L-amino acid oxidase from <i>Hebeloma cylindrosporum</i>	59
3.4 Summary and outlook.....	67

4 Biocatalytic cyanide-free synthesis of chiral nitriles	68
4.1 Enantioselective aldoxime dehydration with aldoxime dehydratase from <i>Bacillus</i> sp. OxB-1	68
4.1.1 Mechanism of the chemocatalytic water elimination of aldoximes	68
4.1.2 Chiral nitrile formation with aldoxime dehydratases	69
4.2 Motivation and substrate selection	73
4.3 Substrate synthesis	75
4.4 Formation of chiral nitriles by dehydration of aromatic aldoximes	81
4.4.1 Substituted aromatic derivatives of 2-phenylpropionaldoxime	81
4.4.2 Identified lead structure for chiral aldoxime dehydration	83
4.4.3 Dehydration of bulky 2-phenylpropionaldoxime derivatives	89
5 Initial development towards a cascade for the synthesis of fatty nitriles from fatty acids	95
5.1 Novel biocatalytic synthesis of adiponitrile and fatty nitriles	95
5.2 Motivation	97
5.3 Initial development of a cascade reaction towards fatty nitriles	98
5.3.1 Alcohol oxidation with alcohol dehydrogenases	98
5.3.2 Chemical alcohol oxidation	100
5.3.2.1 TEMPO-catalyzed oxidation of fatty alcohols	100
5.3.2.2 Palladium-catalyzed oxidation of fatty alcohols	101
5.3.3 Synthesis of fatty aldoximes <i>via</i> condensation of aldehydes with hydroxylamine	102
5.3.4 Fatty nitrile synthesis <i>via</i> aldoxime dehydratase-catalyzed dehydration of fatty aldoximes	103
5.4 Preparative application of the fatty nitrile synthesis cascade	106
5.5 Fermentative production of aldoxime dehydratases	108
5.5.1 Fermentation of cytochrom P450 monooxygenases	108
5.5.2 Expression of Oxds in shaking flask and fed-batch scale	109
5.5.3 Motivation	110
5.5.4 Bioreactor setup and analytical aspects	110
6 Improvement of heme incorporation by a protein sequence based enzyme engineering approach	120

6.1 Enzyme engineering: A key technology for improved catalyst performance	120
6.1.1 Methods of enzyme engineering.....	120
6.1.2 Identification of aggregation hotspots with the software INTMSAlign_HiSol.....	121
6.1.3 Heme incorporation in heterologous expression	122
6.2 Motivation	124
6.3 Rational mutant library design for aldoxime dehydratase from <i>Bacillus</i> sp. OxB-1	125
6.3.1 Identification of mutation sites with INTMSAlign_HiSol	125
6.3.2 Generation and purification of the mutant library.....	127
6.4 Evaluation of the mutant library	131
6.4.1 Effect of the mutants on the specific enzymatic activity.....	131
6.4.2 Protein mass-spectrometry	133
6.5 Conclusion and outlook.....	139
6.6 The effect of the cofactor flavin mononucleotide on aldoxime dehydration activity	141
7 Summary and outlook.....	143
8 Zusammenfassung und Ausblick	147
9 Experimental section	152
9.1 General information and analytics	152
9.1.1 Chemicals.....	152
9.1.2 Devices	152
9.1.3 Analytical methods	153
9.1.3.1 Nuclear magnetic resonance-spectroscopy.....	153
9.1.3.2 Mass spectrometry.....	153
9.1.3.3 High-performance liquid chromatography.....	154
9.1.3.4 Gas chromatography.....	155
9.1.3.5 Thin layer chromatography.....	155
9.1.3.6 Infrared spectroscopy.....	155
9.1.3.7 CHN analysis	155
9.1.4 Microorganisms and genes.....	156
9.1.4.1 Strains.....	156
9.1.4.2 Plasmids	156

9.1.4.3 Enzymes	156
9.1.5 Buffers and solutions	157
9.2 Computational methods	158
9.2.1 Determination of aggregation hotspots	158
9.2.2 Secondary structure determination	159
9.3 Chemical methods	160
9.3.1 General procedure 1 (GP1): TEMPO-catalyzed oxidation of fatty alcohols	160
9.3.1.1 Attempted synthesis of <i>n</i> -octanal	160
9.3.1.2 Attempted synthesis of <i>n</i> -decanal	160
9.3.1.3 Attempted synthesis of <i>n</i> -dodecanal	161
9.3.2 General procedure 2 (GP2): Palladium(II) acetate catalyzed oxidation of fatty alcohols with molecular oxygen	161
9.3.2.1 Attempted synthesis of <i>n</i> -octanal	161
9.3.2.2 Synthesis of <i>n</i> -dodecanal	162
9.3.2.3 Synthesis of <i>n</i> -hexadecanal	162
9.3.3 General procedure 3 (GP3): Nitroaldol condensation of aromatic aldehydes with nitromethane	163
9.3.3.1 Synthesis of (<i>E</i>)-1-fluoro-4-(2-nitrovinyl)benzene	163
9.3.3.2 Synthesis of (<i>E</i>)-2-(2-nitrovinyl)thiophene	164
9.3.4 General procedure 4 (GP4): Synthesis of nitroalkanes by Michael-addition of magnesium halides to nitroalkenes.....	164
9.3.4.1 Synthesis of <i>rac</i> -(1-nitrobutan-2-yl)benzene.....	165
9.3.4.2 Synthesis of <i>rac</i> -(3-methyl-1-nitrobutan-2-yl)benzene	166
9.3.4.3 Synthesis of <i>rac</i> -(1-cyclohexyl-2-nitroethyl)benzene	166
9.3.4.4 Synthesis of <i>rac</i> -1-fluoro-4-(1-nitropropan-2-yl)benzene	167
9.3.4.5 Synthesis of <i>rac</i> -2-(1-nitropropan-2-yl)thiophene	168
9.3.5 General procedure 5 (GP5): Synthesis of aldoximes by disproportionation of nitroalkanes with benzyl bromide.....	168
9.3.5.1 Synthesis of <i>rac</i> -2-phenylbutanal oxime.....	169
9.3.5.2 Synthesis of <i>rac</i> -3-methyl-2-phenylbutanal oxime	170
9.3.5.3 Synthesis of <i>rac-E/Z</i> -2-cyclohexyl-2-phenylacetaldoxime.....	172

9.3.5.4	Synthesis of <i>rac</i> -4-fluorophenyl-propanal oxime.....	173
9.3.5.5	Synthesis of <i>rac</i> - <i>E/Z</i> -2-(thiophen-2-yl)propanal oxime.....	174
9.3.6	General procedure 6 (GP6): Synthesis of aldoximes by condensation of aldehydes with hydroxyl amine salts.....	175
9.3.6.1	Synthesis of <i>Z</i> -phenylacetaldoxime.....	175
9.3.6.2	Synthesis of <i>rac</i> - <i>E/Z</i> -2-phenylpropionaldoxime.....	176
9.3.6.3	Synthesis of <i>n</i> -octanal oxime.....	177
9.3.6.4	Synthesis of <i>n</i> -nonanal oxime.....	177
9.3.6.5	Synthesis of <i>n</i> -decanal oxime.....	178
9.3.6.6	Synthesis of <i>n</i> -dodecanal oxime.....	179
9.3.7	General procedure 7 (GP7): Synthesis of racemic nitriles by copper(II) catalyzed dehydration of aldoximes.....	179
9.3.7.1	Synthesis of <i>rac</i> -2-phenylacetonitrile.....	180
9.3.7.2	Synthesis of <i>rac</i> -2-phenylpropane nitrile.....	180
9.3.7.3	Synthesis of <i>rac</i> -2-phenylbutane nitrile.....	181
9.3.7.4	Synthesis of <i>rac</i> -3-methyl-2-phenylbutane nitrile.....	181
9.3.7.5	Synthesis of <i>rac</i> -2-cyclohexyl-2-phenylacetonitrile.....	182
9.3.7.6	Synthesis of <i>rac</i> -4-fluorophenyl-propane nitrile.....	183
9.3.7.7	Synthesis of <i>rac</i> -2-(thiophen-2-yl)propionitrile.....	183
9.4	Microbiological methods.....	185
9.4.1	General procedure 8 (GP8): Preparation of chemo-competent cells.....	185
9.4.2	General procedure 9 (GP9): Site-directed mutagenesis <i>via</i> polymerase chain reaction.....	185
9.4.3	General procedure 10 (GP10): Photometric determination of DNA concentration.....	185
9.4.4	General procedure 11 (GP11): Transformation of plasmids.....	186
9.4.5	General procedure 12 (GP12): Protein expression in shaking flasks.....	186
9.4.5.1	Auto-induction medium.....	186
9.4.5.2	TB-medium pUC18-OxdB.....	186
9.4.5.3	TB-medium pET22b-OxdB.....	187
9.4.6	Fermentative production of aldoxime dehydratase from <i>Bacillus</i> sp. OxdB-1.....	187

9.4.6.1 Media	188
9.4.6.2 Process control	188
9.4.6.3 Sampling.....	189
9.4.6.3 Determination of the glycerol concentration	189
9.4.7 General procedure 13 (GP13): Determination of the cell dry weight	189
9.5 Biochemical methods.....	190
9.5.1 General procedure 14 (GP14): Preparation of protein fractions	190
9.5.2 General procedure 15 (GP15): Acidic cell lysate activation.....	190
9.5.3 General procedure 16 (GP16): Protein purification	190
9.5.4 General procedure 17 (GP17): Determination of the protein concentration.....	191
9.5.5 General procedure 18 (GP18): Sodium dodecylsulfate acrylamide gel electrophoresis.....	191
9.5.6 General procedure 19 (GP19): Determination of the plasmid stability.....	193
9.5.7 Protein activity assays	193
9.5.7.1 General procedure 20 (GP20): L-Amino acid oxidase assay	193
9.5.7.2 General procedure 21 (GP21): ADH-assay	193
9.5.8 General procedure 22 (GP22): Biocatalytic deamination of amino acids to α -keto acids.....	194
9.5.8.1 Byproduct determination <i>via</i> $^1\text{H-NMR}$ -spectrometry	194
9.5.8.2 Comparison of different catalase enzymes.....	195
9.5.8.3 Time course	196
9.5.8.4 Determination of the enzyme stability.....	197
9.5.8.5 Variation of the substrate and catalyst loading	198
9.5.8.6 Investigation of substrate and product inhibition.....	199
9.5.8.7 Investigation of different buffer systems	200
9.5.9 General procedure 23 (GP23): Biocatalytic oxidation of fatty alcohols to fatty aldehydes.....	200
9.5.10 General procedure 24 (GP24): Biocatalytic dehydration of aldoximes to nitriles	201
9.5.10.1 Arylaliphatic aldoximes.....	201
9.5.10.2 Linear fatty aldoximes	204

9.5.10.3 Activity determination of whole-cells obtained in high cell-density fermentation	205
9.5.10.4 Activity determination of OxdB variants whole-cell catalysts <i>via</i> biotransformation of Z-phenylacetaldoxime.....	207
9.5.10.5 Activity determination purified OxdB variants <i>via</i> biotransformation of Z-phenylacetaldoxime.....	208
10 Register of illustrations	210
10.1 Figures.....	210
10.2 Schemes.....	215
10.3 Tables.....	220
11 List of abbreviations.....	224
12 References.....	230
13 Appendix	242

1 Biocatalysis as a tool in organic synthesis: Achievements, scope and limitations

A major issue in current research of this millennium is the sustainability of resources, processes and products. Acknowledging the limited amount of the available fossil resources, biorenewables are a hot topic. The production of fuels and energy as well as chemical feedstocks and processes are in the focus.^[1,2] In the end of the last millennium, the term of “green chemistry” was established by *Anastas and Warner*. This term refers to a more sustainable chemistry regarding the resources, processes and products. Twelve principles which a green process should meet were defined.^[3] Major issues are the avoiding of waste and the use highly toxic compounds as well as the use of catalysts for achieving a better atom economy. Catalysis and asymmetric reactions play an outstanding role for achieving green reactions. The Nobel laureate *Noyori* pointed out the necessity of sustainable chemistry in this century.^[4] As enzymes can be considered as green catalysts, biocatalysis is an interesting tool for achieving this target. Biocatalysis responds positively to ten of the twelve principles of green chemistry (Table 1).^[1,5] The other principles are not related to the process but to the product itself. Advantages of enzymatic transformations are the higher atom economy, less waste production, and the mild reaction conditions. Enzymatic reactions often allow novel, more efficient synthetic pathways in the production of chemicals. Their very high selectivity (chemo-, regio- and stereo-) outperforms many homogeneous catalysts.^[6]

Table 1. Principles of green chemistry and how biocatalysis as a method addresses them.^[1]

Green chemistry principle	Biocatalysis
Waste prevention	Significantly reduced waste
Atom economy	More atom- and step-economical
Less hazardous synthesis	Generally low toxicity
Design for safer products	Not relevant (product not process)
Safer solvents and auxiliaries	Usually performed in water
Energy efficiency	Mild conditions / energy-efficient
Renewable feedstocks	Enzymes are renewable
Reduced derivatization	Avoids protection / deprotection steps
Catalysis	Enzymes are catalysts
Design for degradation	Not relevant (product not process)
Real-time analysis	Applicability to biocatalytic processes
Inherently safer processes	Mild and safe conditions

1 Biocatalysis as a tool in organic synthesis: Achievements, scope and limitations

An established method for the evaluation of the waste production is the so called *E*-factor, which is defined as the amount of waste generated per amount of product. As a general trend, the waste amount is increasing with smaller reaction scale in the different segments of the chemical industry. In the bulk chemistry segment, reactions are often carried out in the gasphase or neat, which avoids the formation of solvent waste. Especially in the fine chemistry and the pharmaceutical segment, higher functionalization of the educts and more complex reactions are necessary, thus, more waste is produced (Table 2).^[7-9]

Table 2. Annual production scale and *E*-factors in the different segments of the chemical industry.^[7-9]

Industrial segment	Annual production [t·a ⁻¹]	<i>E</i> -Factor [kg _{waste} ·kg _{product} ⁻¹]
Oil refinery	10 ⁶ -10 ⁹	<0.1
Bulk chemistry	10 ⁴ -10 ⁶	<1-5
Fine/Special chemistry	10 ² -10 ⁴	5-50
Pharmaceuticals	10 ¹ -10 ³	25-(>100)

Biocatalysts have become an important tool in organic chemistry as well as the chemical industry throughout all their segments.^[1,5,10-15] Biocatalysis itself has been known to humans since the antique. Even a few thousand years ago, humans already utilized yeasts to produce ethanol for alcohol beverages by fermentation of sugars. Regarding the term biocatalysis, it has to be differentiated between fermentation and biotransformation. Products of fermentative processes are obtained *via* microbial transformations of a carbon source in the metabolism of a microorganism.^[14] Bacteria or fungi can produce specific products such as fatty acids, amino acids, and other value-added compounds, e.g. natural antibiotics.^[16] The closely related metabolic engineering is a research field of its own. In the following, when referred to biocatalysis, biotransformation is meant. In biotransformations, a distinct product is formed in a classical catalytic reaction (cascade) form defined educts. In the beginning of the 20th century, one of the first biocatalytic reactions was the synthesis of (*R*)-mandelonitrile from benzaldehyde.^[14] Since then, many biocatalysts have already found an application in organic synthesis.^[2,14]

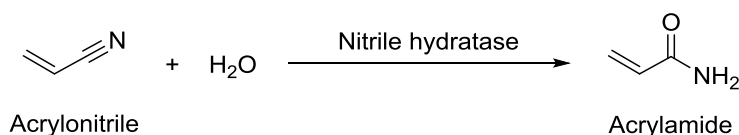
Enzymes can be used in different forms for synthetic application. Reactions can be catalyzed by enzyme crude extracts, purified enzymes, (recombinant) whole-cell catalysts and immobilized enzymes. The most common expression systems for recombinant proteins are modified strains of *Escherichia coli* (*E. coli*).^[17] Immobilization of enzymes (and whole-cells) is a powerful technique for adjusting properties of the catalyst regarding its stability against temperature and organic solvents. Immobilization can be performed *via* binding to a support, entrapment or cross-linking techniques. An example for a cross-linking technique is the

1 Biocatalysis as a tool in organic synthesis: Achievements, scope and limitations

synthesis of so-called cross-linked enzyme aggregates (CLEAs). A further advantage of immobilization is that the immobilized proteins are not soluble in water, thus, can be separated easier. This procedure enables recycling and reuse of the enzymes, which can be a big cost-reducing factor.^[18]

The petrochemistry field is typically not addressed directly by biocatalysis with isolated catalysts. Biocatalytic processes for production of petrochemicals are less prominent compared to the other segments of the chemical industry. There is a hard competition with highly efficient processes such as the steam-cracking of alkanes forming shorter terminal alkenes. Recently, Evonik Industry investigated an enzyme able to synthesize these alkenes and claimed a patent for its application.^[19] Apart from production of chemicals, enzymatic treatments for removal of undesired contents are technically applied,^[20] e.g. the treatment of wastewater from petrochemical processes.^[21] Most petrochemicals are the smallest building blocks known in chemical synthesis. These compounds are also used for the energy generation or contained in fuels. This whole field is about to change gravely in the future in consideration of the limited fossil resources.^[22] Biocatalytic processes such as fermentations utilizing sugars, cellulose and organic waste as novel (bio-)renewable feedstocks for the production of hydrogen, ethanol, and other value-added materials as fatty acids are frequently investigated.^[23]

In the bulk chemistry segment, high chemoselectivity and production efficiencies of the reactions are required. Side reactions as polymerizations induced by acid-base catalysis have to be evaded. The low price of the products makes this field highly competitive. Low catalyst loadings and high space time yields of the processes are necessary for successful implementation of biocatalysis in this field.^[13] An example of enzymes applied in bulk chemistry are nitrile hydratases, which are utilized to synthesize acrylamide from acrylonitrile (Scheme 1). The very high chemoselectivity of this reaction under mild conditions, avoiding hydrolysis of the amide to the carboxylic acid and polymerization, is superior to chemical hydration processes. In Germany and Japan, these processes are carried out with cells of *Rhodococcus rhodochorus* J1 expressing nitrile hydratase in a scale of 650,000 tons per year.^[10,24]

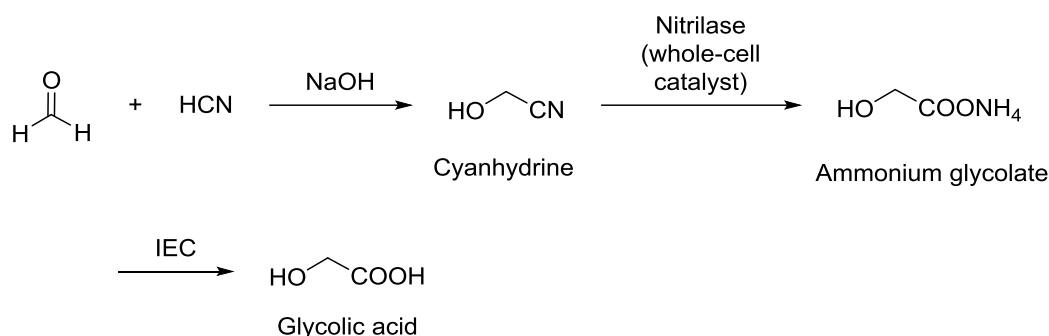


Scheme 1. Nitrile hydratase-catalyzed acrylamide production from acrylonitrile.^[10,24]

In the synthesis of glycolic acid from formaldehyde and cyanide, another enzymatic hydrolysis plays a key role. Glycolic acid has several applications in the food industry, as an industrial

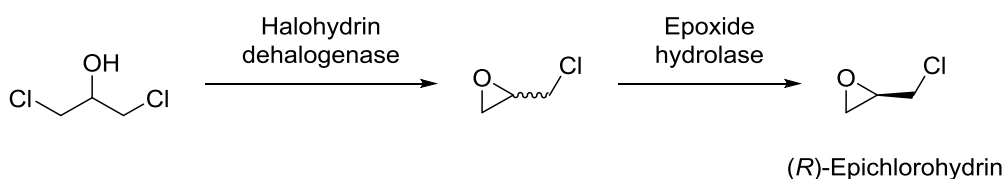
1 Biocatalysis as a tool in organic synthesis: Achievements, scope and limitations

cleaner and as a building block in organic chemistry. The annual sales of this compound currently date at around 290 million US-\$ with a growing prognosis. A synthesis route run by DuPont involving a biocatalytic hydration of the intermediate cyanhydrine proceeds under mild conditions catalyzed by nitrilase (Scheme 2). This reaction requires a different chemoselectivity of the hydrolysis compared to the acrylamide production. The formed ammonium glycolate is converted to glycolic acid by ion-exchange chromatography (IEC). Both wild-type nitrilases and recombinant enzymes contained in whole-cells are suitable for this reaction with a high productivity.^[13,25]



Scheme 2. Synthesis of glycolic acid from formaldehyde, hydrogen cyanide, and sodium hydroxide *via* cyanhydrine formation (99 % yield), subsequent nitrilase-catalyzed hydrolysis (99 % yield) and IEC.^[13,25]

(*R*)-Epichlorohydrin, an intermediate in the synthesis of the drug Rivaroxaban, can be synthesized enzymatically from 1,3-dichloro-2-propanol in two steps (Scheme 3). First, the racemic epoxide is formed by a halohydrin dehalogenase-catalyzed cyclization. Then, the optically pure (*R*)-epichlorohydrine (>99 % ee) is obtained in a kinetic resolution of the racemic compound catalyzed by a (*S*)-selective epoxide hydrolase. With an optimized reaction system, the product is obtained with a yield of 42.7 % at 512 mM substrate concentration.^[13,26]

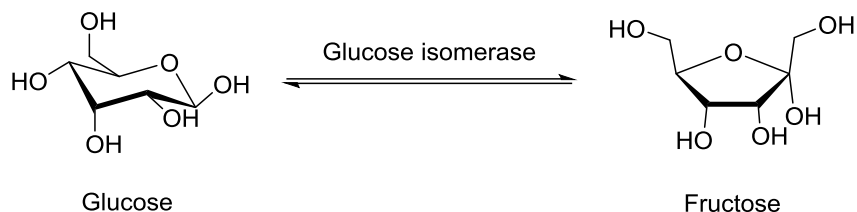


Scheme 3. Synthesis of (*R*)-epichlorohydrine from 1,3-dichloro-2-propanol by dehalogenation with a halohydrin dehalogenase followed by the kinetic resolution of the epoxide with a (*S*)-selective epoxide hydrolase.^[13,26]

Sweeteners are highly demanded in the food industry. As D-fructose is considered as the sweeter sugar compared to D-glucose, the glucose isomerization is an attractive method for sweetness increasing (Scheme 4). The resulting fine chemical high-fructose corn syrup, a fructose enriched mixture of both isomers, is produced in 10⁷ tons per year scale in the industry. As the chemical isomerization requires harsh conditions such as a high temperature

1 Biocatalysis as a tool in organic synthesis: Achievements, scope and limitations

and a strongly basic pH value, the biocatalytic isomerization with glucose isomerase is preferred here.^[13,27,28]



Scheme 4. Isomerization of D-glucose to D-fructose catalyzed by glucose isomerase.^[13,27,28]

An overview about the granted patents in the years from 2014 to 2019 shows the most prominent enzyme classes in recent application orientated research (Figure 1). Hydrolases are still the most dominating enzyme class with approximately 40 % of the total share. In the second rank, nearly equally at half of the hydrolase level, transaminases and redox enzymes each have a share of approximately 20 %. Lyases are also an upcoming enzyme class, however, their share is still smaller.^[29]

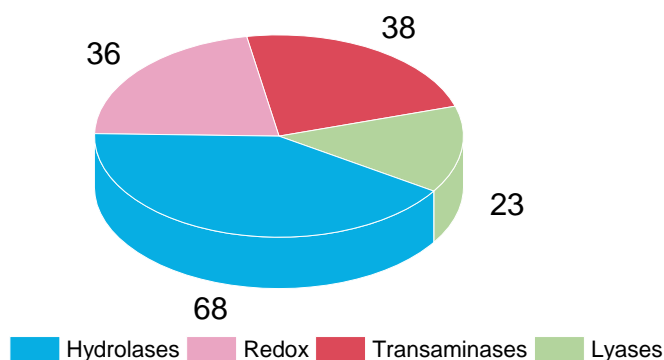
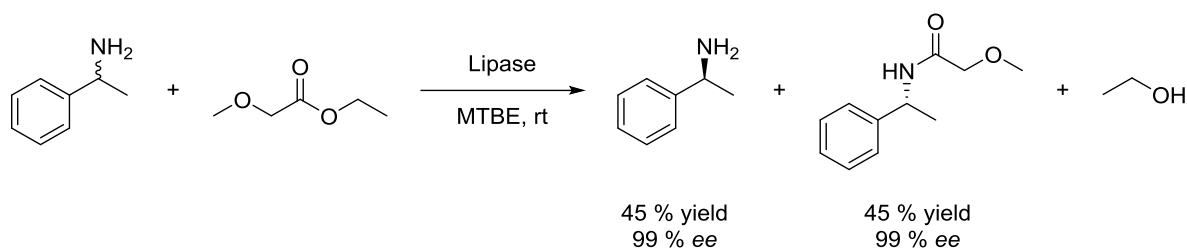


Figure 1. Overview of total numbers of granted patents in the years from 2014 to 2019 related to the application of the most prominent enzyme classes. Less relevant classes are neglected in the circle diagram (Adapted from P. Domínguez de María, G. de Gonzalo, A. R. Alcántara, *Catalysts* **2019**, *9*, 802. Creative Common CC BY license).^[29]

Hydrolases have numerous applications in organic synthesis due to their properties. Especially lipases are selective catalysts for the resolution of chiral esters, amides, carboxylic acids, and amines. Many lipases tolerate a high amount of organic solvent and high reaction temperatures, which facilitates their application in organic synthesis.^[1,30] An example for a process running at multi-thousand tons per year scale is the lipase-catalyzed resolution of 1-phenylethylamine under mild conditions. This process is carried in pure *tert*-butylmethylether (MTBE) at room temperature with ethyl methoxyacetate as acyl-donor (Scheme 5).^[31–33]

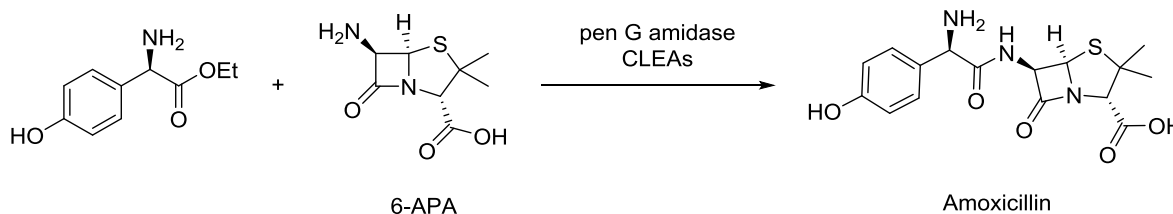
1 Biocatalysis as a tool in organic synthesis: Achievements, scope and limitations



Scheme 5. Kinetic resolution of 1-phenylethylamine by a lipase-catalyzed amidation with ethyl methoxyacetate as acyl-donor.^[31–33]

Enzymatic reactions are of interest for the pharmaceutical industry as the number of reaction steps towards the product can be often reduced drastically by employing biocatalysis. Enzymes often exhibit high chemo- and stereoselectivity, which is necessary for the high demands of this industry branch.^[13] Advantages of enzymes in this segment are their compatibility for one-pot reactions, the reduced waste production achieved by applying biocatalytic steps and the typical high product purity of biotransformations. The purity is necessary as the product is directly applied to humans.^[11,13] However, the implementation of biocatalytic reactions in drug synthesis routes can be challenging regarding their development costs. It is often uncertain whether drug candidates will pass the clinical phases, so cheap and easy-to-establish routes (regarding development) are often preferred.^[34] Alternative biocatalytic synthesis routes for known pharmaceuticals tend to be investigated after sale-start and for generic drugs.^[35–37]

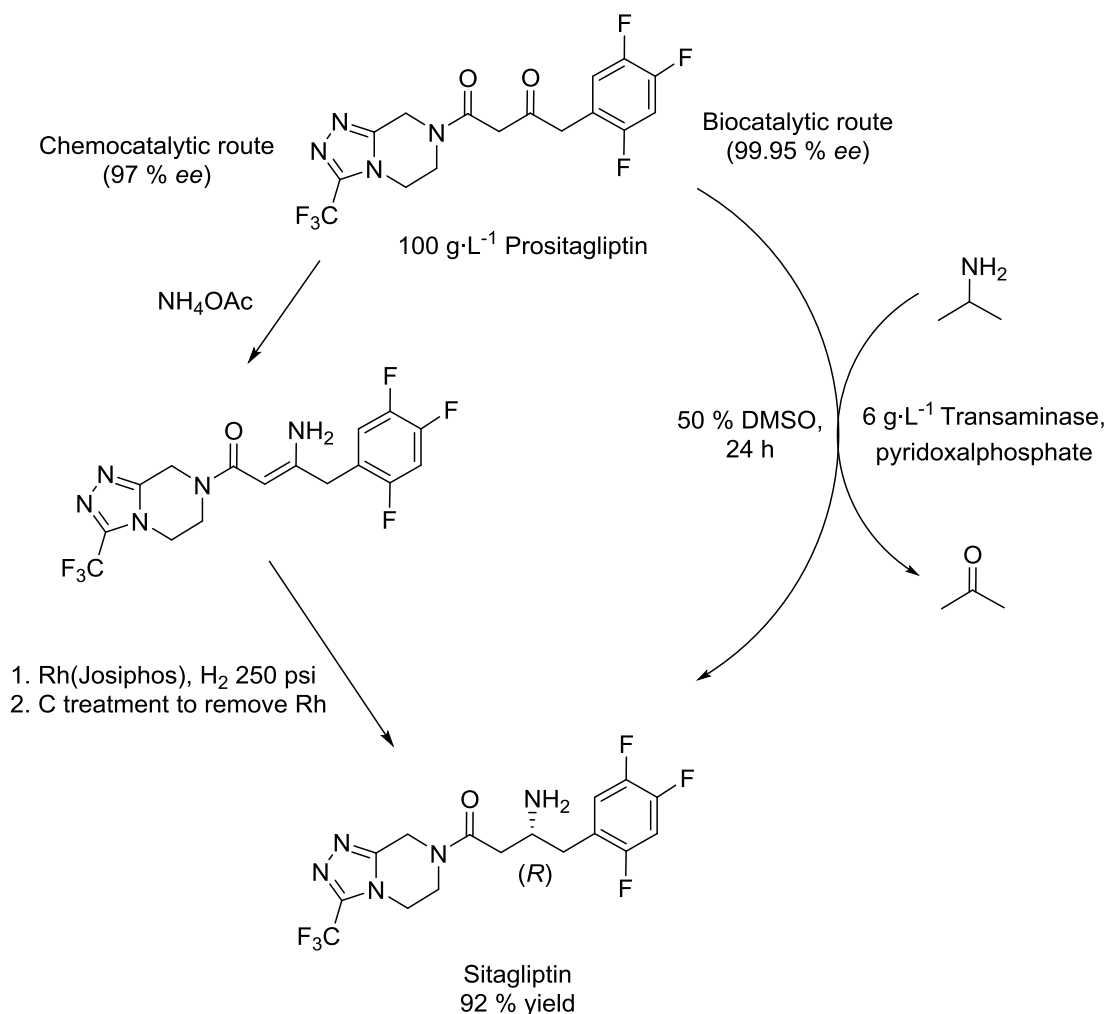
Early examples for (immobilized) enzymes in the pharmaceutical industry are related to the synthesis of semi-synthetic penicillin antibiotics. The important intermediate 6-aminopenicillanic acid (6-APA) is formed by hydrolysis of penicillin G (pen G) catalyzed by immobilized penicillin G amidase (pen G amidase) in a reversible reaction. Pen G is obtained from fermentative processes of fungi.^[16,38] Amoxicillin and other semi-synthetic penicillin antibiotics can be synthesized *via* condensation of 6-APA with synthetic esters catalyzed by pen G amidase (Scheme 6) or alternatively with another enzyme, penicillin G acylase (not shown). These processes are run in industrial scale replacing the classical chemical synthesis.^[1,38,39]



Scheme 6. Synthesis of the antibiotic amoxicillin from 6-APA by amide formation catalyzed by pen G amidase CLEAs.^[16,38]

1 Biocatalysis as a tool in organic synthesis: Achievements, scope and limitations

An impressive example for the power of biocatalysis in combination with directed evolution is the biocatalytic synthesis of the drug Sitagliptin from its precursor Prositagliptin (Scheme 7). The final synthesis step to this molecule is a formal reductive amination of a ketone group. The established chemocatalytic route proceeds by enamine formation with ammonium acetate and subsequent asymmetric hydrogenation with a chiral rhodium complex yielding the product with 97 % ee. The use of a heavy metal-catalyst in the last reaction step is a drawback as removal of trace amounts of heavy metals *via* active coal treatment is necessary for keeping the quality standards of pharmaceuticals. For the biocatalytic route, a transaminase has been engineered from a non-active (*R*)-selective wild-type enzyme only converting 0.7 % of the substrate (at 2 g·L⁻¹ loading). By combining computer-aided design with saturation mutagenesis and multiple rounds of DNA shuffling, an enzyme converting 100 g·L⁻¹ substrate (with 6 g·L⁻¹ enzyme) in the presence of 50 % DMSO in 24 hours was designed. The product could be isolated with 92 % yield at a perfect ee-value of 99.95 %.^[37]



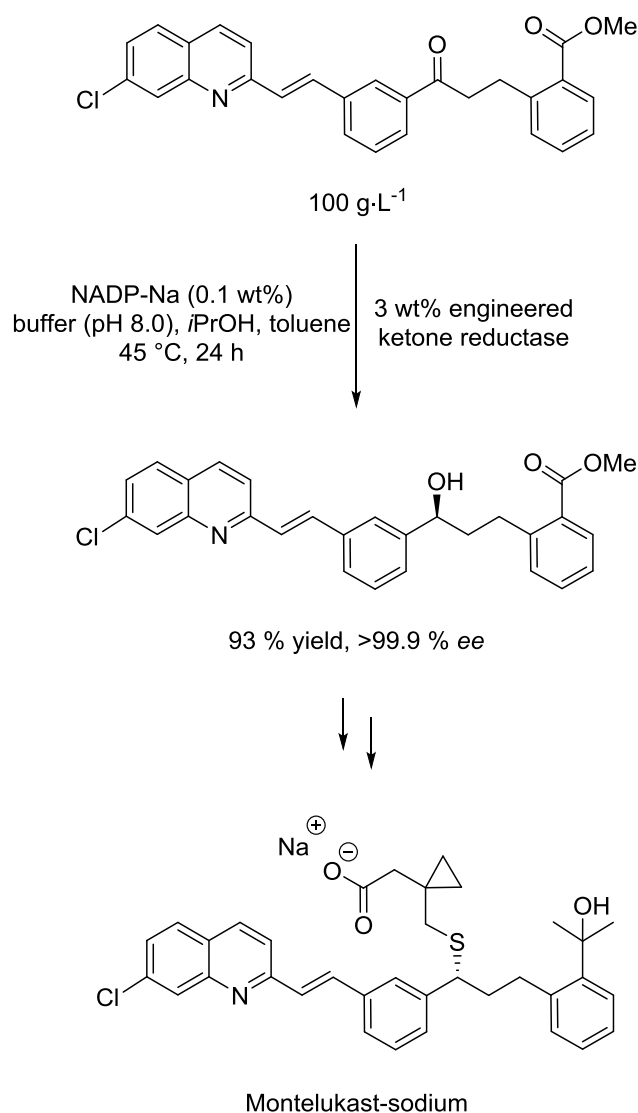
Scheme 7. Comparison of the chemocatalytic (left side) and a novel biocatalytic route for the synthesis of Sitagliptin from its precursor Prositagliptin.^[37]

1 Biocatalysis as a tool in organic synthesis: Achievements, scope and limitations

Another example which shows the possibilities of biocatalysis with engineered proteins is the implementation of a ketoreductase-catalyzed reduction in the synthesis of a precursor of Montelukast-sodium, an antiasthmatic drug (Scheme 8). The biocatalytic ketone reduction replaces an asymmetric reduction with a moisture sensitive chiral borate, which is required in a 1.5 to 1.8 fold excess and does not give sufficient enantiopurity of the product.^[35] Especially due to the bulkiness and the hydrophobic structure of the substrate, the wild-type enzyme only showed an extremely low volumetric production of $0.5 \text{ g}\cdot\text{L}^{-1}$ in one day reaction time. The demands to an engineered protein were a high thermal stability and the robustness against high amounts of polar, water miscible solvents. Further demands were perfect enantioselectivity, favorable kinetic properties (low K_m and high k_{cat}) and no inhibitory effects caused by neither the co-substrate *iso*-propanol and the acetone formed in the reactions.^[35] The final mutant was generated *via* several rounds of mutagenesis, which were analyzed with a very efficient high-performance liquid chromatography (HPLC) method. An efficient process could be carried out in 230 kg scale using the engineered protein. At a substrate loading of now $100 \text{ g}\cdot\text{L}^{-1}$, yields between 90 to 98 % can be obtained with $3 \text{ g}\cdot\text{L}^{-1}$ enzyme in one day reaction time at $45 \text{ }^\circ\text{C}$. A product purity of $>98 \%$ was achieved at a perfect *ee*-value of $>99.9 \%$.^[35]

There are other examples of pharmaceuticals or important intermediates as Atorvastatin, Ezetimibe, Sulopenem (intermediates), and (*S*)-licarbezepine (drug), for which engineered ketone reductases play a major role in their synthesis routes.^[5] The above-mentioned processes are only striking examples for numerous syntheses in the pharmaceutical industry employing biocatalytic reactions, but also show the need of engineering proteins for the actual application. Wild-type enzymes rarely meet all requirements of a process especially for the fine chemical and pharma segment. Therefore, protein engineering is considered as a necessary tool for application of enzymes in organic synthesis. Much progress has been reported in this field in the last thirty years.^[14,15]

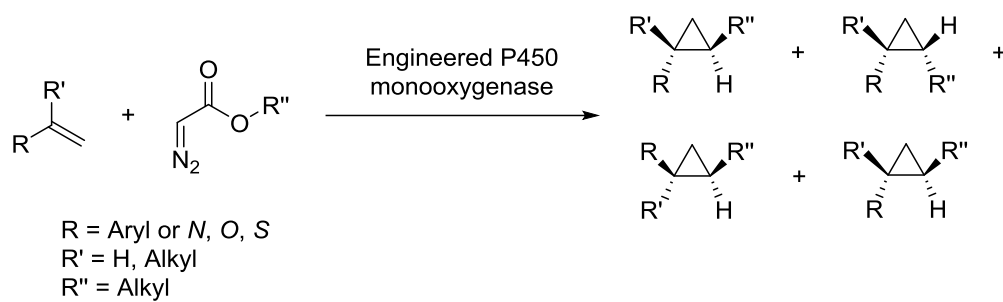
1 Biocatalysis as a tool in organic synthesis: Achievements, scope and limitations



Scheme 8. Biocatalytic ketone reduction with an engineered ketone reductase as a key step in the synthesis of the drug Montelukast-sodium.^[12]

The development of directed evolution of proteins was a major achievement contributing to the success of biocatalysis. For her achievement in this field, *Arnold* was awarded the Nobel Prize in Chemistry 2018.^[40] Besides biocatalyst optimization, directed evolution is also a suitable tool for designing total new reactivity not present in nature. A great example for such a reaction was given with an engineered cytochrome P450 (CYP) monooxygenase. Instead of the naturally catalyzed oxene transfer, carbenes were transferred from diazoesters to olefins forming cyclopropanes in asymmetric reaction with high enantio- and diastereoselectivity.^[41] Besides terminal alkenes, also heteroatom-substituted terminal alkenes were suitable substrates for these engineered enzymes (Scheme 9).^[42]

1 Biocatalysis as a tool in organic synthesis: Achievements, scope and limitations



Scheme 9. Cyclopropanation of (heteroatom-substituted) olefins with azoesters catalyzed by engineered CYP monooxygenases.^[41,42]

2 State of the art

2.1 Synthetic methods for the synthesis of α -keto acids and nitriles

In this doctoral thesis, various aspects of enzyme catalysis were investigated with mainly two kinds of enzymes, which are involved in the natural metabolism of amino acids to carboxylic acids in microorganisms. While amino acid oxidases (AAOs) oxidize amino acids to α -keto acids releasing ammonia and hydrogen peroxide, aldoxime dehydratases (Oxds) catalyze the dehydration of aldoximes to nitriles. Both enzymes are related to flavin cofactors. These two enzyme classes will be applied in synthesis of valuable compounds located in the bulk and fine chemistry segment. The aim was the development of alternative synthetic routes for these compounds. The biocatalytic processes or the enzyme itself will be optimized.

2.1.1 Enantiomerically pure amino acids and α -keto acids

L- α -Amino acids are the blocks of which all naturally occurring peptides and proteins are made of (20 proteinogene), therefore they occur in all organisms. More than 700 different amino acids have been identified in nature. Chemically, these compounds contain an amino group in the α -position of a carboxyl group. Their opposite enantiomer, the D-amino acids, are also present in nature, however, they are not used in the biosynthesis of peptides.^[43] α -Amino acids are closely related to α -keto acids, compounds which contain a carbonyl moiety instead of the amino moiety (Figure 2).^[44] L-Amino acids are applied in the food industry, e.g. additives like aspartate or its monosodium salt, and as feed additives for animal food. They can also be used in the synthesis of bioactive polypeptides for the pharmaceutical industry.^[45]

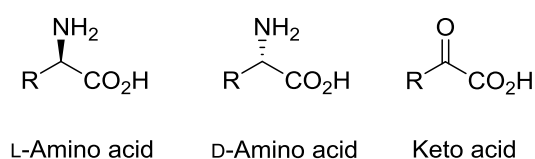
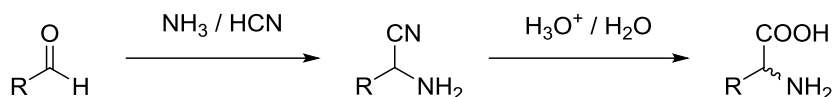


Figure 2. Basic structure of L- α -amino acids, D- α -amino acids, and α -keto acids.

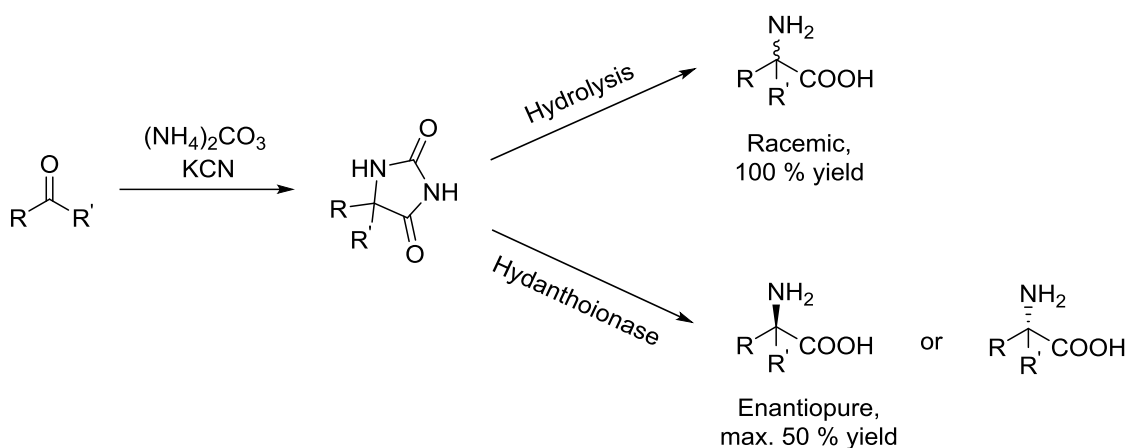
Historically, they were synthesized by the Strecker-synthesis from aldehydes, ammonia and hydrogen cyanide. In the first reaction step, an aminonitrile is obtained by the addition of hydrogen cyanide to the *in situ* formed imine. Acidic hydrolysis of the aminonitrile yields the racemic α -amino acids (Scheme 10). As a drawback however, this process only yields the racemic mixtures instead of the enantiomerically pure amino acids and employs the highly toxic hydrogen cyanide as a reagent.^[46] The Strecker-synthesis can also be carried out in asymmetric fashion if auxiliaries are used.^[47]

2 State of the art



Scheme 10. Schematic procedure of the production of α -amino acids by the Strecker-reaction. An aldehyde gets transformed into an α -aminonitrile by ammonia and hydrogen cyanide, which is acidly hydrolyzed to the amino acid.^[46]

The common chemical production of amino acids is now performed with the Bucherer-Bergs-synthesis, a variant of the Strecker-synthesis. Instead of ammonia and hydrogen cyanide, ammonium carbonate and sodium cyanide are used to form hydantoiones. These compounds can be hydrolyzed to amino acids by chemical hydrolysis in basic media or with enantioselective hydantoionases yielding enantiomerically pure amino acids in a kinetic resolution (Scheme 11). Drawbacks of the Bucherer-Bergs synthesis are the long reaction times, elevated process temperatures and the toxicity of potassium cyanide.^[46]



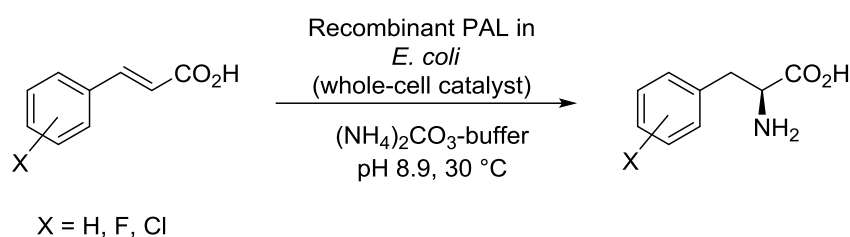
Scheme 11. Synthesis of amino acids by the Bucherer-Bergs-synthesis forming hydantoiones and subsequent hydrolysis or resolution with hydantoionases.^[46]

While the chemical synthesis is common for the production of racemic amino acids, especially methionine and alanine and the achiral glycine, most L-amino acids are produced by means of enzymatic reactions or fermentative processes. Wild-type strains or engineered variants of *E. coli*, *Corynebacterium glutamicum* (*C. glutamicum*), and others are used for the production of most proteinogenic amino acids in industrial scale.^[45,48] The bacteria are usually grown in presence of cheap hydrolyzed carbohydrates in large reactors of 50-500 kL-scale.^[48] Especially, genetically modified strains of *C. glutamicum* (gene deletion, gene insertion, etc.) are frequently investigated as a platform for the production of many amino acids.^[49] An approach towards racemic amino acids from lignocellulose as a non-food competing biorenewable resource *via* electrochemical reduction of α -keto acids has been investigated recently. For example, lactic acid, glycolic acid, and α -hydroxyglutaric acid can be obtained *via* hydrothermal degradation of lignocellulose. By means of chemical or biocatalytic oxidation, the corresponding α -keto acids can be formed. The racemic α -amino acids can be obtained by a

2 State of the art

four electron reduction of the α -keto acids at a titan(IV) oxide/titan-mesh-electrode in the presence of hydroxylamine as an amine donor *via* the aldoximes as intermediates.^[50]

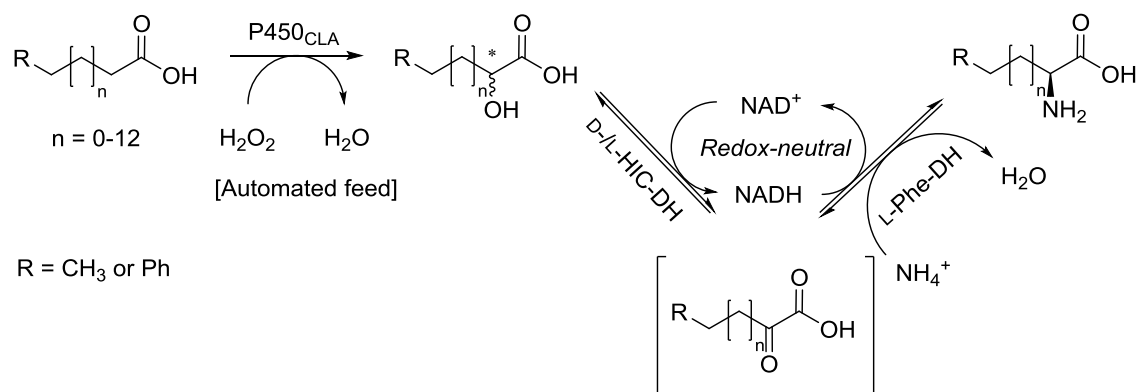
For unnatural amino acids as well as D-amino acids however, fermentative production is not an option. Therefore, chemical synthesis or resolution of racemic amino acids is required. Homologation of various nickel(II) complexes with glycine or alanine is an asymmetric method to yield enantiomerically enriched unnatural amino acids.^[51] Unnatural α -amino acids containing electron withdrawing groups can also be obtained photochemically from a total protected aspartate in presence of a ruthenium catalyst.^[52] Enzymatic production of unnatural amino acids with different phenylalanine-ammonia lyases (PAL) expressed in *E. coli* has been investigated recently. These enzymes accept also halogenated derivatives of L-phenylalanine as substrates. In presence of a high excess of ammonium carbonate as ammonia source, up to 50 mM of halogenated *trans*-cinnamic acid were converted to the halogenated derivatives of L-phenylalanine (Scheme 12).^[53]



Scheme 12. Synthesis of halogenated derivatives of L-phenylalanine from *trans*-cinnamic acid with whole-cell catalysts expressing phenylalanine-ammonia lyases.^[53]

A reaction cascade consisting of three enzymatic transformations with a peroxygenase, an alcohol dehydrogenase (ADH) and an amino acid dehydrogenase (AADH) can form amino acids (especially aliphatic amino acids or phenylalanine) from carboxylic acids. The stereoselectivity depends on the selectivity of the enzyme used. The peroxygenase catalyzes the hydroxylation of the carboxylic acid in α -position by utilization of hydrogen peroxide given with a feed strategy. Next, an ADH (here a D- or L-selective α -hydroxyisocaproate dehydrogenase: HIC) oxidizes the α -hydroxy carboxylic acid to the α -keto acid, which is converted to the corresponding α -amino acid in a reductive amination catalyzed by an AADH (here L-phenylalanine dehydrogenase: L-Phe-DH). Ammonia is the amine donor in this system. The cofactor nicotinamide adenine dinucleotide (NAD) is recycled *in situ* by the two enzymes of the second step in this so called redox-neutral hydrogen borrowing cascade (Scheme 13).^[54]

2 State of the art



Scheme 13. Enzymatic cascade implying hydroxylation with a peroxygenase, alcohol oxidation with HIC and reductive amination with AADH forming (unnatural) L-amino acids from carboxylic acids.^[54]

α -Keto acids represent the deaminated form of the α -amino acids. This compound class plays an important role in the biosynthesis of acetyl-coenzyme A and in the Krebs-cycle.^[55] They are applied in the food industry as supplements, contained in animal feed and are given for prevention of nitrogenemia for renal failure patients.^[56] Furthermore, α -keto acids are precursors in the synthesis of pharmaceuticals and some representatives as α -ketoisocaproate have a medical application in unmodified form (Table 3).^[57] The α -keto acid derived from alanine, pyruvate, is the natural byproduct formed in reactions catalyzed by amine transaminases (carbonyl to amine). According to this, transamination reactions forming aldehydes or ketones from amines require pyruvate as a co-substrate.^[58] This α -keto acid is therefore involved in several biocatalytic cascades with transaminases and their cofactor recycling.^[59] Naturally occurring and synthetic α -keto acids can be used as acylating agents in organic chemistry. In comparison to other acylating agents, only carbon dioxide is formed as the byproduct in these reactions. A recent review from *Penteado et al.* gives a comprehensive overview about synthesis protocols of amides and the scope of this reaction (Figure 3).^[55]

Table 3. Application of selected α -keto acids.^[57]

Green chemistry principle	Biocatalysis
Pyruvate	Improve exercise endurance capacity Weight-control supplement Nutraceutical Antioxidant Precursor of pharmaceuticals
α -Ketoglutaric acid	Ammonium ion receptor Precursor of chemical compounds Improve athletic performance and wound healing The poly α -ketoglutaric acid is used in tissue scaffolding and therapeutic delivery
α -Ketoisovalerate	The precursor of 1-butanol Hepatitis B virus infection and chronic glomerulonephritis Feed of lamb, pigs, chickens
α -Ketoisocaproate	Precursor of biofuel Hepatitis B virus infection and chronic glomerulonephritis Depression of silenced tumor with organoselenium compounds Stimulate insulin secretion Increase muscular power Promote the milk production and composition
Phenylpyruvate	Diet sweetener aspartame, indole-3-acetic acid precursor
α -Keto- γ -methylthiobutyric acid	Poultry industry, anti-cancer drug
2,5-Diketo-D-gluconic acid	Precursor of 2-keto-L-gluconic acid
2-Ketobutyric acid	Precursor for chemical synthesis of pesticide, spice and food additive

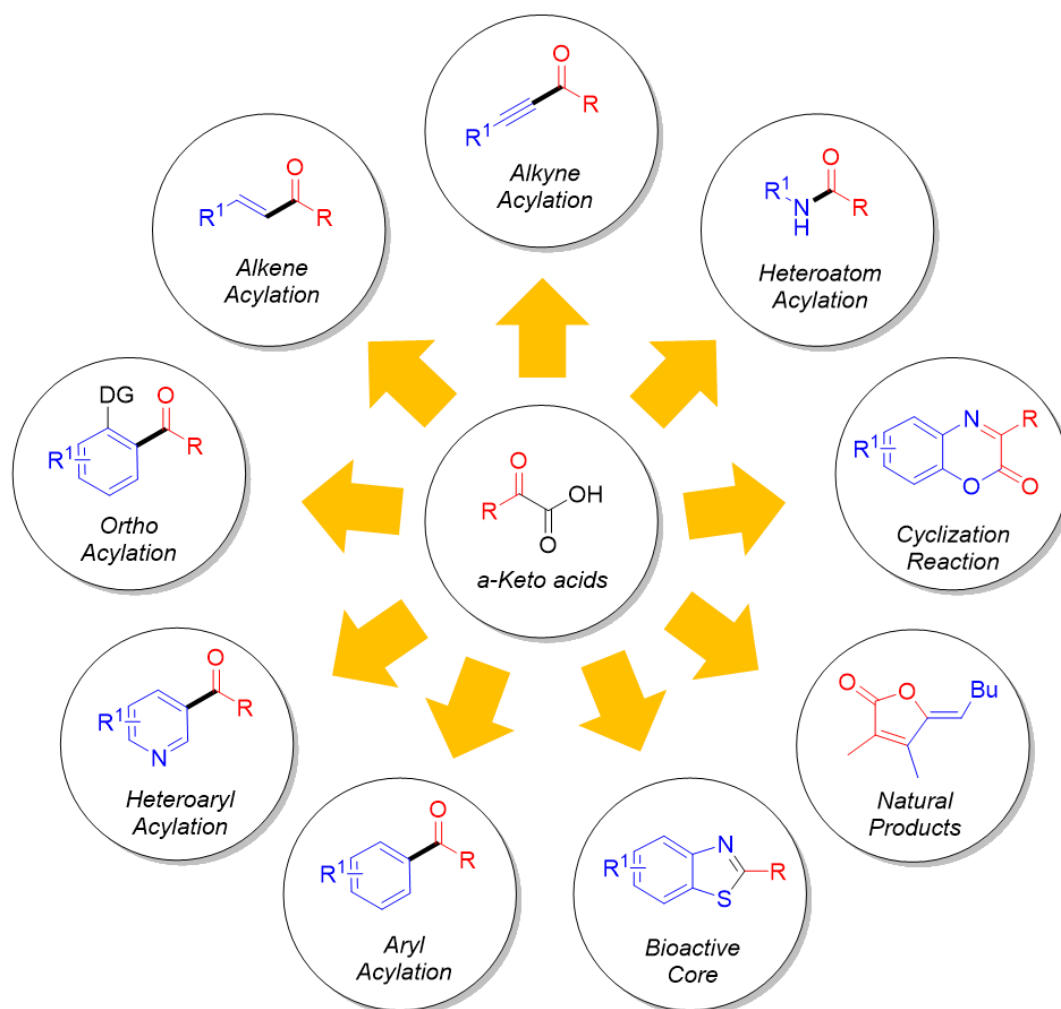
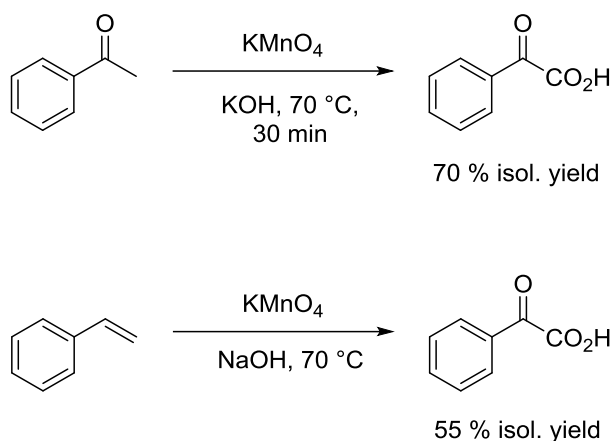


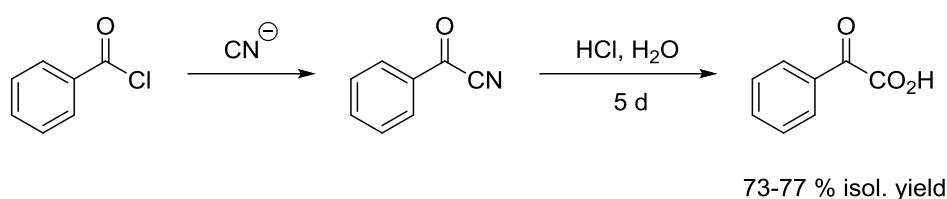
Figure 3. Application of α -keto acids as acylating agents in organic chemistry (Adapted with permission from F. Penteado, E. F. Lopes, D. Alves, G. Perin, R. G. Jacob, E. J. Lenardão, *Chem. Rev.* 2019, 119, 7113–7278, Copyright © 2019, American Chemical Society).^[55]

In analogy to α -amino acids, α -keto acids can be also prepared by chemical processes. *Waters* and *Cooper et al.* gave comprehensive overviews about methods of α -keto acid preparation.^[44,60] Historically, preparations of phenylglyoxylic acid were performed by oxidation of acetophenone or styrene with potassium permanganate in strong basic medium (Scheme 14).^[61,62] Another method is the acidic hydrolysis of benzoyl cyanide, where yields of 73 to 77 % were obtained after a reaction time of five days.^[63] The preparation of the benzoyl cyanide requires harsh reaction conditions involving benzoyl chloride and a cyanide source (Scheme 15).^[64]

2 State of the art

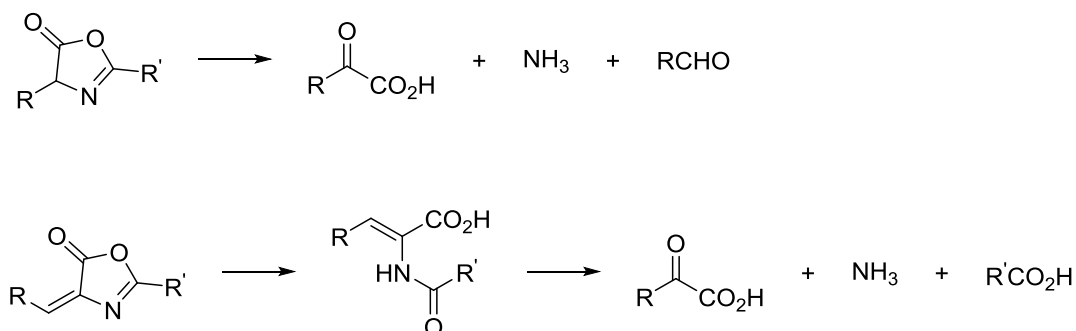


Scheme 14. Oxidation of acetophenone (upper) or styrene (lower) with potassium permanganate under basic conditions yielding phenylglyoxylic acid.^[61,62]



Scheme 15. Synthesis of phenylglyoxylic acid from benzoyl cyanide, which is prepared from benzoyl chloride by substitution with cyanide salts.^[63,64]

An convenient synthesis route towards α -keto acids utilizes oxalozones as intermediates. Oxalozones are five-membered heterocycles containing a C-N double bond and a lactone moiety. The hydrolysis of both saturated and unsaturated oxalozones yields α -keto acids, ammonia and an aldehyde or carboxylic acid depending on if saturated or unsaturated oxalozones are used (Scheme 16).^[44] If oxalozones are prepared from α -amino acids and trifluoroacetic acid anhydride, fair to excellent yields of the α -keto acids between 58 and 91 % were achieved. This method is also suitable for the synthesis of chiral β -methyl- α -keto acids.^[65]

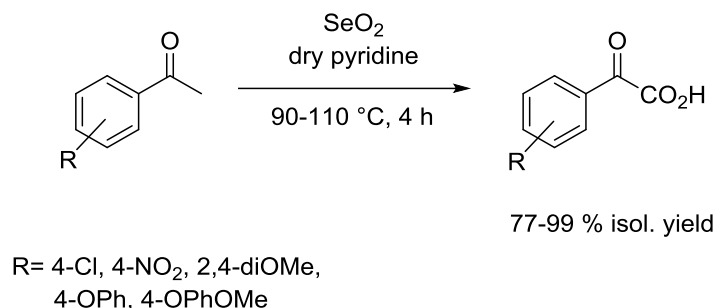


Scheme 16. Hydrolysis of saturated (upper) and unsaturated (lower) oxalozones yielding α -keto acids, ammonia and aldehydes (upper) or carboxylic acids (lower).^[44,65]

Derivatives of phenylglyoxylic acid can be synthesized by the heating of acetophenone derivatives and selenium(IV) oxide in dry pyridine. For different substitution patterns with varying electronic and mesomeric effects, yields of the α -keto acids between 77 and 99 %

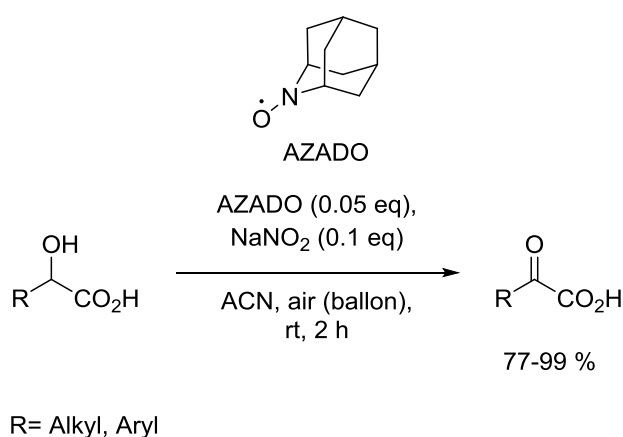
2 State of the art

were obtained (Scheme 17).^[66] A perfluoroorganic selenium compound can be a catalyst for oxidation of methylketones to α -keto acids as well.^[67]



Scheme 17. Oxidation of acetophenone derivatives with selenium(IV) oxide in dry pyridine yielding phenylglyoxylic acid derivatives.^[66]

Furthermore, a catalytic oxidation of 2-hydroxycarboxylic acids is suitable to produce several α -keto acids in yields between 77 and 99 %. This reaction proceeds at room temperature in the presence of the AZADO-radical and sodium nitrite in acetonitrile with molecular oxygen as the oxidant (Scheme 18).^[68]

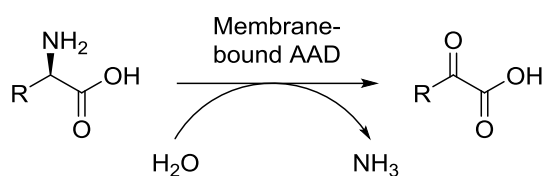


Scheme 18. AZADO (structure on top of the arrow)-catalyzed oxidation of 2-hydroxycarboxylic acids under air forming α -keto acids.^[68]

Despite of their high costs and environmental pollution caused by the waste and/or reagents, α -keto acids are mostly prepared chemically in the industry. In view of the emerging biotechnological industry, enzymatic and microbial production processes will possibly replace the chemical synthesis of the biological α -keto acids in the future. In general, α -keto acids can be produced by an enzymatic deamination of α -amino acids in biotransformations or in fermentative processes using natural biosynthesis pathways. An important advantage of enzymatic transformations compared to fermentative processes is the facile downstream. There are two enzymes present in nature, which catalyze the deamination reaction: AAOs (see further in chapter 2.2.2) and amino acid deaminases (AADs). AADs are membrane-bound enzymes, which catalyze the unoxidative deamination of α -amino acids to their corresponding

2 State of the art

α -keto acids releasing only ammonia (Scheme 19).^[56] Especially AADs of the *Proteus* genus have been a target of enzyme engineering. With a combination approach of metabolic engineering of whole-cell catalysts and engineered AADs, highly improved titers of α -keto acids were obtained. For example, the titer of the α -ketoglutaric acid production was raised from 12.79 g·L⁻¹ to 89.11 g·L⁻¹ with an improved system consisting of an AAD from *Proteus mirabilis* expressed in *Bacillus subtilis* strain 168. Deletion of genes responsible for the degradation of α -keto acids improved the product stability in the fermentative process. Application of random mutagenesis on the AADs led to an improved enzyme overexpression and performance.^[56] A bottleneck in the fermentative α -keto acid production is still the requirement of α -amino acid supply in the culture medium, which makes these processes less economical.^[69]



Scheme 19. Non-oxidative deamination of L-amino acids to α -keto acids catalyzed by membrane-bound AADs.^[56]

2.1.2 Nitriles

Nitriles are a compound class containing a C-N triple bond. The simplest nitrile is hydrogen cyanide, a gaseous, acidic and highly toxic compound. Its salts are crystalline compounds of also high toxicity.^[70] An industrially very relevant nitrile is acrylonitrile, which is an intermediate in the synthesis of acrylamide. For instant, the annual production of acrylonitrile was 5.8 million tons in the year 2008 with growing tendence. Adiponitrile (hexane- 1,6-dinitrile) is an aliphatic dinitrile of high relevance, as it is an intermediate in the synthesis of polyamides. Besides the polymer industry, nitriles have further applications in the industry. Other (aromatic) nitriles find application as fine chemicals, for example as precursors of agrochemicals and pharmaceuticals. Niacin (Nicotinamide), a product derived from nicotinonitrile, is a feed additive itself and also plays an important role as precursor of pharmaceuticals. Chiral nitrile groups are found as structural motifs in several pharmaceuticals,^[71] such as Saxagliptin^[72] and Vildagliptin (Figure 4).^[73]

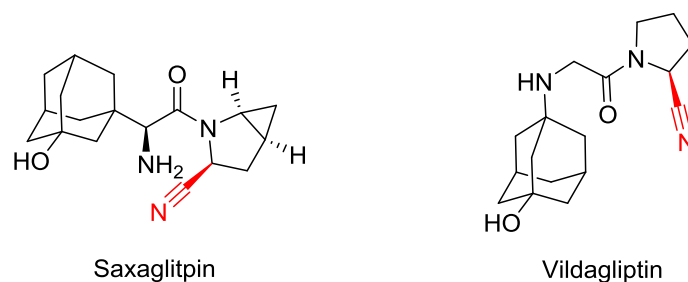
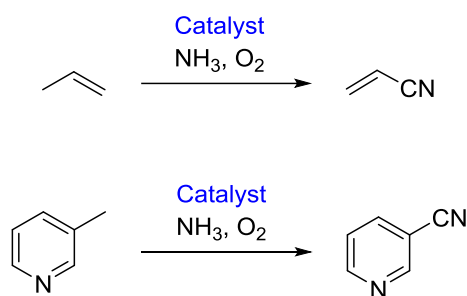


Figure 4. Structures of the drugs Saxagliptin and Vildagliptin bearing chiral nitrile moieties (marked in red).^[72,73]

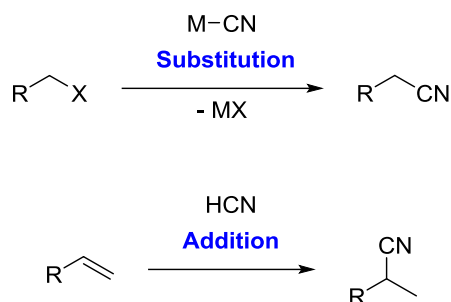
There is a vast number of reactions known, which obtain nitriles in organic synthesis. The following section introduces only selected strategies of (chiral) nitrile compound synthesis and present industrially relevant processes. Typical synthesis strategies of industrial relevance are the ammoxidation,^[74] addition or substitution reactions.^[46,71,75,76] The ammoxidation is a gas phase oxidation of alkanes, alkenes or aromatics to nitriles. In the presence of oxygen, ammonia, and a metal-catalyst, a terminal cyano group is formed (Scheme 20). For example, acrylonitrile, methylacrylonitrile, (tere-)phthalodinitrile and nicotinonitrile are prepared by this method. This reaction can be carried out smoothly in industrial scale and is moreover classified as a “green” oxidation method,^[77] therefore it has been frequently investigated since its development.^[78] Undesired byproducts are carbon dioxide formed by overoxidation processes or hydrogen cyanide and other nitriles formed by degradation of educt and product occurring during the reaction. A drawback are the elevated temperatures necessary for the reaction.^[77]



Scheme 20. Ammoxidation of propylene (upper) and 3-picoline (lower) forming acrylonitrile and nicotinonitrile.^[74]

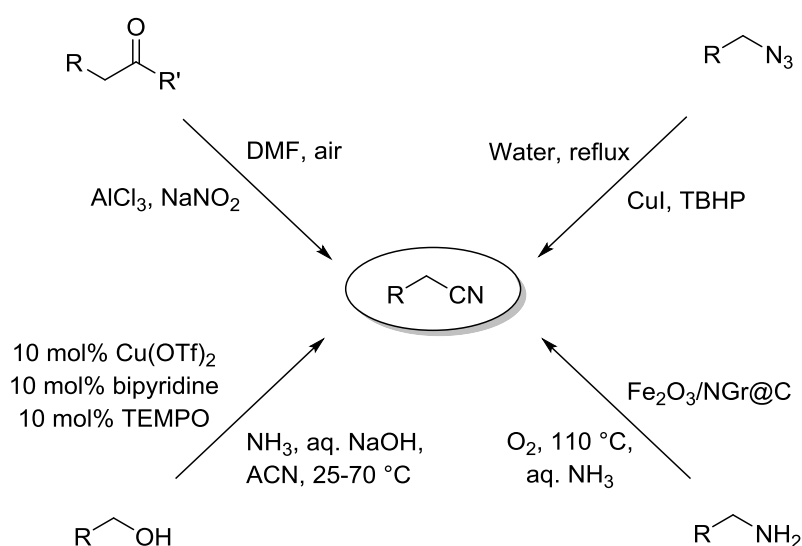
Substitution reactions with hydrogen cyanide or its salts are based on the Kolbe-nitrile synthesis (Scheme 21, upper).^[79] As these reactions usually require harsh conditions or the use of the highly toxic cyanide ions, different synthesis routes would be desirable.^[46,71,75,76]

Cyano groups can also be introduced into molecules by hydrocyanation, the addition of hydrogen cyanide to C-C double bonds (Scheme 21, lower). An example of this reaction in the chemical industry is the hydrocyanation of 1,3-butadiene forming adiponitrile run by DuPont at several million ton scale.^[80]



Scheme 21. Synthesis of nitriles by substitution or addition reactions.^[46,71,75,76,80]

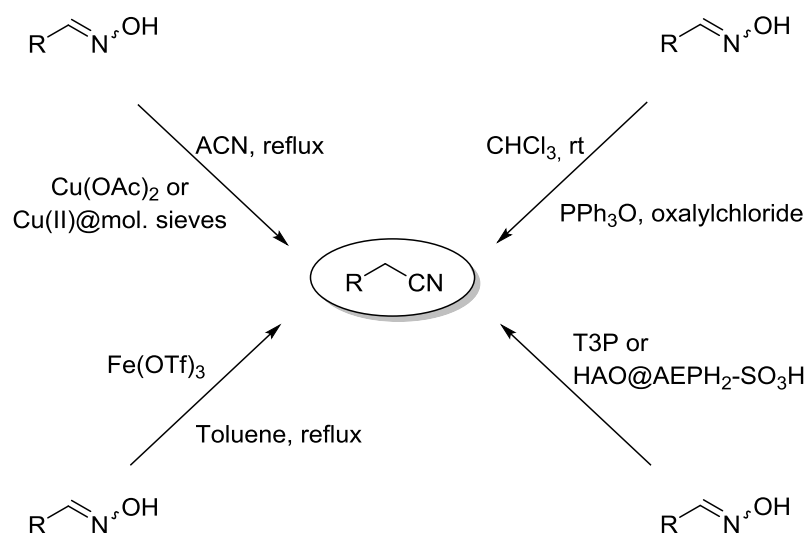
Nitriles are also accessible *via* oxidative transformations of carbonyl species, amines and azides (Scheme 22). A catalytic oxidation of primary alcohols or aldehydes in a copper-TEMPO-air system (TEMPO: 2,2,6,6-Tetramethylpiperidinyloxy) is suitable for the synthesis of nitriles under basic conditions with ammonia as a nitrogen donor. Arylic and aliphatic nitriles can be synthesized using this method.^[81] Nitriles can also be synthesized from aldehydes or ketones in an oxidation involving a C-C bond cleavage with aluminum(III) chloride and sodium nitrite as a nitrogen source. By *in situ* aldoxime formation followed by a Beckmann-rearrangement nitriles are formed.^[82] Alternatively, nitrogen containing organic compounds can be used as educts for nitrile synthesis as well. An oxidative method with an iron(III) oxide-based nanocatalyst prepared by pyrolysis of nitrogen introduced graphene ($\text{Fe}_2\text{O}_3/\text{NGr@C}$) is suitable for the synthesis of terminal aliphatic or aromatic nitriles.^[83] Moreover, primary azides can be oxidized to nitriles in an aqueous *tert*-butylhydroperoxide (TBHP) solution in the presence of copper(I) iodide.^[84]



Scheme 22. Oxidative pathways for nitrile synthesis from alcohols, carbonyl-compounds, azides and amines.^[81-84]

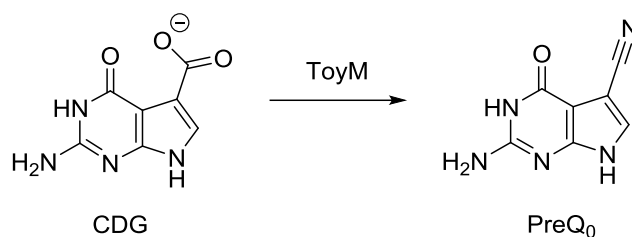
2 State of the art

Also aldoximes can be transformed into racemic nitriles by several dehydration methods (Scheme 23). For example, a metal-free catalytic dehydration of *in situ* activated aldoximes can be performed with triphenylphosphane oxide and a slight excess of oxalylchloride as oxidating agent. The *in situ* formed species in this reaction degrades by loss of hydrogen chloride, carbon monoxide and carbon dioxide releasing triphenylphosphane oxide and the nitrile.^[85] A derivative of phosphoric acid, namely propanephosphoric acid anhydride (T3P) and a sulfonated hydroxyapatite nanocatalyst functionalized with 2-aminoethyldihydrogenphosphate (HAP@AEPH₂-SO₃H) are also reagents for the rapid formation of nitriles from aldoximes. These reactions can be combined with the condensation of aldehydes with hydroxylamine forming the aldoximes *in situ* without product isolation.^[86,87] Copper(II) ions can catalyze the transfer of a water molecule from aldoximes to acetonitrile, thus forming nitriles and acetamide.^[88,89] The metal-catalyzed dehydration of aldoximes can be also performed in the absence of other nitriles with iron(III) triflate in toluene.^[90]



Scheme 23. Selected methods of aldoxime dehydration for the synthesis of racemic nitriles.^[85-90]

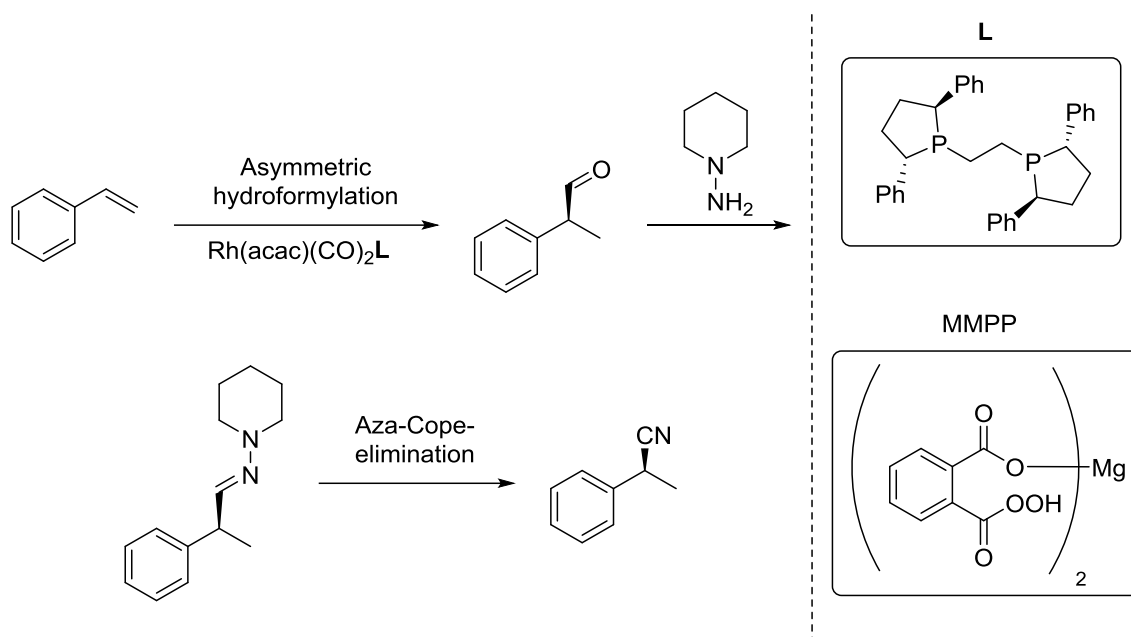
The actinobacterium *Streptomyces rimosus* utilizes a unique enzyme for the transformation of carboxylic acids into nitriles, the nitrile synthetase ToyM (Scheme 24). In particular, this enzyme catalyzes the transformation of 7-carboxy-7-deazaguanine (CDG) to 7-cyano-7-deazaguanine (PreQ₀) utilizing two equivalents of adenosine triphosphate (ATP). The reaction proceeds by formation of an amide intermediate while utilizing of one equivalent of ATP with ammonia as the nitrogen source. The same enzyme is also active for the following transformation of the amide into the nitrile using another equivalent of ATP.^[91] Although possessing a very interesting reactivity, the dependence on the cofactor ATP is a highly limiting factor for an application in organic synthesis. ATP is very expensive and suitable methods of *in situ* cofactor regeneration are not state of the art yet.



Scheme 24. Transformation of CDG to PreQ₀ catalyzed by the nitrile synthetase ToyM.^[91]

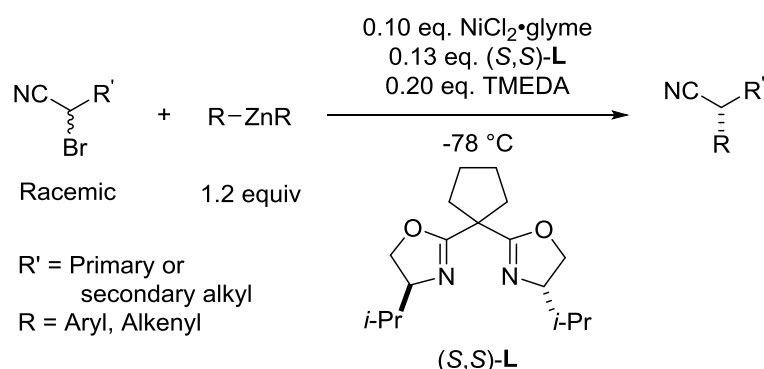
Chiral nitriles can be obtained *via* various approaches. Starting from chiral molecules (or chiral nitriles) with already existing stereoinformation, nitriles can be prepared under retainment of the chiral information as well as under stereoinversion. Chiral ketonitriles can be prepared *via* a radical β -fragmentation of β -hydroxyazide structures in terpene structure induced by iodine, diacetoxyiodine and irradiation with retaining stereoinformation. With the same system, aldonitriles can be obtained from carbohydrate structures containing the β -hydroazide motif.^[92] α -Metallated chiral nitriles prepared *via* deprotonation with Grignard-reagents are stable against stereoinversion for a short time at -104 °C. If quenched with an electrophile *in situ* or after ten seconds, chiral nitriles with an *ee*-value of up to 96 % can be prepared.^[93] Copper(I)-catalyzed α -silylation of chiral α -trifloxynitriles proceeds under stereoinversion with high *ee*-values of up to 99 %.^[94] Aluminum(III) chloride promoted ammoxidation of enantiomerically enriched methylenes with *tert*-butylnitrite as nitrogen source in presence of catalytic amounts of *N*-hydroxyphthalimide also proceeds under retainment of the axial stereoinformation.^[95]

The hydrogenation of alkoxy-cinnamic nitriles with rhodium and a chiral phosphane ligand can yield chiral nitriles with up to 99.9 % *ee*.^[96] Besides an asymmetric hydrogenation of alkanes containing a cyano group, this moiety can also be introduced into a molecule in asymmetric fashion. *Li et al.* showed an impressive method of enantioselective hydrocyanation with a rhodium catalyst while avoiding the highly toxic hydrogen cyanide as cyanide source (Scheme 25). The hydrocyanation proceeds by an asymmetric hydroformylation with a chiral rhodium complex and benzoic acid as an additive. The aldehyde obtained in the hydroformylation is condensed *in situ* with 1-aminopiperidine forming a chiral imide as a stable intermediate. The benzoic acid assists in accelerating the condensation, thus, preventing racemization. The cyano group is formed in an aza-Cope-elimination induced by *N*-oxidation of the heterocycle with magnesium monoperoxyphthalate (MMPP). Nitriles can be prepared in high yields with *ee*-values between 88 to 94 % from several aromatic and heteroaromatic as well as cyclic aliphatic alkenes.^[80]



Scheme 25. Hydrocyanation of alkenes (here styrene) by avoiding hydrogen cyanide. The reaction proceeds by an asymmetric hydroformylation followed by enamine formation and an aza-Cope-elimination induced by MMPP.^[80]

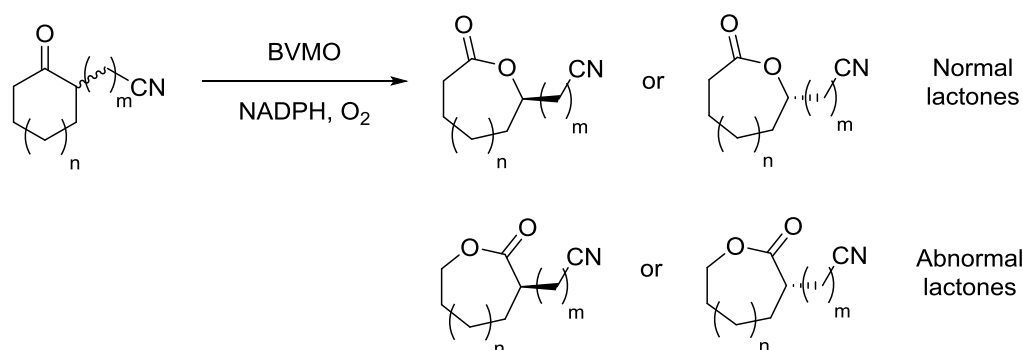
An asymmetric synthesis of chiral nitriles from racemic α -brominated nitriles in a stereoconvergent Negishi-cross-coupling with diaryl- or dialkenylzinc can yield chiral secondary nitriles (Scheme 26). The coupling proceeds with a chiral nickel catalyst and forms enantiomerically enriched nitriles with high yields at *ee*-values between 76 to 94 %. However, the reaction conditions are not desirable as a high catalyst loading of 13 mol% of the chiral ligand (at a catalyst loading of 10 mol% nickel) and low temperatures ($-78\text{ }^\circ\text{C}$) are required in order to obtain the nitrile in high yields at good enantioselectivity. Nevertheless, this method is suitable for the enantioselective synthesis of non-terminal chiral nitriles with a varying backbone.^[97]



Scheme 26. Negishi-cross-coupling of α -brominated nitriles with diaryl or dialkenylzinc forming enantiomerically enriched nitriles in presence of a chiral nickel catalyst.^[97]

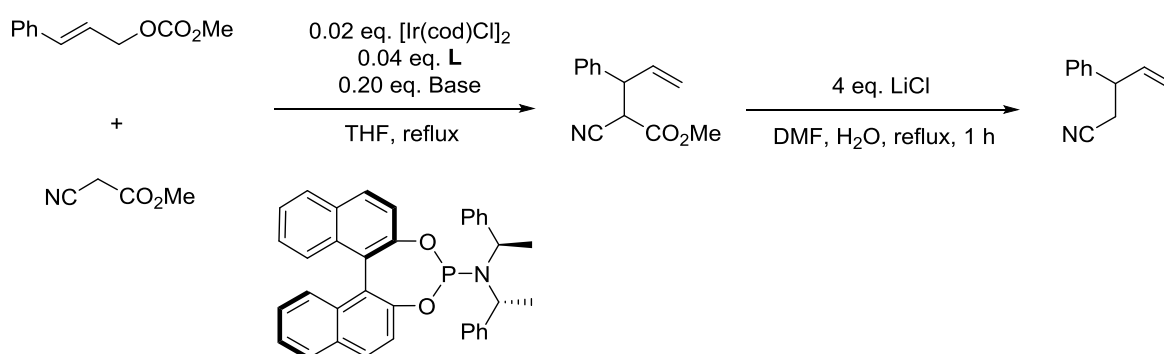
2 State of the art

A regio- and enantioselective synthesis of nitrilolactones was reported with Bayer-Villiger monooxygenases (BVMOs) from racemic nitriloketones. BVMOs were screened for ketones of different ring sizes and side group chain lengths (Scheme 27). Especially 2-(1-cyanoethyl)cyclohexanone, 2-(1-cyanopropyl)cyclohexanone, and 2-(1-cyanopropyl)cycloheptanone were converted highly selective by several cyclohexane monooxygenases in the screening. Depending on the combination of substrate and enzyme, E-values of >200 were achieved in the kinetic resolutions.^[98]



Scheme 27. Enantioselective Bayer-Villiger oxidation of nitriloketones catalyzed by BVMOs forming normal and abnormal nitrilolactones.^[98]

Iridium-catalyzed allylation of cyanoacetate methylesters can form homoallylic chiral nitriles in presence of a chiral phosphane ligand (Scheme 28). The methoxycarbonyl group can be removed in a Krapcho-demethoxycarboxylation with lithiumchloride under heating to reflux. This method yields nitriles with very high ee-values of up to 99 % and relatively low catalyst loadings of 2 % iridium (and 4 % of the chiral phosphane ligand). However, this method is limited for the synthesis of homoallylic nitriles.^[99]



Scheme 28. Iridium(II)-catalyzed allylation of cyanoacetate methylester followed by a Krapcho demethoxycarboxylation forming allylic nitriles.^[99]

2 State of the art

Most presented routes for the chiral nitrile synthesis (apart from the hydrocyanation) require a nitrile (or cyanide ion) as the educt or an enantiomerically pure educt for the transformation. An alternative to the chemical preparation of chiral nitriles is represented by the inclusion crystallization in a host framework of an L-phenylalanine derivative and 4-hydroxybenzoic acid (Figure 5). Most crystallized nitriles were obtained in yields of up to 91 % with an *ee*-value of up to 92 %. The 2-(*o*- or *m*-methylphenyl)-propionitrile derivatives did not crystallize or were obtained as racemic compounds.^[100]

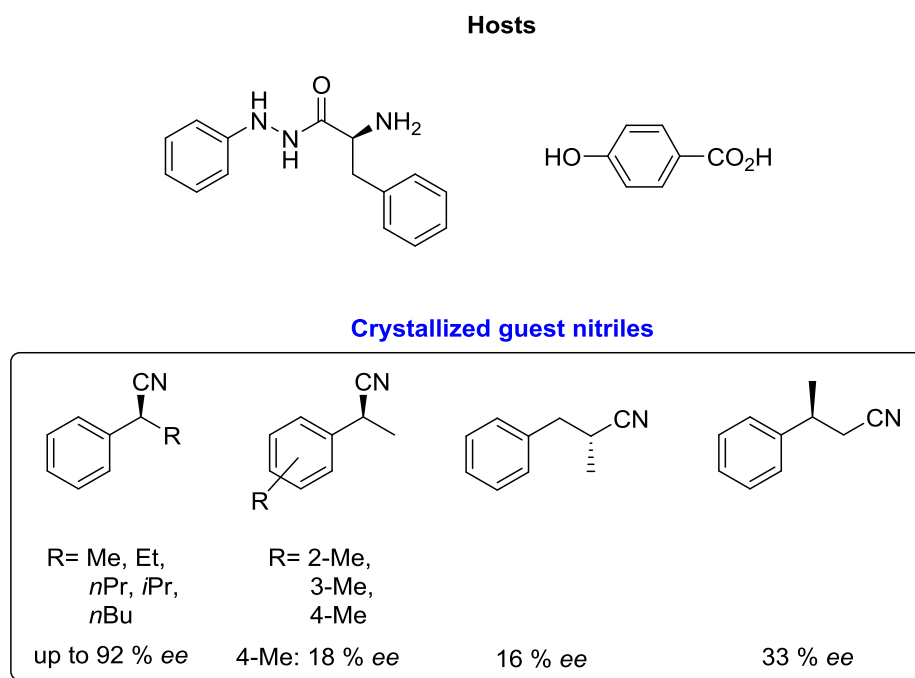


Figure 5. Crystallized chiral guest nitriles in a host framework consistent of an L-phenylalanine derivative and 4-hydroxybenzoic acid.^[100]

2.2 Oxidative transformations with amino acid oxidases and amine oxidases

2.2.1 Flavoenzymes: An overview

This chapter has already been published partly in alternative form as part of a book chapter by the author of this thesis and her co-authors focusing mostly on amine oxidases (AOs) and AAOs.^[101] Oxidases are flavoenzymes and belong to the family of oxidoreductases (EC 1). This class of enzymes is dependent on flavine cofactors (Figure 6), usually flavin mononucleotide (FMN, in green) or flavin adenine dinucleotide (FAD, in light red).^[102] Flavoenzymes have several catalytic functions in organisms such as in (non-)redox processes, DNA repair, cell folding, apoptosis, light emission, energy production, etc.^[103]

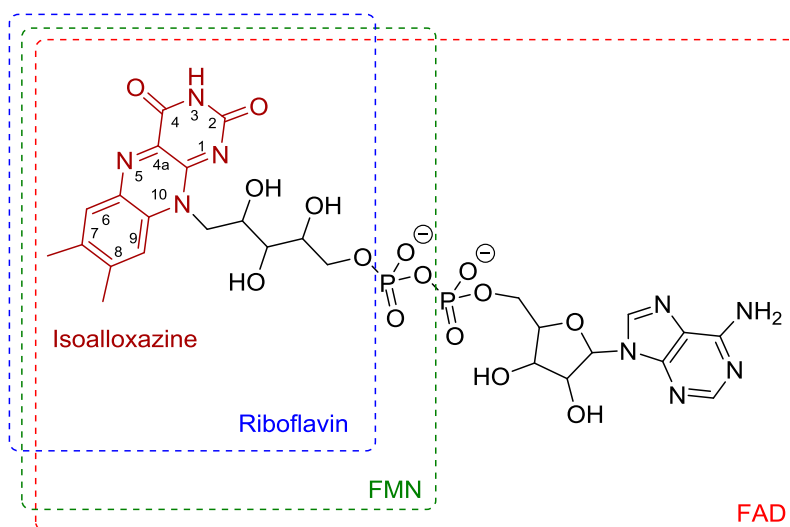


Figure 6. Structures of isoalloxazine (red), riboflavin (blue), FMN (green) and FAD (light red).^[102]

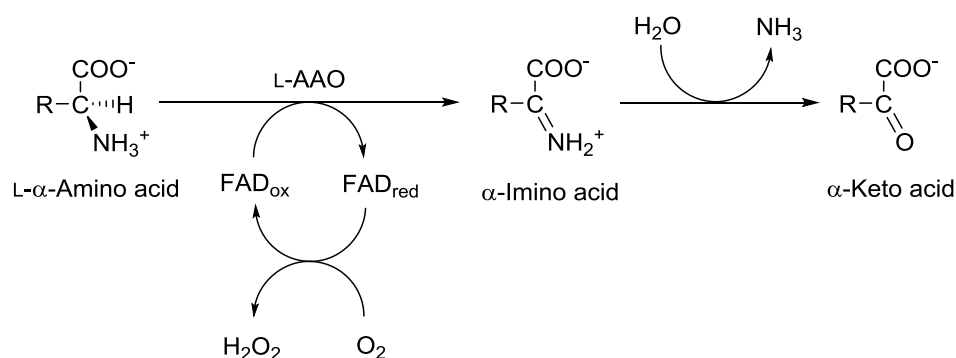
One category of this enzyme class is able to oxidize substrates containing an amine moiety (EC 1.4.3). Enzymes of interest are especially mono amine oxidases (MAOs, EC 1.4.3.4) and AAOs both catalyzing the oxidative deamination of amines and α -amino acids, respectively. The AAOs exhibit selectivity for the L- or D-amino acids, separating them into L-amino acid oxidases (L-AAO, EC 1.4.3.2) and D-amino acid oxidases (D-AAO, EC 1.4.3.3). All three mentioned kind of enzymes utilize molecular oxygen as a substrate and release ammonia and hydrogen peroxide. Oxidases are suitable catalysts for the synthesis of chiral organic compounds by oxidation of C-N bonds due to their high stereo- and regioselectivity.^[104]

2.2.2 Amino acid oxidases: A variable biocatalyst

2.2.2.1 General information and catalytic function

As flavoproteins, L-AAOs contain flavin derivatives as cofactors: In this special case the cofactor FAD is covalently linked to a specific FAD-binding site, which is usually located at the N-terminus of the protein.^[105] Due to their FAD-content, these enzymes have a red color. Most enzymes are thermostable up to 60 °C and are stable in a broad pH range. Their optimum pH is around pH 7.0. Storage at 4 °C often leads to an activity loss.^[106]

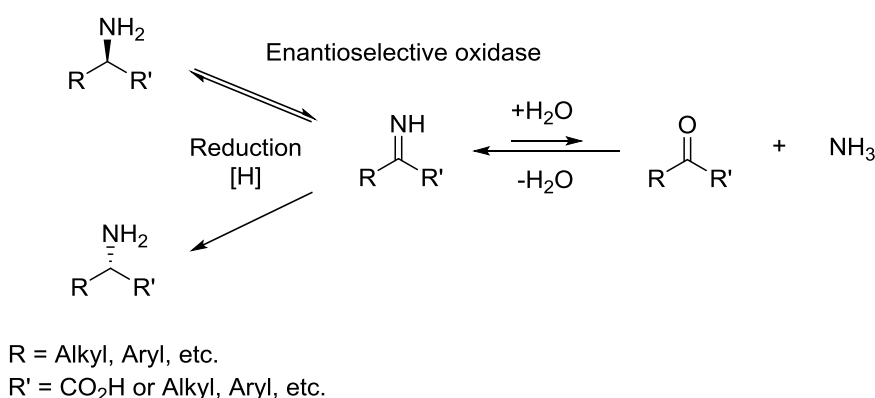
The protein structures of the homodimers of L-AAOs from snake venoms and *Rhodococcus opacus* (*R. opacus*) have already been determined, which was helpful for understanding the catalytic functions of these enzymes.^[107,108] The catalytic cycle of the L-amino acid oxidation is assumed to proceed first *via* a hydrogen abstraction from the amino moiety to the oxidized form of the FAD (FAD_{ox}), thus, reducing it to the reduced form (FAD_{red}).^[109] α -Imino acids are formed in this reaction step as intermediates, which had been proved by *Hafner and Wellner*.^[110] The FAD_{red} then gets oxidized by molecular oxygen, which acts as an electron acceptor. The oxygen therefore abstracts an electron from the FAD_{red} forming a superoxide radical (O₂⁻), which generates a radical species at the C4-position. Oxidation at the N5-position of the isoalloxazine under formation of hydroperoxide then oxidizes the cofactor back to its FAD_{ox} state.^[111] Hydrolysis of the α -imino acid releases ammonia under formation of the corresponding α -keto acid (Scheme 29).^[109] In principle, the same mechanism also applies for D-AAOs.^[112] Previously, a different mechanism involving carbanion species was also discussed in literature. However, more evidences prove the above-mentioned mechanism.^[107]



Scheme 29. Catalytic mechanism of the α -keto acid synthesis by L-AAOs.^[109]

2.2.2.2 Synthetic pathways with amino acid oxidases

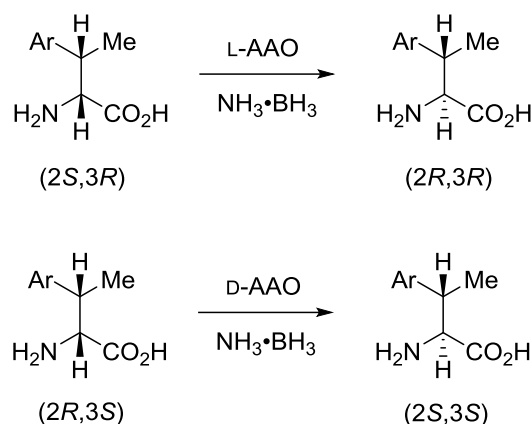
In general, there are two synthetic applications of these enzymes with different targets. As the product of the catalytic cycle is an α -imino acid, AAOs can be used for the synthesis of α -keto acids (see in chapter 2.2.2.3). Another synthetic strategy is the resolution of racemic amino acids or their stereoinversion by coupling the AAO-catalyzed oxidation with an unselective reducing agent. Borazane has been demonstrated to be suitable in combination with both L-AAO^[113] and D-AAO.^[114] The prerequisite for this synthetic application is a high selectivity of the AAO for the oxidation of one enantiomer of the amino acid. While the preferred isomers get permanently oxidized by the AAO, the unselective reducing agent reduces the imine to both enantiomers of the amino acids. This leads to the accumulation of the unaccepted isomer after several cycles of oxidation and reduction. As the imine hydrolysis is also an equilibrium reaction, the accumulation of the unaccepted isomer also shifts this on the imine side (Scheme 30). Depending on the selectivity, a theoretical yield of 100 % can be achieved both for the dynamic kinetic resolution (defined as 100 % of one enantiomer) and the stereoinversion.



Scheme 30. Deracemization of chiral amines or amino acids by oxidases. A cyclic sequence of enantioselective oxidation coupled with a non-selective reduction enriches the non-converted enantiomer.^[113]

2 State of the art

Roff *et al.* gave an example for the synthetic applicability of this method for the stereoinversion of (2*S*, 3*R*)- and (2*R*, 3*S*)- β -methyl-L-arylphenylalanine derivatives with L-AAO from snake venom or D-AAO from *Trigonopsis viride* obtaining the opposite enantiomers (2*R*, 3*R*) and (2*S*, 3*S*). High yields of 68 % to 92 % were achieved with perfect enantio- and diastereoselectivity (Scheme 31). The chiral branched amino acid derivatives were synthesized from L-threonine methylester by halogenation, subsequent Suzuki-cross-coupling with aryl boronic acids and hydrogenation with a chiral ruthenium catalyst.^[115]



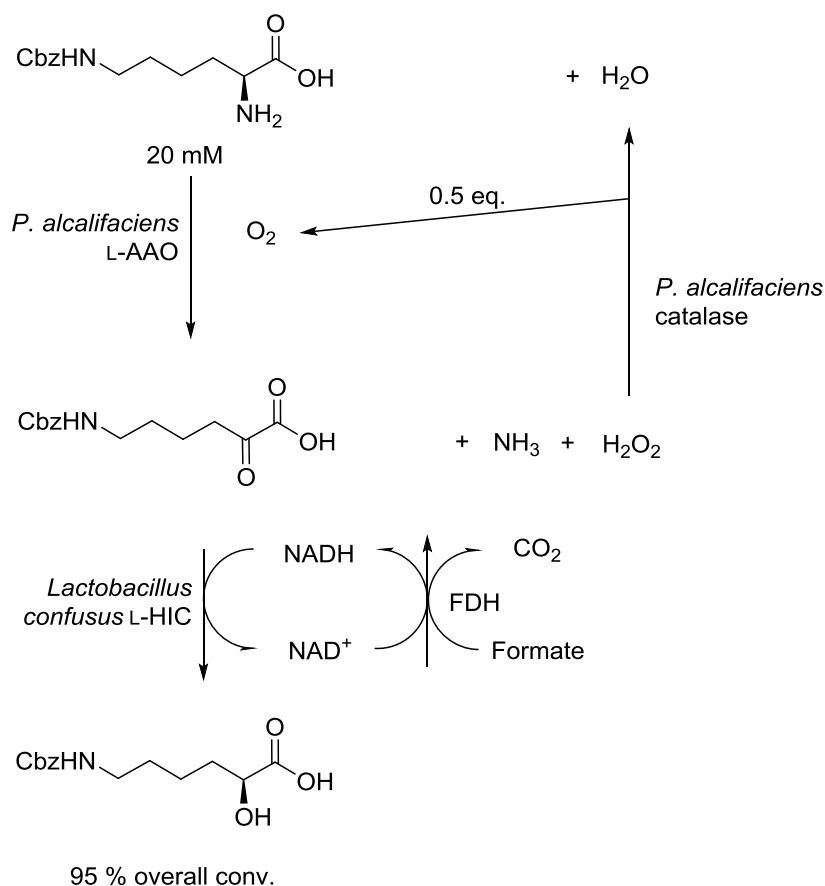
Scheme 31. Synthesis of β -methyl-arylphenylalanine derivatives by L-AAO or D-AAO implying stereoinversion.^[115]

2.2.2.3 L-Amino acid oxidases

L-AAOs are widely distributed in nature, they occur in numerous snake^[105,116] and insect venoms.^[117] But also the enzymes originating from fungi,^[118,119,120] bacteria,^[107,121,122] and algae^[123] are known. While the formation of hydrogen peroxide causes the toxicity in venoms, the enzymes are also involved in the metabolism of L-amino acids in nature.^[109]

The oxidation of Cbz- N_ϵ -L-lysine catalyzed by venom from *Crotalus adamanteus* (*C. adamanteus*, eastern diamondback rattlesnake), which contains the L-AAO, formed the corresponding keto-acid with a yield of 76 % in a five gram reaction scale.^[124] Alternatively, this reaction could also be catalyzed by the L-AAOs from *Trichoderma viride* (*T. viride*) or *Providencia alcalifaciens* (*P. alcalifaciens*). The *P. alcalifaciens* L-AAO has higher activity for the Cbz-protected lysine derivative. The *P. alcalifaciens* cells also contain a catalase enzyme. A sequential reaction cascade applying these cells combined with the NAD-dependent L-HIC from *Lactobacillus confusus* yielded 18.9 mM of Cbz-L-Oxylysine (corresponding to 95 % conversion) starting from Cbz- N_ϵ -L-lysine (Scheme 32).^[125]

2 State of the art



Scheme 32. Formation of Cbz- N_{ϵ} -L-oxyllysine from Cbz- N_{ϵ} -L-lysine in a four enzyme system.^[125]

The production of the native L-AAO in the fungus *Aspergillus fumigatus* can be induced by supply of amino acids such as L-threonine and L-methionine.^[126] The enzyme is capable of the resolution of racemic hydrophobic amino acids such as of alanine, phenylalanine and tyrosine. However, only for racemic alanine a perfect resolution was achieved. For DL-phenylalanine and DL-tyrosine, the products were obtained with 80 % and 84 % enantiopurity, respectively.^[127]

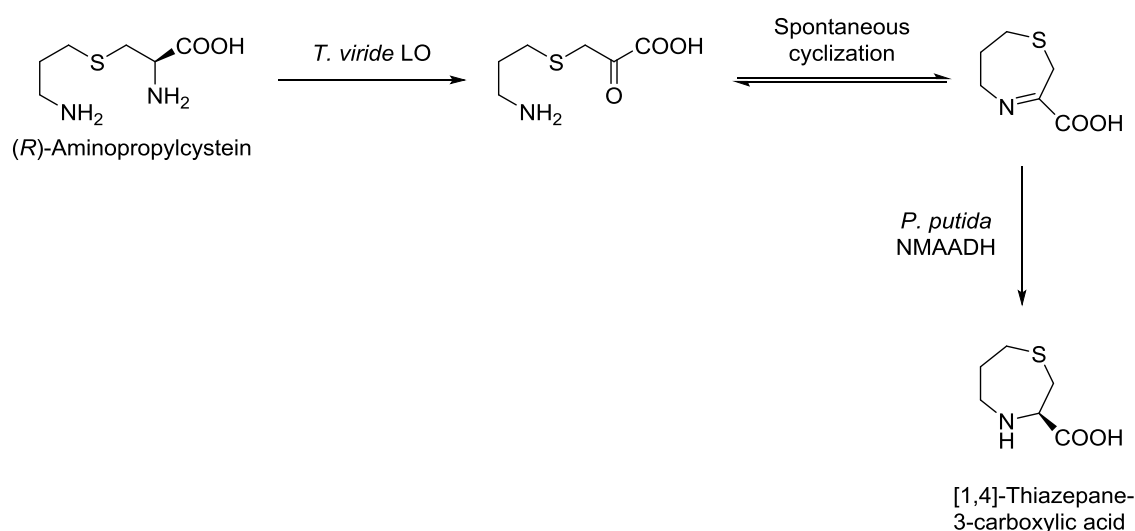
The L-AAO from *R. opacus* has a more broad substrate spectrum and converts most proteinogenic α -amino acids.^[122] Expression of this enzyme in the yeast *Streptomyces lividans* was successful, whereby soluble, active enzyme was obtained. However, expression in *E. coli* only led to the formation of protein aggregates, which were inactive in their solubilized form even after reactivation treatment. Higher concentrations of L-alanine inhibit this enzyme.^[128] When it comes to the oxidation of L-3,4-dihydroxyphenylalanine, the L-AAO from *R. opacus* surpasses the performance of the L-AAO from *C. adamanteus*. The product of this reaction, 3,4-dihydroxyphenylpyruvic acid, is used as a pharmaceutical and is itself an intermediate in the synthesis of rosmarinic acid.^[129]

2 State of the art

The production of the D-amino acids from racemic mixtures of homoserine, glutamine, citrulline and N_ϵ -acetyllysine at 100 mM substrate concentration have been reported with the purified L-AAO from *Rhodococcus* sp. AIU Z-35-1 (40 mU of enzyme, 1.0 mL reaction scale). A racemic mixture of arginine was also resolved to D-arginine with 60 mU enzyme under the same conditions.^[130] This enzyme shows excellent properties as no substrate inhibition and a broad substrate scope. It shows the highest activity for Cbz- N_ϵ -L-lysine, however, the deamination of the ϵ -amino group in Cbz- N_α -L-lysine is also catalyzed.^[131]

The L-aspartate oxidase from the hyperthermophilic archaeon *Sulfolobus tokodaii* expressed as active holoprotein is known for the deamination of L-aspartate to its corresponding α -keto acid. The enzyme has a high pH tolerance and thermal stability (stable < 80 °C). A racemic solution of 50 mM DL-aspartate were quantitatively converted with a perfect enantiopurity of the D-enantiomer using low amounts of enzyme (300 U·L⁻¹).^[132]

L-Lysine oxidase (LO, EC 1.4.3.14) catalyzes the oxidation of the α,ω -amino group of L-lysine.^[133] LO from *T. viride* and N -methyl-L-AADH (NMAADH) from *Pseudomonas putida* (*P. putida*) ATCC12633 expressed in *E. coli* convert aminopropylcystein into [1,4]-thiazepane-3-carboxylic acid a one-pot reaction system (Scheme 33).^[134] Thereby, the α,ω -diamino acid (aminopropylcystein) is oxidized to the α -keto acid by LO from *T. viride*. Next, the α -keto acid spontaneously converts into the imino acid by cyclization. Finally, the imine moiety is reduced to the corresponding L-cyclic amino acid by the NADPH dependant NMAADH from *P. putida* ATCC12633.^[134]



Scheme 33. The reaction from aminopropylcystein to [1,4]-thiazepane-3-carboxylic acid by the combination of LO from *T. viride* and NMAADH from *P. putida* ATCC12633.^[134]

2 State of the art

Besides the narrow substrate scopes of several microbial enzymes, a main bottleneck for the application of L-AAOs remains the expression in heterologous hosts, which often leads to formation of insoluble protein aggregates.^[135] The expression of L-AAOs often leads to the production of inactive enzyme, which has to be activated. An example for such a reactivation is the SDS-treatment of an L-AAO from *Hebeloma cylindrosporium* (*H. cylindrosporium*).^[120] Furthermore, the lack of a suitable *in vivo* screening method due to cell viability caused by the cytotoxicity of L-AAOs makes methods of directed evolution hard to apply.^[135]

2.2.2.4 D-Amino acid oxidases

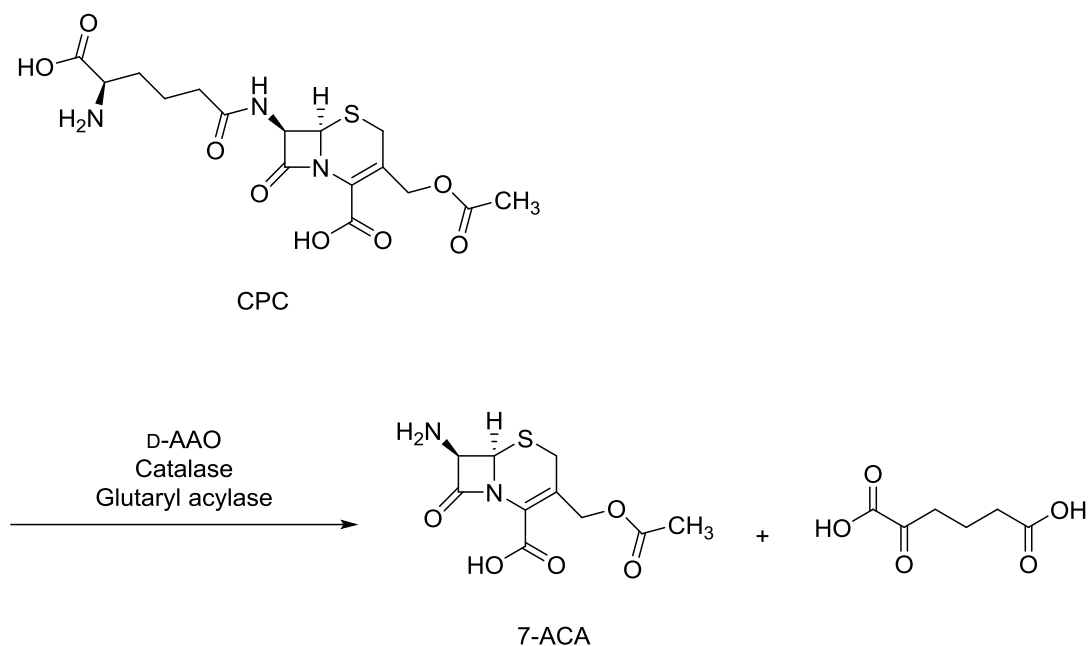
In contrast to the limited applicability of L-AAOs, which results mostly from their poor expression in heterologous hosts and their narrow substrate scopes, D-AAOs are more prominent in synthesis.^[135] Higher expression levels and broader substrate scopes simplify the application of this enzyme in organic synthesis. As the α -keto acid synthesis has already been exemplified with the L-AAOs, the part about D-AAOs will focus on industrially relevant processes involving this enzyme class.^[136]

D-Amino acid oxidases (D-AAOs) are flavoproteins and catalyze the stereospecific oxidative deamination of D-amino acids to the corresponding α -keto acids, ammonium, and hydrogen peroxide. The enzymes widely exist in various organisms such as bacteria,^[137] fungi,^[138] plants^[139] and humans,^[140] and so on.^[141] D-AAOs are well known because they are considered as a model flavo-oxidase catalyst in basic research. The principles of α -keto acid synthesis and deracemization of amino acids are similar to those of L-AAOs. The following part will focus on the application of D-AAOs in biotechnological processes,^[142] especially the production of 7-aminocephalosporanic acid (7-ACA) and (S)-2-amino-3-(6-*o*-tolylpyridin-3-yl)propanoic acid (ATPPA), an important intermediate in the synthesis of glucagon-like peptide mimetics or GLP-1 receptor modulators.^[142]

7-ACA is an important intermediate in many industrial processes for quasi-synthetic cephalosporin antibiotics synthesis. Formerly, the chemical synthesis of 7-ACA was the mainly applied synthesis route in industry. The main drawback of this method are the harsh reaction conditions, especially the use of hydrogen peroxide. As a greener alternative, enzymatic syntheses have been studied.^[143] However, most of these methods are still using hydrogen peroxide. *López-Gallego et al.* developed a one-pot reaction system for the production of 7-ACA from cephalosporin C (CPC) with D-AAO, catalase, and glutaryl acylase, which are applied as immobilized enzymes (Scheme 34).^[144] By co-immobilizing D-AAO and catalase, this reaction proceeds without hydrogen peroxide addition. As α -ketoacid-pyl-7-ACA is a strong inhibitor for the D-AAO, a subsequent reaction step by means of glutaryl acylase-catalyzed

2 State of the art

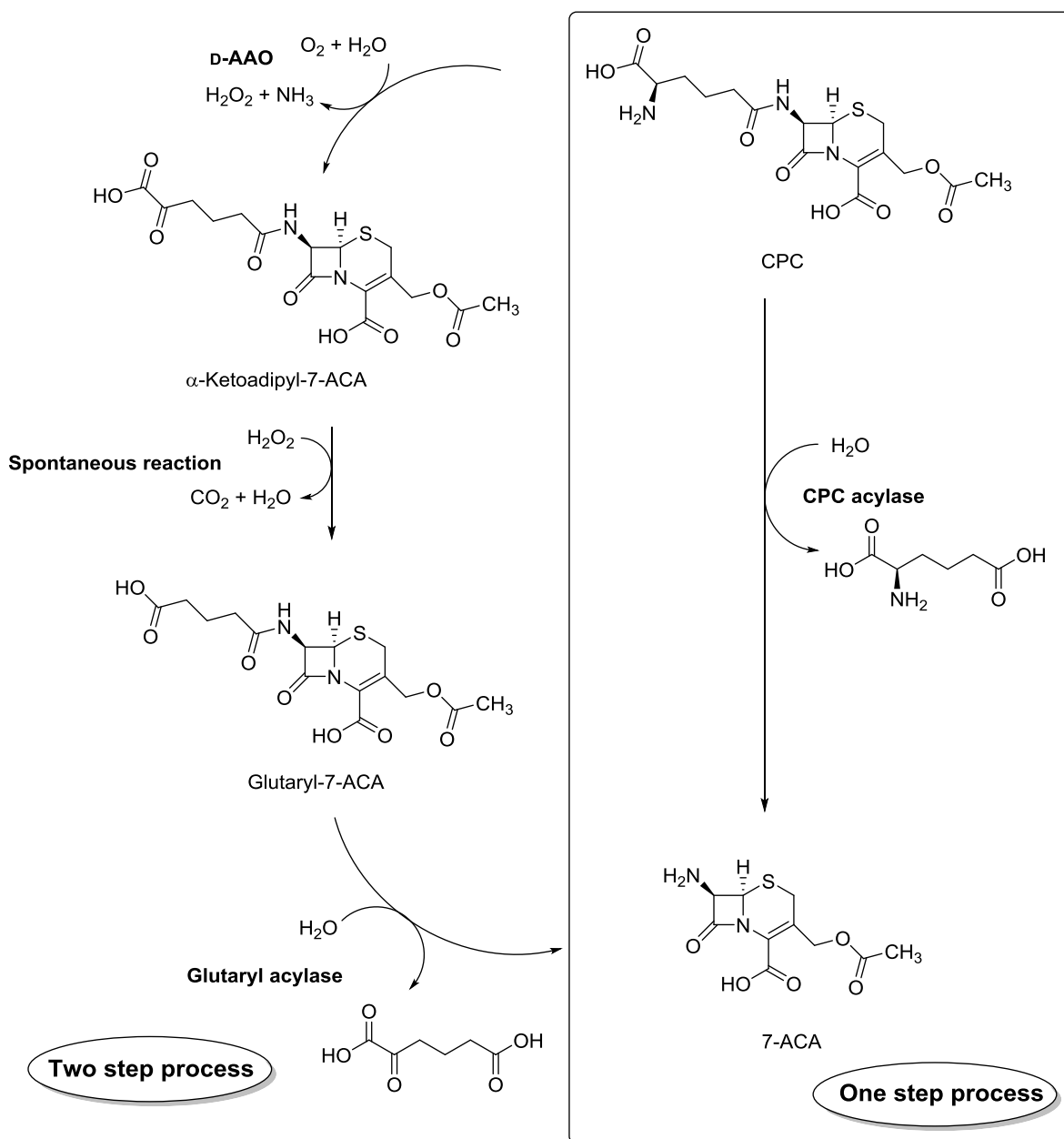
cleavage of the amide group binding the side chain is necessary. Thus, α -ketoadipyl-7-ACA is removed from the first reaction equilibrium by hydrolysis and the one-pot reaction system proceeds smoothly.^[144]



Scheme 34. The conversion of CPC into 7-ACA with an enzymatic system comprising of D-AAO, catalase, and glutaryl acylase.^[144]

Furthermore, *López-Gallego et al.* have studied an improvement of the CPC hydrolysis using a mutant of glutaryl acylase in the absence of hydrogen peroxide (Scheme 35).^[145] This study was focussed on the intermediate α -ketoadipyl-7-ACA, which gets oxidatively decarboxylated to glutaryl-7-ACA. In this step hydrogen peroxide acts as the oxidant, thus, avoiding its accumulation. A mutagenesis study revealed that a variant of glutaryl acylase from *Pseudomonas* SY-77 (Y178F_F375H) was most suitable. When utilizing the wild-type enzyme 40 % yield of 7-ACA were obtained. 80 % yield of 7-ACA were obtained using the mutant, which corresponds to a 3-fold mass excess compared to the initial process involving D-AAO and catalase.^[145] Alternatively, the hydrolysis of CPC to 7-ACA can be catalyzed with CPC acylase, which is also attractive for industrial 7-ACA production.^[146]

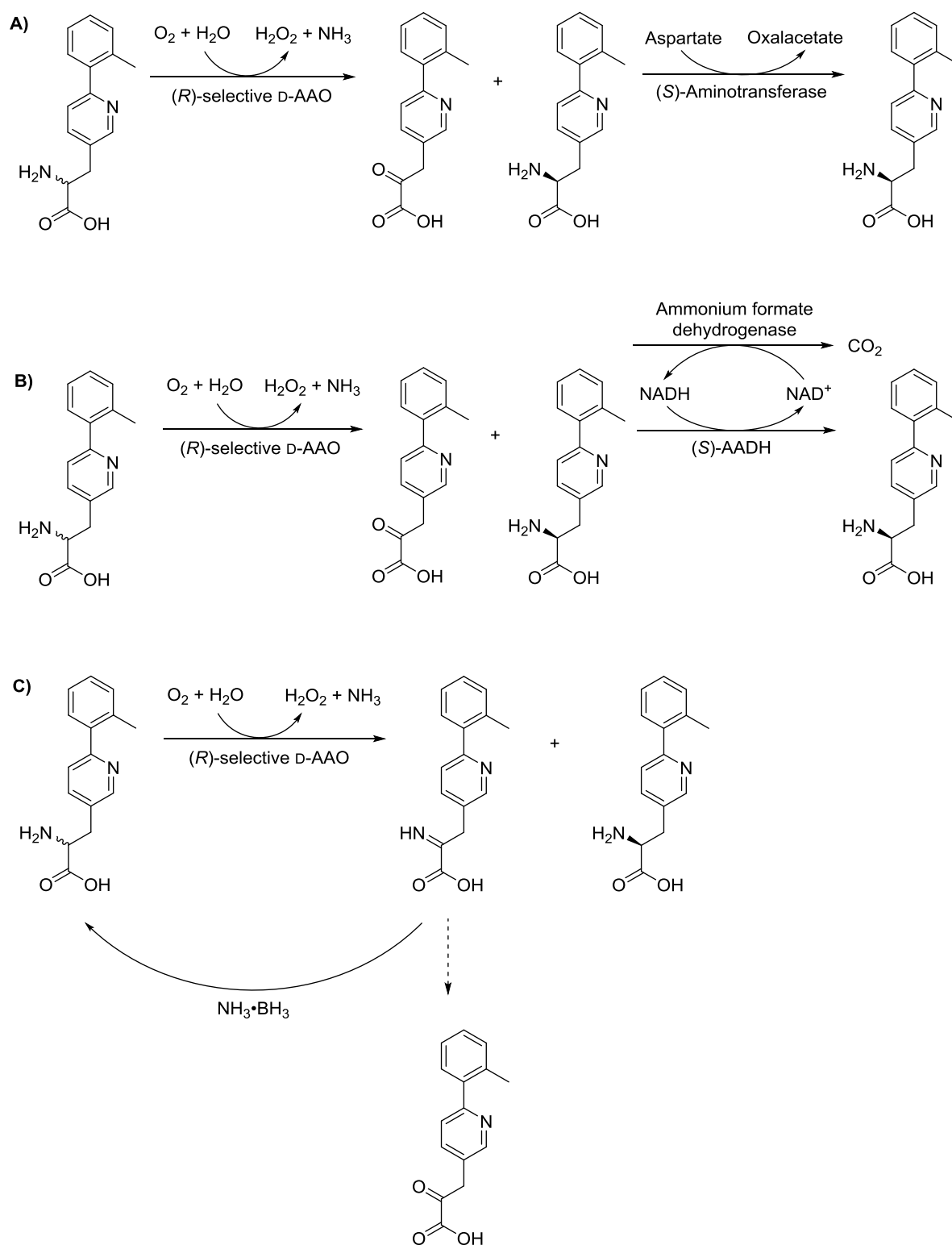
2 State of the art



Scheme 35. The two step (left) or one step (right) conversion of CPC into 7-ACA.^[146]

(S)-ATPPA is an important intermediate in the production of an antidiabetic drug candidate. Three enzymatic methods for the deracemization of racemic ATPPA forming the (S)-enantiomer were studied (Scheme 36). In the first method, the contained (R)-ATPPA was selectively oxidized to the corresponding α -keto acid by the (R)-selective D-AAO from *Trigonopsis variabilis* (*T. variabilis*) expressed in *E. coli*, which was subsequently aminated to the (S)-amino acid by the (S)-selective aminotransferase from *Burkholderia* sp. expressed in *E. coli* (A). (S)-ATPPA was produced in 73 % isolated yield at >99 % ee by this method.^[147]

2 State of the art



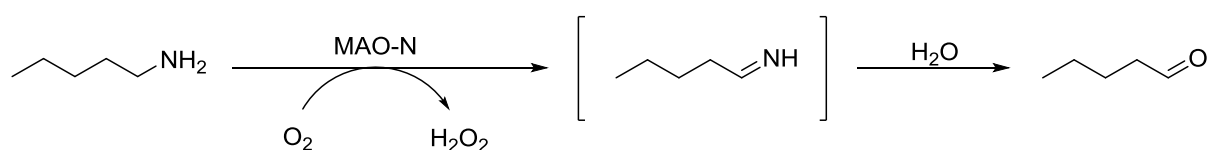
Scheme 36. The conversion of racemic ATPPA into (S)-ATPPA A) using (R)-selective D-AAO and (S)-aminotransferase, B) using (R)-selective D-AAO and (S)-selective AADH, and C) by dynamic kinetic resolution using (R)-selective D-AAO combined with unselective chemical imine reduction.^[147]

2 State of the art

Regarding the second method for producing of (S)-ATTPA, the kinetic resolution and subsequent reduction was realized by combination of the (R)-ATTPA oxidation catalyzed by D-AAO from *T. variabilis* with a reduction catalyzed by the (S)-AADH from *Sporosarcina ureae* using NADH as a cofactor (B). In this method, (S)-amino acid was produced with 54 % isolated yield (68 % conversion) and >99 % ee. In addition, the chemoenzymatic dynamic kinetic resolution of the racemic substrate was studied as a third method (C). In this system, (S)-ATPPA was obtained using Celite-immobilized (R)-selective D-AAO from *T. variabilis* combined with the unselective chemical imine reduction with borazane. In this method, the (S)-amino acid was produced with 68 % isolated yield (81 % conversion) and >99 % ee.^[147]

2.2.3 Amine oxidases: Another enzyme for the resolution of amines

AOs are widely present in nature, for example, in bacteria, fungi, mammals including human, and so on. They can be separated into two groups. While type I is dependent on copper, type II is dependent on flavin derivatives as cofactors. Both groups of enzymes catalyze the oxidation of amines to imines, while only type II AOs release the “free” imine from the active site, thus, being applicable in synthesis.^[148] In most cases however, type II AOs (from here on mentioned by AO) catalyze the oxidative deamination of amino groups by converting amines into the corresponding imines, which are usually hydrolyzed into the corresponding carbonyl compounds. Mono amine oxidases (MAOs) are the most prominent enzymes amongst this class. Simple aliphatic amines such as *n*-butylamine, amylamine, and to a lower extent also benzylamine can be oxidized to imines using wild-type of MAOs with molecular oxygen as an oxidant (Scheme 37).^[133] In 1995, the flavin-dependent monoamine oxidase N (MAO-N, EC 1.4.3.4) was isolated from the fungus *Aspergillus niger*.^[149] Later, heterologous expression of this enzyme in *E. coli* and its purification to homogeneity was reported.^[150]



Scheme 37. The conversion of an amine (here *n*-pentylamine) to the corresponding aldehyde by oxidation with MAO-N and subsequent hydrolysis of the formed imine.^[133]

MAO-N has an outstanding role amongst MAOs and has been utilized and engineered for several applications in amine resolution tailoring its reactivity and selectivity. There are several original works applying the previously described method for deracemization of chiral amino acids (Scheme 30) with MAO-N and its engineered variants. This enzyme has been proved to be a powerful tool in the synthesis of enantiomerically pure chiral amines. All primary,

2 State of the art

secondary and tertiary amines are substrates of this enzyme. The first example of this synthetic strategy was the synthesis of α -L-methylbenzylamine.^[151]

Furthermore, AOs find application in several resolutions of primary and secondary amines and nature products containing amine functions as tetrahydro- β -carbolines (THBCs) and 1,2,3,4-tetrahydroquinoline (THQ) and its derivatives. THBCs are important and extensive bioactive alkaloids in nature, for example, harmicine as an antileishmanil compound and reserpine, ajmalicine, and the stimulant yohimbine as antihypertensive drugs (Figure 7).^[152] THQ is an optically active substance which is important for the chemical industry, e.g. in the synthesis of pharmaceuticals, agrochemicals, and so on.^[153,154]

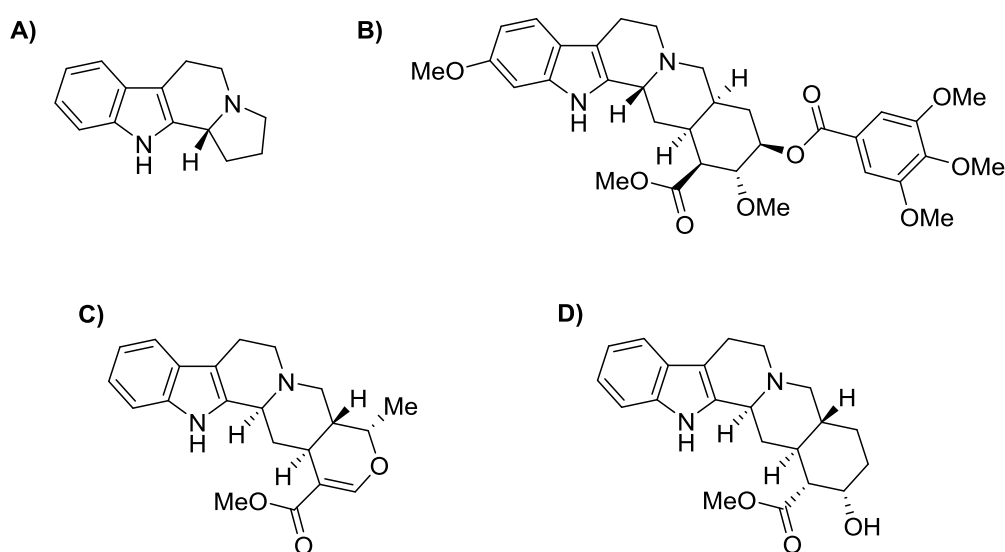
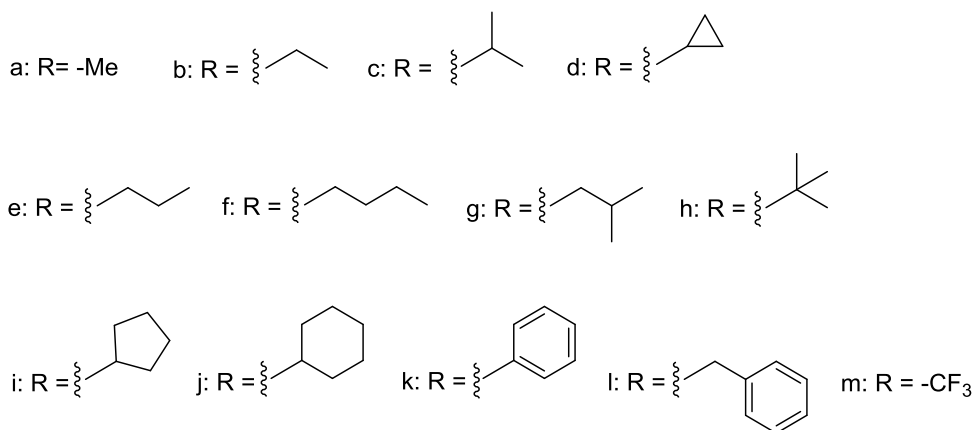
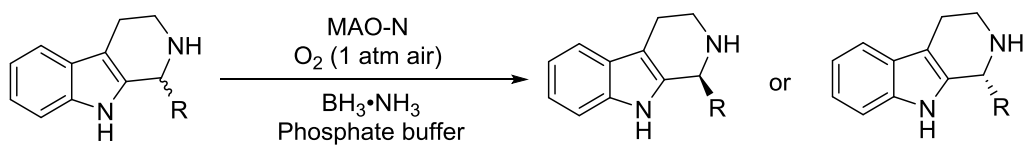


Figure 7. Examples for alkaloids with the β -carboline backbone. A) Harmicine, B) reserpine, C) ajmalicine, d) stimulant yohimbine.^[152]

Chemo-enzymatic deracemization of various racemic alkaloids with the β -carboline backbone was investigated by combination of MAO-N and the non-selective reductant borazane. Thus, with this reaction system an isolated yield of up to 93 % and *ee*-value of up to 99 % could be reached (Table 4).^[152] MAO-N variants can exhibit different enantioselectivity against various racemic alkaloids with the β -carboline backbone. Moreover, docking simulations demonstrated that MAO-N showed (*R*)-selectivity against various racemic alkaloids. The screening of substrates in combination with docking simulations allow predictions about the impact of mutations of MAO-N on the selectivity.^[152]

2 State of the art

Table 4. Enantioselectivity of MAO-N variants D9 and D11 with various racemic alkaloids containing the β -carboline backbone.^[152]



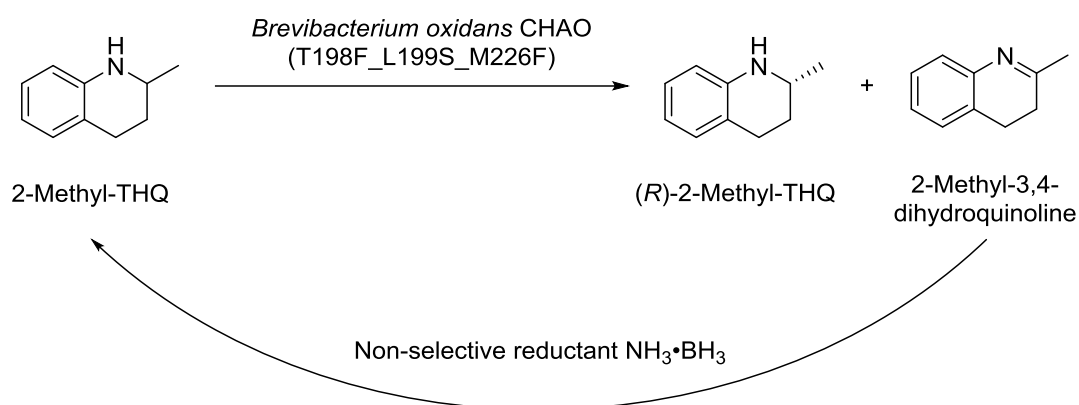
Entry	Time [h]	ee [%]	
		MAO-N D9	MAO-N D11
a	24	>99 (<i>R</i>)	a
b	84	36 (<i>R</i>)	b
c	72	40 (<i>S</i>)	c
d	48	86 (N.D.)	d
e	48	99 (<i>S</i>)	e
f	48	96 (<i>S</i>)	f
g	48	58 (<i>S</i>)	g
h	48	62 (<i>S</i>)	h
i	48	85 (<i>S</i>)	i
j	48	80 (<i>S</i>)	j
k	72	30 (<i>S</i>)	k
l	48	-	l
m	48	-	-

N.D. not determined

2 State of the art

The optically active substance THQ is important for the industry, e.g. in the synthesis of pharmaceuticals, agrochemicals, and so on.^[153,154] The biocatalytic access towards this compounds with MAO-N is well established. *Wang et al.* constructed various mutants of 11 amino acids placed within 5 Å distance from the cyclohexanone substrate and screened those mutants with various amines as substrates.^[155]

Another AO finding application is a mutant of the cyclohexylamine oxidase (CHAO) (T198F_L199S_M226F) from *Brevibacterium oxidans* IH-35A. Expressed in *E. coli*, it was described as the best catalyst for the conversion of racemic 2-methyl-THQ into (*R*)-2-methyl-THQ reaching 76 % isolated yield at 98 % ee (Scheme 38).^[155] This was the first report of the oxidation of a THQ derivate with a CHAO as a catalyst.



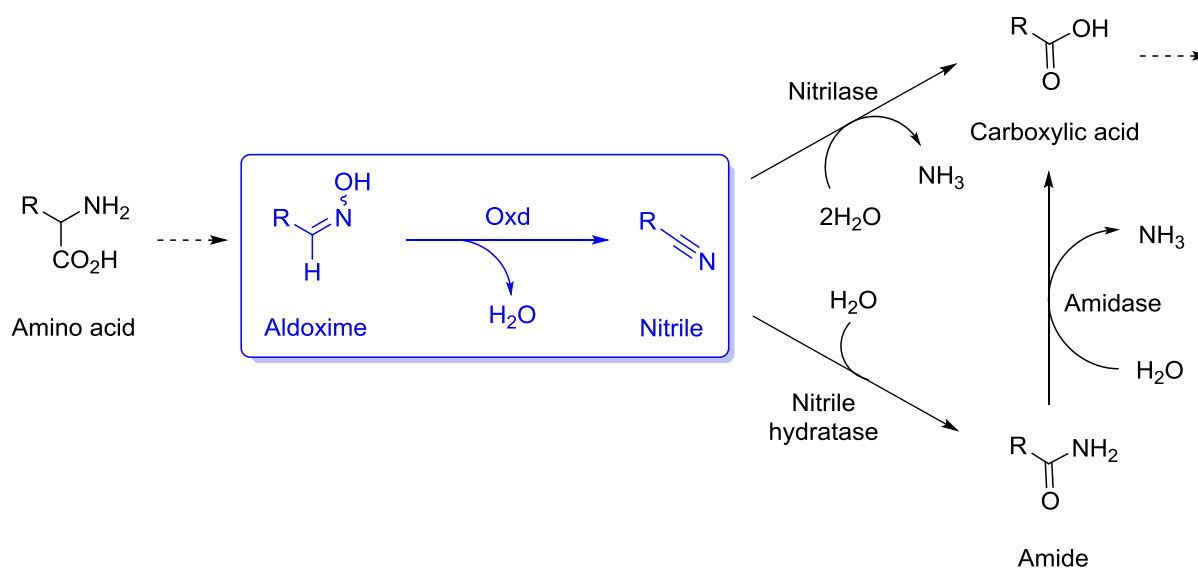
Scheme 38. The dynamic kinetic resolution of racemic 2-methyl-THQ forming (*R*)-2-methyl-THQ using a CHAO variant (T198F_L199S_M226F) from *Brevibacterium oxidans* IH-35A expressed in *E. coli*.^[155]

2.3 Aldoxime dehydratases: Special nitrile producing lyases

Parts of this chapter have also been published in different form as a mini-review by the author of this thesis (as a co-author in a joint work).^[156]

2.3.1 Isolation and expression of aldoxime degrading enzymes

Aldoximes were supposed to be intermediates in the biosynthesis of nitriles, which are intermediates in the biosynthesis of amides and carboxylic acids. The biosynthesis route of carboxylic acids can proceed *via* two different pathways from the nitrile, a single step hydrolysis catalyzed by nitrilase or sequentially catalyzed by nitrile hydratase forming amides and amidase forming nitriles under release of ammonia (Scheme 39). Earlier research on the biosynthesis of carboxylic acids in high plants suggested the formation and degradation of aldoximes in the biosynthesis pathway. As no enzyme was successfully purified and characterized, no clear evidence for an aldoxime dehydrating enzyme has been found until the end of the last millennium.^[157,158]



Scheme 39. Oxds are special heme containing lyases involved in the “aldoxime-nitrile-pathway” of microbes. These enzymes catalyze the dehydration of aldoximes to nitriles, which are metabolized by nitrile hydratases and amidases or by nitrilases.^[159–161]

A screening from soil by the acclimation culture technique led to the isolation and identification of the aldoxime degrading bacterium *Bacillus* sp. OxB-1 and its aldoxime dehydrating enzyme (OxB).^[157] This enzyme catalyzes the dehydration of *Z*-phenylacetaldoxime (*Z*-PAOx) to phenylacetoneitrile (PAN). Shortly after, this enzyme was purified from a recombinant *E. coli* to homogeneity, characterized^[162] and high-level overexpressed intracellularly in *E. coli*.^[163] Especially, the amount of oxygen saturation during expression was reported to have a strong impact on the protein activity obtained. Micro-aerobic conditions were proved to yield the

2 State of the art

highest culture activity.^[163] Since the discovery of this enzyme class, only a handful of these enzymes have been identified, isolated and characterized yet.^[164–170] According to a broad screening with intact cells of microorganisms (975 species), wide distribution of aldoxime dehydration activity was observed (188 strains). Most activities were observed with bacteria and fungi, while only some yeasts showed this activity. Furthermore, the aldoxime dehydration activity was observed in combination with nitrile hydration activity for all proved examples. Presence of aldoximes and nitriles in the culture medium induce the production of aldoxime-nitrile degrading enzymes.^[160]

Further recombinant Oxds from the bacteria *Pseudomonas chloraphis* B23 (OxdA),^[165] *Rhodococcus globerulus* A-4 (OxdRG),^[164] *Rhodococcus erythropolis* (OxdRE),^[166] *Rhodococcus* sp. YH3-3 (OxdYH3-3)^[170] and the head blight fungus *Fusarium graminearum* MAFF305135 (OxdFG) are known.^[167] Via an approach combining southern hybridization and PCR-techniques with the sequence of OxdRE as a probe, genes coding aldoxime- and nitrile-degrading enzymes were found proving the connection of these enzymes in the natural pathway. One Oxd with a new primary structure was identified in the gene of *Pseudomonas* sp. K-9 (OxdK).^[161] This enzyme was subsequently expressed in *E. coli* and characterized.^[168] A recently attempted BLAST search in the GeneBank database suggested the distribution of Oxds in the *Bradirhizobium* sp. family. Amongst sequence fragments with identity of 42 to 48 % compared to the gene sequence of OxdK, one protein was overproduced in *E. coli* and characterized as an aldoxime dehydratase (OxdBr1).^[169]

2.3.2 Properties of aldoxime dehydratases

2.3.2.1 Properties and structure

Due to their special properties (Table 5) and catalytic activity, Oxds were allocated in a category for unique enzymes (EC 4.99.1.5 to 4.99.1.7). Oxds have a typical molecular weight of approximately 40 kDa and occur as a monomer (OxdB, OxdBr1, OxdFG) or homodimer (OxdA, OxdK, OxdRE, OxdRG) in their native state. Spectroscopic investigations suggested that these proteins contain a protoheme IX unit (heme b, Figure 8) which is non-covalently bound to the protein. Interestingly, heme b is only partly contained in the wild-type or recombinant enzyme. The heme content varies between 33 % (recombinant OxdB) and 69 % (recombinant OxdA).^[166,168] Depending on the expression system, different contents between 32 and 43 % of heme b were incorporated into OxdRE.^[166] The heme b unit causes a characteristic band in the absorbance spectrum of the enzyme, the so called solet peak. Depending on the oxidation state of the iron of the heme group, the peak is shifted between ~410 nm for the ferrous (+II) and ~430 nm for the ferric form (+III) for most Oxds.^[167] For an

2 State of the art

unknown reason, the solet peak of OxdFG in its ferrous form is located at 420 nm. A different constitution of the active site is might be the cause.^[167] As a consequence of the presence of heme units in Oxds, the enzymes have a strong red color.

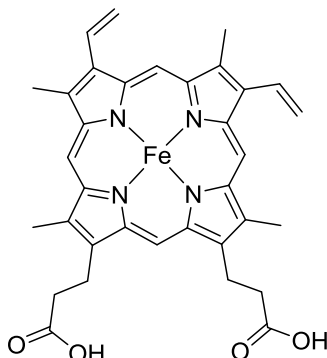


Figure 8. Structure of protoheme IX (heme b).^[171]

Oxds are stable in a pH milieu close to the neutral point (pH 7.0), depending on the enzyme pH ranges between 4.5 (OxdFG) or 6.0 (most others) and 8.0 (OxdA, OxdB, and OxdFG) or 9.5 (OxdRE and OxdRG) are tolerated. OxdBr1 shows a narrower stable pH range. The highest activity can be found at pH 5.5 (OxdA, OxdRG), 7.0 (OxdB, OxdK, OxdBr1) or 8.0 (OxdRE and OxdRG). This enzyme class is not stable against higher temperatures. Most enzymes are inactivated at temperatures $>40\text{ }^{\circ}\text{C}$ or $>45\text{ }^{\circ}\text{C}$. OxdBr1, OxdFG and OxdK are more sensitive towards higher temperatures. The optimum temperature for all Oxds is between 20 and 30 $^{\circ}\text{C}$. Only OxdA and OxdBr1 have a higher temperature optimum of 45 $^{\circ}\text{C}$ and 40 $^{\circ}\text{C}$, respectively, although the enzymes are inactivated fastly at these temperatures.^[162,164–169]

The oxidation state of the cofactor heme b has a strong impact on the catalytic activity of Oxds. Even though substrate binding to the heme iron was observed in both oxidation states of the iron, notable dehydration activity was only observed in the ferrous state.^[172,173] Moreover, most Oxds exhibit higher activity in the presence of flavin cofactors such as FMN and FAD. Reducing agents such as sodium dithionite and 2-mercaptoethanol are reported to have a stabilizing effect on the enzyme and improve the dehydration activity. Under anaerobic conditions, highly increased dehydration activities of Oxds are reported.^[162,166] Possibly, oxygen can not only act as oxidant for the heme iron but also inhibit the enzymes to some extent.

2 State of the art

Table 5. Properties of selected Oxds expressed recombinantly in *E. coli*.^[162,164–169]

Property	OxdA	OxdB	OxdBr1	OxdFG	OxdK	OxdRE	OxdRG
Molecular weight (M_t)							
Native	76,400	42,000	40,700	34,100	85,000	80,000	80,000
Sequence	40,127	40,150	40,713	44,070	44,511	44,794	44,817
Tag	-	-	(N)6His	(N)6His	(N)6His	(N)6His	(N)6His
Number of subunits	2	1	1	1	2	2	2
Soret peak (nm)							
(ferrous form)	408	407	404	420	408	409	409
(ferric form)	428	432	427	431	428	428	428
Heme content [%]	69	33	N.D.	N.D.	35	32	37
Optimum							
pH (in KPB*)	5.5	7.0	7.0	5.5	7.0	8.0	8.0
Temperature [°C]	45	30	40	25	20	30	30
Stability							
pH	6.0-8.0	6.5-8.0	5.0-7.5	4.5-8.0	5.5-6.5	6.0-9.5	6.0-9.5
Temperature [°C]	<40	<45	<30	<20	<30	<40	<40

N.D. not determined, *potassium phosphate buffer

The crucial residues for aldoxime dehydration activity of Oxds were identified *via* alanine substitution studies. The incorporation of the heme cofactor is suggested to be mediated by a non-covalent bond formed between the heme iron and a histidine residue of the protein. Another histidine residue is reported to have a crucial role in the catalytic function of Oxds. Spectroscopic analysis showed that the aldoxime binds to the ferrous heme iron *via* the nitrogen atom of the aldoxime moiety. However, if the heme iron is in the ferric state, the substrate binding proceeds *via* the oxygen atom of the aldoxime moiety. Catalytic activity is only observed when the substrate is *N*-bound to the enzyme.^[172,174] The determination of the crystal structures of OxdRE and OxdA (Figure 9) and further site-directed mutagenesis contributed to a more comprehensive understanding of the catalytic mechanism of aldoxime dehydration.^[175,176]

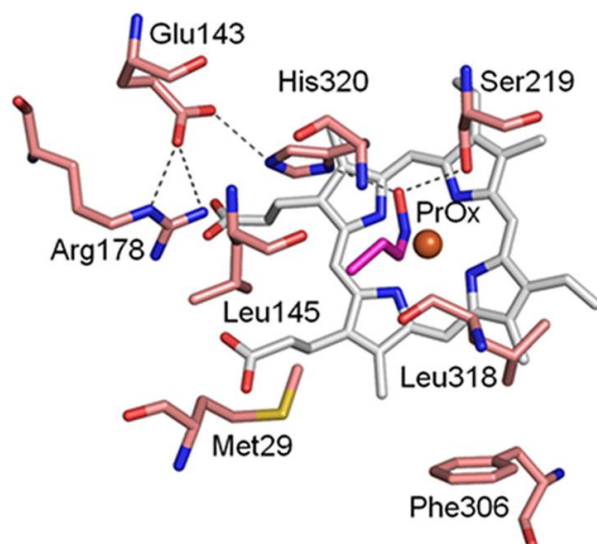
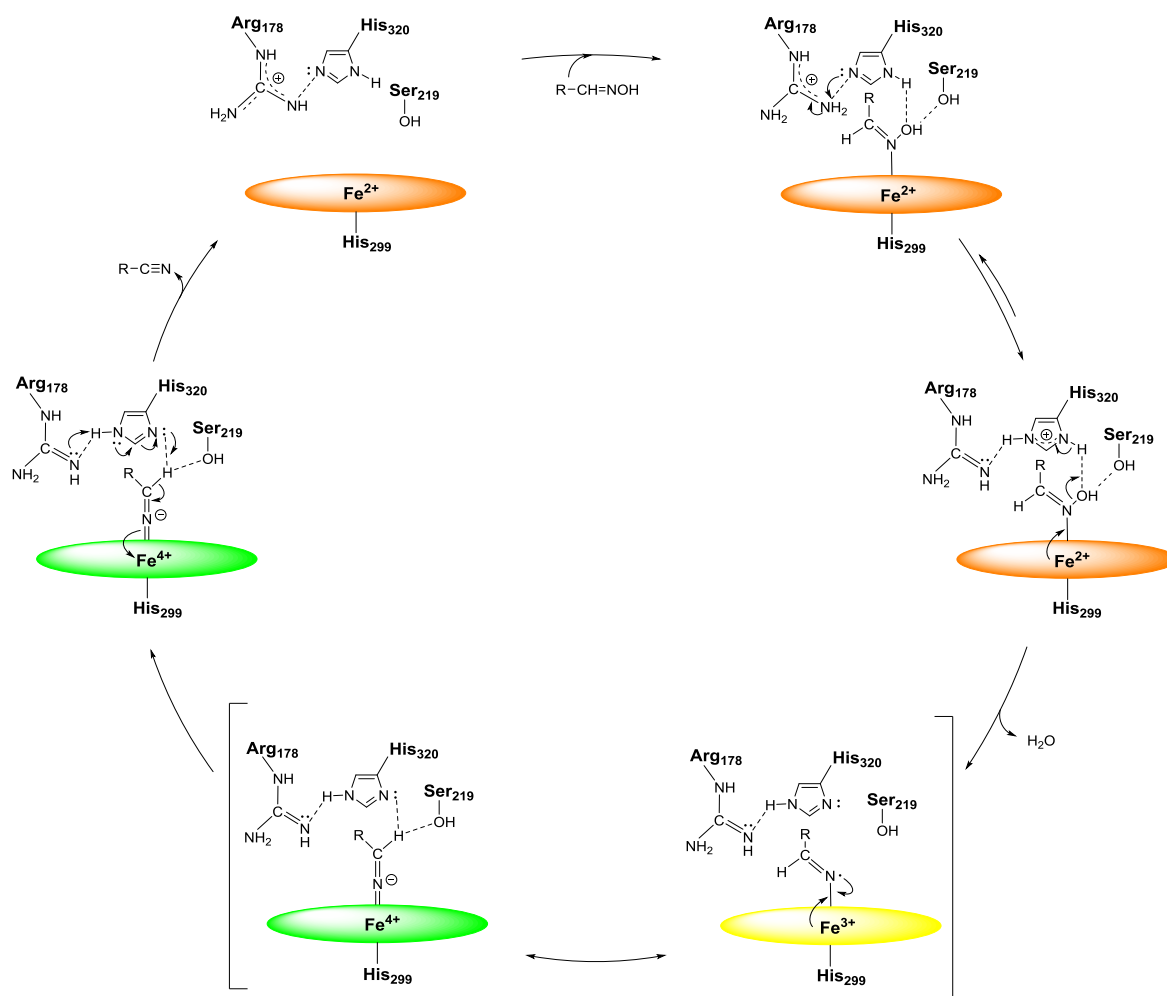


Figure 9. Structure of the active site of the Michaelis-complex of OxdRE with bound *n*-propionaldoxime from the distal heme side. Oxygen, nitrogen and sulfur atoms are colored in red, blue and yellow, respectively. The dashed lines show possible hydrogen bonds. This figure was originally published in the *Journal of Biological Chemistry*. H. Sawai, H. Sugimoto, Y. Kato, Y. Asano, Y. Shiro, S. Aono, *J. Biol. Chem.* **2009**, *284*: 32089-32096, Copyright © 2009, the American Society for Biochemistry and Molecular Biology.^[176]

2.3.2.2 Catalytic mechanism of aldoxime dehydratases

The dehydration of the aldoximes is not a redox reaction but proceeds by acid-base catalysis (Scheme 40). For example, the active site of OxdA contains the amino acid residues Arg₁₇₈ and His₃₂₀ forming a catalytic dyad, Ser₂₁₉ which assists the substrate binding, and a heme b group with another histidine (His₂₉₉) coordinating the central iron atom. The aldoxime enters the active site and binds *N*-coordinated to the iron(II) of the heme unit. The hydroxyl moiety of the aldoxime is linked to the Ser₂₁₉ and His₃₂₀ by formation of hydrogen bonds. First, the His₃₂₀ is protonated *via* proton transfer from the Arg₁₇₈. Then, water is released from the substrate *via* heterogeneous cleavage of the N-O bond of the aldoxime and the N-H bond of the His₃₂₀. Electron transfer from the iron(II) to the nitrogen generates a radical at the nitrogen atom and oxidizes the iron to the oxidation state +3. A further electron transfer from the iron(III) to the nitrogen atom generates a highly oxidized iron(IV) species under formation of a Fe-N double bond. The hydrogen atom at the α -carbon atom of the aldoxime gets abstracted from the His₃₂₀ which re-protonates the catalytic dyad. In this step, the two electrons are transferred back from the nitrogen to the iron under formation of a C-N triple bond releasing the nitrile and reducing the iron to the oxidation state +2.^[175]

2 State of the art

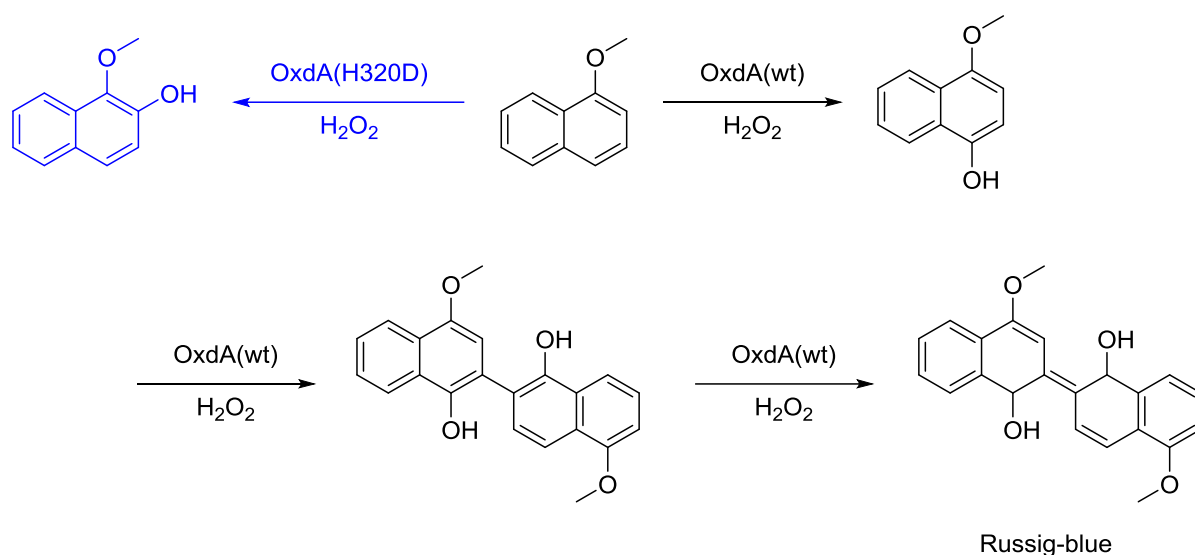


Scheme 40. Proposed mechanism of the dehydration of aldoximes catalyzed by Oxds (active site of OxdA shown). The ovals refer to the heme b unit in the active site of the Oxds with different oxidation state of the iron atom: Brown (+II), yellow: (+III), green: (+IV) (Reprinted with permission from T. Betke, J. Higuchi, P. Rommelmann, K. Oike, T. Nomura, Y. Kato, Y. Asano, H. Gröger, *ChemBioChem* **2018**, *19*, 769-778, Copyright © 2018, John Wiley & Sons, Inc.).^[175]

2.3.2.3 Other reactions catalyzed by aldoxime dehydratases

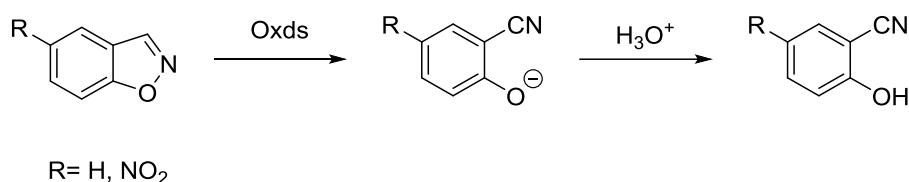
Many heme proteins are known for their redox-catalysis functions. As Oxds contain a heme group and are derived from CYP enzymes, it lays close that also have redox activity. The *Kobayashi* group demonstrated that wild-type OxdA also exhibited catalase, peroxidase and peroxygenase activity. A mutation in the active site of one histidine crucial for aldoxime dehydration (H320D) increases the catalytic efficiency of these redox reactions remarkably. Wild-type OxdA is able to catalyze the synthesis of the dye Russig-blue from 1-methoxynaphthalene *via* three peroxygenation reactions (Scheme 41). Furthermore, a new oxidation product of 1-methoxynaphthalene was observed with the OxdA_H320D mutant, which was not known to be obtained by other enzymatic peroxygenation reactions.^[177]

2 State of the art



Scheme 41. Oxidation of 1-methoxynaphthalene catalyzed by wild-type OxdA and OxdA_H320D mutant forming Russig-blue or 2-hydroxy-1-methoxynaphthalene.^[177]

Besides redox activities, some Oxds were found to catalyze the Kemp-elimination, a base-catalyzed reaction in organic chemistry. High catalytic efficiencies were observed for the Kemp-elimination of benzisoxazole and its 5-nitro-substituted derivative forming 2-cyano-phenol derivatives with wild-type OxdA, OxdB and OxdRE (Scheme 42). An alanine scanning study revealed that the reaction occurred in the active site of OxdB with distal histidine residues involved in the catalytic mechanism.^[178]



Scheme 42. Kemp-elimination of (5-nitro-)benzisoxazole catalyzed by Oxds and subsequent protonation forming 2-cyano-(5-nitro-)phenol.^[178]

2.3.3 Synthesis of nitriles with aldoxime dehydratases

While several publications focused on the characterization and general understanding of the enzyme class Oxds, only a limited number of original works describes their application for organic synthesis of nitriles. All of the recent synthetic transformations were performed with OxdB^[179] or OxdYH3-3 in form of whole-cell catalysts in their original hosts or recombinant in *E. coli*.^[159,170] These Oxds generally suffer from low stability and liability to oxidation when the purified protein is contained in buffer solution, which reduces the enzymatic activity significantly.^[178] However, improved enzyme stability is observed for the enzyme contained in whole-cells.^[180] For the other Oxds, an application in biocatalytic nitrile synthesis is not reported yet. Nevertheless, kinetic data (K_m -value and the maximal reaction velocity v_{max}) give an idea

2 State of the art

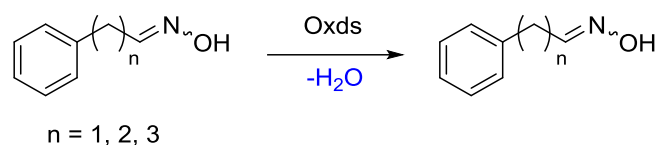
about the scope of these enzymes. The activity assay for determination of Oxd activity is based on the detection of nitrile formation in biotransformations by HPLC or gas chromatography (GC). These kinetic data still have to be taken carefully, as the assay conditions (e.g. aerobic or anaerobic) and the purification protocol have a strong impact on the enzymatic activity.^[162,178] Depending on the enzyme, arylaliphatic, (hetero-)aromatic and aliphatic aldoximes are accepted as substrates. For OxdBr1, no kinetic data and synthetic transformations are reported yet.^[169]

2.3.3.1 Arylaliphatic aldoximes

Arylaliphatic aldoximes are typical substrates of Oxds (Table 6). *Z*-PAOx serves as model substrate for most Oxds, however, OxdYH3-3 does not accept this substrate or any other tested arylaliphatic aldoxime (Entries 6 and 13).^[181] OxdB has a K_m -value of 0.872 mM at a maximal velocity of 19.5 U·mg⁻¹ for *Z*-PAOx (Entry 1).^[162] The highest v_{max} -value found for this substrate was 28.2 U·mg⁻¹ with OxdFG (Entry 2).^[167] For the other enzymes, a v_{max} -value between 0.14 and 5.41 U·mg⁻¹ was observed (Entries 3 to 5). The *Z*-aldoxime with a chain length enlarged by one carbon atom, 3-phenylpropionaldoxime, was also smoothly converted with the tested Oxds (Entries 7 to 12).^[162,164,166–168] The highest v_{max} -value for this substrate of 20.4 U·mg⁻¹ was found with OxdFG (Entry 9).^[167] Besides, OxdB and OxdK exhibit notable v_{max} -values of 14.3 U·mg⁻¹ and 12.1 U·mg⁻¹ for this substrate, respectively (Entries 7 and 10).^[162,168] An even larger substrate (*E/Z*-mixture) is still accepted by OxdB, OxdFG and OxdK (Entries 14 to 16) while it is not converted by OxdRG (Entry 17). The v_{max} -value for this substrate is notably lower for OxdB and OxdK, while still 14.1 U·mg⁻¹ are observed with OxdFG. The K_m -values for these arylaliphatic aldoximes are between 0.872 and 5.88 mM depending on the substrate-enzyme combination. For example, a large deviation of the K_m -value (6-fold) for *Z*-PAOx and 4-phenylbutanal oxime is observed with OxdB.^[162,164,167,168] PAN could be synthesized in a very good isolated yield of 89 % with whole-cells of *E. coli* expressing OxdB. Even the high substrate loading of 0.5 M *Z*-PAOx was completely converted within eight hours (Entry 1). Also 3-phenylpropionitrile was isolated in an excellent yield of 90 % (99.5 % conversion) from a similar system at 0.75 M substrate concentration (*Z*-isomer) after 20 hours reaction time (Entry 7). If a mixture of isomers of 3-phenylpropionaldoxime is given, 0.1 M substrate were completely converted after 17 hours (Entry 8).^[179]

2 State of the art

Table 6. Kinetic data, conversions and isolated yields for biotransformations of arylaliphatic aldoximes with Oxds.

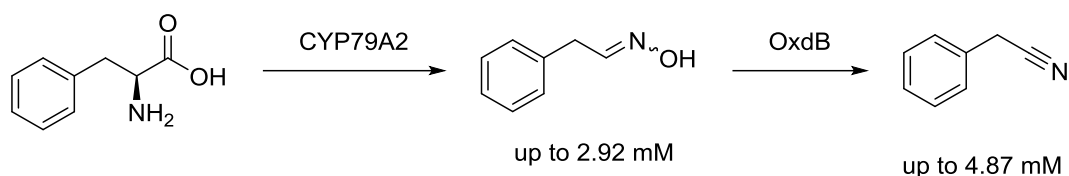


Entry	n	Oxd	E/Z	K _m [mM]	v _{max} [U·mg ⁻¹]	Conv. (isol. Yield) [%]	Reference
1	1	B	Z	0.872	19.5	100 (89)	[162,179]
2	1	FG	Z	3.52	28.2	-	[167]
3	1	K	Z	0.991	2.61	-	[168]
4	1	RE	Z	5.37	5.41	-	[166]
5	1	RG	Z	1.40	0.14	-	[164]
6	1	YH3-3	E/Z	N.A.	N.A.	N.A.	[181]
7	2	B	Z	1.36	14.3	99.5 (90)	[179]
8	2	B	E/Z	-	-	100	[157,179]
9	2	FG	Z	2.76	20.4	-	[167]
10	2	K	Z	0.975	12.1	-	[168]
11	2	RE	Z	5.88	4.59	-	[166]
12	2	RG	Z	2.31	0.392	-	[164]
13	2	YH3-3	E/Z	N.A.	N.A.	N.A.	[181]
14	3	B	E/Z	5.24	3.35	-	[162]
15	3	FG	E/Z	1.79	14.1	-	[167]
16	3	K	E/Z	0.882	2.53	-	[168]
17	3	RG	E/Z	N.D.	N.D.	-	[164]

N.A. not accepted, N.D. not determined.

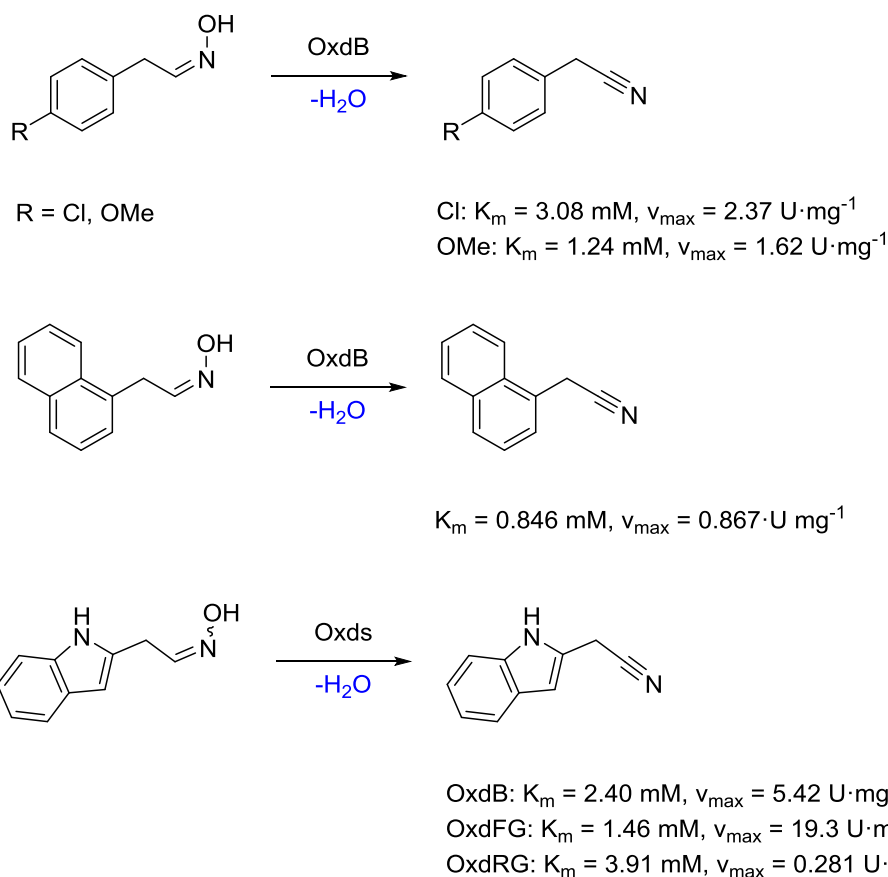
A metabolically engineered system following the natural “aldoxime-nitrile-pathway” was suitable for the production of PAOx and PAN from L-phenylalanine in a fermentative process (Scheme 43). The phenylalanine N-monooxygenase from *Arabidopsis thaliana* (CYP79A2), pGro7 as an expression improving protein and OxdB were co-expressed in *E. coli*. In this enzymatic cascade, L-phenylalanine is first oxidatively decarboxylated by CYP79A2 to PAOx, which is subsequently dehydrated by OxdB. Under optimized culture conditions, product concentrations of up to 2.92 mM PAOx (without expression of OxdB) or 4.87 mM PAN in the culture medium were obtained.^[182]

2 State of the art



Scheme 43. Bioengineered pathway for the synthesis of PAN from L-phenylalanine by oxidation with CYP79A2 and dehydration of the *in situ* produced aldoxime with OxdB.^[182]

OxdB is also active towards *para*-substituted derivatives of Z-PAOx (Scheme 44). For *p*-chloro-PAOx and 4-methoxy-PAOx, K_m -values of 3.08 and 1.24 mM at v_{\max} -values of 2.37 U·mg⁻¹ and 1.62 U·mg⁻¹ were observed. Naphthylacetaldoxime is also accepted by OxdB with a slightly lower maximal velocity and a low K_m -value of 0.846 mM.^[162] Indole-2-aldoxime, a derivative of tryptophane, is accepted by OxdB, OxdFG and OxdRG. The v_{\max} -values observed for this substrates are in the same range compared to those of the other arylaliphatic aldoximes.^[162,164,167]



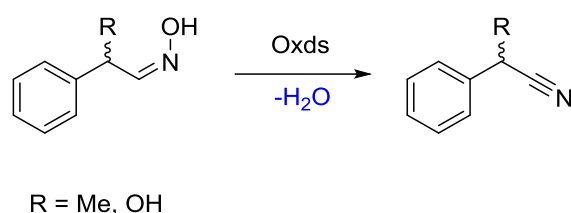
Scheme 44. K_m - and v_{\max} -values for PAOx derivatives with OxdB, OxdFG and OxdRG.^[162,164,167]

Besides these achiral arylaliphatic aldoximes, chiral derivatives of PAOx can be substrates of Oxds (Table 7). The methyl-branched derivative, 2-phenylpropionaldoxime (2-PPOx), has been converted to 2-phenylpropionitrile (2-PPN) with 37.1 % conversion using an *E. coli* whole-cell catalyst expressing OxdB (Entry 1).^[179] Also OxdFG, OxdK, OxdRE and OxdRG

2 State of the art

convert this substrate with v_{\max} -values in similar ranges to those of PAOx and 3-phenylpropionaldoxime (Entries 2 to 5).^[162,164,166–168] Again, OxdYH3-3 does not accept this substrate structure (Entry 6).^[181] OxdB was not active for an aldoxime with a hydroxyl moiety in this position (Entry 7). OxdFG and OxdRG converted this substrate, however, with a lower catalytic efficiency (Entries 8 and 9).^[164,167] The inductive effect of the hydroxyl moiety is probably unfavorable for the stabilization of the substrate in the active site of the enzymes. In principle, chiral nitrile synthesis would be possible starting from these branched derivatives of PAOx (see in detail in chapter 4.1.2).

Table 7. Kinetic data and conversions for chiral derivatives of PAOx with various Oxds.



Entry	R	Oxd	<i>E/Z</i>	K_m [mM]	v_{\max} [U·mg ⁻¹]	Conv. (isol. Yield) [%]	Reference
1	Me	B	<i>E/Z</i>	-	-	37.1	[179]
2	Me	FG	<i>E/Z</i>	3.71	18.1	-	[167]
3	Me	K	<i>E/Z</i>	4.07	6.93	-	[168]
4	Me	RE	<i>E/Z</i>	10	7.93	-	[166]
5	Me	RG	<i>E/Z</i>	11.9	0.81	-	[164]
6	Me	YH3-3	<i>E/Z</i>	N.A.	N.A.	-	[181]
7	OH	B	<i>E/Z</i>	N.A.	N.A.	-	[162]
8	OH	FG	<i>E/Z</i>	1.79	2.32	-	[167]
9	OH	RG	<i>E/Z</i>	3.23	0.572	-	[164]

N.A. not accepted

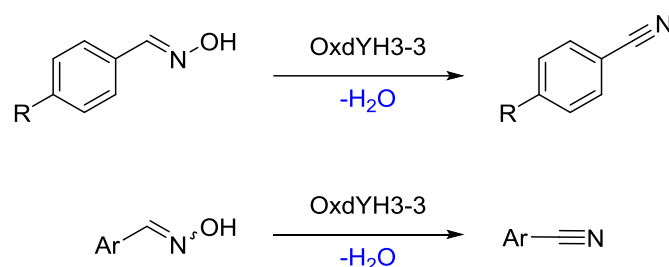
2.3.3.2 Aromatic and heteroaromatic aldoximes

Aromatic *E*-aldoximes with a substituent in *para*-position were not converted with OxdB or OxdRG.^[162,164] Despite not being active at all for arylaliphatic aldoximes, OxdYH3-3 expressed in its original host *Rhodococcus* sp. YH3-3 was proved to catalyze the synthesis of aromatic nitriles (Table 8).^[159,181] The difference of the substrate scope is probably caused by the low similarity of these enzymes. For aromatic benzaldoxime derivatives with a substituent in *para*-position, conversions of up to 24 % were observed for *p*-tolualdoxime as substrate (Entry 1). *p*-Anisolintrile was isolated in 6 % yield (Entry 2). Conversions of 7.2 and 0.06 % were observed for *p*-chlorobenzaldoxime and *p*-nitrobenzaldoxime, respectively (Entries 3 and 4). Also heteroaromatic *E*-aldoximes are substrates for OxdYH3-3, but no or only marginal activity

2 State of the art

towards this substrate was observed with OxdA, OxdB, OxdRE and OxdRG (data now shown).^[162,164–166,181] For these substrates, higher yields were observed with *Rhodococcus* sp. YH3-3 cells. For example, 50 mM of *E*-pyridine-3-aldoxime was dehydrated to 3-cyanopyridine, which was isolated with an excellent yield of 98 % (Entry 5). However, 3-cyanopyridine was only obtained in a poor solution yield of 20 % if the *Z*-isomer is converted (Entry 6). Also other (substituted) pyridines are substrates of OxdYH3-3. *E*-Pyrazinealoxime and *E*-pyridine-2-aldoxime are converted to their corresponding nitriles with 22 % conversion (Entry 10) or obtained with 30 % yield (Entry 7), respectively. *O*-Acetyl-*E*-3-cyanopyridine was obtained in a good isolated yield of 73 % in a reaction from its aldoxime at 100 mM concentration (Entry 11). *E*-Furfuryl-2-aldoxime is also a favorable substrate for this enzyme (Entry 9). Larger derivatives as *E*-indole-3-aldoxime and *E*-pyridine-3-aldoxime-*N*-oxide are only accepted very poorly (Entries 8 and 12).^[181]

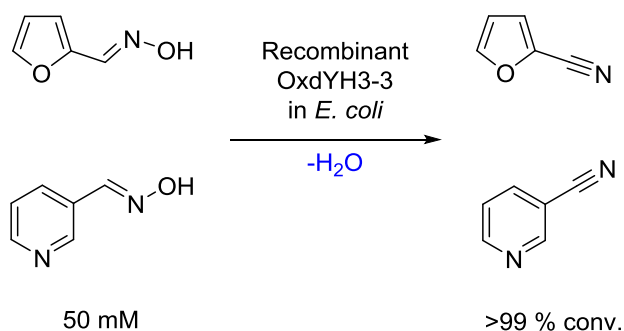
Table 8. Conversions or yields of biotransformations of (hetero-)aromatic aldoximes with whole-cells of *Rhodococcus* sp. YH3-3.^[181]



Entry	Aromatic moiety	Substrate conc. [mM]	<i>E/Z</i>	Conv. (isol. Yield) [%]
1	4-Toluoyl	10	<i>E</i>	24
2	4-Anisoyl	10	<i>E</i>	(6)
3	4-Chlorophenyl	10	<i>E</i>	7.2
4	4-Nitrophenyl	100	<i>E</i>	0.06
5	3-Pyridinyl	50	<i>E</i>	(98)
6	3-Pyridinyl	50	<i>Z</i>	20
7	2-Pyridinyl	100	<i>E</i>	(30)
8	3-Indolyl	100	<i>E</i>	0.07
9	2-Furfuryl	100	<i>E</i>	62
10	2,5-Pyrazinyl	100	<i>E</i>	22
11	2-Acyl-3-pyridinyl	100	<i>E</i>	(73)
12	3-Oxopyridinyl	100	<i>E</i>	(0.2)

2 State of the art

Recently, recombinant expression of OxdYH3-3 in *E. coli* was reported.^[170] The protein was mostly expressed in the insoluble form and was therefore not purified. *E*-furfuryl-2-aldoxime and *E*-pyridine-3-aldoxime were fully converted to their nitriles with the recombinant whole-cell catalyst after nine hours reaction time at 50 mM substrate loading (Scheme 45). The initial conversion of *E*-pyridine-3-aldoxime was higher compared to *E*-furfuryl-2-aldoxime.^[170]



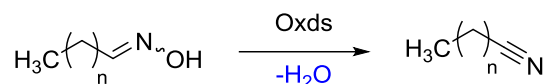
Scheme 45. Dehydration of *E*-furfuryl-2-aldoxime and *E*-pyridine-3-aldoxime to 2-furonitrile and 3-cyanopyridine catalyzed by recombinant OxdYH3-3 in *E. coli* BL21(DE3).^[170]

2.3.3.3 Linear and branched aliphatic aldoximes

Aliphatic aldoximes are also substrates of Oxds. It can be separated between linear aliphatic and branched aliphatic aldoximes. Linear aliphatic aldoximes with a chain length between two and six carbon atoms have been investigated as substrates of Oxds (Table 9). These enzymes are suitable to convert these linear aldoximes independent of their chain length.^[162,164–168,179,181] Partially, very high v_{\max} -values with specific substrate-enzyme combinations were obtained (e.g. Entries 9, 15, 16, and 19).^[162,167,168] Very high to total conversion (97 to 100 %) of acetonitrile (100 mM substrate), *n*-propionitrile (50 mM substrate), *n*-butyronitrile (100 mM substrate), *n*-pentane nitrile (250 mM substrate) and capronitrile (300 mM substrate) was observed with a recombinant OxdB whole-cell catalyst (Entries 2, 3, 8, 14, and 19). The nitriles were isolated in moderate yields between 46 and 56 % (Entries 8, 14, and 19).^[179] Despite that OxdYH3-3 is not active for arylaliphatic nitriles, *n*-butyronitrile could be isolated in a moderate yield of 45 % in a preparative biotransformation of *n*-butanal oxime with *Rhodococcus* sp. YH3-3 whole-cells (Entry 13).^[181]

2 State of the art

Table 9. Kinetic data, conversions and isolated yields for biotransformations of linear aliphatic aldoximes with Oxds.



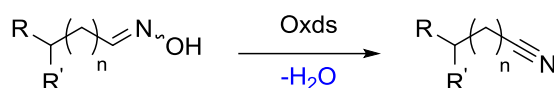
Entry	n	Oxd	<i>E/Z</i>	K_m [mM]	V_{max} [U·mg ⁻¹]	Conv. (isol. Yield) [%]	Reference
1	0	A	<i>E/Z</i>	11	(5.6) [*]		[165]
2	0	B	<i>E/Z</i>	-	-	97	[179]
3	1	B	<i>E/Z</i>	4.32	3.28	99.3	[179]
4	1	K	<i>E/Z</i>	0.778	2.90		[168]
5	1	RE	<i>E/Z</i>	2.17	5.78		[166]
6	1	RG	<i>E/Z</i>	5.13	0.43		[164]
7	2	A	<i>E/Z</i>	0.25	(5.4) [*]		[165]
8	2	B	<i>E/Z</i>	11.1	9.49	100 (46)	[162,179]
9	2	FG	<i>E/Z</i>	2.87	20.4		[167]
10	2	K	<i>E/Z</i>	2.16	14.8		[168]
11	2	RE	<i>E/Z</i>	2.64	6.02		[166]
12	2	RG	<i>E/Z</i>	1.73	0.689		[164]
13	2	YH3-3	<i>E/Z</i>	-	-	(45)	[181]
14	3	B	<i>E/Z</i>	2.42	12.6	100 (53)	[162,179]
15	3	FG	<i>E/Z</i>	10.1	88.8		[167]
16	3	K	<i>E/Z</i>	3.78	19.9		[168]
17	3	RE	<i>E/Z</i>	1.13	4.59		[166]
18	3	RG	<i>E/Z</i>	1.13	1.64		[164]
19	4	B	<i>E/Z</i>	6.12	32.3	99.5 (56)	[162,179]
20	4	FG	<i>E/Z</i>	0.802	3.60		[167]
21	4	K	<i>E/Z</i>	3.12	15.3		[168]
22	4	RG	<i>E/Z</i>	2.94	1.66		[164]

*The value given in parenthesis corresponds to the k_{cat} -value in [min⁻¹].

2 State of the art

Beside linear aliphatic aldoximes, their branched derivatives are also accepted by Oxds (Table 10). For all substrates suitable enzymes were found.^[162,164,166–168,179] While *iso*-butyraldoxime (at 10 mM substrate concentration) was only converted to 35.3 % of the corresponding nitrile (Entry 1), *iso*-valeronitrile (200 mM substrate concentration) was isolated in 50 % yield (99.6 % conversion) with whole-cells expressing OxdB (Entry 5).^[179] In general, OxdB preferred substrates with longer chain lengths over the shorter ones.^[162,179] Furthermore, cyclohexane-carbaldoxime was accepted by OxdK, OxdRE, and OxdRG while it was not accepted by OxdB (Entries 12 to 15).^[162,166,168] Moreover, an application of Oxds in the synthesis of citronellyl nitrile and other compounds used in the fragrance industry has been patented by BASF recently.^[183]

Table 10 Kinetic data, conversions and isolated yields of biotransformations of branched linear aliphatic aldoximes with Oxds.



Entry	n	R	R'	Oxd	E/Z	K _m [mM]	v _{max} [U·mg ⁻¹]	Conv. (isol. Yield) [%]	Reference
1	0	Me	Me	B	E/Z	-	-	35.3	[179]
2	0	Me	Me	K	E/Z	0.538	5.87	-	[168]
3	0	Me	Me	RE	E/Z	1.41	8.33	-	[166]
4	0	Me	Me	RG	E/Z	5.54	0.041	-	[164]
5	1	Me	Me	B	E/Z	3.58	7.72	99.6 (50)	[167,179]
6	1	Me	Me	FG	E/Z	2.66	23.1	-	[167]
7	1	Me	Me	K	E/Z	1.33	35.1	-	[166]
8	1	Me	Me	RE	E/Z	2.43	5.71	-	[166]
9	1	Me	Me	RG	E/Z	3.97	0.239	-	[164]
10	2	Me	Me	B	E/Z	2.98	10.1	-	[162]
11	2	Me	Me	RG	E/Z	6.76	1.32	-	[164]
12	0	-Cy-		B	E/Z	N.A.	N.A.	-	[162]
13	0	-Cy-		K	E/Z	5.96	16.8	-	[168]
14	0	-Cy-		RE	E/Z	0.99	4.76	-	[166]
15	0	-Cy-		RG	E/Z	1.13	0.386	-	[164]

N.A. Not accepted.

3 Biocatalytic synthesis of phenylpyruvate with an L-amino acid oxidase

3.1 Recent developments regarding fungal L-amino acid oxidases

Recently, the heterologous expression of an active L-AAO from the fungus *Rhizoctonia solani* as a fusion protein with a maltose-binding protein as a solubility-tag in *E. coli* has been reported. This study was employing a novel method for the direct determination of the produced α -keto acid *via* reversed phase-HPLC (RP-HPLC) measurements. Usually, the activities of L-AAOs are determined in a coupled assay measuring the hydrogen peroxide formation as an indirect indicator for the reaction progress.^[119]

Nuutinen et al. reported an L-AAO from the fungus *Hebeloma cylindrosporum* (*H. cylindrosporum*) expressed in the heterologous host *E. coli* (*hcLAAO1*). This enzyme could be activated after expression by treatment with sodium dodecylsulfate (SDS). However, the applicability of this enzyme for synthetic transformations suffers from the narrow substrate spectrum.^[120] Recently, *Bloess et al.* reported another L-AAO from a putative gene of *H. cylindrosporum* (*hcLAAO4*, constructed with a linked hexahistidine-tag). An inactive form of this enzyme was obtained from heterologous expression in *E. coli*. *hcLAAO4* can be activated by acidic treatment after purification. In contrast to several other L-AAOs, a broad substrate spectrum was found for *hcLAAO4* (Figure 10). Activity was observed for most proteinogenic amino acids (except L-proline, L-cysteine, L-serine, L-threonine and L-aspartate). Furthermore, esters of L-alanine, L-glutamic acid, L-leucine, L-methionine, L-tyrosine and L-phenylalanine were converted by this enzyme. This feature might be interesting for a synthetic application of this enzyme. Moreover, the K_m -values for all tested substrates were in sub-millimolar range (e.g. 0.48 mM for L-phenylalanine), which underlines the potential of this enzyme.^[184]

3 Biocatalytic synthesis of phenylpyruvate with an L-amino acid oxidase

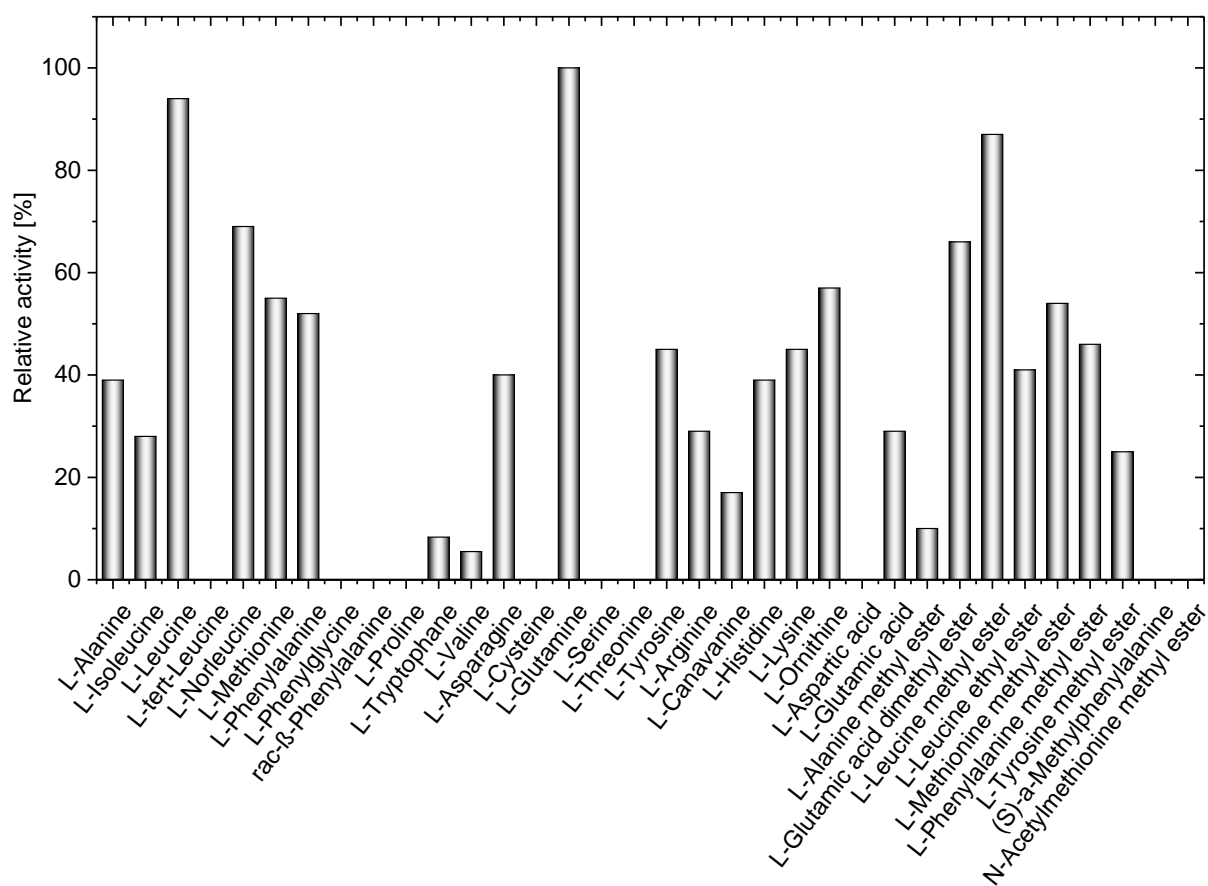
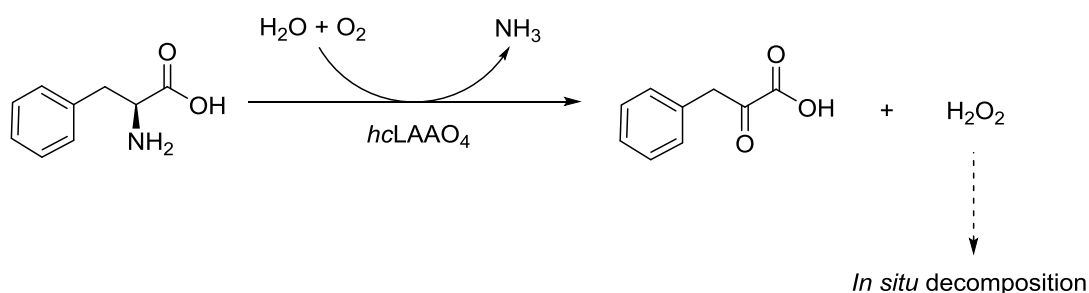


Figure 10. Substrate spectrum of recombinant, acidic activated *hcLAAO4*.^[184]

3.2 Motivation

In this chapter, the novel *hcLAAO4* will be utilized in biotransformations exploring an application of this enzyme in α -keto acid synthesis. The enzyme in this study will be obtained from the *Fischer von Mollard* group (Bielefeld University) in purified form or as whole-cells containing the expressed enzyme. Besides the enzyme produced from *E. coli*, also the enzyme produced from *P. pastoris* will be utilized and compared.

The focus will be laid on characterizing the enzyme and the process regarding relevant parameters of preparative biotransformations. As this enzyme also accepts α -amino acid esters,^[184] it could be a valuable tool for the synthesis of α -keto esters in organic synthesis. The experiments will be carried out with L-phenylalanine as a model substrate facilitating the analytical procedures. This substrate was chosen because of its hydrophobicity and the enzymatic activity of *hcLAAO4*, which is close to those of L-amino acid esters (Scheme 46). Furthermore, the expected reaction product, phenylpyruvate, finds an application as a precursor in the synthesis of the diet sweetener aspartame and indole-3-acetic acid.



Scheme 46. Overview about a process for production of phenylpyruvate from L-phenylalanine with *hcLAAO4*.

3.3 Process properties of the L-phenylalanine oxidation with L-amino acid oxidase from *Hebeloma cylindrosporium*

The enzyme was obtained as previously described from the *Fischer von Mollard* group as purified and activated enzyme (of known activity) or as whole-cells. The lysate was prepared with a protocol following the acidic activation of the purified protein with citric acid buffer pH 3.0, which was applied after cell lysis in a high-pressure homogenizer. A gel electrophoretic analysis (SDS-PAGE) performed by *Bloess* visualizes the level of enzyme expression and the increased purity of the enzyme after Ni²⁺-NTA affinity chromatography (Figure 11, band at ~67.5 kDa).^[185] The overproduction of the enzyme in the crude extract is on a medium level. The activation of the lysate does not affect the enzyme purity, thus, no or only marginal amounts of protein (desired and undesired) is lost in the activation step. The affinity chromatography purification step increases the purity remarkably, however, homogeneity is not reached. The purity was considered as sufficient for biotransformations and process characterization.

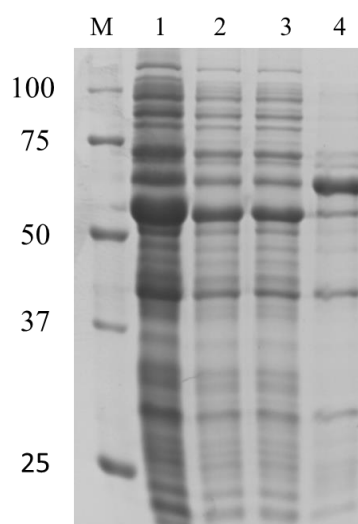
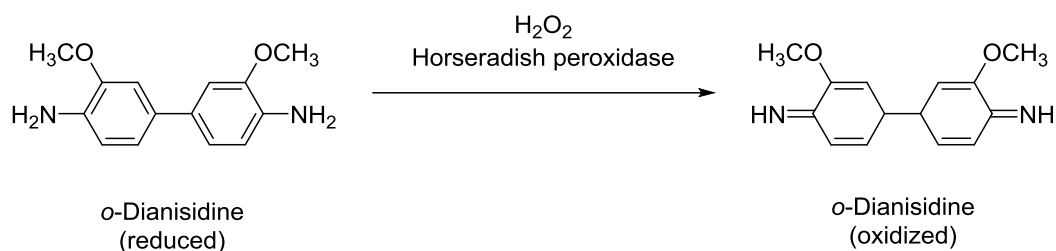


Figure 11. Verification of the purification of *hclAOO4* (~67.5 kDa) *via* SDS-PAGE by *Bloess*. M: Marker, Lane 1: Crude extract, lane 2: Activated lysate, lane 3: Activated lysate after filtering, Lane 4: Ni-NTA purified enzyme.^[185]

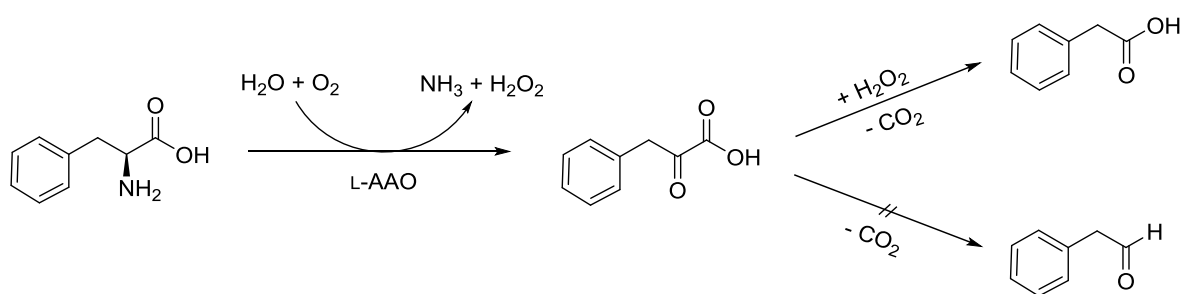
The activated lysate as well as the purified protein were applied in biotransformations. Similar amounts of enzyme regarding the activity (determined according to GP20) were utilized. The activity assay for the determination of the L-AAO activity was dependent on the initial production rate of hydrogen peroxide, which is formed as a side product of the L-phenylalanine oxidation. This rate was monitored *via* the oxidation of the dye *o*-dianisidine catalyzed by horseradish peroxidase (Scheme 47). The oxidized form of the dye can be observed spectroscopically at a wavelength of 436 nm.^[186]

3 Biocatalytic synthesis of phenylpyruvate with an L-amino acid oxidase



Scheme 47. Oxidation of *o*-dianisidine with hydrogen peroxide as oxidant catalyzed by horseradish peroxidase.

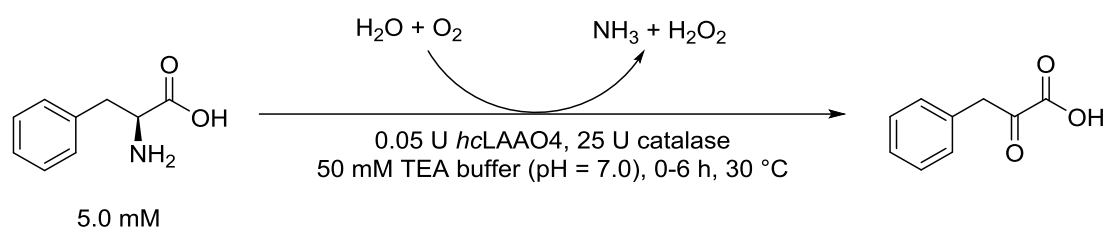
In order to determine the product formed in the actual reaction system, an established method for analysis by RP-HPLC in comparison to a calibration curve was used.^[119] Slightly different retention times were observed for L-phenylalanine and phenylpyruvate compared to literature (see methods). As an initial reference, the biotransformation of L-phenylalanine was carried out with purified *hcLAAO4* regardless of the hydrogen peroxide formation. At full conversion of the substrate, phenylpyruvate was not detected. Another product eluting at a retention time of 6.5 min was observed instead. This retention time would fit to both phenylacetic acid and phenylacetaldehyde (both have a retention time at 6.5 min). NMR spectroscopic analysis of the reaction solution verified that no phenylacetaldehyde is contained in the solution (Appendix, Figure 40). Phenylacetic acid is assumed to be formed through an oxidative decarboxylation of phenylpyruvate reducing the chain length by one carbon atom as suggested in literature for analogue systems.^[129] Decarboxylation will probably proceed by oxidation of the α -keto acid with hydrogen peroxide forming the peroxy- α -keto acid as an intermediate, which rearranges to the carboxylic acid under release of carbon dioxide (Scheme 48, mechanism not shown). No evidence for a spontaneous non-oxidative release of carbon dioxide was found as no aldehyde was observed.



Scheme 48. Possible decomposition pathways of phenylpyruvate produced in biotransformations catalyzed by L-AAO. The oxidative decarboxylation to phenylacetic acid is observed while no evidence was found for the formation of phenylacetaldehyde *via* non-oxidative decarboxylation.

3 Biocatalytic synthesis of phenylpyruvate with an L-amino acid oxidase

In nature, L-AAOs often occur together with catalase enzymes, a hydrogen peroxide degrading enzyme class. Many processes involving hydrogen peroxide forming oxidases require the addition of catalase enzymes in order to prevent the overoxidation of the product (see chapter 2.2). As a first benchmark of the process characteristics, this overoxidation had to be avoided. Therefore, two different catalase enzymes, commercially available bovine catalase (Sigma Aldrich) and a human catalase expressed in *E. coli*,^[187] were tested. As an alteration of the initial biotransformation, 25 U of catalase was added to the reaction solution (Scheme 49). This refers to a ratio of 10 U per μmol of substrate.



Scheme 49. Standard biotransformation of L-phenylalanine to phenylpyruvate catalyzed by *hcLAAO4*.

In the presence of catalase, the formation of phenylpyruvate was observed with a low byproduct formation of the carboxylic acid. The bovine catalase showed to be superior to the one from human. Over several data points, a higher specific product formation of 92 % (arithmetic middle of six values) was observed with the bovine catalase, while 85 % specific product formation (arithmetic middle of five values) were observed with human catalase. Henceforth, all further experiments were performed with bovine catalase. Figure 12 visualizes a typical RP-HPLC chromatogram of the analysis of the biotransformation in presence and absence of bovine catalase. Furthermore, it was shown that phenylpyruvate was stable under the reaction conditions (except hydrogen peroxide) and was not degraded by any other pathway.

3 Biocatalytic synthesis of phenylpyruvate with an L-amino acid oxidase

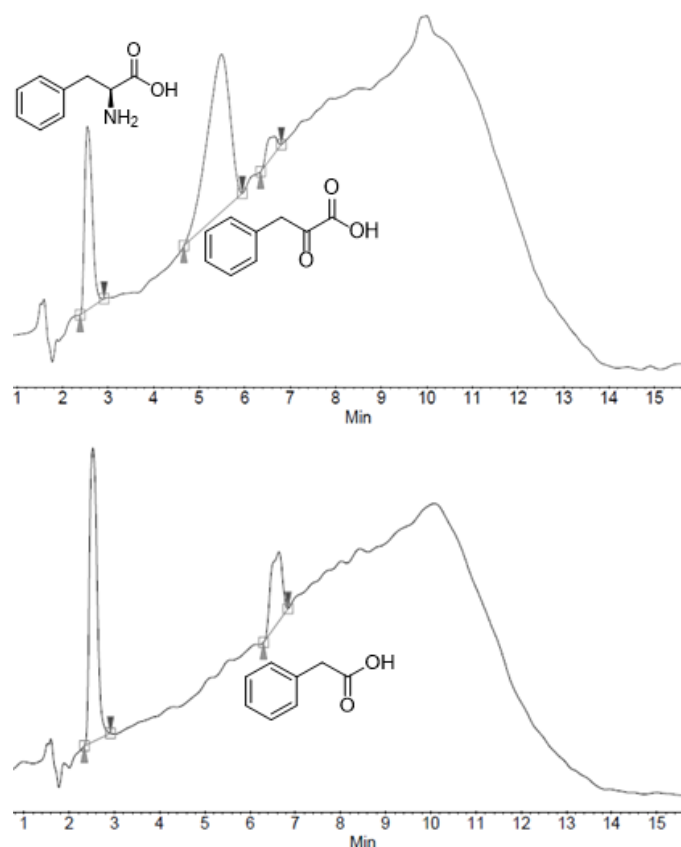


Figure 12. RP-HPLC chromatograms of the reaction mixtures with the addition of 50 U·mL⁻¹ catalase (upper) and without addition (lower).

First, the effect of the host cell for protein expression (*E. coli* or *P. pastoris*) and the form of *hcLAAO4* used (lysate or purified) were investigated. Crude extracts or lysates are often an attractive option for cheaper catalysts in bioprocesses. Protein purification steps necessary are a bottleneck for application due to their costs.^[17] In order to compare lysate and purified protein, a time course of the biotransformation of L-phenylalanine with 5.0 mM substrate concentration and a low catalyst loading (0.05 U corresponding to 0.02 U per μmol substrate) was measured. Each data point was determined by an individual batch, as the reaction was carried out in micro-scale (500 μL) and had to be stopped by boiling (Figure 13). After 30 minutes reaction time, 41 % of the substrate were converted when using the purified enzyme from *E. coli*. If the activated lysate was used, a lower conversion of 26 % was reached at this time. Whereas full conversion in the biotransformation with the purified enzyme was achieved already after two hours, the use of the lysate led to full conversion after three hours reaction time. Although using same amount of enzyme according to its activity, the observed conversions to phenylpyruvate were lower for the activated lysate at the same reaction time. These results indicate a higher stability of the purified enzyme compared to the lysate under the reaction conditions. Cross-effects from other proteins contained in the lysate might reduce the productivity of *hcLAAO4* as well. In addition to the expression in *E. coli*, enzyme obtained from expression in *P. pastoris* was also tested for biotransformations at 5.0 mM substrate

3 Biocatalytic synthesis of phenylpyruvate with an L-amino acid oxidase

concentration under the same conditions. If *hcLAAO4* from *P. pastoris* is used, full conversion was also observed after three hours (lysate and purified enzyme). For this host, the initial reaction velocity was even higher for the lysate compared to the purified enzyme. The overall product formation was slightly faster when the enzyme expressed in *E. coli* was used. The expression host probably does not have a major impact on formation of the oxidation product phenylacetic acid. Low amounts of ~5 % byproduct were observed in all biotransformations. The byproduct formation was higher with the purified enzyme from *P. Pastoris*, especially after six hours reaction time. The reason for this is unknown.

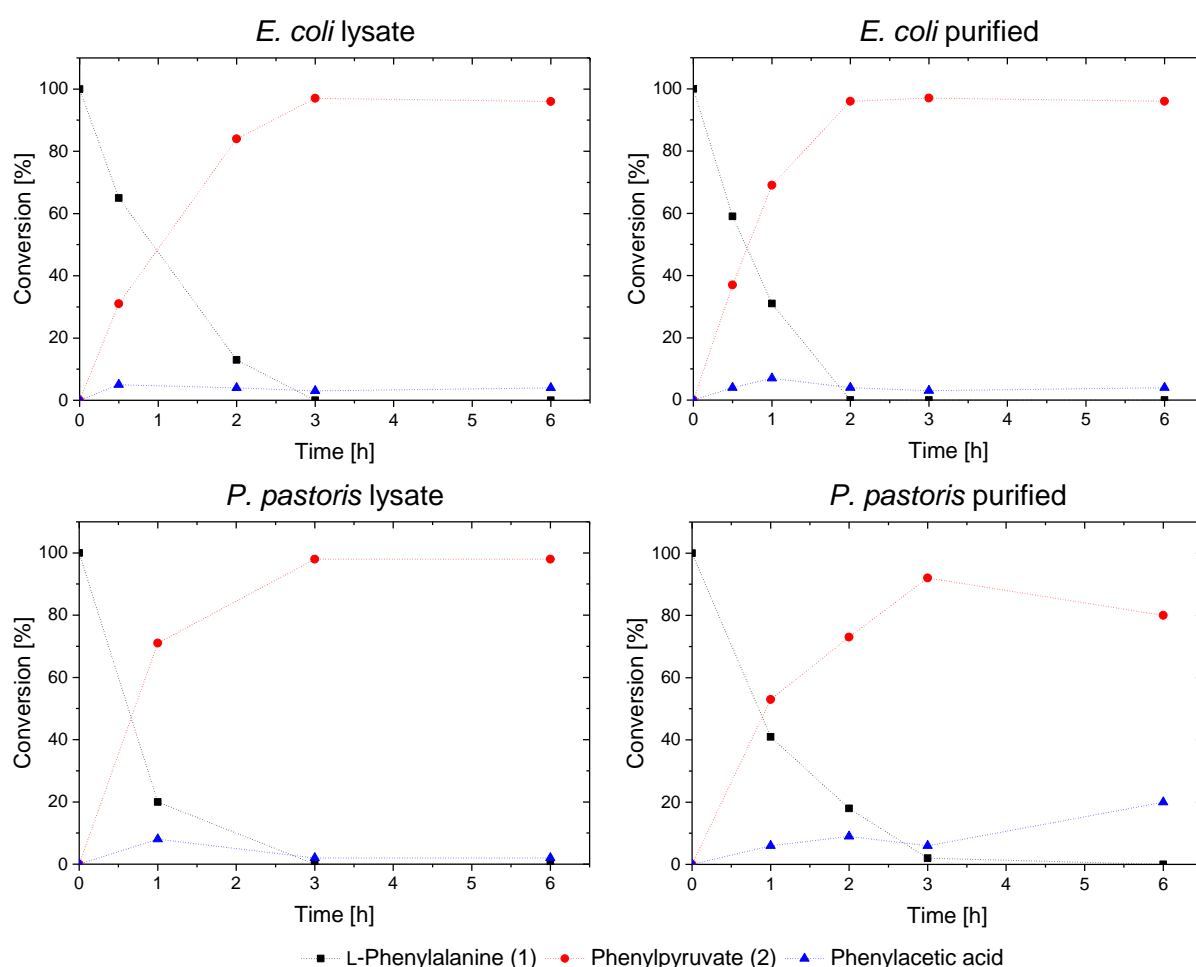


Figure 13. Time course of the standard biotransformation of L-phenylalanine with 0.05 U *hcLAAO4* given as lysate or purified enzyme obtained from expression in *E. coli* or *P. pastoris*.

Second, a stability test was carried out with the purified enzyme obtained from both expression systems. Therefore, the reaction solution containing all components except the substrate was incubated at -20 °C for one week before usage. The biotransformation was initiated by the addition of L-phenylalanine and the conversion to phenylpyruvate and phenylacetic acid was determined with RP-HPLC measurements. For the incubated enzyme, full conversion of 5.0 mM substrate was observed after a longer reaction time of four hours for the enzyme expressed in *E. coli* and five hours for the enzyme expressed in *P. pastoris*, respectively. The

3 Biocatalytic synthesis of phenylpyruvate with an L-amino acid oxidase

reaction progress is notably slower compared to when using fresh enzyme. The catalase activity was not gravely affected by the storage, byproduct formation was observed in the same range as the directly prepared reactions.

Higher salt concentrations (also of buffer salts) can have an effect on the enzymatic activity and stability.^[188] Furthermore, reaction systems with a high buffer salt concentration can facilitate the workup of a reaction, especially for liquid-liquid extractions. The influence of a higher concentration of triethanolamine buffer (TEA-buffer) on the reaction system with 0.05 U of purified *hcLAAO4* from *E. coli* was tested up to salt concentrations of 500 mM (standard 50 mM). A notable impact on the conversion of phenylpyruvate and the specific product formation was not observed regardless of the buffer concentration. The specific product formation was >95 % in all reactions.

Inhibitory effects have a strong impact on bioprocess development. In order to investigate these effects on the enzymatic activity of *hcLAAO4*, the biotransformation of L-phenylalanine was carried out in presence of the product or higher substrate concentrations. Conversions of phenylpyruvate and phenylacetic acid were monitored after one hour reaction time using a catalyst loading of 0.05 U purified *hcLAAO4* from *E. coli*. A decrease of the enzymatic activity was not observed when up to 5.0 mM phenylpyruvate were added to the reaction solution. Higher amounts of this α -keto acid were not soluble in the reaction system, thus, an inhibitory effect was not observed. The low solubility of α -keto acids in aqueous buffer systems could be advantageous for an application of *hcLAAO4* in α -keto acid synthesis. The product would precipitate from the aqueous reaction solution, thus, simplifying the workup enormously. In the following, the effect of substrate concentrations of up to 40 mM L-phenylalanine on the productivity of the biotransformation and the specific product formation was tested (Table 11). When a substrate concentration of 5.0 mM was present, 3.7 mM of L-phenylalanine were converted to 3.4 mM phenylpyruvate and 0.3 mM phenylacetic acid (Entry 1). This corresponds to a specific product formation of 92 %. After the same reaction time, an overall conversion of 4.6 mM was observed when the substrate amount was 10 mM (Entry 2). In this case, the specific product formation decreased to 89 %. For higher substrate concentrations of 20 and 30 mM, the overall conversion further increased to 5.0 and 6.8 mM, respectively (Entries 3 and 4). The specific product formation was only slightly affected. The highest tested substrate concentration was 40 mM L-phenylalanine (Entry 5). An overall conversion of 8.0 mM was observed at this substrate concentration. However, the specific product formation decreased to 84 %. Even though the lowest tested substrate concentration of 5.0 mM is notably above the doubled K_m (0.96 mM for L-phenylalanine),^[184] the productivity of the biotransformation remarkably increased with higher substrate loadings. These results suggest no inhibitory effect

3 Biocatalytic synthesis of phenylpyruvate with an L-amino acid oxidase

of the substrate on the activity of *hcLAAO4*. Furthermore, the increased production rate is a favorable factor for synthetic applications. In addition to the higher productivity, the amount of produced phenylacetic acid increased with higher substrate concentrations. Whether the byproduct is formed or not depends on the relative turnover frequencies of the oxidative decarboxylation and the hydrogen peroxide degradation catalyzed by bovine catalase. One molecule of hydrogen peroxide can form maximally one molecule of phenylacetic acid as it is consumed in this step. If hydrogen peroxide accumulates in the reaction solution, the oxidative decarboxylation becomes more likely. This accumulation of hydrogen peroxide is probably caused by a higher turnover frequency of the *hcLAAO4*-catalyzed L-amino acid oxidation observed at higher substrate concentrations. The addition of higher amounts of catalase would prevent this byproduct formation, however, this might be an additional cost factor.

Table 11. Conversions and (by-)product formation in the biotransformations after one hour reaction time at higher substrate concentrations with 0.05 U *hcLAAO4* from *E. coli*.

Entry	Conc. L-Phe [mM]	Conv. [%]	Conc. phenylpyruvate [mM]	Conc. phenylacetic acid [mM]	Specific product formation [%]
1	5.0	73	3.4	0.3	92
2	10	46	4.1	0.5	89
3	20	25	4.5	0.5	90
4	30	23	6.0	0.8	88
5	40	20	6.7	1.3	84

In the following, the effect of an increased catalyst loading was investigated by analyzing the conversions of 5.0 to 20 mM L-phenylalanine after a constant reaction time of seven hours (Figure 14). 5.0 mM of the substrate were nearly totally converted to phenylpyruvate with 0.05 U *hcLAAO4* from *E. coli*. If the substrate loading is increased to the double amount (10 mM), a conversion of 54 % at a specific product formation of 91 % phenylpyruvate was achieved with the same amount of enzyme. At 20 mM substrate concentration, 46 % of the L-phenylalanine were converted to phenylpyruvate with a specific product formation of 87 %. With a higher catalyst loading of 0.10 U purified *hcLAAO4*, substrate concentrations up to 15 mM of L-phenylalanine were fully converted. A conversion of 91 % was observed when 20 mM of the substrate were present in the reaction solution. Full conversion of 20 mM L-phenylalanine was achieved when the catalyst loading was increased to 0.20 U purified *hcLAAO4*. When 0.30 U purified *hcLAAO4* were used, a complete conversion of 20 mM L-phenylalanine was observed even after four hours reaction time (data not shown). In accordance to the previous observations, an increased formation of the byproduct was observed at higher substrate loadings regardless of the catalyst loading. Furthermore, the increase of the catalyst loading also led to a higher byproduct formation at lower substrate concentrations.

3 Biocatalytic synthesis of phenylpyruvate with an L-amino acid oxidase

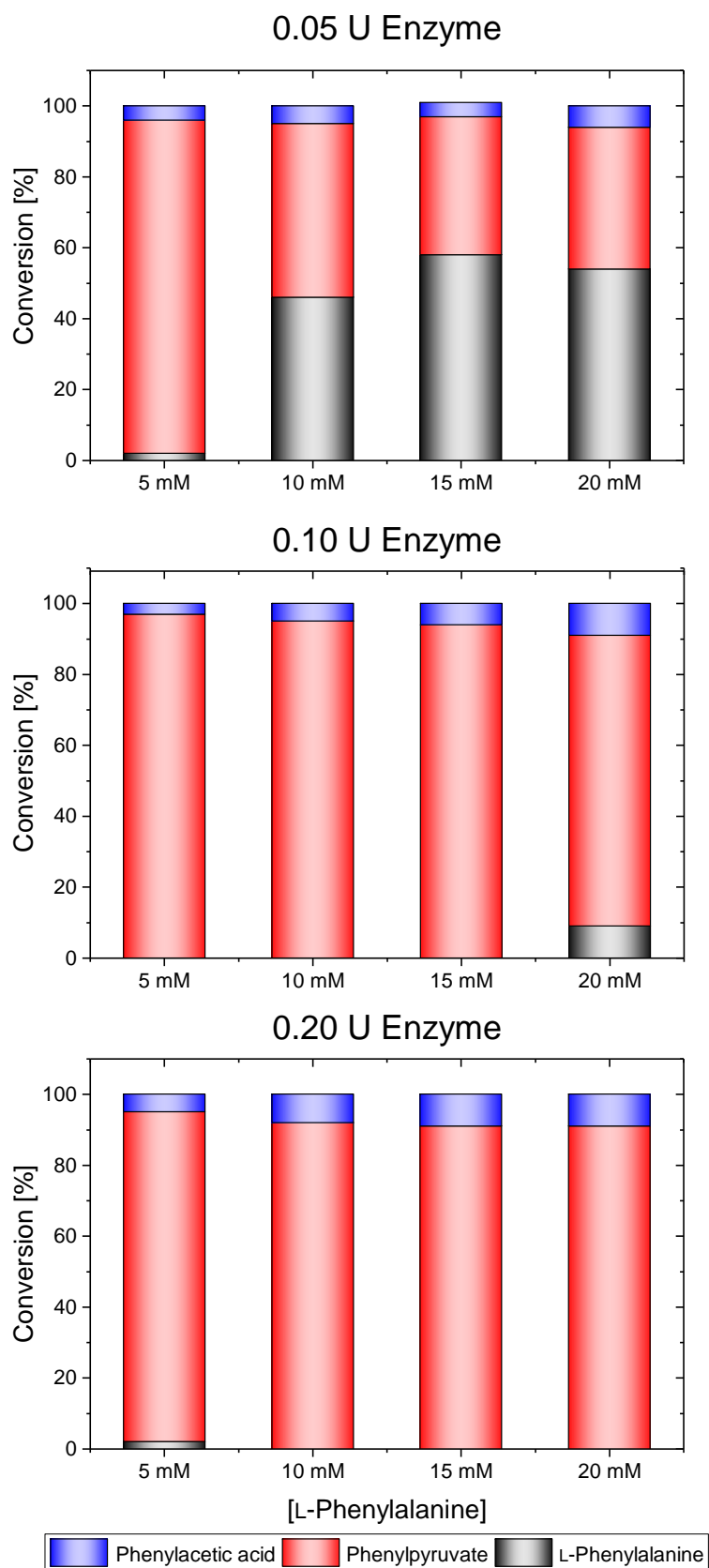


Figure 14. Results of the biotransformations with purified *hcLAAO4* (0.05 U, 0.10 U, and 0.20 U) obtained through expression in *E. coli* for substrate concentrations ranging from 5.0 to 20 mM.

3.4 Summary and outlook

In summary, the *hcLAAO4* has been shown to be a suitable catalyst for the production of phenylpyruvate from L-phenylalanine. The enzyme showed an enhanced turnover at higher substrate concentrations. Inhibitory effects of buffer salts, substrate and product were not observed for the *hcLAAO4*. The commercially available bovine catalase was suitable to prevent the degradation of phenylpyruvate in the reaction system. Specific product formations of constantly over 90 % were observed in the preparative transformations. Full conversion of 20 mM L-phenylalanine (3.3 g L^{-1}) was obtained within seven hours (0.20 U enzyme) or four hours (0.30 U) in analytical scale (10 μmol). Although showing slight inactivation after long incubation times in the reaction media, the catalyst seemed to be robust for the process. In conclusion, these results indicate a promising applicability of the enzyme in biotransformations for α -keto acid synthesis. The next step in bioprocess design would be to investigate the conversion of higher substrate loadings for reaching an application relevance. As the tested substrate concentrations were close to the solubility limit of the substrate, a co-solvent screening might be helpful. This would be important for transferring this model reaction system towards the synthesis of α -keto esters from amino acid esters, as their water solubility is much lower compared to the polar α -amino acid. The construction a fusion-protein of the *hcLAAO4* with a catalase might be a suitable approach to enhance the hydrogen peroxide quenching.

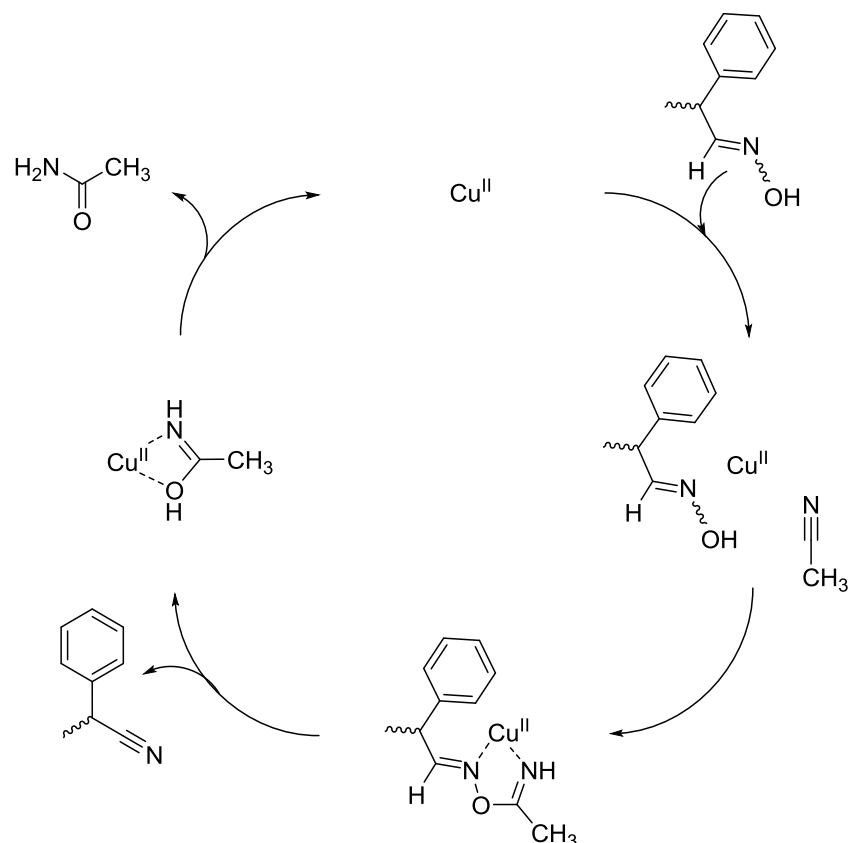
4 Biocatalytic cyanide-free synthesis of chiral nitriles

4.1 Enantioselective aldoxime dehydration with aldoxime dehydratase from *Bacillus* sp. OxB-1

4.1.1 Mechanism of the chemocatalytic water elimination of aldoximes

Until now, no enantioselective chemocatalytic method of aldoxime dehydration has been reported in literature. An example for such a non-selective reaction is the copper(II)-catalyzed dehydration of aldoximes in the presence of acetonitrile occurring at temperatures >80 °C. This reaction proceeds in heterogeneous fashion with copper(II)-ions immobilized on molecular sieves (4 Å)^[88] as well as homogeneously with copper(II) acetate.^[89] In the reaction, water is not released as a free molecule but transferred to the acetonitrile forming acetamide and the nitrile. A five-membered intermediate with both the aldoxime and acetonitrile coordinating to the copper under formation of a C-O-bond is postulated (Scheme 50).^[88] For this reaction, no impact of the geometry of the aldoxime moiety on the reactivity is known, the reaction proceeds equally with both *E*- and *Z*-isomer. The reaction can also be catalyzed by the produced nitrile instead of acetonitrile, thus forming the corresponding amide as a side product. However, this pathway is not preferred for most compounds.

The mechanism of the copper(II)-catalyzed aldoxime dehydration (Scheme 50) also explains that this reaction cannot be stereospecific by definition, as no new stereocenter is formed in the reaction. Furthermore, the configuration of the aldoxime is unaffected by the reaction. In theory, an enantioselective progress of the reaction could be realized with a chiral ligand bound to the copper. This reaction represents a kinetic resolution of a racemate, thus only a conversion of 50 % could be realized for perfect enantioselectivity. Considering the reaction conditions, especially the high temperatures, the free enthalpy difference of two transition states would probably be marginally for this system. An effective resolution would be more likely in a highly chiral environment at lower temperatures.

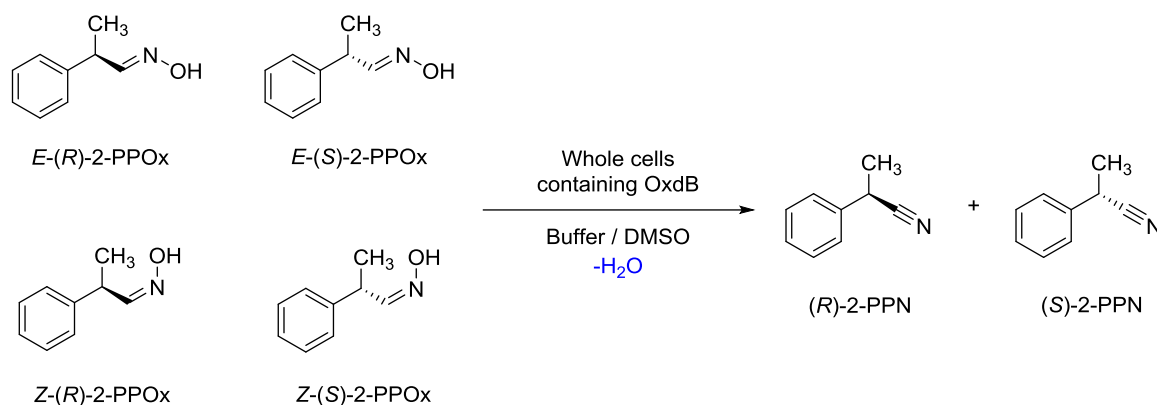


Scheme 50. Proposed mechanism for the aldoxime dehydration to nitriles catalyzed by copper(II)-ions by transfer of water to acetonitrile forming acetamide. The mechanism is shown for the dehydration of 2-PPOx to 2-PPN in analogy to the proposed mechanism of the dehydration of benzaldoxime.^[88]

4.1.2 Chiral nitrile formation with aldoxime dehydratases

The case described above would be given if the dehydration of aldoximes is catalyzed by Oxds under physiological conditions. Several publications have proposed that enantioselective dehydration with Oxds would be possible if chiral aldoximes are given as substrates. Recently, a study from *Metzner et al.* was focused on this topic.^[180] They used the most simple derivative of PAOx, 2-PPOx, which is only different by one methyl group in the α -position of the aldoxime moiety, as a model substrate for their study of enantioselective aldoxime dehydration with OxdB. A racemic mixture of *E/Z*-2-PPOx contains the two enantiomers of both the *E*- and *Z*-isomer of the aldoxime. The configuration of the stereocenter in α -position to the aldoxime moiety remains untouched in the reaction. Both (*R*)- and (*S*)-isomer will be transformed in the (*R*)- and (*S*)-nitrile. In the study, OxdB was applied as a whole-cell catalyst to improve the enzyme stability in the biotransformation (Scheme 51).^[180]

4 Biocatalytic cyanide-free synthesis of chiral nitriles



Scheme 51. Dehydration of a racemic mixture of *E/Z*-2-PPOx forming both enantiomers of 2-PPN catalyzed by OxdB.^[180]

If a racemic mixture of 2-PPOx (*E/Z* 80:20) was converted completely to 2-PPN at 30 °C, no enantioselectivity was observed (Table 12, Entry 1). At a lower temperature of 8 °C however, a maximum of 60 % conversion was achieved even at elevated reaction times. In this case the (*S*)-nitrile was produced with an *ee*-value of 65 % (Entry 2). If substrate solutions containing the *E*-isomer enriched aldoxime were used in the biotransformation, better enantioselectivity with a maximum of 98 % *ee* at a conversion of 50 % were achieved (Entries 3 and 4). With a *Z*-enriched substrate solution, the opposite enantiomer was obtained, however with much lower selectivity (Entry 5).^[180]

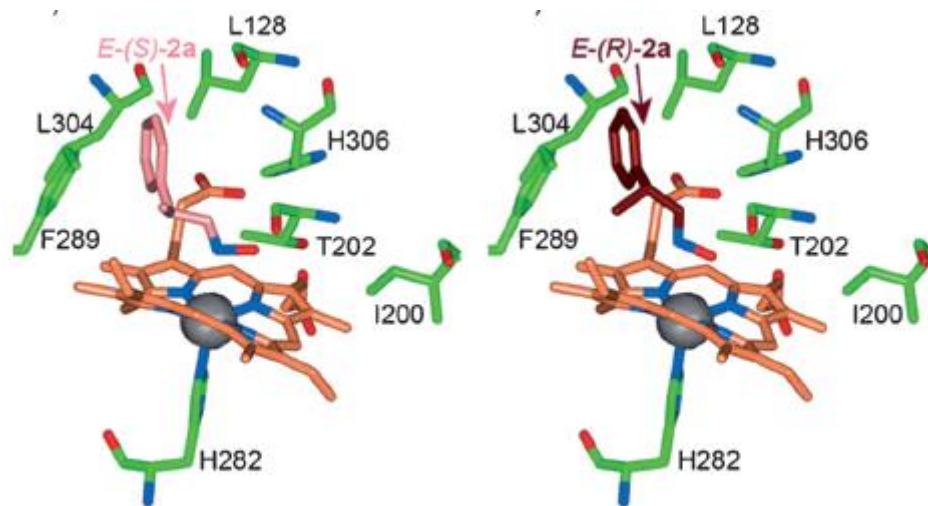
Table 12. Conversions and *ee*-values of the biotransformation of racemic *E/Z*-2-PPOx mixtures of varying *E/Z*-ratios towards 2-PPN with OxdB.^[180]

Entry	<i>E/Z</i> -ratio	T [°C]	Conv. [%]	<i>ee</i> [%]
1	80:20	30	>99	0
2	80:20	8	60	65 (<i>S</i>)
3	90:10	8	53	88 (<i>S</i>)
4	99:1	8	50	98(<i>S</i>)
5	8:92	8	15	67 (<i>R</i>)
6	8:92	8	96	4 (<i>S</i>)

The difference in enantioselectivity for the isomers of 2-PPOx was explained *via* a molecular modeling approach. By docking both configurations of *E*- and *Z*-isomer in the active site in a model and comparing the distances between the heme iron and the nitrogen-atom of the aldoxime, the relative energies of the transition states were estimated (Figure 15). In addition, the data was consistent for the achiral substrate PAOx explaining the preference of the enzyme for *Z*-PAOx (Entries 1 and 2). While for the *E*-isomer of 2-PPOx the distances of both enantiomers have a high difference (0.33 Å) favoring the (*S*)-enantiomer (Entries 3 and 4), the difference is only slight for *Z*-isomer (0.04 Å) with a preference for the (*R*)-enantiomer (Entries

4 Biocatalytic cyanide-free synthesis of chiral nitriles

5 and 6). The distances obtained from in calculations are in good agreement to the experimental data, proving a strong differentiation for the two enantiomers of the *E*-isomer and a poor one for the *Z*-isomer. Moreover, the *Z*-isomer was preferably accepted by the enzyme according to the model representing the experimental findings.^[180]

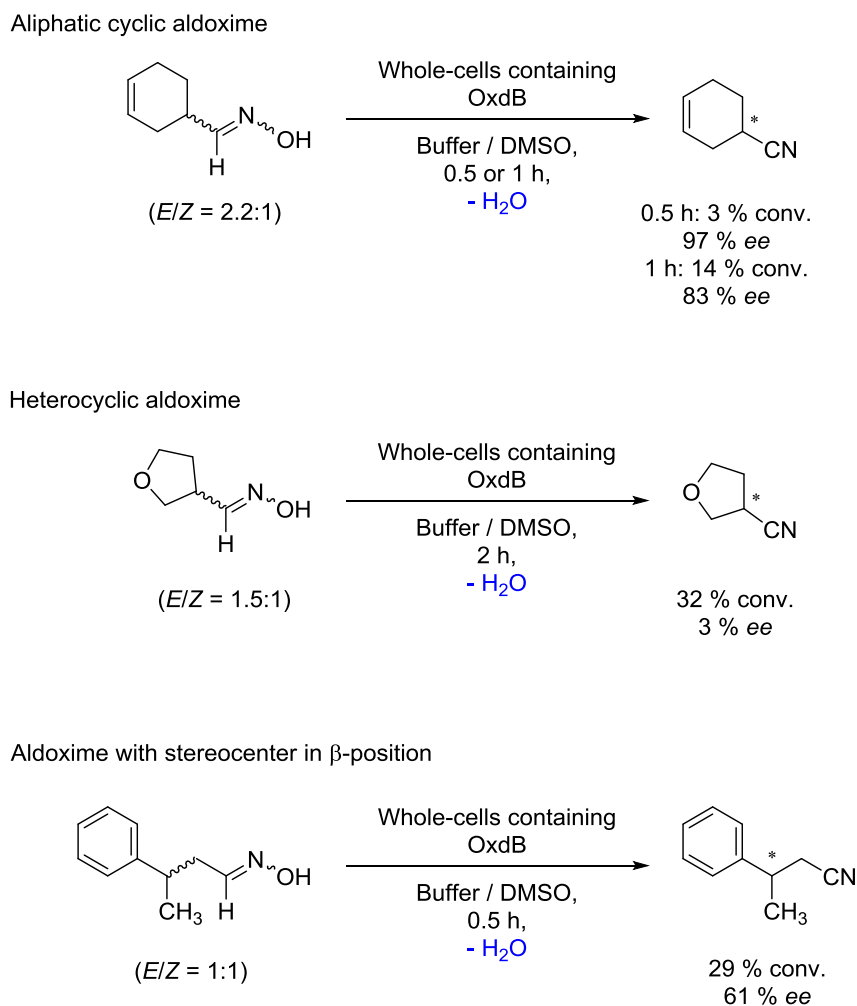


Entry	Substrate	Fe–N [Å]	Fe–O [Å]
1	<i>E</i> -PAOx	2.87	3.26
2	<i>Z</i> -PAOx	2.76	3.50
3	<i>E</i> -(<i>S</i>)-2-PPOx	2.88	3.31
4	<i>E</i> -(<i>R</i>)-2-PPOx	3.21	2.80
5	<i>Z</i> -(<i>S</i>)-2-PPOx	2.73	3.66
6	<i>Z</i> -(<i>R</i>)-2-PPOx	2.69	3.22

Figure 15. Molecular model of OxdB showing the positions of a) *E*-(*S*)-2-PPOx and b) *E*-(*R*)-2-PPOx in the active site and comparison of the Fe–N and Fe–O distances for all isomers and enantiomers of PAOx and 2-PPOx (Adapted with permission from R. Metzner, S. Okazaki, Y. Asano, H. Gröger, *ChemCatChem*, 6, 3105-3109. Copyright © 2014, John Wiley & Sons, Inc.).^[180]

4 Biocatalytic cyanide-free synthesis of chiral nitriles

Highly enantioselective nitrile formation can subsequently be only achieved with a highly isomerically enriched *E*-isomer. In principle, both enantiomers of the nitrile are accessible with the same enzyme, which is a quite unique observation in enzyme chemistry. This study also included other chiral aldoximes for which only less selective transformations were observed with *E/Z*-mixtures (Scheme 52).



Scheme 52. Enantioselective dehydrations of racemic mixtures of 3-hexen-1-aldoxime, tetrahydrofuran-3-aldoxime, and 3-phenylbutanal oxime with OxdB.^[180]

4.2 Motivation and substrate selection

Together with the coworkers *Betke* and *Rommelmann*, the study of *Metzner et al.* should be expanded by testing a broad variety of substrates with different substitution patterns in order to gain a deeper understanding of this unique enantioselective dehydration reaction. It is of high interest, whether other Oxds show the same properties as OxdB. Therefore, five Oxds available in recombinant form in *E. coli* hosts (OxdA, OxdB, OxDFG, OxdRE and OxdRG) were chosen.

The aldoximes, which will be tested for enantioselective dehydration with Oxds, were separated between the coworkers. Most aldoximes are accessible directly *via* condensation of the corresponding aldehydes with hydroxylamine. However, a different synthesis route will be necessary for more complex aldoximes, which corresponding aldehydes are not commercially available. For these aldoximes, a synthesis route featuring two new C-C bond formations will be developed. While *Betke* and *Rommelmann* focussed on aliphatic and cyclic aliphatic aldoximes,^[189,190] two derivatives of 2-PPOx bearing a heteroaromatic moiety instead of the phenyl group were chosen. Furthermore, halogen substituted derivatives of 2-PPOx were of interest for this substrate study and the substrates were again separated between the coworkers. In this work, the *para*-fluoro derivative of 2-PPOx (4-FPPOx) was chosen. Besides the derivatives of 2-PPOx changing the aromatic moiety, the effect of the other substituent in α -position to the aldoxime moiety will be investigated as well. Aldoximes bearing an ethyl (EtPAOx), *iso*-propyl (*i*PrPAOx) or cyclohexyl group (CyPAOx) in this position were chosen as target molecules. With this substrate study (Figure 16), it might be estimated which substrate size fits in the active site of these Oxds without using the crystal structure of the enzymes. From another synthetic perspective, these molecules may be accessible *via* hydroformylation of aromatic terminal or internal alkenes containing the desired structural motif. *Metzner et al.* showed that the enantioselectivity of the dehydration is strongly related to the isomeric purity of the aldoximes.^[180] An effective separation method for these aldoximes has to be developed as well.

4 Biocatalytic cyanide-free synthesis of chiral nitriles

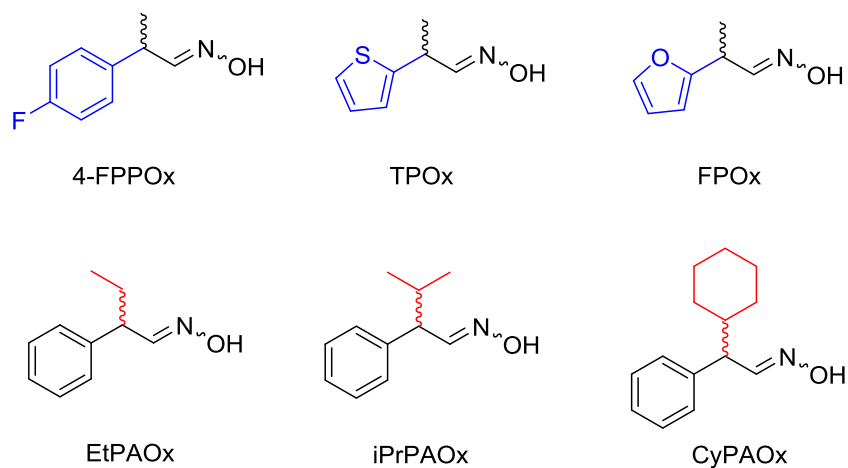
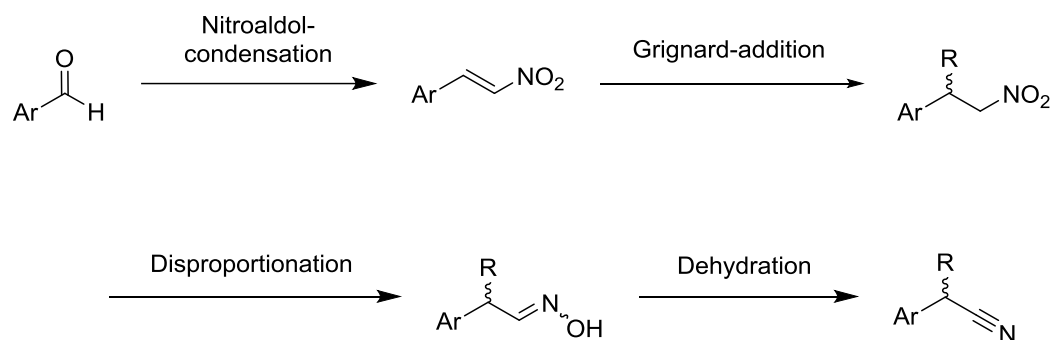


Figure 16. Structures of target substrates for the investigation of the enantioselectivity of the Oxd catalyzed dehydration.

4.3 Substrate synthesis

The synthesis of 2-(furan-2-yl)propionaldoxime (FPOx)^[191] and biocatalytic dehydration thereof was already carried out in previous experiments by the author of this thesis. In these experiments, only recombinant OxdB in *E. coli* JM109 was used.^[192]

Obtaining the selected new aldoximes was the first target. A possible synthetic route under formation of two C-C bonds starting from the commercially available benzaldehyde derivatives was chosen (Scheme 53). The first C-C bond can be introduced in a Nitroaldol-condensation with nitromethane forming *E*-nitroalkenes, which already bear a nitrogen-containing group.^[193] The next C-C bond (e.g. methyl group) can be formed by Michael addition^[194] of e.g. a Grignard-reagent. In this step, also other aliphatic groups can be introduced, thus, being also suitable for the bulky substrates. The key step for the aldoxime formation will be the disproportionation of the nitro moiety.^[191] Finally, a chemical dehydration of the aldoximes can form racemic nitriles, which are necessary as a reference for the Oxd-catalyzed dehydrations (see Scheme 23).

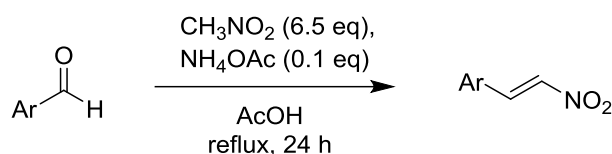


Scheme 53. Synthesis routes chosen for obtaining the racemic chiral aldoximes starting from aryl aldehydes or *trans*- β -nitrostyrene.

A Nitroaldol-condensation is a powerful method for C-C bond formation introducing also a nitrogen-containing functionality.^[193] In the reaction of aryl aldehydes with nitromethane in acetic acid, isomerically pure *E*-nitroalkenes were formed (Table 13). Recrystallization from ethanol yielded the *para*-fluorine substituted nitrostyrene derivative (Entry 3) in a medium yield of 39 % and the heteroaromatic derivatives in fair to good yields of 60 and 73 % (Entries 1 and 2). Repeated recrystallization steps of the residue would increase the yield of this reaction. For the synthesis of the unsubstituted bulky substrates, this reaction step was not necessary as *E*-*trans*- β -nitrostyrene is cheaply commercially available.

4 Biocatalytic cyanide-free synthesis of chiral nitriles

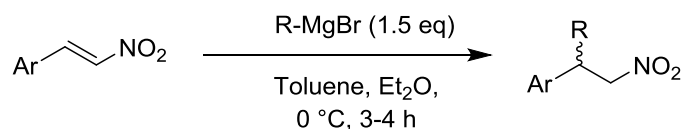
Table 13. Reaction conditions and isolated yields of the Nitroaldol-condensation of (hetero-)arylic aldehydes.



Entry	Ar	Isol. yield [%]
1	Thiophen-2-yl	60
2	Furan-2-yl	73
3	4-Fluorophenyl	39

The formed *E*-nitroalkenes represent a Michael-system. The addition to this specific structural motif is proceeding regioselective towards the β -position of the nitro group.^[194,195] In the next step, the methyl group or the desired bulky substituents was introduced by addition of (cyclic) aliphatic Grignard-reagents (Table 14). Racemic chiral nitroalkanes were obtained in this reaction and purified *via* automated column chromatography. The yields were moderate in a range between 30 to 53 % (Entries 1 and 3 to 6) for most compounds. Solely, the 2-furanyl-substituted nitroalkane was isolated in a very good yield of 86 % by gravity column chromatography (Entry 2).

Table 14. Reaction conditions and isolated yields of the addition of the aliphatic Grignard-reagents to *E*-nitroalkenes.



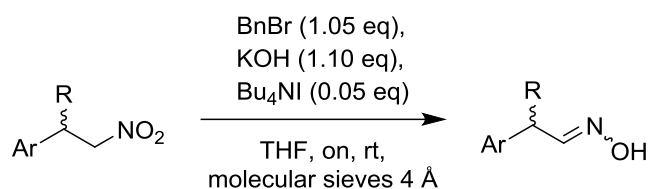
Entry	Ar	R	Isol. yield [%]
1	Thiophen-2-yl	Me	30
2	Furan-2-yl	Me	86
3	4-Fluorophenyl	Me	50
4	Ph	Et	42
5	Ph	<i>i</i> Pr	42
6	Ph	Cy	53

Subsequently, racemic mixtures of the isomers of the aldoximes were prepared *via* disproportionation with benzyl bromide (forming benzaldehyde as side-product) in analogy to a literature known method (Table 15).^[191] Automated column chromatography was the purification method of choice. The heteroaromatic aldoximes were obtained in 52 % and 58 % yield for 2-(thiophen-2-yl)propionaldoxime (TPOx, Entry 1) and FPOx (Entry 2), respectively.

4 Biocatalytic cyanide-free synthesis of chiral nitriles

4-FPPOx was obtained in an excellent yield of 96 % with this method (Entry 3). The bulky derivatives of 2-PPOx were obtained only in moderate yields between 37 and 48 % (Entries 6 to 8). Benzaldoxime, which can be formed as byproduct in this reaction, interfered during the column chromatography for these compounds. Due to their similar hydrophobicity, the separation between the desired aldoxime and byproduct was hardly given with any solvent mixture tested. In addition to the new aldoximes, *Z*-PAOx and *E/Z*-2-PPOx (without isomer separation) were synthesized as references *via* condensation of the corresponding aldehydes and hydroxylamine (not displayed). Both aldoximes were obtained in 41 % isolated yield from recrystallization or column chromatography (Entries 4 and 5).

Table 15. Reaction conditions and isolated yields of the disproportionation of nitroalkanes to aldoximes with benzylbromide.



Entry	Ar	R	Isol. yield [%]
1	Thiophen-2-yl	Me	52
2	Furan-2-yl	Me	58
3	4-Fluorophenyl	Me	96
4*	Ph	H	41
5*	Ph	Me	41
6	Ph	Et	37
7	Ph	<i>i</i> Pr	37
8	Ph	Cy	48

*These aldoximes were synthesized by an alternative method *via* condensation of the corresponding aldehydes and hydroxylamine.

4 Biocatalytic cyanide-free synthesis of chiral nitriles

Because biotransformations of *E/Z*-mixtures of aldoximes does not lead to an enantioselective dehydration progress with OxdB, the isomers were attempted to be separated.^[180] Automated column chromatography with an equipped UV/vis-detector was chosen therefore (Figure 17). This method is based on the different polarities of *E*- and *Z*-isomers due to the spatial orientation of the hydroxyl moiety.

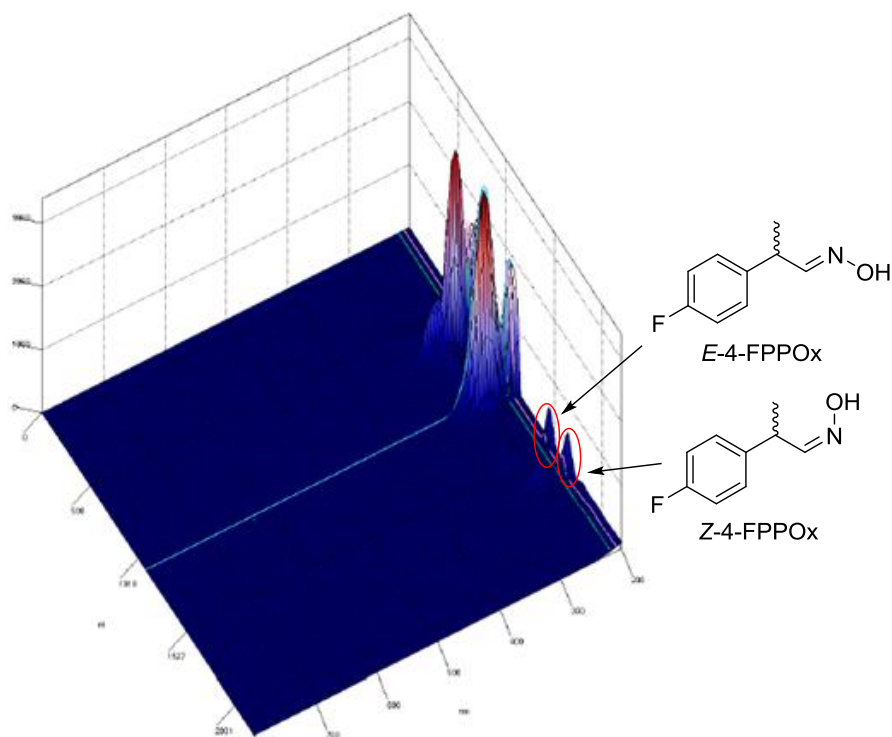


Figure 17. Visualization of the automated column chromatography of the crude product of 4-FPPOx synthesis (detection wavelength between 200 and 800 nm). *E*-4-FPPOx elutes before *Z*-4-FPPOx.

Both the *E*- and the *Z*-isomer of the synthesized 2-PPOx derivatives aldoximes were separated to an isomeric purity of up to 98 % (Table 16, Entries 5 to 10). However, for the heteroaromatic aldoximes the separation was not possible (Entries 3 and 4). Here the structural difference of the isomers is only marginal, thus, a difference in interaction with the silica was not given. Furthermore, some aldoximes can be prone to isomerization at ambient temperatures due to a low inversion barrier of between *E*- and *Z*-isomer. These substrates were only used as isomeric mixtures in biotransformations. No separation was attempted for the isomers of *Z*-PAOx, 2-PPOx and CyPAOx (Entries 1, 2, and 11).

4 Biocatalytic cyanide-free synthesis of chiral nitriles

Table 16. Isomeric ratios of the aldoximes separated with automated column chromatography.

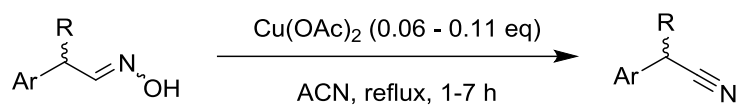
Entry	Substrate	<i>E/Z</i>	Isomer ratio [<i>E:Z</i>]
1	PAOx	<i>Z</i>	<1:99
2	2-PPOx	<i>E/Z</i>	70:30
3	TPOx	<i>E/Z</i>	70:30
4*	FPOx	<i>E/Z</i>	37:63
5	4-FPPOx	<i>E</i>	92:8
6	4-FPPOx	<i>Z</i>	3:97
7	EtPAOx	<i>E</i>	96:4
8	EtPAOx	<i>Z</i>	3:97
9	iPrPAOx	<i>E</i>	97:3
10	iPrPAOx	<i>Z</i>	2:98
11	CyPAOx	<i>E/Z</i>	15:85

*FPOx was purified *via* non-automated column chromatography. It was not possible to further separate the isomers.

In order to confirm the product formation in the biotransformation, the corresponding nitriles were necessary as a reference. Due to the simplicity of this procedure, the syntheses were carried out according to the protocol of *Ma et al.* utilizing copper(II) acetate as a catalyst for the transfer of water from the aldoxime to acetonitrile.^[89] All desired nitriles were obtained in moderate to very high yields (Table 17). Especially the yields for the bulky aldoximes (Entries 6 to 8) were exceeding 80 % for all substrates including an excellent yield of 99 % for 2-phenylbutyronitrile (EtPAN). 2-(Furan-2-yl)propionitrile (FPN) was only obtained in a yield of 16 % by an alternative dehydration method. This experiment was performed before the establishment of the copper(II) acetate-mediated dehydration. As the reference compound was obtained, no new synthesis attempt was necessary.

4 Biocatalytic cyanide-free synthesis of chiral nitriles

Table 17. Reaction conditions and isolated yields of the copper(II) acetate-catalyzed dehydration of aldoximes to the corresponding racemic nitriles.



Entry	Ar	R	Isol. yield [%]
1	Thiophen-2-yl	Me	68
2*	Furan-2-yl	Me	16
3	4-Fluorophenyl	Me	50
4	Ph	H	68
5	Ph	Me	63
6	Ph	Et	99
7	Ph	<i>i</i> Pr	80
8	Ph	Cy	93

*This nitrile was synthesized *via* triphenylphosphaneoxide-catalyzed dehydration with oxalylchloride.

4.4 Formation of chiral nitriles by dehydration of aromatic aldoximes

4.4.1 Substituted aromatic derivatives of 2-phenylpropionaldoxime

With the separated isomers of the aldoximes in hand, the next step in this study was the biocatalytic aldoxime dehydration with Oxds. As previously mentioned, five recombinant aldoxime dehydratases were available as catalysts. These Oxds were expressed in microaerobic shaking flask cultures with a glucose-based auto-induction medium (AI-medium), as a convenient alternative to their individual optimized expression protocols. The overexpression of the Oxds was verified *via* SDS-PAGE analysis (Figure 18). Sufficient overexpression of the Oxds (~40 kDa) at comparable expression levels of soluble protein was verified in the analysis. Besides the typical *E. coli* inclusion bodies, some inclusion bodies of Oxds were contained in the insoluble fraction. A detailed analysis thereof was not necessary for the research target at this point.

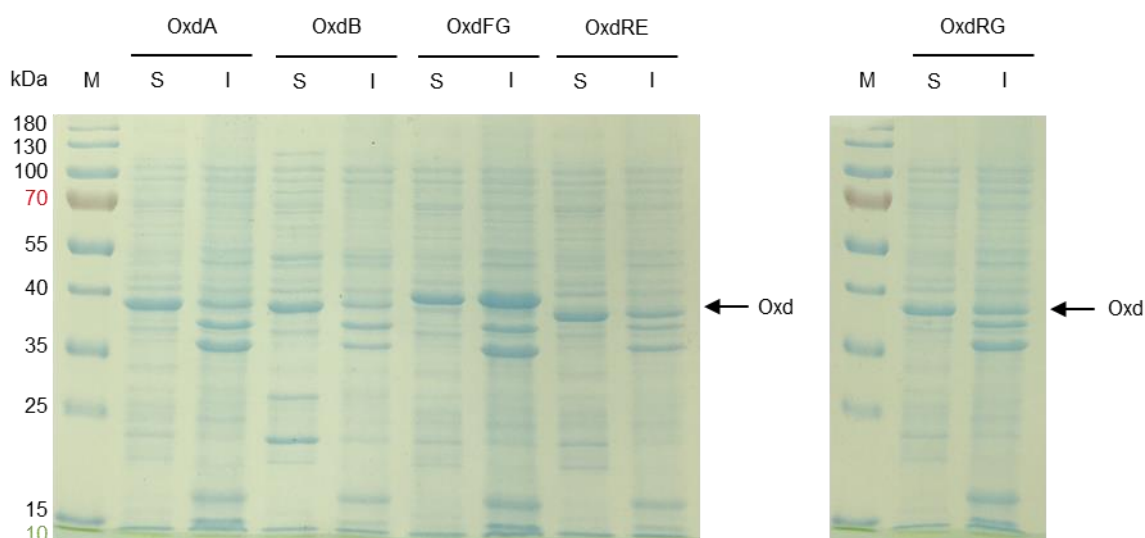


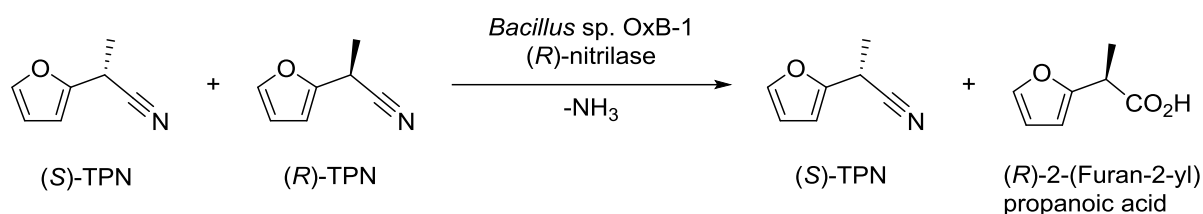
Figure 18. Expression analysis of Oxds *via* SDS-PAGE. M: Marker, Lane I: OxdA (soluble fraction), Lane II: OxdA (insoluble fraction), Lane III: OxdB (soluble fraction), Lane IV: OxdB (insoluble fraction), Lane V: OxdFG (soluble fraction), Lane VI: OxdFG (insoluble fraction), Lane VII: Oxdre (soluble fraction), Lane VIII: Oxdre (insoluble fraction), Lane IX: OxdRG (soluble fraction), Lane X: OxdRG (insoluble fraction).

Metzner et al. already investigated suitable reaction conditions for the Oxd-catalyzed aldoxime dehydration.^[180] Even though the activities are remarkably lower compared to when run at 30 °C, the dehydrations were performed at 8 °C in order to avoid isomerization of the substrates. A neutral pH of 7.0 was chosen as the best compromise of the individual characteristics of the enzymes (chapter 2, Table 5). Oxds were utilized as whole-cell catalysts for an increased enzyme stability as previously described in literature.^[179,180] The conversions of the biotransformations were determined with RP-HPLC in comparison to a calibration curve and the *ee*-values were determined from the relative integrals of the isomers in normal phase

4 Biocatalytic cyanide-free synthesis of chiral nitriles

HPLC (NP-HPLC) on chiral columns. First, the *E/Z*-mixtures heteroaromatic aldoximes were investigated (Table 18).

Due to the research goal of the original work, FPOx has been only tested in biotransformations with OxdB (Entry 1). Even though starting from a mixture containing 67 % *Z*-isomer, (*R*)-FPN was produced with 76 % ee at a conversion of 27 % after one hour reaction time. Taking into account that high enantiopurity of the formed nitrile was only achieved with highly isomerically pure 2-PPOx, this is a promising result. The absolute configuration of the nitrile was determined by comparison to pure enantiomers with chiral GC analysis. The retention time of the (*R*)-enantiomer was identified by digesting a racemic mixture of FPN with a highly (*R*)-selective nitrilase from *Bacillus* sp. OxB-1 overexpressed in *E. coli* forming the corresponding acid, leaving the (*S*)-enantiomer untouched (Scheme 54).



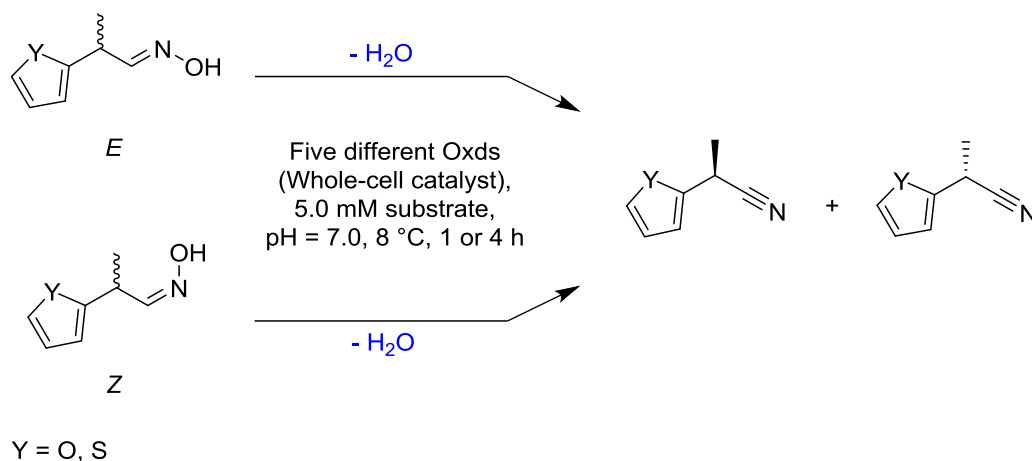
Scheme 54. Principle of the identification of the absolute configuration of FPN by resolution with the highly selective (*R*)-selective nitrilase from *Bacillus* sp. OxB-1.

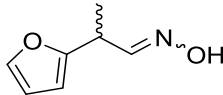
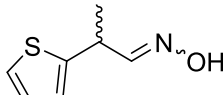
For a mixture of TPOx containing 70 % *E*-isomer, less enantioselective reaction progress was observed. One enantiomer of TPN could be obtained with 90 % ee when using OxDFG, however, only at a low conversion of 7 %. TPN-formation with OxdB was less selective, an ee-value of 23 % of the same enantiomer was achieved at a conversion of 10 %. In the biotransformations with OxDA, Oxdre, and OxDRG the opposite enantiomer of TPN was obtained with ee-values between 23 and 34 % at conversions between 18 and 45 %. The absolute configurations of TPN were not determined (indicated by the elution order of the enantiomers in the NP-HPLC measurements: “+” or “-” in brackets). Here, the first time a different selectivity of the Oxds has been observed. For 2-PPOx, the (*S*)-nitrile is preferably formed from the *E*-aldoxime while the (*R*)-nitrile is formed from the *Z*-aldoxime. Also for FPOx, the (*R*)-nitrile was formed from a *Z*-aldoxime enriched mixture with OxdB. One could speculate that OxDA, Oxdre, and OxDRG form the (*S*)-enantiomer of TPN starting from the *E*-isomer enriched TPOx solution. The opposite enantioselectivity of OxdB and OxDFG could be explained with the low conversions, which result from the low activity for this substrate or rather the given isomer. Under the presumption that OxdB and OxDFG convert only *Z*-FPOx, the theoretical maximum conversion of both enantiomers would be 30 %, thus, the maximal conversion of a perfect kinetic resolution would be 15 %. In this case, (*R*)-TPN will probably be formed in the biotransformations. These considerations could explain the opposite

4 Biocatalytic cyanide-free synthesis of chiral nitriles

enantioselectivity. The activities for the heteroaromatic substrates are in a range of up to $40 \text{ mU} \cdot \text{mg}_{\text{bww}}^{-1}$, which is low considering absolute number but still remarkable acknowledging the low temperature and the enzyme loading. Whole-cell catalysts contain mostly several other components as water, salts, lipids, and other enzymes.

Table 18. Conversions and ee-values for the biotransformation of isomeric mixtures of heteroaromatic derivatives of 2-PPOx with Oxds performed at 8 °C.



Entry	Substrate	Oxd	Conv. [%]	ee [%]
1	 <i>E/Z</i> 33:67	A	N.D.	N.D.
		B*	27	76 (<i>R</i>)
		FG	N.D.	N.D.
		RE	N.D.	N.D.
		RG	N.D.	N.D.
2	 <i>E/Z</i> 70:30	A	18	34 (-)
		B	10	23 (+)
		FG	7	90 (+)
		RE	28	27 (-)
		RG	45	32 (-)

*OxdB was expressed in *E. coli* JM109 under different conditions as described in the original work; (+) and (-) refer to the elution order of TPN in chiral NP-HPLC, no absolute configuration has been determined.

4.4.2 Identified lead structure for chiral aldoxime dehydration

While this thesis was focussed on the heteroaromatic derivatives of 2-PPOx, *Betke* and *Rommelmann* investigated other (aryl-)aliphatic, long-chain aliphatic, and cyclic aliphatic aldoximes.^[189,190] Also in their work, enantioselective transformations with at least one enzyme for all substrates has been observed. High ee-values over 90 % have been achieved for some substrates even at more elevated conversions of >25 %. Summarizing the results of this substrate screening and the results from *Metzner et al.*,^[180] a privileged substrate structure

4 Biocatalytic cyanide-free synthesis of chiral nitriles

could have been proposed (Figure 19). Especially 2-PPOx, was dehydrated highly enantioselectively by all Oxds (Rommelmann, Table 20, Entry 1) and represents this structure.^[189]

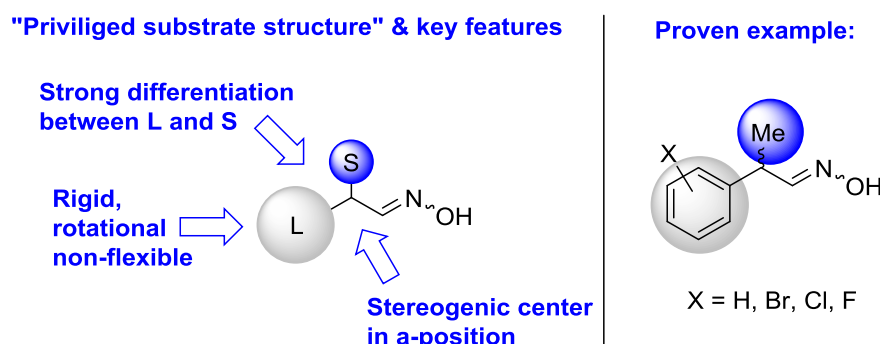


Figure 19. Proposed lead structure of substrate for which Oxds exhibit enantioselectivity (Adapted from T. Betker, P. Rommelmann, K. Oike, Y. Asano, H. Gröger, *Angew. Chem. Int. Ed.* **2017**, *56*, 12361-12366. Copyright © 2017, John Wiley & Sons, Inc.).^[196]

The key feature of this substrate structure is a stereogenic center in α -position to the aldoxime moiety with a strong differentiation of the substituents in size, where the larger substituent (L) should be rigid and rotational non-flexible, while the smaller one (S) should be flexible. For substrates not matching all criteria, such as long-chain aliphatic aldoximes, lower enantioselectivities have been observed. In order to prove this structure and investigate the effects of substituents on the aryl moiety, biotransformations have been carried out with halogen-substituted derivatives of 2-PPOx. In this work, 4-FPPOx as a representant of fluorine-derivatives is tested. Rommelmann and Betke utilized chlorine- and bromine-substituted 2-PPOx derivatives with different substitution patterns.^[189,190] These results will be discussed in combined form in the following part (Table 19).

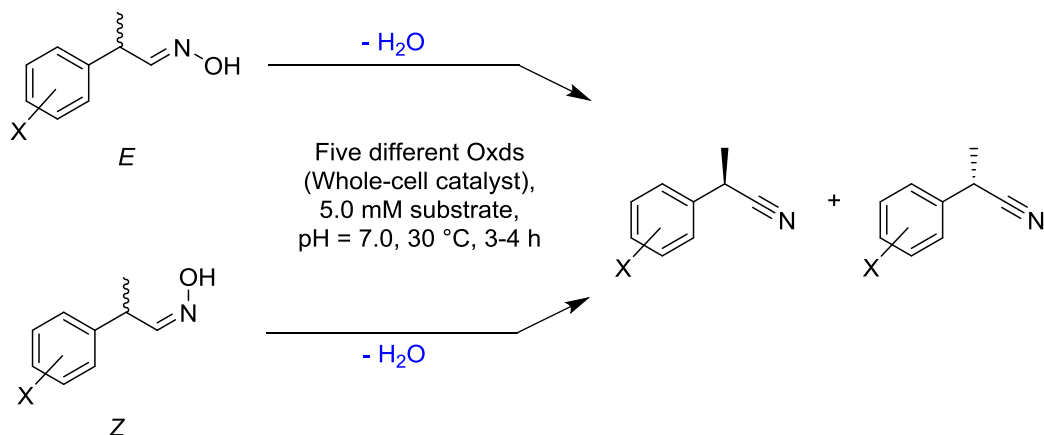
For each tested aldoxime, at least one enantiomer of the corresponding nitrile (usually both) was obtained with very good ee-values higher than 90 % at elevated conversions. All enzymes had substrates for which they were highly selective and those for which only slight activity and selectivity was observed. Especially OxDFG converted many substrates with high selectivity. The impact of the substitution pattern was comparable for all halogens substituents. The absolute configuration was only determined for selected nitriles and remained uninvestigated for the others. Therefore, these nitriles were synthesized and isolated in larger scale biotransformations, which allowed the determination of the absolute configuration by measurement of the specific rotation in comparison to literature values.^[189,190] The observation in the initial experiments, that the racemic *E*-aldoxime is favorably converted to the (*S*)-nitrile and the *Z*-aldoxime to the (*R*)-nitrile, was confirmed for all tested substrates containing the privileged structure motif. Furthermore, all five Oxds exhibited the same enantioselectivity for nearly all investigated substrates.

4 Biocatalytic cyanide-free synthesis of chiral nitriles

In detail, 4-FPPOx was a favorable substrate for OxdFG (Entries 1 and 2). Both enantiomers of the corresponding nitrile were accessible with this enzyme at high ee-values of 83 and 94 % at high conversions of 41 and 46 %, respectively. Also OxdA (for *E*-isomer) and OxdB (for *Z*-isomer) were suitable for achieving high ee-values of 4-FPPN of 97 and 93 %, however, at lower conversions. The activity and enantioselectivity was lower in the case of OxdRE and OxdRG regardless of the isomer given. Both isomers of the other *para*-substituted aldoximes were converted only by OxdB and OxdFG (Entries 7, 8, 13, and 14). Especially, selective dehydration was observed for the *E*-isomer of *para*-bromine substituted 2-PPOx, where the corresponding nitrile was obtained with 99 % ee with OxdB (at 15 % conversion) and 96 % ee with OxdFG (at 33 % conversion). The *E*-isomer of *ortho*-chlorine substituted 2-PPOx was also converted highly selective especially by OxdA, OxdRE, and OxdRG (Entry 3) reaching ee-values of the (*S*)-nitrile between 97 and 99 % at moderate to elevated conversions. For its opposite isomer however, only poor selectivity was obtained with any enzyme (Entry 4). A similar selectivity was also observed for the *ortho*-bromine-substituted aldoxime (Entries 9 and 10). The *Z*-isomer of this aldoxime was not converted at all with any enzyme. For the *meta*-substituted 2-PPOx derivatives, all Oxds showed a *vice versa* preference for the *Z*-isomer. The corresponding *meta*-chloro- and *meta*-bromo-substituted 2-PPN derivatives were obtained highly selective with over 87 % ee at moderate to high conversions for most enzyme-substrate combinations (Entries 6 and 12). The more challenging *E*-isomers were only converted by OxdFG with lower activity and selectivity. (Entries 5 and 11).

4 Biocatalytic cyanide-free synthesis of chiral nitriles

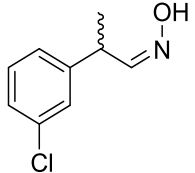
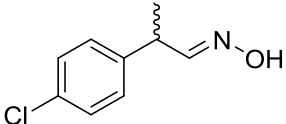
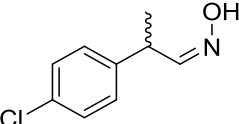
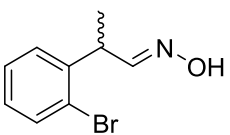
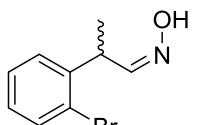
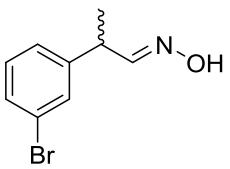
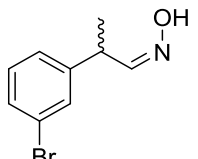
Table 19. Conversions and ee-values for the biotransformation of halogen-substituted 2-PPOx derivatives with isomerically pure aldoximes with Oxds performed at 8 °C.



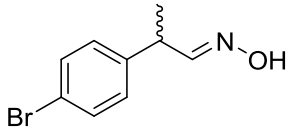
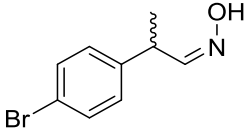
X = F, Cl, Br

Entry	Substrate	Oxd	Conv. [%]	ee [%]
1	 <i>E/Z</i> 92:8	A	15	97 (+)
		B	7	73 (+)
		FG	41	83 (+)
		RE	5	64(+)
		RG	6	67 (+)
2	 <i>E/Z</i> 3:97	A	6	52 (-)
		B	10	93 (-)
		FG	46	94 (-)
		RE	3	71 (-)
		RG	3	60 (-)
3*	 <i>E/Z</i> 99:1	A	12	97 (S)
		B	2	87 (S)
		FG	12	91 (S)
		RE	33	97 (S)
		RG	16	99 (S)
4*	 <i>E/Z</i> 1:99	A	5	2 (S)
		B	12	22 (S)
		FG	8	24 (R)
		RE	14	26 (R)
		RG	6	2 (R)
5*	 <i>E/Z</i> 99:1	A	-	-
		B	-	-
		FG	14	51 (S)
		RE	-	-
		RG	-	-

4 Biocatalytic cyanide-free synthesis of chiral nitriles

6*		A	10	93 (R)
		B	3	67 (R)
		FG	37	87 (R)
		RE	20	91 (R)
		RG	9	91 (R)
<i>E/Z</i> 1:99				
7*		A	-	-
		B	5	94 (+)
		FG	4	85 (+)
		RE	-	-
		RG	-	-
<i>E/Z</i> 99:1				
8*		A	-	-
		B	4	39 (-)
		FG	31	94 (-)
		RE	-	-
		RG	-	-
<i>E/Z</i> 1:99				
9**		A	39	88 (S)
		B	7	9 (S)
		FG	9	85 (S)
		RE	21	91 (S)
		RG	23	91 (S)
<i>E/Z</i> 99:1				
10**		A	-	-
		B	-	-
		FG	-	-
		RE	-	-
		RG	-	-
<i>E/Z</i> 4:96				
11**		A	-	-
		B	-	-
		FG	37	87 (S)
		RE	-	-
		RG	-	-
<i>E/Z</i> 96:4				
12**		A	38	94 (R)
		B	41	89 (R)
		FG	51	88 (R)
		RE	33	94 (R)
		RG	45	90 (R)
<i>E/Z</i> 5:95				

4 Biocatalytic cyanide-free synthesis of chiral nitriles

13**  <i>E/Z</i> 99:1	A	-	-
	B	15	99 (+)
	FG	33	96 (+)
	RE	-	-
	RG	-	-
14**  <i>E/Z</i> 10:90	A	-	-
	B	27	83 (-)
	FG	46	84 (-)
	RE	-	-
	RG	-	-

*These experiments were performed by *Rommelmann*.^[189] **These experiments were performed by *Betke*.^[190] The (+) and (-) refer to the elution order of the nitrile in chiral NP-HPLC measurements.

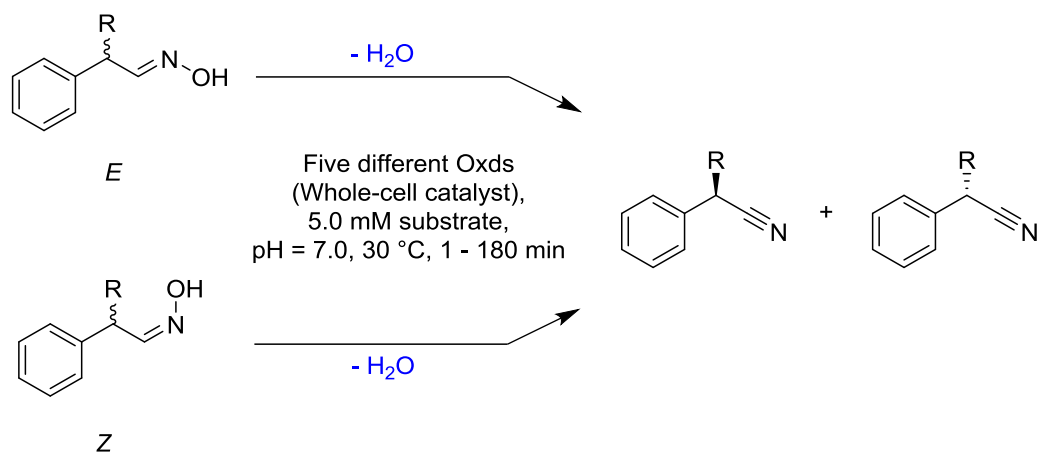
Considering that only wild-type enzymes were used in the experiments, very high enantioselectivity was observed for all tested substrates bearing this structural motif. All tested enzymes were suitable to produce nitriles enantioselectively. For substrates with larger substituents (chloro- and bromo-substituted), lower enzymatic activity was observed. With a glance on the crystal structure of OxdA and OxdRE, and docking simulations of OxdB, it can be assumed that the required space of the aromatic moiety is close to the limit of the cavity size in the active site. As a future perspective, further docking simulations with these substituted aromatic substrates would help to obtain further understanding of the enantioselectivity of Oxds and allow predictions for other substrates. Mutants designed with docking simulations may help to increase the substrate scope and selectivity of Oxds. While OxdA, OxdRE, and OxdRG have a high sequential similarity, OxdB and OxdFG are different compared to these enzymes. For these two enzymes, the crystal structure is not determined yet. Soaking of protein crystals with one of 2-PPOx derivatives could help to understand the larger substrate scope of OxdB and OxdFG. In conclusion, a promising applicability of Oxds for chiral nitrile synthesis was shown. Moreover, an interesting and unique feature in enzyme catalysis has been observed. In principle, both enantiomers of the nitriles can be produced with the same enzyme. The absolute configuration depends on the isomer of the aldoxime used.

4.4.3 Dehydration of bulky 2-phenylpropionaldoxime derivatives

High enantioselectivity of aldoxime dehydration with Oxds was limited on the defined structure (Figure 19). The differentiation between the substituents at the stereocenter in α -position to the aldoxime moiety was considered as an important feature. In the following part, the dehydration of bulky derivatives of 2-PPOx was investigated in order to check the limitations of substrate acceptance and further explore the proposed privileged structure motif, thus proving it.

Initially, the impact of the size of the smaller substituent in α -position was tested with isomeric mixtures of the bulky aldoximes (EtPAOx, *i*PrPAOx, CyPAOx). Considering the bulkiness the substituents, the activities were measured at 30 °C first to get an idea to what extent these substrates are suitable for Oxds (Figure 20). All five enzymes showed activity for the mixture of isomers of EtPAOx. For the aldoxime with an *iso*-propyl group in the α -position, all Oxds except OxdB were active. No enzyme showed activity for CyPAOx, the most bulky substrate. The highest activity for EtPAOx was observed with OxdFG with $10 \text{ mU}\cdot\text{mg}_{\text{bww}}^{-1}$, the other Oxds showed activities between 6.1 and $8.4 \text{ mU}\cdot\text{mg}_{\text{bww}}^{-1}$ and were therefore slightly less active. The activities for EtPAOx were approximately a power of ten lower compared the *E/Z*-mixture of 2-PPOx, where activities in the range of $130 \text{ mU}\cdot\text{mg}_{\text{bww}}^{-1}$ (OxdB) to $250 \text{ mU}\cdot\text{mg}_{\text{bww}}^{-1}$ (OxdA) were observed. For *i*PrPAOx, very low activities $<1.0 \text{ mU}\cdot\text{mg}_{\text{bww}}^{-1}$ were observed. With an increased size of the smaller substituent of this substrate, the activity decreased approximately by the power of ten. The activity of Oxds for these kind of aldoximes decreased with an increased space requirement. The most bulky substrate was not accepted. These results indicate a limitation of the cavity size in two spatial directions (where the aromatic and aliphatic substituent are positioned).

4 Biocatalytic cyanide-free synthesis of chiral nitriles



R = H, Me, Et, *i*Pr, Cy

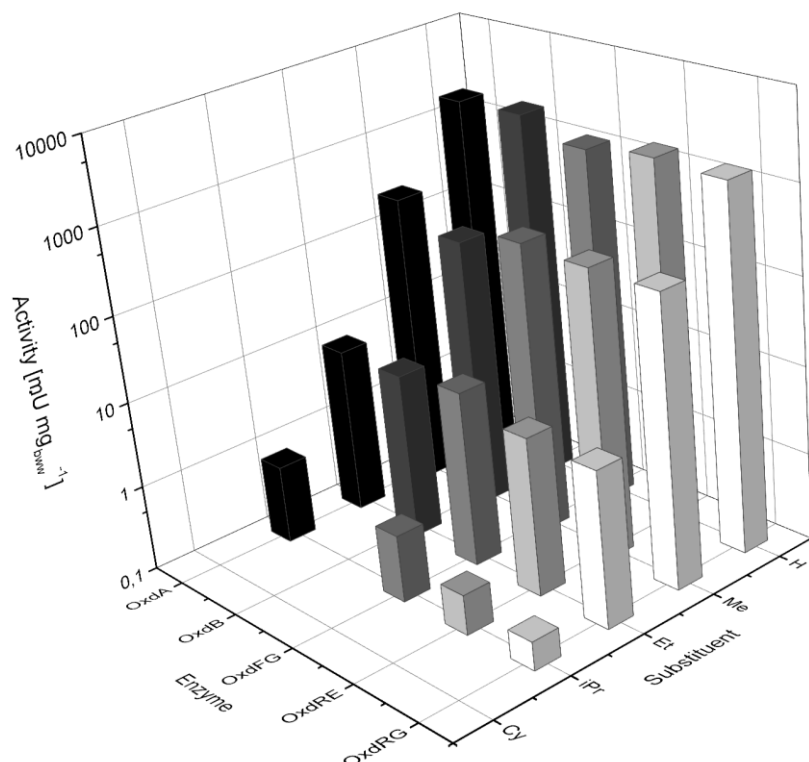


Figure 20. Activities of Oxds towards PAOx, racemic *E/Z*-mixtures of 2-PPOx and bulky derivatives thereof measured in biotransformations at 30 °C.

In the following, biotransformations were carried out with the separated isomers of both EtPAOx and *i*PrPAOx according to the previous method at 8 °C (Table 20). The isomerization of the bulkier substrates seem to be slower compared to those 2-PPOx and its other derivatives. This reaction system again is representing a simple kinetic resolution. While Oxda, Oxdre and OxdrG produced one enantiomer of EtPAN with moderate *ee*-values between 59 % and 73 % at low conversions of up to 24 % starting the *E*-isomer of EtPAOx, more selective transformations were observed with OxdB and Oxdfg (Entry 2). When using OxdB,

4 Biocatalytic cyanide-free synthesis of chiral nitriles

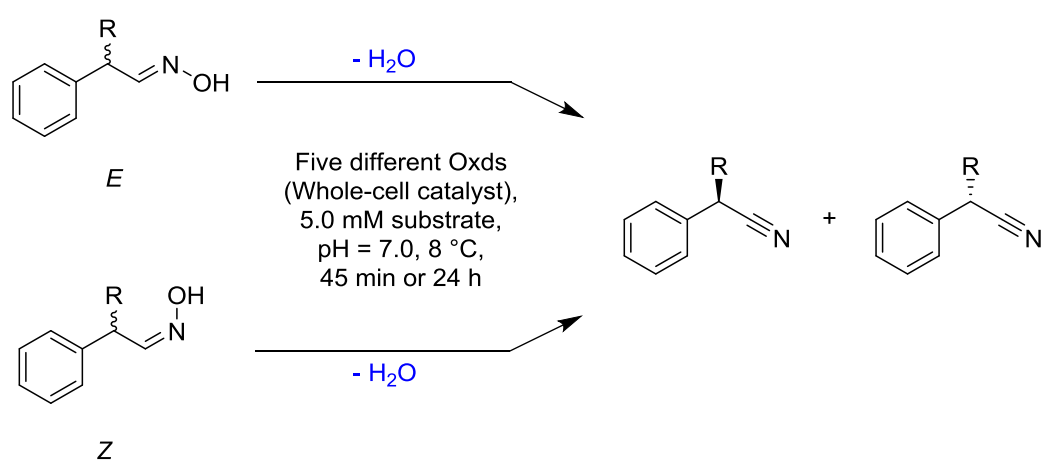
a very high *ee*-value of 71 % regarding the conversion of 58 % was observed. The same applies for the *ee*-value of 94 % achieved at 51 % conversion observed with OxDFG. The selectivity of OxdB and OxDFG corresponds to an *E*-value exceeding 30, which suggests excellent applicability of these kinetic resolutions. In general, it is hard to determine accurate *E*-values if the value exceeds 100 due to the natural errors of the measurement (HPLC). In this case, both the conversion and the *ee*-value are determined separately *via* RP-HPLC and NP-HPLC measurements, respectively. The calculation of the *E*-value becomes inaccurate when conversions of over 50 % were observed. If the conversions or *ee*-values only vary inside a range of ± 1 %, which is a reasonable natural error, theoretically impossible values might be obtained. Therefore, *E*-values are not given more accurate.

For *Z*-EtPAOx the opposite image of selectivity has been obtained (Entry 3). The biotransformation with OxdB led to a moderate *ee* of 82 % at 29 % conversion. For OxDFG a moderate *ee* of 74 % was achieved at 44 % conversion. These values correspond to *E*-values of 14 and 11, respectively, which suggest no or only poor applicability for kinetic resolutions. In contrast to the *E*-isomer, highly selective reaction progress was observed with OxDA, OxDRE, and OxDRG. This is represented by *ee*-values of 72 % (OxDRE, OxDRG) to 75 % (OxDA) at conversions of 58 % (OxDRE, OxDRG) and 57 % (OxDA), respectively. These results also correspond to *E*-values exceeding 30 for all three enzymes. In accordance to previous observations, all Oxds produced favorably the opposite enantiomer of the corresponding nitrile whether starting from the *E*- or *Z*-isomer of EtPAOx. Assuming an analogue substrate binding in the active site compared to 2-PPOx and its halogen-substituted derivatives, a similar selectivity for EtPAOx is likely. Thus, (*S*)-EtPAN might be from *E*-EtPAOx and (*R*)-EtPAN from *Z*-EtPAOx. Due to a lack of reference of the enantiomerically pure nitriles, a determination of the absolute configuration was not possible without crystallization of the product, thus, this hypothesis remained unproved. The enantioselectivity was in the same range compared to 2-PPOx. For *E*-2-PPOx, *Rommelmann* observed *ee*-values of 91 to 94 % at conversions of 25 and 26 % (Entry 1) with all five Oxds.^[189] The *E*-values of this transformations between 27 and 42 (at an isomeric purity of 94 %) indicate similar selectivity compared to *E*-EtPAOx (OxDB, OxDFG). OxDA, OxDRE and OxDRG were less selective for *E*-EtPAOx. With a higher isomeric purity of 99 % of *E*-2-PPOx however, *Metzner et al.* observed an *E*-value of >100 using OxdB.^[180] The isomeric purity of *E*- and *Z*-EtPAOx was also not perfect with 96 and 97 %. The small amounts of the opposite isomer contained can be neglected at conversions higher than 50 %, as all favored enantiomer is converted at this point anyway.

4 Biocatalytic cyanide-free synthesis of chiral nitriles

Only the *Z*-isomer of *i*PrPAOx was accepted by the Oxds (Entry 5) active for this substrate, while the *E*-isomer was only accepted by Oxdfg (Entry 4). The *ee*-value of *i*PrPAN did not exceed 56 % observed at a conversion of 2 % for *E*-*i*PrPAOx with Oxdfg. In the biotransformations of *Z*-*i*PrPAOx with Oxda and Oxdre, only low *ee*-values of 29 and 22 % were achieved at conversions of 9 and 6 %, respectively. The selectivity with Oxdfg was even lower for the *Z*-isomer. OxdrG, the enzyme with the lowest relative activity for *i*PrPAOx, formed a racemic nitrile even at a low conversion of 4 %. In spite of the low enantioselectivity, the *vice versa* enantioselectivity was again observed with Oxdfg.

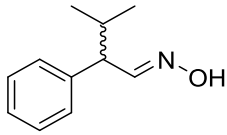
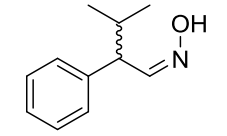
Table 20. Conversions and *ee*-values for the biotransformation of isomerically pure 2-PPOx and bulkier derivatives thereof with Oxds performed at 8 °C.



R = Me, Et, *i*Pr

Entry	Substrate	Oxd	Conv. [%]	<i>ee</i> [%]
1*	 <i>E/Z</i> 94:6	A	25	91 (S)
		B	26	94 (S)
		FG	25	93 (S)
		RE	26	92 (S)
		RG	25	92 (S)
2	 <i>E/Z</i> 96:4	A	24	73 (-)
		B	58	71 (-)
		FG	51	94 (-)
		RE	16	64 (-)
		RG	13	59 (-)
3	 <i>E/Z</i> 3:97	A	57	75 (+)
		B	29	82 (+)
		FG	44	74 (+)
		RE	58	72 (+)
		RG	58	72 (+)

4 Biocatalytic cyanide-free synthesis of chiral nitriles

4	 <i>E/Z</i> 97:3	A	-	-
		B	-	-
		FG	2	56 (-)
		RE	-	-
		RG	-	-
5	 <i>E/Z</i> 2:98	A	9	29 (+)
		B	-	-
		FG	5	40 (+)
		RE	6	22 (+)
		RG	4	0

*These experiments were performed by *Rommelmann*;^[189] The (+) and (-) refer to the elution order of the nitrile in chiral NP-HPLC measurements.

The observed results with the bulkier derivatives of 2-PPOx fit also to the proposed privileged substrate structure and serve as a proof for it. The bulkiness of the substituent decreased the reactivity of the enzymes remarkably ($\sim 10 \text{ mU} \cdot \text{mg}_{\text{bww}}^{-1}$ at 30 °C for *E/Z*-EtPAOx). Nevertheless, conversions of 50 % and higher were achieved in the kinetic resolutions with isomerically pure aldoximes at 8 °C. Moreover, it is interesting that a larger substrate size, while decreasing the activity, leads to a nearly complete loss of enantioselectivity. While the aldoxime with an ethyl group at the stereocenter was converted selectively, the addition of a single methyl group decreased the selectivity enormously. While the ethyl substituent is still quite small, the *iso*-propyl substituent is larger, thus, the differentiation in size compared to the phenyl substituent is smaller. Additionally, in *t*PrPAOx both substituents (Ph, *t*Pr) bear a similar symmetry element, a rotary mirror, which is not the case for the substituents in EtPAOx (Ph, Et). The ethyl group has a higher rotational flexibility compared to the *iso*-propyl group. Possibly, if a substrate is slightly too large to fit in the cavity, substrate binding is only seen in specific constitutions of the active site occurring in a low percentage. However, selectivity might not be given in these constitutions, thus, less selective reaction progress might be observed.

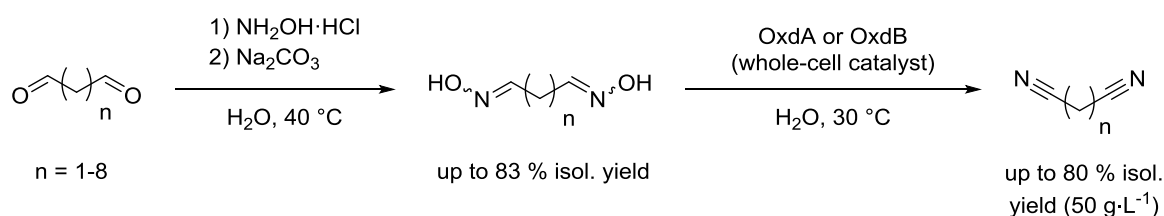
4 Biocatalytic cyanide-free synthesis of chiral nitriles

Docking simulations and crystallization experiments could give an explanation for the enantioselectivity. The rationalization of the enantioselectivity of Oxds is one bottleneck for their application chiral nitrile synthesis with not-tested molecules and for successful introduction of manipulations into the active site. Another bottleneck is still the preparation of the isomerically pure aldoximes. Even for the tested systems, not all aldoximes were obtained with high isomeric purity, which is crucial for successful dehydration giving optically pure nitriles. This hurdle could be overcome by using a synthesis route yielding only one isomer of the aldoximes or by their separation by crystallization. The establishment of a dynamic kinetic resolution featuring aldoxime racemization might be a suitable approach to theoretically produce the nitrile in 100 % yield. Engineering of Oxds towards a higher enantiopreference for one enantiomer would be facilitating such a resolution.

5 Initial development towards a cascade for the synthesis of fatty nitriles from fatty acids

5.1 Novel biocatalytic synthesis of adiponitrile and fatty nitriles

Recently, *Betke et al.* reported the use of OxdA and OxdB in a synthetic cascade reaction forming adiponitrile (Scheme 55, $n = 6$). The novel approach towards this dinitrile also proves that an Oxd-catalyzed dehydration of (di)aloximes can be a synthetic alternative to common synthesis routes for aliphatic (di)nitriles such as hydrocyanation. Adiponitrile was synthesized at yields of up to 80 % from substrate loadings of $50 \text{ g}\cdot\text{L}^{-1}$ hexane-1,6-dialdoxime in 100 mL reaction scale. Also in one liter reaction volume, full conversion was obtained at the same substrate loading achieving an isolated yield of 62 %. However, the substrate scope of the aliphatic dialdoximes was quite narrow. The activity of Oxds decreased for dialdoximes with shorter or longer chain lengths apart from six or seven carbon atoms.^[197]



Scheme 55. Synthesis of aliphatic dinitriles from dialdehydes *via* condensation of dialdehydes with hydroxylamine hydrochloride and subsequent biocatalytic dehydration with OxdA or OxdB.^[197]

Especially in consideration of the low prices of bulk chemicals, the high substrate loading (or space-time yield) necessary for efficient processes is a challenging factor for enzyme catalysis in this segment. There are still only a few enzymes applied as catalysts in this field, especially nitrile hydratases or nitrilases (see chapter 1).^[10,24] Another challenging factor is the efficient production of enzymatic catalysts. In order to keep the costs low, efficient high-cell density fermentative processes producing the enzymes from cheap carbon sources such as glycerol or glucose are necessary.^[198,199] Beside adiponitrile, aliphatic nitriles are of high interest for the chemical industry. They are widely applied in organic synthesis e.g. as solvents and are key intermediates in the production of surfactants, agrochemicals and also pharmaceuticals.^[71] Also fatty amines, which are used in detergents, softeners, lubricants, fungicides, etc. are derived from the nitriles.^[200] In analogy to adiponitrile, most approaches to these aliphatic nitriles are using the highly toxic hydrogen cyanide as nitrile source.^[75,201] A process under milder conditions for synthesis of these nitriles, preferably avoiding hydrogen cyanide, would be desirable.

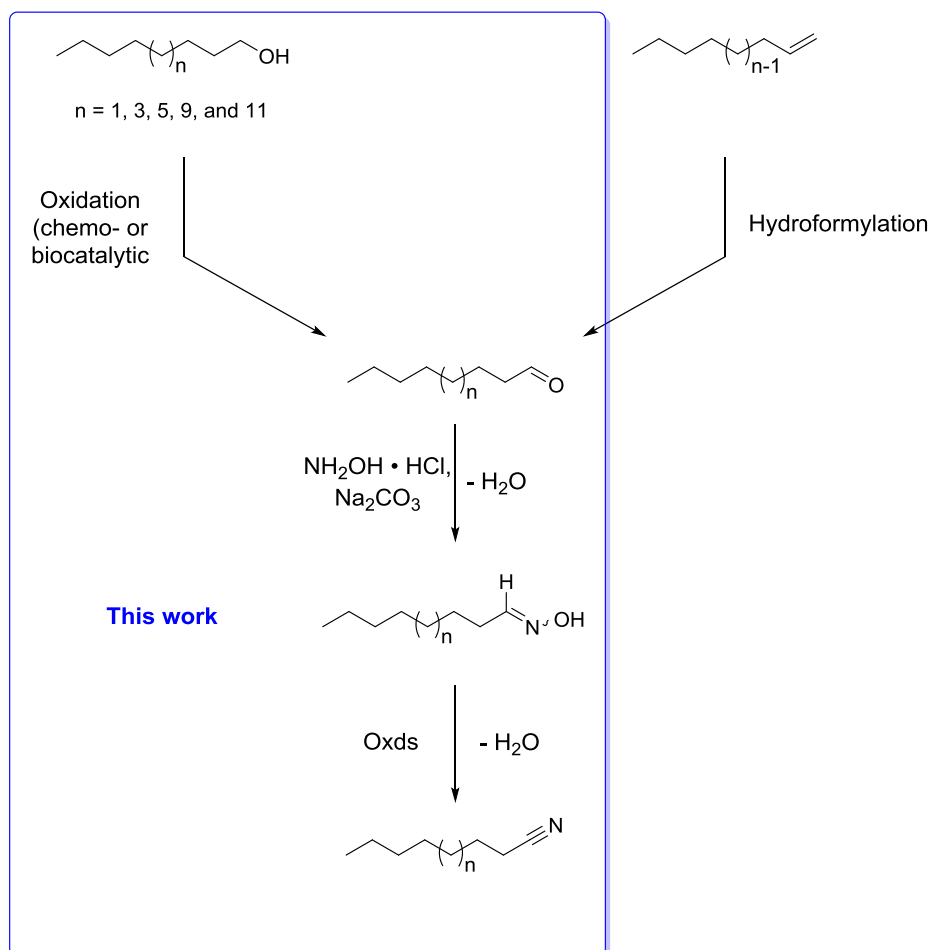
Regarding a sustainable synthesis route, the educts have to be considered as well. For example, fatty acids are discussed as an alternative feedstock in the chemical industry. They

5 Initial development towards a cascade for the synthesis of fatty nitriles from fatty acids

can be produced from biorenewable sources, e.g. the fermentation of microbes and isolation from plants by cleavage of triglycerides. Most fatty acids occurring in nature have chain lengths with an even number of carbon atoms.^[202] They can be efficiently hydrogenated to fatty alcohols.^[203] Therefore, another important step towards nitrile production employing aldoxime dehydration is the synthesis of aldoximes from alcohols. While the typical preparation of aldoximes by condensation of aldehydes with hydroxylamine hydrochloride proceeds usually smoothly to full conversion, the selective oxidation from alcohols towards aldehydes is more challenging. Hydroxylamine as a nitrogen source is not a green chemical yet, however, microbial synthesis of this compound from ammonia (which is also perspectivevely available greenly) is under investigation and is possible in principle.^[204] Many selective oxidations of alcohols to aldehydes require unfavorable conditions such as low temperature or toxic agents. An example for a greener oxidation method is the TEMPO-catalyzed oxidation using for example hydrogen peroxide as oxidant. Alternatively, an enzymatic approach would also be possible for example with ADHs.

5.2 Motivation

The main research goal in this chapter is getting an initial insight in the nitrile production from biorenewable sources. The future goal would be to establish a reaction cascade from fatty alcohols towards the corresponding nitriles (Scheme 56).



Scheme 56. Hypothetical reaction sequence for the formation of fatty nitriles starting from fatty alcohols (blue) or alkenes.

In the following, each reaction step towards the nitrile will be investigated. Therefore, catalytic methods with cheap reagents, which are at least by some extent considered as green, will be used. First, biocatalytic and chemical oxidation reactions of alcohols with even numbered chain lengths will be attempted and compared to each other. The condensation of aldehydes with hydroxylamine is considered trivial in the first place. Nevertheless, the aldoximes have to be synthesized as substrates for testing the activity of Oxds towards them. Besides substrates with even-numbered chain lengths, an odd-numbered substrate will also be tested for its compatibility. However, this substrate will not be generated from the alcohols but *via* hydroformylation of a terminal alkene (increasing the chain-length by one carbon atom). The hydroformylation experiments were carried out by Plass.^[205]

5.3 Initial development of a cascade reaction towards fatty nitriles

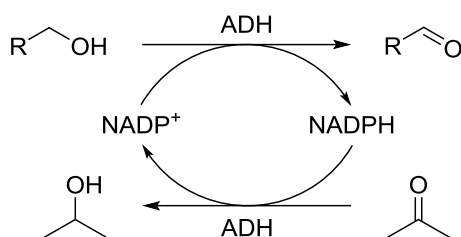
5.3.1 Alcohol oxidation with alcohol dehydrogenases

ADHs are widely applied for the reduction of alcohols towards chiral alcohols. Usually, the reduction reaction of ADHs is the favored direction of this equilibrium, thus oxidative transformations of alcohols to aldehydes or ketones are rarely reported. The selectivity of most ADHs towards secondary alcohols makes this task even more challenging.^[206] *Biermann* reported only low conversions for the oxidation of short-chain primary alcohols to the corresponding aldehydes. Nevertheless, aliphatic alcohols like 1-hexanol were at least accepted by two ADHs to a limited extent.^[207]

In order to investigate the alcohol oxidation with ADHs, a photometric assay for screening of the available catalysts would have been desirable. However, due to the high hydrophobicity of long-chain aliphatic alcohols, resulting in very low water solubility, a photometric approach without high ratios of a water miscible co-solvent is not possible. The aliphatic fatty alcohols could not be solubilized at 5.0 mM substrate concentration even in the presence of 10 or 20 % DMSO. Higher concentrations of DMSO would lead to a decreased enzyme stability or inhibition effects frequently reported for ADHs.^[208] Therefore, instead of determining enzymatic activities in the first place, the product formation was monitored in biotransformations, which were analyzed *via* GC analysis.

The ADHs from *Lactobacillus kefir* DSM 20587 (LkADH)^[209] and *P. pastoris* CBS 7435 (PpADH)^[210] were chosen for these experiments, as they were reported to accept primary alcohols in the study by *Biermann*.^[207] These enzymes were available in whole-cells from previous experiments of this working group. Biotransformations were performed in the presence of acetone. The two ADHs are able to reduce acetone to *iso*-propanol by means of NADPH oxidation (Scheme 57). The NADP⁺ consumed in the ADH-catalyzed oxidation can be recovered *in situ* by coupling the acetone reduction. An advantage of this reaction setup is the additional function of acetone as a co-solvent, which increases the solubility of the fatty alcohols in the buffer. Alternatives for cofactor regeneration would have been an approach coupled to the NAD(P)H-oxidation with so called NADH-oxidases, enzymes oxidizing the cofactor with molecular oxygen as oxidant forming only water as a byproduct.^[211]

5 Initial development towards a cascade for the synthesis of fatty nitriles from fatty acids



Scheme 57. Principle of the cofactor regeneration for ADH-catalyzed oxidation of primary alcohols *via* coupling the reduction of the co-substrate acetone with the same enzyme.^[211]

The aliphatic alcohols with a chain length of eight, ten and twelve carbon atoms were tested as substrates for the two available ADHs (Figure 21). The enzymes were applied as crude extracts. For 1-octanol at 20 mM substrate concentration, 2 % conversion to octanal was observed after one day reaction time with the PpADH. The LkADH converted 12 % of this primary alcohol to the aldehyde. For 1-decanol and 1-dodecanol, the conversion to the corresponding aldehyde was less than 1 % with the Lk-ADH. Also biotransformations with the PpADH only led to slightly higher conversions of 2 % for 1-decanol and 4 % for 1-dodecanol, respectively. These results indicate a general acceptance of this substrate structure with these two ADHs, however, their synthetic relevance is of no great impact. Biermann also observed only 2 % conversion of 1-hexanol to the corresponding aldehyde with the LkADH.^[207] Primary aliphatic alcohols are not a favored substrate structure of ADHs, which usually prefer secondary alcohols with one large and one small substituent. One reason for the unfavored activities is the high energetic level of the transition state occurring during the oxidation of primary alcohols. A further challenging point is the equilibrium of the reaction, which is on the side of the alcohol and not the aldehyde.^[212] The equilibrium position does not facilitate the oxidation also under the aspect of cofactor recycling. The aldehyde or ketone reduction as the reverse reaction, can be coupled with the oxidation of *iso*-propanol to acetone. In this setup, the formed acetone leaves the reaction solution by evaporation, thus, shifting the equilibrium on the product site. However, a coupling of the oxidation reaction would require a high excess of acetone and limiting the substrate loading further and add additional costs.

5 Initial development towards a cascade for the synthesis of fatty nitriles from fatty acids

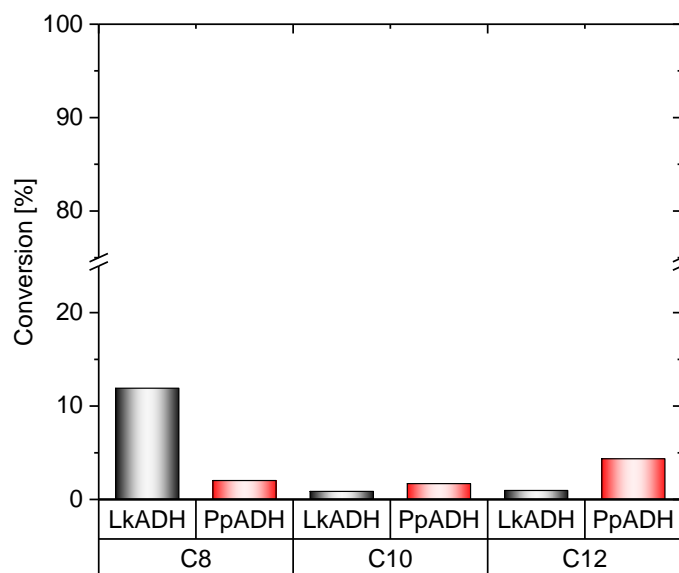
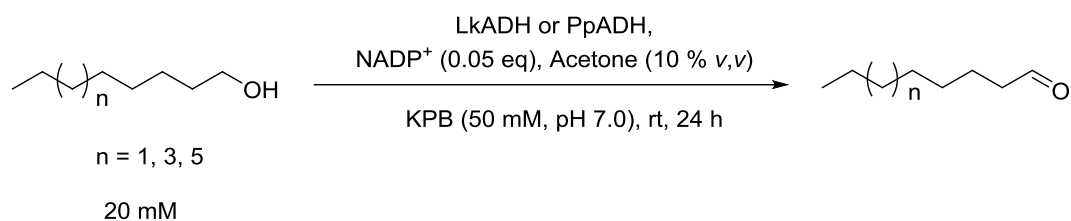


Figure 21. Conversions of biocatalytic oxidations of fatty alcohols (C₈ to C₁₂) to their corresponding aldehydes catalyzed by LkADH or PpADH.

5.3.2 Chemical alcohol oxidation

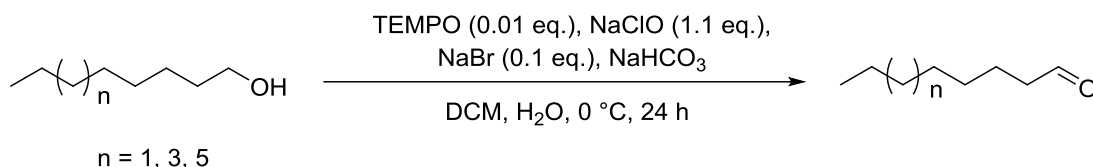
5.3.2.1 TEMPO-catalyzed oxidation of fatty alcohols

The TEMPO-catalyzed oxidation was tested for the C₈ to C₁₂-alcohols as an alternative to the biocatalytic oxidation with ADHs. The TEMPO-catalyzed oxidation is a catalytic reaction mediated by the metastable TEMPO-radical. This radical oxidizes the alcohol to the aldehyde, by being reduced. Oxidants such as sodium hypochlorite solved in water (or only given as pentahydrate crystals) are suitable to recycle the TEMPO-radical *in situ*.^[213] Sodium hypochlorite is also contained in bleach as a very cheap oxidant.^[214] Initial attempts for oxidation of the fatty alcohols *via* TEMPO-catalyzed oxidation with sodium hypochlorite as oxidant were carried out according to the conditions by *Biermann*.^[207] 1-Octanol, 1-decanol and 1-dodecanol were oxidized within a system consisting of the catalyst, sodium bromide as phase-transfer catalyst, sodium hydrogencarbonate and the oxidant in 1.1 equivalents (Table 21). Even under these unoptimized conditions, conversions between 20 and 26 % were observed according to ¹H-NMR analysis. TLC-experiments (with a universal iodine stain) suggested only very slight overoxidation of the aldehydes to the corresponding carboxylic acid.

5 Initial development towards a cascade for the synthesis of fatty nitriles from fatty acids

At this point, it was assumed that especially the oxidation power was not sufficient, thus, the usage of higher amounts of sodium hypochlorite would lead to improved conversions. These results were promising as an initial starting point for a more detailed investigation of the TEMPO-catalyzed oxidation carried out by *Busch and Hinzmann*.^[215]

Table 21. Reaction conditions of the TEMPO-catalyzed oxidation and conversions of the aldehydes according to ¹H-NMR spectroscopy.



Entry	Aldehyde	Conv. [%]
1	C ₈	20
2	C ₁₀	26
3	C ₁₂	23

5.3.2.2 Palladium-catalyzed oxidation of fatty alcohols

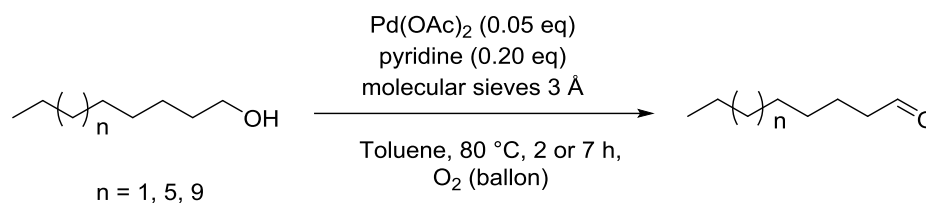
As an alternative, another homogeneous catalytic method reported in literature was tested.^[216] The oxidation of selected linear aliphatic alcohols to the corresponding aldehydes catalyzed by palladium(II) acetate was attempted. This catalytic system oxidizes the primary alcohols selectively in the absence of water by only requiring molecular oxygen as a green oxidant. Substrates with chain length of eight, twelve and 16 carbon atoms were tested (Table 22). An initial reaction with 1-octanol at 0.1 M substrate concentration in the presence of 5 mol% catalyst in 4 mL-scale was converted not totally towards the aldehyde (according to iodine-stained TLC). Workup *via* column chromatography yielded only a mixture of product and educt. The small scale of the reaction is assumed to be an especially disadvantageous setup. The oxidations performed in larger scale (30 mL) with the longer chain alcohols at longer reaction times led to full conversions (according to TLC). Yields of 50 and 30 % were achieved for 1-dodecanol (Entry 2) and 1-hexadecanol (Entry 3), respectively. For the fatty aldehydes decanal and hexadecanal *Nishimura et al.* reported isolated yields of 93 and 95 % (<96 % conversion), respectively.^[216]

A drawback of this synthetic protocol is the column chromatography necessary for workup of the reaction solution in order to remove the palladium-catalyst. Other methods such as celite filtration for removal of palladium could be investigated to optimize the yield. Nevertheless, full conversion proved in preparative scale was satisfactory for the initial test without any optimization of the purification and reaction conditions. Especially, small amounts of water are

5 Initial development towards a cascade for the synthesis of fatty nitriles from fatty acids

reported to have a negative effect on the conversion of this reaction.^[216] Both the TEMPO-catalyzed oxidation and the palladium(II) acetate-catalyzed oxidation were continued by Busch.^[215]

Table 22. Reaction conditions of the palladium(II) acetate-catalyzed oxidation of alcohols to aldehydes and the isolated yields.



Entry	Aldehyde	Isol. yield [%]
1*	C ₈	-
2	C ₁₂	50 (470 mg)
3	C ₁₆	30 (370 mg)

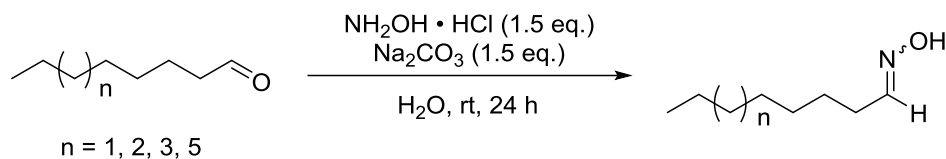
*Conversion was not complete (42 % according to ¹H NMR spectroscopy).

5.3.3 Synthesis of fatty aldoximes *via* condensation of aldehydes with hydroxylamine

In order to complete the cascade reaction towards fatty nitriles, the fatty aldoximes were required to be synthesized. All target substrates were not known in literature, but the classical condensation reaction of the corresponding aldehyde with hydroxylamine hydrochloride in water or a biphasic system is proceeding smoothly in most cases. For the initial studies, only the shorter-chain aldehydes up to a chain length of twelve carbon atoms were synthesized in a ten gram scale batch reaction. The reaction was performed in a biphasic system without addition of any additional organic solvent), as all fatty aldehydes are liquids (Table 23). Complete conversion was observed in all reactions according to TLC analysis and the product was removed from the reaction solution *via* liquid-liquid extraction. The new aldoximes were obtained in moderate yields of 24 to 40 % by recrystallization of the crude product from ethanol. The product loss is assumed to be occurring during the recrystallization step, which was neglectable in the initial stage of this project. The yields could possibly be raised by optimizing this procedure and repeating the recrystallization step for a few times. Most important was to obtain the new aldoximes for the transformation with Oxds (next chapter). At this point, it was neglected whether the *E*- or *Z*-isomer was formed preferably.

5 Initial development towards a cascade for the synthesis of fatty nitriles from fatty acids

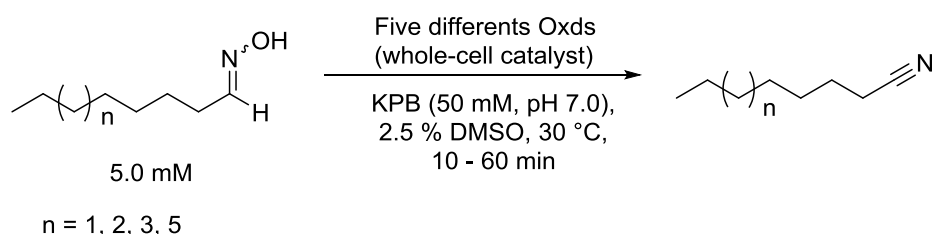
Table 23. Reaction conditions and yields of the condensation of fatty aldehydes with hydroxylamine hydrochloride forming the corresponding fatty aldoximes.



Entry	Aldoxime	Isol. yield [%]
1	C ₈	24
2	C ₉	32
3	C ₁₀	40
4	C ₁₂	39

5.3.4 Fatty nitrile synthesis *via* aldoxime dehydratase-catalyzed dehydration of fatty aldoximes

The aliphatic nitriles are known resources and commercially available, thus, they were not synthesized in this work. These compounds do not bear an aromatic group or a π -system, so GC was the desired method for analysis. For testing the substrate acceptance of the Oxds, biotransformations were performed with the synthesized aldoximes in analytical scale (500 μL reaction volume, Scheme 58).



Scheme 58. Biotransformation of fatty aldoximes with Oxds.

All Oxds showed activity for the tested substrates up to a chain length of twelve carbon atoms measured with 5.0 mM substrate concentration (Figure 22). While octanal oxime was dehydrated to octane nitrile with a conversion of up to 21 to 24 % even after ten minutes, conversions in a similar range were observed after 30 minutes reaction time for nonanal oxime. For these two substrates, all five tested Oxds showed only slight differences in their activities. For decanal oxime and dodecanal oxime, a further decrease of the enzymatic activity was observed. While 28 % conversion of decanal oxime were obtained in one hour reaction time with OxdB, the other Oxds (OxdA, OxdRE, OxdRG) converted the half amount of substrate in the same reaction time. The amount of formed nitrile was with 7 % even lower when using OxdFG. A maximum of only 3 % dodecane nitrile was formed in one hour reaction time with

5 Initial development towards a cascade for the synthesis of fatty nitriles from fatty acids

OxdRE or OxdRG. The other whole-cell catalysts were even less productive for this substrate. In general, all tested Oxds accept fatty aliphatic aldoximes and produce the corresponding nitriles, as observed *via* GC analysis. It was observed that an increased chain length led to lower activities. While the smaller substrates were accepted in a similar fashion from the Oxds, OxdRE and OxdRG converted dodecanal oxime slightly better. The aliphatic aldoximes tested here would hardly fit into the active site of Oxds in a linear configuration (estimated from comparison with the crystal structures and docking simulations available). Their rotational flexibility might make them fit well in the active site in their intricated configurations.

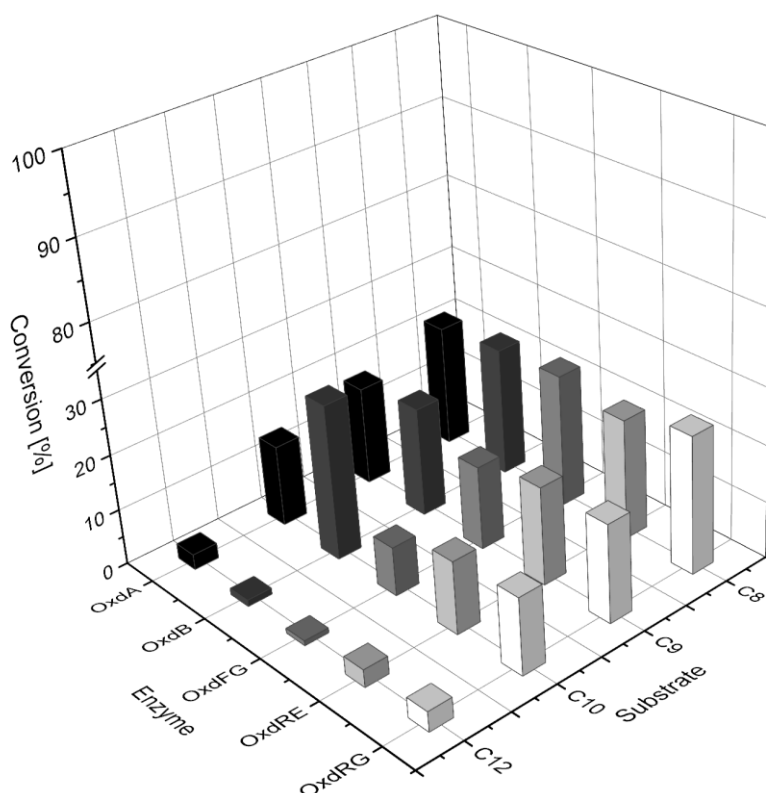


Figure 22. Conversions of biocatalytic aldoxime dehydration of fatty aldoximes with five Oxds after 10 (C₈), 30 (C₉), and 60 minutes (C₁₀, C₁₂).

While OxdFG often showed very good selectivity in the kinetic resolution of arylaliphatic aldoximes, the transformations of aliphatic aldoximes were not favored. The lower conversions might also be caused by the lower stability of this enzyme compared to the other Oxds (see chapter 2, Table 5). A biotransformation of nonanal oxime was performed at 10 mM substrate loading for three hours reaction time with all Oxds at 50 g·L⁻¹ enzyme loading in analytical scale (Figure 23) as a prove for quantitative nitrile production. While for OxdFG, OxdRE, OxdRG only low conversions not exceeding 35 % were observed, OxdA and OxdB were proved to be more suitable for preparative transformations. With OxdA a conversion of 82 % was achieved. Only OxdB fully converted this aldoxime to the corresponding nitrile.

5 Initial development towards a cascade for the synthesis of fatty nitriles from fatty acids

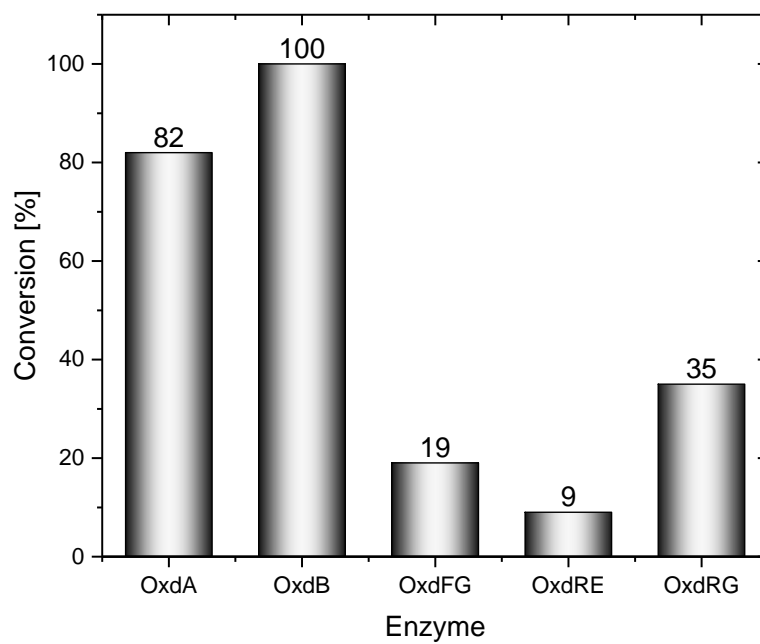


Figure 23. Conversions of 10 mM nonanal oxime to nonane nitrile with five Oxds after three hours reaction time.

5.4 Preparative application of the fatty nitrile synthesis cascade

Hinzmann et al. continued the investigation of the dehydration of aliphatic aldoximes with OxdB in larger scale.^[217] Even at elevated substrate concentrations of up to $1.4 \text{ kg}\cdot\text{L}^{-1}$ of 1-octanal oxime, a conversion of 93 % was observed. Full conversion of octane nitrile at $1.0 \text{ kg}\cdot\text{L}^{-1}$ total substrate loading was observed in a 250 mL batch reaction with $33 \text{ g}\cdot\text{L}^{-1}$ wet cells and a substrate feeding strategy. Workup was simple as the nitrile was forming a second phase, which just had to be separated in order to obtain pure nitrile in 86 % isolated yield (Figure 24). In consideration that OxdB is a heme-containing enzyme, the stability in this reaction medium is impressive.^[217]

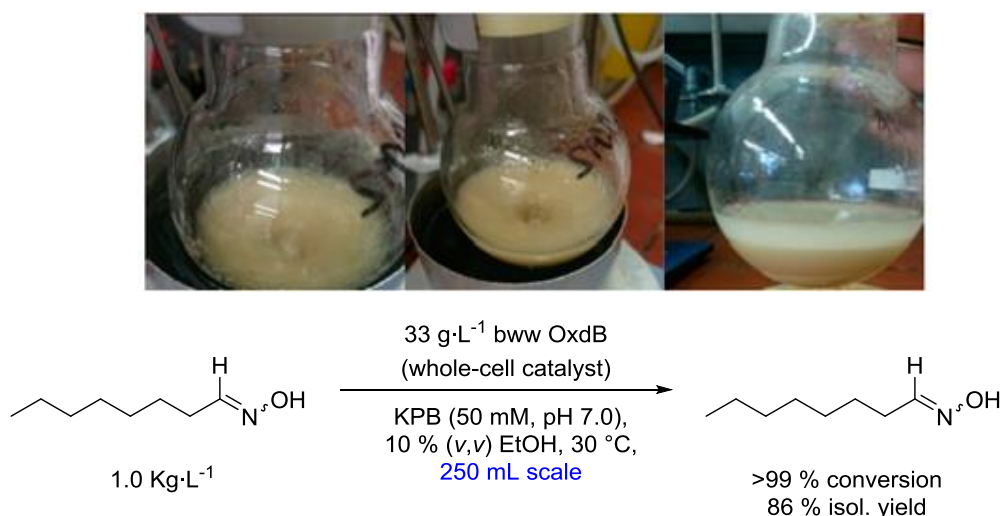
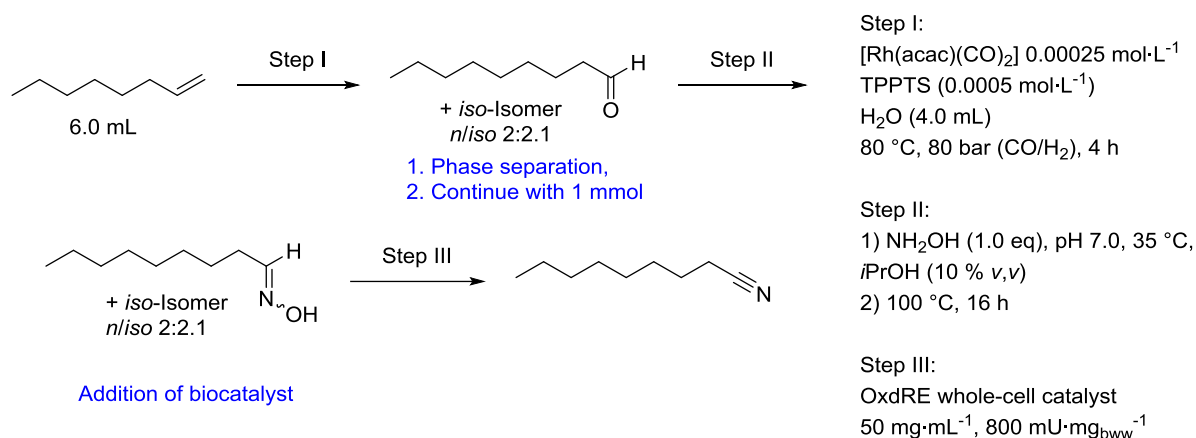


Figure 24. Dehydration of octanal oxime to octane nitrile catalyzed by Oxds and reaction solution while and after the stirring. Phase separation between the organic phase consisted of only the desired nitrile after the reaction is shown above (Adapted with permission from A. Hinzmann, S. Glinski, M. Worm, H. Gröger, *J. Org. Chem.* **2019**, *84*, 4867–4872. Copyright © 2019, American Chemical Society).^[217]

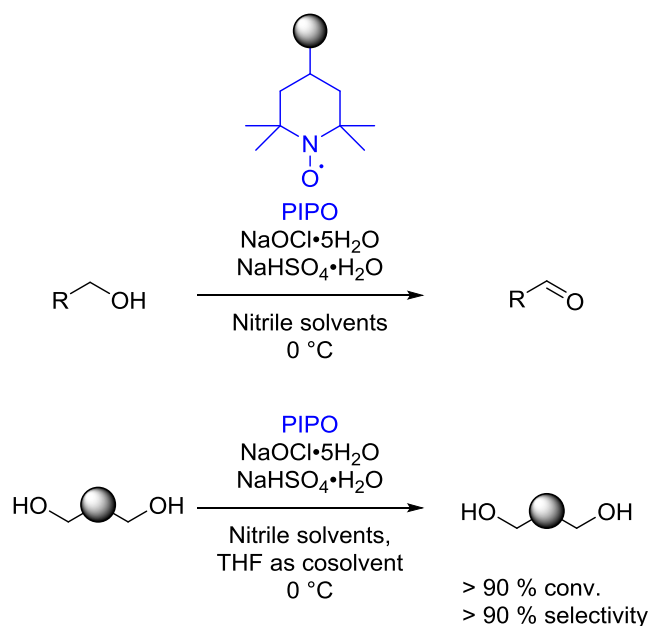
The investigated dehydration of nonanal was successfully implemented in a cascade proceeding *via* hydroformylation of 1-octene (Scheme 59, the principle, actual experiments carried out by *Plass* and other coworkers). In this cascade, first the hydroformylation is performed with 1-octene in presence of water and a rhodium complex, yielding a mixture of *n*- and *iso*-aldehydes. These were only separated by extraction and then condensed with hydroxylamine forming the aldoximes. In order to avoid strong inhibitory effects of remaining hydroxylamine on the Oxds as reported in earlier works,^[179] the reaction mixture was heated before addition of the biocatalyst. The dehydration of the aldoximes is performed with a catalyst loading of $50 \text{ g}\cdot\text{L}^{-1}$ OxdRE whole-cells giving an overall conversion of 67 % nonane nitrile over all steps. OxdB was not chosen as it shows poor activity against the *iso*-aldoxime. Related on the last step, the nitriles (*n*- and *iso*- mixture) were isolated in 41 % yield.^[218]

5 Initial development towards a cascade for the synthesis of fatty nitriles from fatty acids



Scheme 59. Reaction sequence for synthesis of nonane nitrile from 1-octene without workup steps.^[218]

The TEMPO-catalyzed oxidation of fatty alcohols was further investigated by *Hinzmann, Stricker and Busch*.^[215,219,220] Several parameters were investigated and the reaction conditions were optimized (Scheme 60). With the use of a polymer immobilized TEMPO-catalyst (PIPO) and sodium hypochlorite pentahydrate as oxidant, very good conversions exceeding 90 % with high selectivity were observed for the reaction running in nitriles as solvents. Both fatty alcohols and dialcohols were suitable to be oxidized with this protocol.^[221]



Scheme 60. PIPO-catalyzed oxidation of primary (di)alcohols with sodium hypochlorite pentahydrate as oxidant.^[221]

5.5 Fermentative production of aldoxime dehydratases

The synthetic applications described in the last section show a promising applicability of OxdB regarding bulk chemistry synthesis. However, the bottleneck of the enzyme supply in sufficient amounts is still required to be addressed. High cell-density fermentation is necessary for the application of biocatalysts in industrial processes. Therefore, usually highly optimized processes are necessary for efficient production of the desired enzyme (or whole-cell catalyst). The medium should be cheap and broadly applicable.^[198] Aldoxime dehydratases have been discovered about 20 years ago and are not applied in industry yet. Only optimized cultures in shaking flasks have been performed so far.

5.5.1 Fermentation of cytochrom P450 monooxygenases

CYP enzymes, which share the heme cofactor with Oxds, are a frequently investigated enzyme class. Nevertheless, expression of these proteins has been proved to be difficult in larger scale due to functionalization necessary for expression. The liability of the heme iron against oxidation is a further observed problem.^[222] Pflug *et al.* reported the successful fed-batch fermentation of a CYP enzyme from *Bacillus megaterium* (CYP102A1) in *E. coli*. For fermentative processes, the activity and enzyme production rates are usually compared to expression in shaking flasks as reference. In these experiments, the expression of this CYP enzyme under microaerobic conditions proved to be advantageous. When these conditions were applied to a fed-batch process in a 5.0 L bioreactor, fermentation was first carried out with glucose at lower levels of oxygen saturation (DO-value).^[223] Under these culture conditions, the formation of acetate was observed as a product of glucose metabolism. Acetate formation is a technical problem observed for growth of *E. coli* under microaerobic or anaerobic conditions. The exchange of the carbon-source from glucose to glycerol is reported to avoid acetate formation in anaerobic glucose metabolism in *E. coli*.^[199] Moreover, the use of glycerol as carbon source is reported to have an improving effect on recombinant protein expression in fermentation of *E. coli*.^[224] With the switch of the carbon-source, a stable process at DO-levels under 2 % for the production of CYP102A1 was carried out for 29 hours (Figure 25). With this adjustment, the protein could be produced in large amounts showing with production yield and specific activity close to the shaking flask expression.^[223]

Except this successful fermentative process, only Zhang *et al.* reported the batch fermentation of another CYP enzyme from *Rhodococcus* sp. expressed highly active in *E. coli* BL21(DE3) as a whole-cell catalyst. This process was also carried out at low DO-levels <10 % with glucose as carbon source. However, if the batch fermentation was followed by a feed-phase with glycerol based media, lower fermentation yields and low activities were observed. This was

5 Initial development towards a cascade for the synthesis of fatty nitriles from fatty acids

explained by the interference of byproducts from the *E. coli* metabolism. Cell-densities over OD 8 were not achieved for expression of highly active protein with this method.^[225] No new successful reports in this field could be noticed in the last ten years, thus, underlining the difficulty of the expression of oxygen-labile proteins.

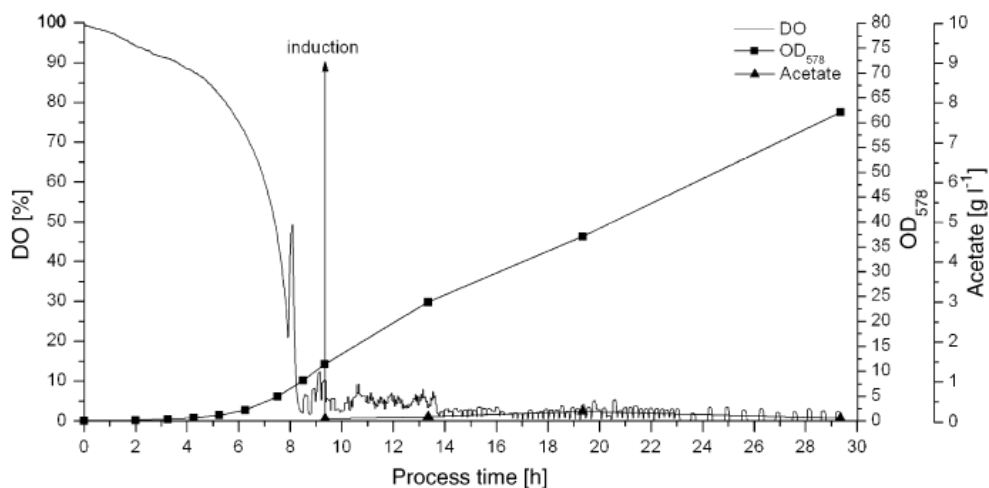


Figure 25. Process parameters such as DO, OD₅₇₈ and acetate formation for the fed-batch fermentation (5.0 L scale) of *E. coli* BL21(DE3) expressing CYP102A1 (Reprinted from *J. Biotechnol.*, 129, Development of a fed-batch process for the production of the cytochrome P450 monooxygenase CYP102A1 from *Bacillus megaterium*, S. Pflug, S. M. Richter, V. B. Urlacher, 481-488. Copyright © 2007, with permission from Elsevier).^[223]

5.5.2 Expression of Oxds in shaking flask and fed-batch scale

In similarity to CYP-enzymes, the effect of oxygen saturation during expression, and therefore the oxidation state of the heme iron, is crucial for Oxds as well. *Kato and Asano* observed a strong dependence of the enzymatic activity of recombinant OxdB on the aeration rates during expression in shaking flasks. Microaerobic conditions were superior compared to other conditions.^[163] While it is difficult to determine oxygen saturations in shaking flasks *via* sensors, larger bioreactors are standardly equipped with inline analytics for monitoring oxygen saturation, pH-value, foam formation, etc.

Betke initially investigated the high-cell density fermentation (2.0 L bioreactor) of OxdB in *E. coli* BL21(DE3)Condon⁺ with an AI-medium-based strategy. An expression level of OxdB slightly below the shaking flask expression was observed after 72 hours of process time. However, the produced whole-cell catalyst showed only 2.5 % of the activity compared to shaking flask expression. The observed activity was not dependent on the oxygen saturation in the medium. Insufficient heme incorporation, oxidation of the heme iron atom to its ferric form or iron depletion leading to incorporation of other metals in the active site of OxdB were

5 Initial development towards a cascade for the synthesis of fatty nitriles from fatty acids

proposed as reasons for the lower activity.^[190] Previous reports suggest that the incorporation of heme b is crucial for the folding of OxdB. If the enzyme is grown in medium containing no iron, the formation of insoluble apoprotein is observed exclusively.^[163]

5.5.3 Motivation

Based on the experiences with the fermentation of OxdB by *Betke* and the successful fermentation of two CYP-enzymes, a high cell-density fermentation process of OxdB will be further examined with the target to produce a whole-cell catalyst. The media, expression vector and process conditions will be examined in order to get a better understanding of this process. Literature known expression systems of OxdB in shaking flasks should be transferred to a bioreactor. Especially the effect of oxygen is to be figured out.

5.5.4 Bioreactor setup and analytical aspects

Three systems suitable for expression of active OxdB are known (Table 24).^[163,178] All these methods use the strain *E. coli* JM109 or a type of BL21(DE3) with the high-copy plasmids pUC18 or pET22b(+). The expression in the pUC18 vector is under control of the M13 promotor, while in pET22b(+) the strong T7 promotor is controlling the protein expression. Despite using different media, all cultures are performed under microaerobic conditions.

Table 24. Expression systems and conditions for the expression of recombinant OxdB in *E. coli*.

Entry	Medium	Vector	Medium	Volume [mL _{Culture} (mL _{Flask})]	Shaking speed [rpm]	Temperature [°C]
1 ^[163]	<i>E. coli</i> JM109	pUC18	LB	250 (500)	150	30
2*	<i>E. coli</i> BL21(DE3) - RIL	pUC18	AI	400 (500)	160	30
3 ^[178]	<i>E. coli</i> BL21(DE3)	pET22b(+)	TB	1400 (2000)	120	26

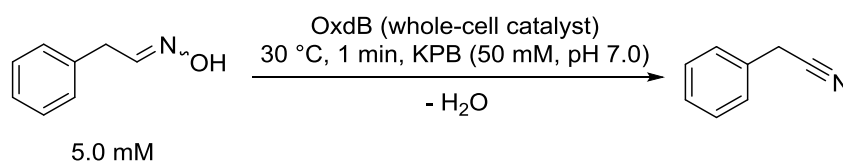
*Used in chapter 4 and 5.

First, the reactor setup was decided in order to transfer the shaking flask expression methods. Two 3.4 L fermenter with an operating volume of 2.0 L were chosen. These reactors have sensors for measuring pH value, oxygen saturation, foam formation and are equipped with a mechanical stirrer, cooling (or heating) and a pump for addition of feed medium. Both the stirrer and the feed pump can be programmed to respond to the monitored values by a functionalized Excel sheet. Samples of the expression medium were taken periodically by using a modified fraction collector for preparative HPLC and cooled at 4 °C. Concentrations of glycerol in the

5 Initial development towards a cascade for the synthesis of fatty nitriles from fatty acids

medium during the batch phase were determined with RP-HPLC measurements in comparison to a calibration curve. A spectroscopic method for determination of concentration of heme-proteins by a CO difference spectral method is frequently applied in hemoprotein related research.^[226] However, the sufficient equipment for this determination under inert gas using gaseous carbon monoxide was not available for this research. This issue was neglected as the target was to produce a highly active whole-cell catalyst for aldoxime dehydration and not production of isolated protein. In contrast to previous experiments in this thesis, which refer to the activity per wet biomass, the specific activity determined in fermentative processes is typically referred to the cell dry weight (in $\text{U}\cdot\text{mg}_{\text{CDW}}^{-1}$). A correlation between the OD and the cell dry weight was calculated for each process and used for the determination of specific activities of the prepared whole-cell catalysts.

First, the activity of the whole-cell catalyst produced with the available expression systems was tested again in order to obtain a reference for the fermentations. Cultivations were performed in accordance to the literature known procedures with some adjustments. Biotransformations of Z-PAOx were carried out according to previously established methods (Scheme 61).



Scheme 61. Dehydration of Z-PAOx to PAN as the standard activity assay for the determination of OxdB activity in whole-cells.

Initial experiments showed that the *E. coli* strain BL21(DE3)-RIL was the favored host for expression of OxdB. However, AI-medium (induction by lactose) can be disadvantageous regarding optimization of a fermentation process. Therefore, additionally TB-medium was tested for expression of OxdB in this strain adapting an IPTG-based expression protocol reported in literature (Table 25).^[163] Both expression protocols feature an initial exponential cell growth phase at 37 °C followed by a temperature decrease to 30 °C for the protein expression. The whole-cell catalyst expressed in TB-medium showed a specific activity of $7.80 \text{ U}\cdot\text{mg}_{\text{CDW}}^{-1}$ referring to $17,700 \text{ U}\cdot\text{L}^{-1}$ (Entry 1). For the AI-based strategy, a slightly lower specific activity of $6.66 \text{ U}\cdot\text{mg}_{\text{CDW}}^{-1}$ was observed, however, at a lower volumetric activity of $10,800 \text{ U}\cdot\text{L}^{-1}$ (Entry 2). Reason for the lower absolute activity is probably the lower biomass obtained in the AI-medium culture. Both a high specific activity of the whole-cell catalyst and large amounts of biomass, directly related to a high absolute activity, are necessary.

5 Initial development towards a cascade for the synthesis of fatty nitriles from fatty acids

Table 25. Specific and volumetric activities of OxdB-whole-cell catalyst expression of under different conditions in *E. coli* BL21(DE3)-RIL harboring the pUC18-OxdB vector.

Entry	Medium	Volume [mL _{Culture} (mL _{Flask})]	Shaking speed [rpm]	Specific activity [U·mg _{CDW} ⁻¹]	Volumetric activity [U·L ⁻¹]
1	TB	250 (500)	150	7.80	17,700
2	AI	400 (500)	160	6.66	10,800

The culture conditions and the feeding strategy were decided as a starting point for the development of a bioprocess for production of the OxdB whole-cell catalyst. First, fermentations were performed under aerobic conditions. These are favorable for the growth of *E. coli*, therefore, these conditions were suitable to obtain an initial insight in the fed-batch fermentation of OxdB. An overpressure of 0.2 bar oxygen was set as standard. The pH-value was adjusted by phosphoric acid (for pH decrease) and ammonia (for pH increase), which also represents an additional nitrogen source for the growth. Pluronic® was the choice as the standard anti-foam agent. The carbon source glycerol (additionally glucose/lactose in AI-medium) was consumed in the initial batch phase. The oxygen available in the bioreactor was also consumed during the batch phase.

The so called DO-spike control was activated at this point. Two different mechanisms for adjustment of the DO-level were activated when the DO-level dropped below 30 % for the first time. The stirrer speed was automatically increased every time when the DO-level dropped below 30 % from this point on. The oxygen saturation in the medium can be increased by a higher stirrer speed, which also promotes faster bacterial growth. A decrease of the oxygen saturation can be achieved by addition of feed-medium every time when the DO-level exceeds 60 %. This medium is comprising of the carbon source glycerol, yeast extract and magnesium(II) chloride, which increases the plasmid stability. The higher availability of the carbon source in the culture medium after addition of feed-medium promotes faster cell growth, which is consuming oxygen. A stable process was carried out according to this protocol for at least 72 hours, in which the major part of the feed-medium was consumed (Figure 26). Processes were carried out separately with AI-medium, TB-medium and HSG-medium, an optimized medium for high cell-density fermentations of *E. coli*.^[227] Protein expression was induced by addition of 1.0 mM of the inducer IPTG at an OD₆₀₀ of ~50 (t = 20 h) when using TB- and HSG-medium. Exponential cell growth was observed until induction for these cultures. A slower linear cell growth (HSG) or a slight linear decrease of biomass (TB) was observed after induction. While the cell growth was nearly linear over the whole process time when using AI-medium, a slower initial growth rate was observed.

5 Initial development towards a cascade for the synthesis of fatty nitriles from fatty acids

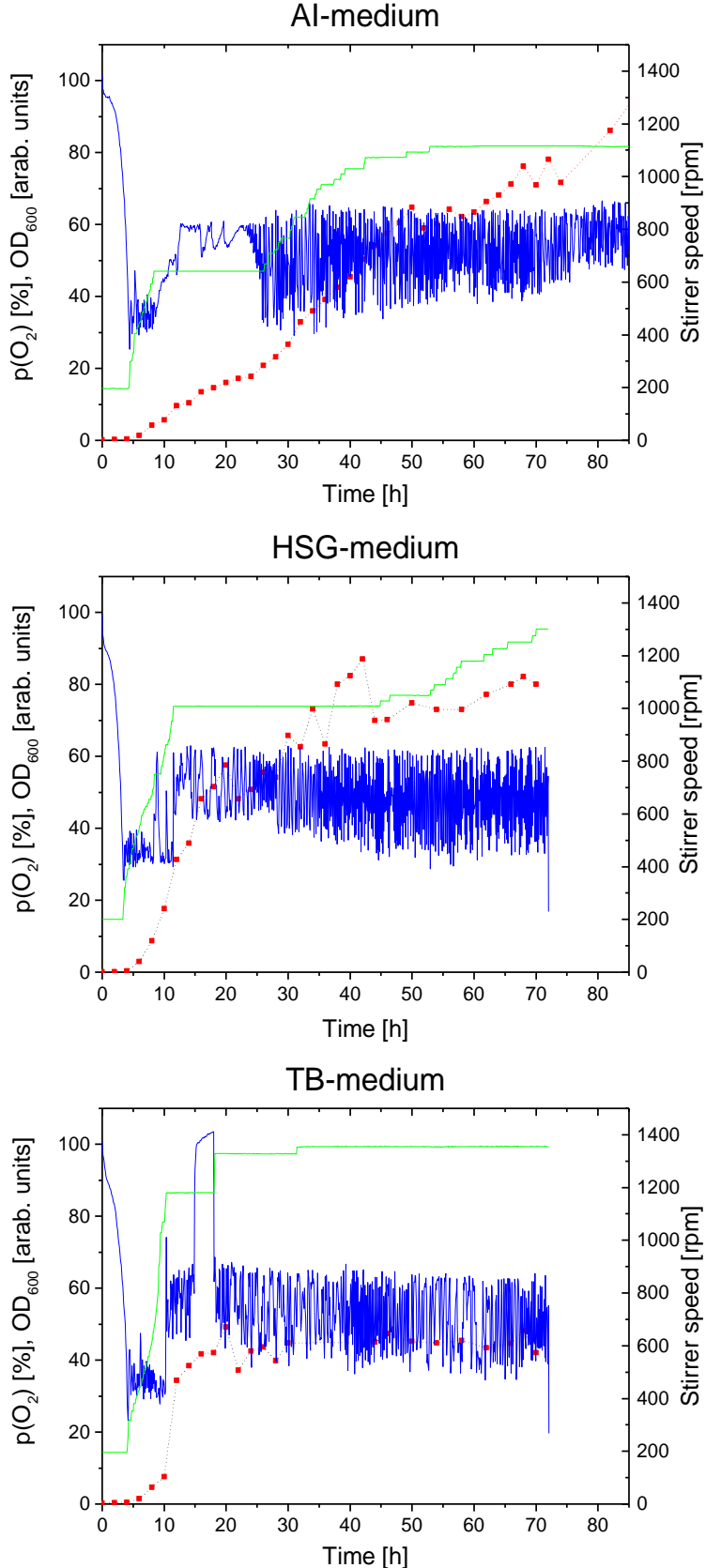


Figure 26. Selected process parameters for the fed-batch fermentations of *E. coli* BL21(DE3)-RIL harboring pUC18-OxdB with different media in the batch phase (Al-medium: upper, HSG-medium: middle, TB-medium: lower). Blue line: DO-level, green line: stirrer speed, red squares: OD_{600} .

5 Initial development towards a cascade for the synthesis of fatty nitriles from fatty acids

Samples were taken over the whole process time and analyzed regarding its activity for the dehydration of Z-PAOx as the standard substrate of OxdB (Figure 27). Therefore, the cells were washed twice with KPB and suspended in the same buffer prior to use. Acknowledging the higher biomass obtained in high cell-density fermentations, the dilution was five times higher compared to the shaking flask cultures. An increase of the specific activity until the maximum after 36 hours was observed in the AI-medium culture from the inoculation. The maximal specific activity was $3.92 \text{ U}\cdot\text{mg}_{\text{CDW}}^{-1}$, which corresponds to a relative specific activity of 59 % compared to shaking flask expression with AI-medium. The absolute culture activity was only approximately 3.5 fold higher compared to shaking flask expression as the OD_{600} in the fermentation was still below 40 at this point. A symmetrical decrease to values close to $0 \text{ U}\cdot\text{mg}_{\text{CDW}}^{-1}$ after the maximum was observed. If the process is carried out for a longer time without addition of feed-medium, the produced cells were not active for aldoxime dehydration (data not shown). This could be explained by the high oxygen saturation in the process window, where no DO-spike control was possible any more. The same applied for the experiments under supervision of *Betke*.^[228] However, only the activity of the harvested cells after the process end were determined. No data for samples in between are available from these experiments. Possibly, activity would have been observed during the DO-spike controlled process time. The high oxygen saturation might be the most reasonable explanation for the inactive whole-cell catalyst produced by *Betke*.

A flat exponential course of the specific activities of the OxdB whole-cell catalyst was observed for the IPTG-induced fermentations with HSG- and TB-medium. Both courses were very similar. A slight activity below $0.20 \text{ U}\cdot\text{mg}_{\text{CDW}}^{-1}$ was observed for both fermentations until the induction point at 20 hours. This suggests leaky expression of the protein, which is also reported to occur for other lac-operon regulated plasmids.^[229] The exponential increase of the activity started after the induction. After 72 hours of process time (end point), a specific activity of 1.24 and $1.26 \text{ U}\cdot\text{mg}_{\text{CDW}}^{-1}$ was observed for TB- and HSG-medium, respectively. For TB-medium, the end point value corresponds to 16 % relative activity compared to shaking flask experiments. HSG-medium was also tested in shaking flasks, however, only slightly active catalyst was obtained in these experiments (data not shown). The oxygen saturation in shaking flasks is limited because the flasks (without baffles) were closed with aluminum foil. The rich nature of HSG-medium might be disadvantageous in this setup. Further optimization of shaking flask expression of OxdB in HSG-medium would have been necessary. Therefore, the activities from the fermentations with in this medium were not compared to a reference. Despite the high OD of ~80 achieved with HSG-medium, only absolute activities 2.5 fold higher than the best shaking flask experiment (TB-medium, Table 25, Entry 1) were obtained. This might be originated from the significantly lower specific activity of the whole-cell catalyst produced in

5 Initial development towards a cascade for the synthesis of fatty nitriles from fatty acids

the fermentations. The biomass obtained after the end of the process was not tested in biotransformations individually. The activity is assumed to be equal to when determined in analytical scale.

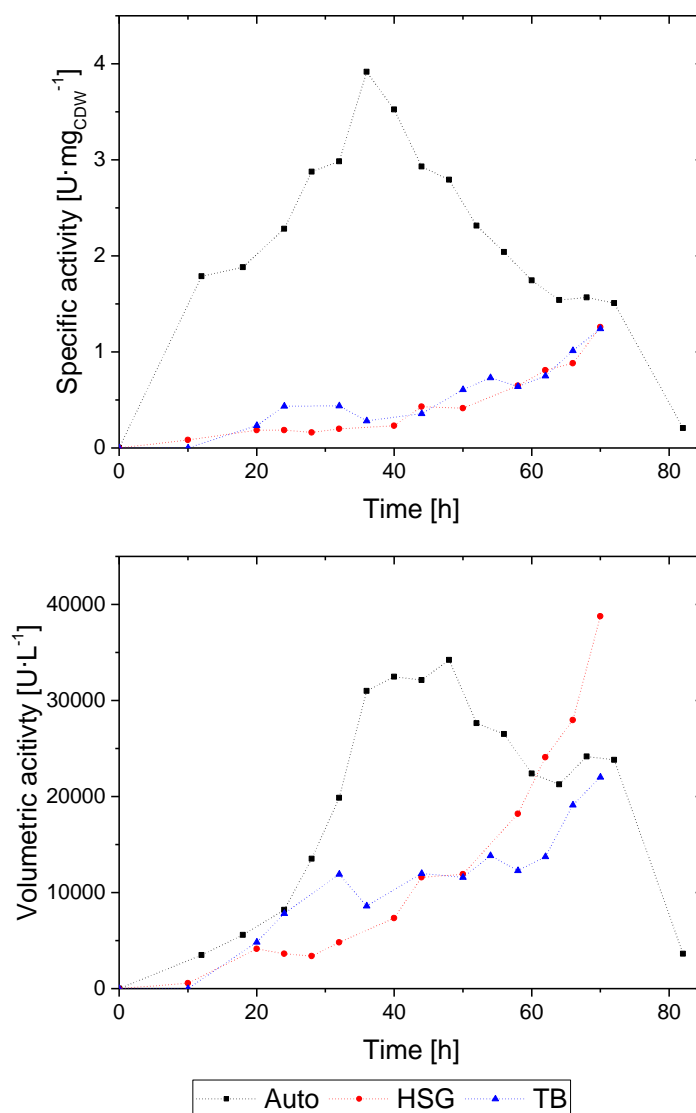


Figure 27. Specific (upper) and volumetric activities (lower) observed in the fed-batch fermentations of *E. coli* BL21(DE3)-RIL harboring pUC18-OxdB comparing different medias used in the batch-phase. Black: AI-medium, red: TB-medium, blue: HSG-medium.

In the following, the protein expression was analyzed *via* SDS-PAGE performed with cells harvested at the induction point ($t = 20$ h) and in one day intervals after induction (Figure 28 to Figure 30). An increase of the OxdB band size (~ 40 kDa) was observed after induction, however, insoluble protein was formed in large amounts regardless of the culture medium and the process time. A major part of the leaky expressed protein was found in the insoluble fraction. Protein was also found in the membrane fraction, which is assumed to be caused by insufficient sonification of the harvested cells. The *E. coli* typical inclusion bodies were also found additionally in the membrane fraction, what supports this hypothesis. The induction with

5 Initial development towards a cascade for the synthesis of fatty nitriles from fatty acids

IPTG increased the protein production in the fermentations with HSG- and TB-medium, what was also observed in the activity course.

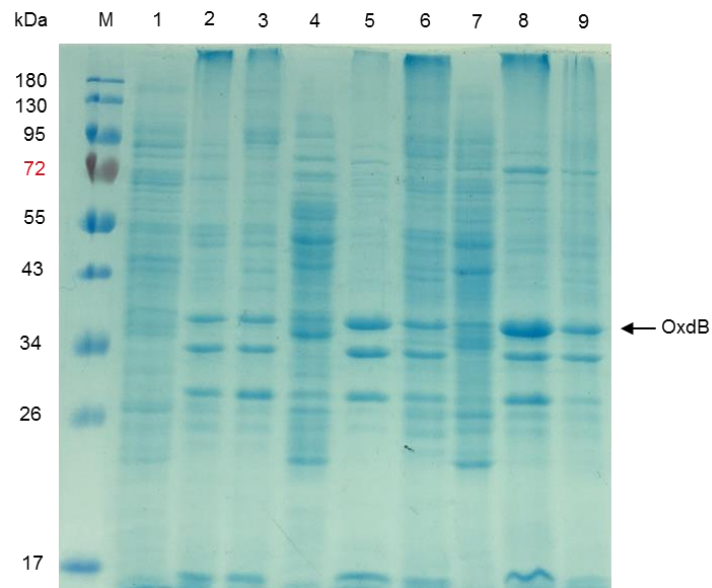


Figure 28. SDS-PAGE analysis of the fed-batch fermentation of *E. coli* BL21(DE3)-RIL harboring pUC18-OxdB with AI-medium in the batch phase. M: Marker, Lane 1: Soluble fraction (0.83 d), Lane 2: Insoluble fraction (0.83 d), Lane 3: Membrane fraction (0.83 d), Lane 4: Soluble fraction (1.83 d), Lane 5: Insoluble fraction (1.83 d), Lane 6: Membrane fraction (1.83 d), Lane 7: Soluble fraction (2.83 d), Lane 8: Insoluble fraction (2.83 d), Lane 9: Membrane fraction (2.83 d).

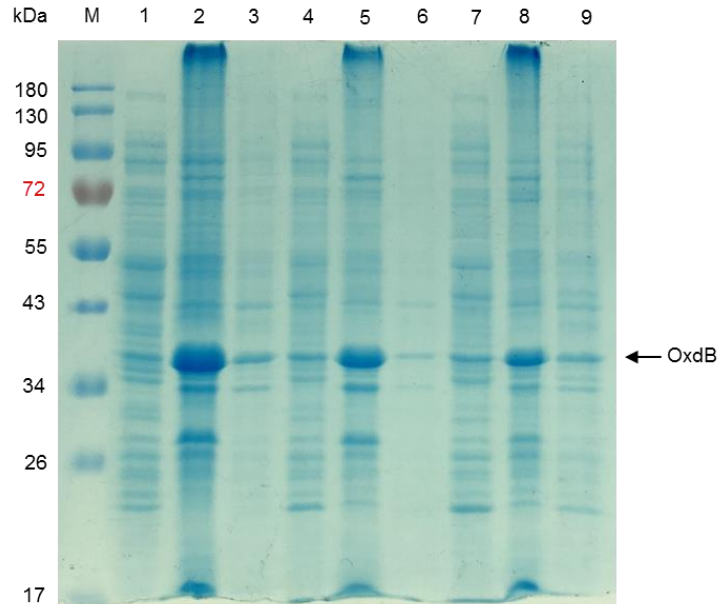


Figure 29. SDS-PAGE analysis of the fed-batch fermentation of *E. coli* BL21(DE3)-RIL harboring pUC18-OxdB with HSG-medium in the batch phase. M: Marker, Lane 1: Soluble fraction (0.83 d), Lane 2: Insoluble fraction (0.83 d), Lane 3: Membrane fraction (0.83 d), Lane 4: Soluble fraction (1.83 d), Lane 5: Insoluble fraction (1.83 d), Lane 6: Membrane fraction (1.83 d), Lane 7: Soluble fraction (2.83 d), Lane 8: Insoluble fraction (2.83 d), Lane 9: Membrane fraction (2.83 d).

5 Initial development towards a cascade for the synthesis of fatty nitriles from fatty acids

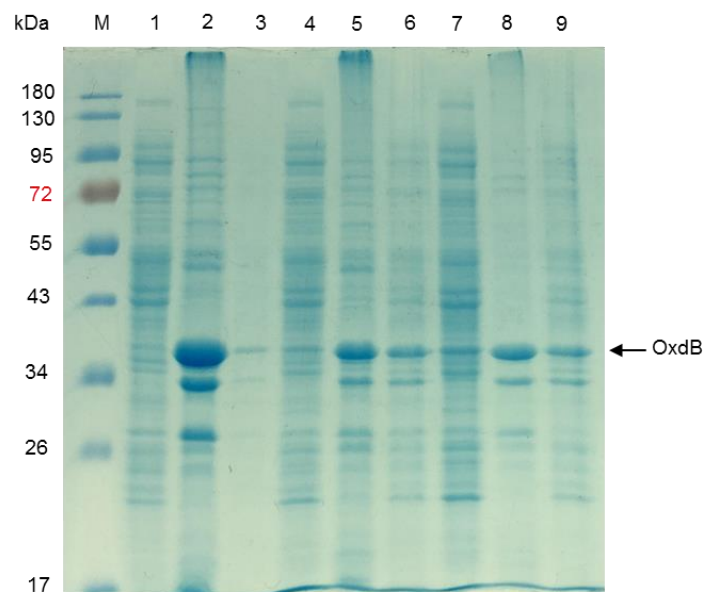


Figure 30. SDS-PAGE analysis of the fed-batch fermentation of *E. coli* BL21(DE3)-RIL harboring pUC18-OxdB with TB-medium in the batch phase. M: Marker, Lane 1: Soluble fraction (0.83 d), Lane 2: Insoluble fraction (0.83 d), Lane 3: Membrane fraction (0.83 d), Lane 4: Soluble fraction (1.83 d), Lane 5: Insoluble fraction (1.83 d), Lane 6: Membrane fraction (1.83 d), Lane 7: Soluble fraction (2.83 d), Lane 8: Insoluble fraction (2.83 d), Lane 9: Membrane fraction (2.83 d).

Even though several attempts of reproduction of these results were made, a reproduction of the cell growth and the activities was not possible. In order to search for a reason, the plasmid stability was investigated. This parameter describes the stability of the expression system against plasmid leakage. While the preculture was showing an excellent plasmid stability close to 100 %, after one day of process time with the AI-medium, the plasmid stability already dropped to 30 to 40 %. Longer process times led to an even further decrease. Plasmid stabilities of 60 % were observed at the induction point when using TB-medium, however, a harsh decrease was observed until the process end. Insufficient plasmid stability might be a cause of the instable fermentation processes. Batch and fed-batch fermentations of *E. coli* BL21(DE3) harboring pET22b(+)-OxdB with a C-terminal hexahistidine-tag were also attempted. These expressions also suffered from low plasmid stability and non-reproducible results under several conditions. The expression plasmids suitable for shaking flask expression of OxdB were proved to be not suitable for high cell-density fermentations. Reasons for the low plasmid stability might be *inter alia* the leaky protein expression,^[230] the expression temperature of 30 °C and other stress factors such as low oxygen saturation.^[231]

In addition to the fermentations at higher DO-values, fermentations at lower DO-values representing microaerobic conditions were attempted. Therefore, different strategies were tested to keep the DO in an interval (at low DO-values) or below a specific value. Several attempts were made by the DO spike control and with constant low stirrer speed (after induction) for IPTG-based strategies. However, no stable process was observed (see

5 Initial development towards a cascade for the synthesis of fatty nitriles from fatty acids

examples of unstable processes in Figure 31). In this cases, only very low activity under 1 % compared to the shaking flask expression was observed.

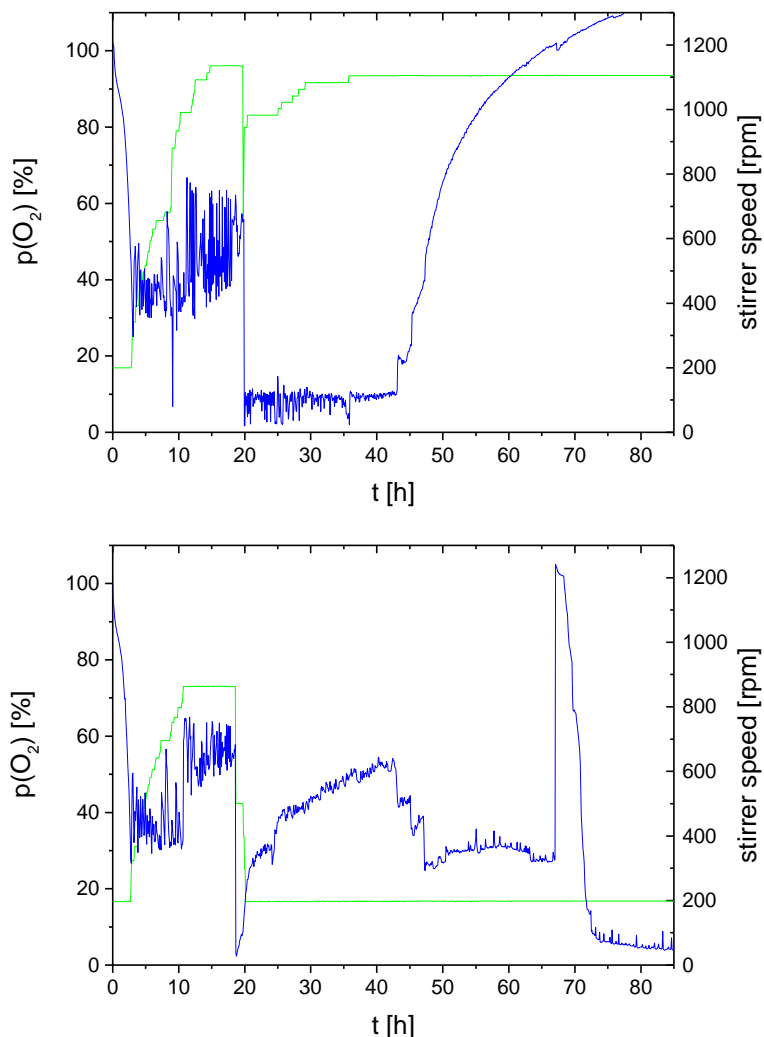


Figure 31. DO-level (blue) and stirrer speed (green) monitored for attempts of fed-batch fermentation of *E. coli* BL21(DE3)-RIL harboring pUC18-OxdB with HSG-medium given in the batch phase. Upper: DO <10 % controlled by DO-spike strategy, lower: Constant stirrer speed after induction.

In conclusion, new insights in the fermentative production of OxdB whole-cell catalysts have been obtained. There is an evidence that one of the reasons for the lower activity observed in fermentations might be oxidation of the heme iron at high DO-values over longer times. Active protein was obtained with both an AI-based and IPTG-induction based strategy at a “normal” oxygen saturation level between 30 and 60 %. The relative activity compared to shaking flasks expression was 59 % for AI-medium and 16 % for TB-medium, respectively. Furthermore, the formation of insoluble protein was observed in high amounts. This might be caused by insufficient heme incorporation, a reason for insoluble expression of OxdB, or incorrect protein folding under high stress conditions.

5 Initial development towards a cascade for the synthesis of fatty nitriles from fatty acids

One could speculate about the reasons for the low whole-cell catalyst activity and the instability of the processes. One reason is assumed to be the low plasmid stability, what is a frequently observed issue for lac-operon regulated plasmids. A switch to a more tightly repressed vector controlled by e.g. the arabinose promoter or the use of a low-copy number plasmid might solve this issue.^[232] Other strains of *E. coli* repressing the lac-promoter more effectively might also be an alternative.^[230] Usually fermentation processes are designed from systems successfully tested in shaking flasks. While the experiments in shaking flasks led to good overexpression of active protein, the whole fermentation process could rarely be carried out smooth. For protein expression at low DO-values, a more robust expression system is necessary. If another expression plasmid or will not increase the robustness of this system, a switch to an organism which grows better under microaerobic conditions might be a successful strategy.

Another limitation was the strongly inhibited cell growth or even the decrease of the biomass amount observed. A typical response of *E. coli* to induction is a slightly decreased linear cell growth. If at the same time too high amounts of the feed medium are inserted, a large excess of the carbon source could be accumulated. The cells might be inactivated by this accumulation. Induction at a higher OD combined with a slower feeding strategy might be advantageous. Besides this, apoptosis was frequently observed, especially at high OD-values. These cells stucked together and their suspension in buffer was impossible. Activity tests with these cells also led to no or only marginal activity.

6 Improvement of heme incorporation by a protein sequence based enzyme engineering approach

6 Improvement of heme incorporation by a protein sequence based enzyme engineering approach

6.1 Enzyme engineering: A key technology for improved catalyst performance

The functional expression of OxdB in a fermentative process was quite challenging. Besides the mentioned optimization methods addressing the expression system, engineering of the protein itself could be an additional and orthogonal approach for improvement of the fermentative processes. The introduction of mutations might lead to a higher production yield of OxdB and a higher specific enzymatic activity as well as whole-cell catalyst activity.

6.1.1 Methods of enzyme engineering

Protein engineering has been developed to a broadly applicable tool for improving performance of a biocatalyst. Most enzymes applied in bioprocesses are modified to suit the special challenges of these systems. Activity, stability and selectivity are typical points addressed by enzyme engineering.^[14,233]

For all types of enzyme engineering a reliable assay is crucial to evaluate the results. The throughput of the assay setup determines the numbers of mutants screenable in a realistic time scale. For medium-throughput screenings, fluorescence or absorption spectrometry based assays in 96- or 256-well plates are common. Numbers of up to 10^5 variants can be tested with spectroscopic methods. These assays often require the use of model substrates, not necessarily related to the target substrate. MS-measurements monitoring the product formation are also broadly applicable, but are more elaborate and therefore often more expensive. For a higher rate of throughput exceeding 10^7 variants, methods based on cell-sorting in microfluidics like fluorescence-activated cell sorting (FACS) are common. FACS is applied to single cells dividing them into distinct subpopulations by electrostatic deflection.^[234,235]

The methods for the introduction of mutations is also related to the assay type. In principle, protein engineering can target the whole gene or only specific regions of the gene. Common methods for targeting the whole gene are random mutagenesis *via* e.g. error prone polymerase chain reaction (PCR) and DNA shuffling methods. They do not require any further information about the protein. Rational approaches are based on information given from the secondary, tertiary or quaternary structure of the protein such as the crystal structure or homology models. A specific site can be modified with methods of saturation mutagenesis. In this approach,

6 Improvement of heme incorporation by a protein sequence based enzyme engineering approach

hotspots are identified and mutated to all possible amino acids in this position. CASTing is a method to address several hotspots at the same time. An even more rational approach with much lesser variants is the introduction of selected point mutations based on a rational model, such as docking simulations.^[234,235]

6.1.2 Identification of aggregation hotspots with the software INTMSAlign_HiSol

Most rational approaches have in common that they require tertiary or quaternary structure information of the target protein. This can be a problem if the crystal structure of the protein is not solved and reliable homology models are not yet available. The software INTMSAlign was designed to construct functional proteins based on sequence data.^[236] Recently, *Matsui et al.* developed a new protein engineering method addressing solubility issues in the expression of heterologous proteins in *E. coli* with this program (Figure 32).^[237] Insufficient capability of the expression system *E. coli* to fold proteins is one of the major issues causing significant amounts of insoluble protein formed during the protein expression. A variation of this program, INTMSAlign_HiSol, was able to identify so called aggregation hotspots. These hotspots are basically mismatches of the hydrophobicity of amino acids located in specific regions. In native proteins, hydrophobic amino acid residues are located (in most cases) in the inner sphere of the protein while hydrophilic amino acid residues are mainly located in the outer sphere.^[237]

The sequence alignment function of INTMSAlign identifies where the target protein contains non-highly conserved amino acids in the same gene family. INTMSAlign_HiSol features an additional tool which calculates the change in hydropathy for a single point mutation in these positions, the so-called HiSol score. Residues with high positive or negative HiSol scores are identified as aggregation hotspots (hydropathy contradiction rule). Hydrophobicity mismatches in α -helices can also cause protein misfoldings (α -helix rule). When both rules are combined, a higher fraction of soluble protein (hit rate 70 %) was observed (hydropathy contradiction rule on α -helix).^[237]

6 Improvement of heme incorporation by a protein sequence based enzyme engineering approach

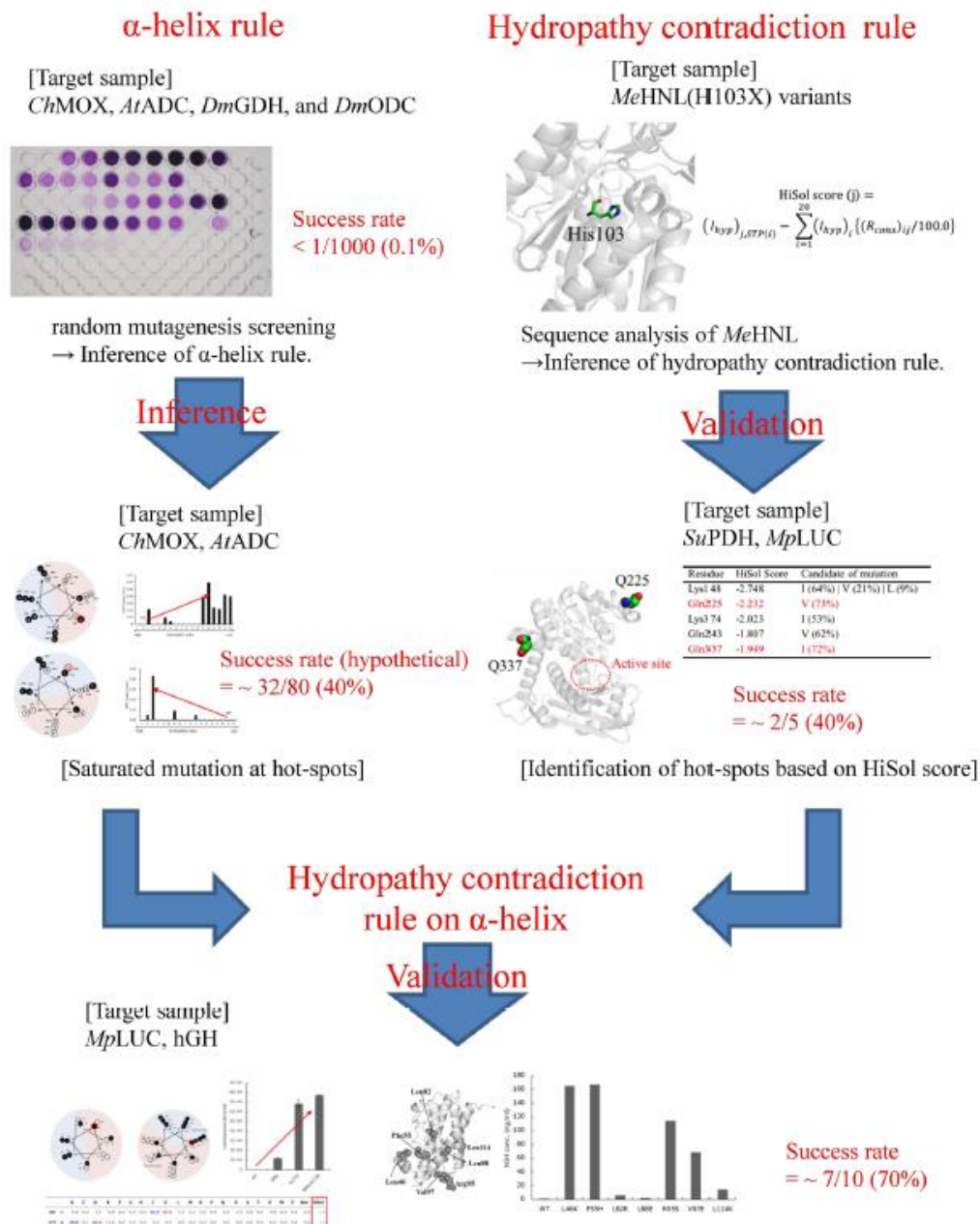


Figure 32. Flowchart of the development of primary and secondary structure based approach to identify aggregation hotspots in proteins using the software INTMSAlign_HiSol (Reprinted from D. Matsui, S. Nakano, M. Dadashipour, Y. Asano, *Sci. Rep.* **2017**, 7, 9558. Creative Common CC BY license).^[237]

6.1.3 Heme incorporation in heterologous expression

For wild-type Oxds, different amounts of heme incorporation into the apoprotein during expression are reported. Although OxdB is not folded correctly in the total absence of iron in the culture medium, which is necessary for heme biosynthesis, the enzyme expressed homologously in *Bacillus* sp. OxB-1 is still bearing heme in only 35 % of the enzyme.^[163] The heme content is different for other Oxds. For example, OxdA contains 69 % heme in the wild-type enzyme when expressed in *E. coli*.^[165] Depending on the expression vector and the

6 Improvement of heme incorporation by a protein sequence based enzyme engineering approach

position of a hexahistidine-tag, the heme content of OxdRE varies between 32 and 43 %.^[166] It is unclear whether the Oxds originally produced in their bacterial hosts have the same low heme content or the heme cofactor is lost during the protein purification steps.^[166] Oxds have rarely been a target of protein engineering. Mutations introduced into the enzymes were used to identify the active site or the properties of the enzyme. The alanine substitution of crucial histidine residues in the active site of OxdA has been investigated. While most mutations in the active site did not have an effect on the heme incorporation, the removal of the His₂₉₉ residue binding to the heme iron prevented heme incorporation completely.^[174]

Insufficient heme incorporation, as suggested from the results in chapter 5.5, is a common challenge in expression of hemoproteins in *E. coli*. A typical strategy for increasing the heme incorporation into proteins is the addition of the heme precursor δ -amino levulinate in the culture medium,^[238] but which is reported to have no effect on OxdB expressed in *E. coli*.^[163] Alternatively, optimization of the expression host can also improve heme incorporation. For example, the *E. coli* strain Nissle 1917 naturally produces the ChuA heme receptor, which improves the heme uptake from the media, thus, improving heme incorporation during protein expression when heme is present in the medium.^[239] Furthermore, the strain RP523 contains a porphobilinogen synthase gene disruption and an uncharacterized permeability mutation that renders this bacterium heme-permeable. Therefore, this strain can be utilized to introduce unnatural heme cofactors into proteins.^[240] Moreover, co-expression of a ferrochelatase, an enzyme assisting heme incorporation, can increase heme incorporation during heterologous expression in *E. coli*.^[241]

6.2 Motivation

For improving the efficiency of the nitrile synthesis with Oxds, the absolute activity obtained from a cell culture has to be raised. This activity is strongly related to the amount of soluble protein expressed and to its specific activity. One could think that increasing the solubility of a protein, as demonstrated by *Matsui et al.*, would also raise its expression level (of already expressible proteins).^[237] A higher expression level is assumed to lead to higher observed activity of the whole-cell catalyst under the premise that factors such as mass transfer in the solution as well as the absorption and excretion of the substrate and product, respectively, could be neglected. An improvement of enzyme solubility could also address the issue of insoluble protein expression observed in the fermentative production of OxdB in chapter 5.5.

Even though Oxds contain several highly conserved residues in their gene family, high differences of the heme incorporation in the wild-type enzymes is observed. Besides mutations of the heme iron-binding histidine, other mutations are reported to have no major effect on the heme incorporation. However, residues located in the second sphere might affect the heme incorporation. Common methods for increasing heme incorporation are only suitable to a limited extent for application in fermentations, especially for the production of whole-cell catalysts. If the hydropathy contradiction rule on α -helices is applied to an Oxd, one could assume that this might also have an effect on the heme incorporation and therefore might improve the expression level of soluble protein. This will be evaluated for OxdB, especially recognizing that the crystal structure is not determined yet. While Oxds have not been target of enzyme engineering for optimization of its catalytic features yet, this would be a pioneering task.

6.3 Rational mutant library design for aldoxime dehydratase from *Bacillus sp. OxB-1*

6.3.1 Identification of mutation sites with INTMSAlign_HiSol

As the first step, aggregation hotspots were located by applying the program INTMSAlign_HiSol on the sequence of OxdB. An overview about highly conserved residues and possible targets was obtained with these calculations (intermediate values, not given as output). The implemented HiSol function then automatically calculated the HiSol score for the identified j -th residue by the following formula

$$\text{HiSol score (j)} = (I_{\text{hyp}})_{j,\text{STP}(i)} - \sum_{i=1}^{20} (I_{\text{hyp}})_i \{(R_{\text{cons}})_{ij}/100\}$$

as a dimensionless value. The formula is explained in more detail in the experimental section (chapter 9.2). There are different scales for determining the hydrophathy of amino acids, which are based on factors such as the hydrophathy of distinct protein regions (Table 26).^[242]

Table 26. Hydrophathy of the 20 proteinogene amino acids according to selected scales.

Amino acid	Group	<i>Eisenberg et al.</i> ^[243]	<i>Engelman et al.</i> ^[244]	<i>Kyte and Doolittle</i> ^[245]	<i>Hoop and Woods</i> ^[246]	<i>Janin</i> ^[247]
Ile	Nonpolar	0.73	3.1	4.5	1.8	0.7
Phe	Nonpolar	0.61	3.7	2.8	-2.5	0.5
Val	Nonpolar	0.54	2.6	4.2	-1.5	0.6
Leu	Nonpolar	0.53	2.8	3.8	-1.8	0.5
Trp	Nonpolar	0.37	1.9	-0.9	-3.4	0.3
Met	Nonpolar	0.26	3.4	1.9	-1.3	0.4
Ala	Nonpolar	0.25	1.6	1.8	-0.5	0.3
Gly	Nonpolar	0.16	1.0	-0.4	0.0	0.3
Cys	Polar	0.04	2.0	2.5	-1.0	0.9
Tyr	Polar	0.02	-0.7	-1.3	-2.3	-0.4
Pro	Nonpolar	-0.07	-0.2	-1.6	0.0	-0.3
Thr	Polar	-0.18	1.2	-0.7	-0.4	-0.2
Ser	Polar	-0.26	0.6	-0.8	0.3	-0.1
His	Charged	-0.40	-3.0	-3.2	-0.5	-0.1
Glu	Charged	-0.62	-8.2	-3.5	3.0	-0.7
Asn	Polar	-0.64	-4.8	-3.5	0.2	-0.5
Gln	Polar	-0.69	-4.1	-3.5	0.2	-0.7
Asp	Charged	-0.72	-9.2	-3.5	3.0	-0.6
Lys	Charged	-1.10	-8.8	-3.9	3.0	-1.8
Arg	Charged	-1.80	-12.3	-4.5	3.0	-1.4

6 Improvement of heme incorporation by a protein sequence based enzyme engineering approach

Depending on the scale, the charged amino acids asparagine, lysine and arginine are the most hydrophilic residues. The non-polar amino acids isoleucine, phenylalanine, valine and leucine are the most hydrophobic residues.^[242] The hydropathy indices according to *Kyte and Doolittle* were used for calculation. The program used the normalized values of this scale (to an average of “0” and a variance of “1” obtained *via* z-transformation, Figure 33).^[245] According to this scale, arginine and lysine with normalized hydropathy indices lower than -1.0 are the most hydrophilic amino acids. Isoleucine and valine are the most hydrophobic amino acids with hydropathy indices higher than 1.5.

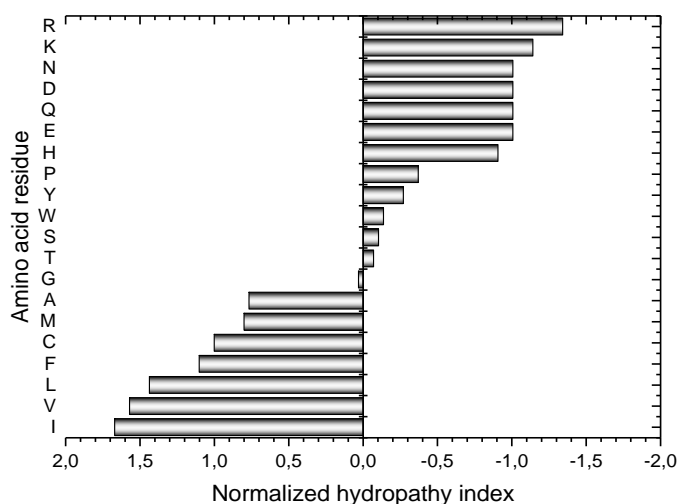


Figure 33. z-Transformed values of the normalized hydropathy indices of the 20 naturally occurring amino acids according to the scale of *Kyte and Doolittle* (Adapted from D. Matsui, S. Nakano, M. Dadashipour, Y. Asano, *Sci. Rep.* **2017**, 7, 9558, Creative Common CC BY license).^[237,245]

Twenty residues exhibited the highest absolute HiSol scores (Table 27). The amino acids which are targets for replacement by more hydrophilic residues gave positive HiSol scores (Entries 1 to 10). The amino acids which are targets for replacement by more hydrophobic residues gave negative HiSol scores (Entries 11 to 20). All other residues of the protein exhibit values in between the displayed values. They were neglected because the effect of mutations is less dominant for residues with a lower absolute HiSol score.^[237] The majority of the twenty identified residues with high absolute HiSol scores was located in strand (45 %) or coil (30 %) structures according to a secondary structure determination utilizing the PSIPRED tool available on the online server.^[248,249] Only five of twenty identified residues (25 %) were located in α -helicies. Other residues located in α -helix structures were not searched because of the less dominant effect proposed for them. Therefore, in contrast to the previous work by *Matsui et al.*, only the hydropathy contradiction rule was applied and all twenty identified residues were investigated. Furthermore, the effect of other secondary structures on the heme incorporation might also be of interest. These twenty residues were not located in the proposed active site of OxdB according to a homology model with OxdA and OxdRE.^[178] The conservation of the

6 Improvement of heme incorporation by a protein sequence based enzyme engineering approach

identified residues in the gene family was spread out between low values of under 20 % (Entries 8 and 11) and up to 90 % (Entry 1).

Table 27. Predicted aggregation hotspots for the sequence of OxdB by the program INTMSAlign_HiSol.^[237] The structure elements were predicted by PSIPRED.^[248,249]

Entry	Position	Original	Changed	Similarity [%]	HiSol score	Secondary structure
1	319	I	E	90.0	2.656	Strand
2	226	I	Q	26.5	2.411	Helix
3	220	L	E	39.7	2.281	Helix
4	149	V	E	65.6	2.278	Coil
5	105	I	R	32.6	2.252	Coil
6	267	L	R	40.0	2.226	Coil
7	316	I	Q	67.9	2.175	Strand
8	180	I	A	13.9	1.890	Coil
9	65	L	H	24.2	1.880	Strand
10	262	V	G	43.8	1.852	Strand
11	317	E	L	17.8	-1.452	Strand
12*	190	K	R	34.5	-	Strand
13	135	D	L	35.0	-1.496	Coil
14	67	Q	T	32.2	-1.533	Strand
15	49	K	V	24.2	-1.582	Helix
16	63	R	L	34.6	-1.882	Strand
17	296	H	L	56.7	-1.943	Coil
18	229	N	M	80.1	-1.974	Helix
19	250	Q	I	29.3	-2.153	Strand
20	283	K	L	57.8	-2.485	Helix

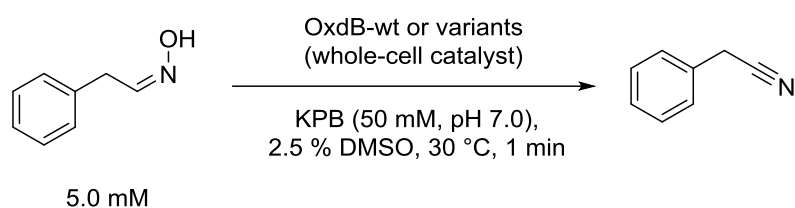
*See experimental section for further details.

6.3.2 Generation and purification of the mutant library

The identified point mutations were introduced by site-directed mutagenesis with the corresponding primers (see Appendix) and the vector pET22b harboring the OxdB gene as template DNA. This vector was chosen because of its C-terminal hexahistidine-tag, which simplifies the protein purification procedures. In an initial screening, OxdB was overexpressed in *E. coli* BL21(DE3) according to a downscaled expression protocol (70 mL medium in shaking flask) reported in literature.^[178] This method was chosen for its facility as an intinial screening. First, the specific activity (related to the wet biomass) of the whole-cell catalyst was determined against Z-PAOx as standard substrate of OxdB (Scheme 62). There is no suitable method available for screening the aldoxime dehydration activity except the *in vivo* approach with

6 Improvement of heme incorporation by a protein sequence based enzyme engineering approach

resting cells. Especially considering the effect of oxygen saturation during expression on the enzymatic activity, the protein expression in the screening should be close to the actual expression conditions. Oxygen saturation in cultures performed in 96- or 256-well plates would be not directly comparable to cultures in shaking flasks. Even the medium volume, flask size and shaking speed are reported to have a high impact on the enzymatic activity of Oxds.^[163] Considering the application of the enzyme in a whole-cell catalyst, the assay conditions should be also close to the biotransformation for nitrile synthesis. Therefore, cultivation in (small) shaking flasks and evaluation of the activity with the standard-assay by RP-HPLC were the chosen for the screening (Scheme 62).



Scheme 62. Activity assay of the determination the whole-cell catalyst activity of OxdB and its variants.

The activity was tested with resting cells harvested from the cultures of all variants (Figure 34). For the wild-type enzyme, a specific activity of $0.82 \text{ U}\cdot\text{mg}_{\text{bww}}^{-1}$ was observed. This is comparable to the other expression system with the pUC18 expression plasmid. However, the absolute cell growth observed was lower. For the mutants, a slightly slower cell growth compared to the wild-type was observed, indicating that the expression of the mutants was more stressful for the cells. For seven variants of OxdB, an improved specific activity (whole-cells) compared to the wild-type enzyme was observed. The highest activity was observed with OxdB-M9 (K65H), where the specific activity improved by 61 %. The whole-cell catalyst expressing OxdB-M12 (K190R) also showed an activity improve of 34 %. For the other five variants, an increase in activity of approximately 20% was observed (OxdB-M8, 13, 15, 18, 20). The other twelve variants showed (slightly) decreased specific activity. These values were obtained only by single determination as initial screening, thus, should be taken with caution. They were intended to give an overview about the study and gave the author a view if this mutation study is leading to form active protein or not. For one variant, no activity was observed (OxdB-M14: Q67T). This mutant was constructed again later (for purification) but not tested in the whole-cell screening again.

The expression level of the OxdB variants did not show high deviations compared to the wild-type enzyme in these experiments (data not shown). Improved expression levels were not observed. Some variants (e.g. OxdB-M5) even showed a remarkably lower expression level. On the first glance, these results did not suggest an improved expression of the protein, which refutes the initial hypothesis that the attempted rational approach might be suitable to improve

6 Improvement of heme incorporation by a protein sequence based enzyme engineering approach

soluble expression of OxdB, for which soluble expression is already known. It has to be notified here, that the expression protocol was optimized only for the wild-type enzyme and different expression conditions may promote higher overexpression of the variants, e.g. better expression at higher temperatures (here tested only at 26 °C). Despite the unchanged or lower expression levels, higher specific activity of the whole-cell catalyst was observed for some variants. Initial studies using an unoptimized purification protocol^[192] suggested that the variants OxdB-M8, M9 and M12 show a remarkably high specific activity of the purified protein, surpassing even the wild-type enzyme (data not shown).

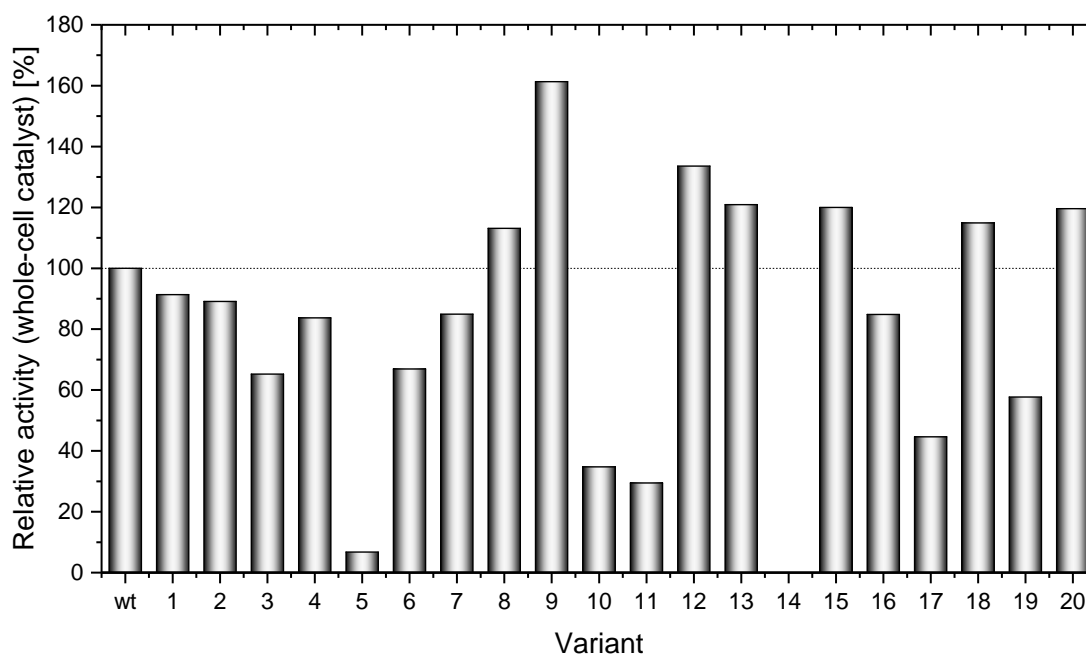


Figure 34. Relative activities of the whole-cell catalysts expressing OxdB variants compared to the wild-type enzyme.

In order to test if this effect can be enhanced, combinations of these three mutants were constructed obtaining OxdB-D1 (L65H_180A), OxdB-D2 (I180A_K190R), and OxdB-D3 (L65H_K190R). In a further step, all 23 variants, including 20 single mutants and three double mutants, were cultivated in larger scale (350 mL TB-medium in 500 mL flask). After harvesting, the cells were immediately disrupted by sonification and the crude extracts were purified over a TALON® metal affinity resin in accordance to an optimized purification protocol.^[178] Combination of all active fractions yielded protein close to homogeneity (Figure 35, bands of all variants see in the appendix, Figure 54 to Figure 56). The purification yields were not further quantified as varying expression levels with each culture were observed for this expression system. This observation might be related to the relatively low plasmid stability.

6 Improvement of heme incorporation by a protein sequence based enzyme engineering approach

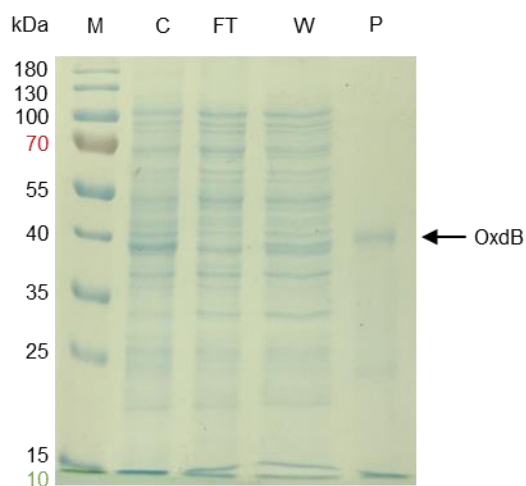


Figure 35. SDS-PAGE visualizing the successful purification of OxdB (here OxdB-M18) *via* affinity chromatography. M: Marker, C: Crude-extract, FT: Flowthrough, W: Wash fraction, P: Eluted protein.

6.4 Evaluation of the mutant library

6.4.1 Effect of the mutants on the specific enzymatic activity

After desalting of the purified enzymes *via* centrifugal filtration, they were tested directly for the biotransformation of Z-PAOx. The activity assay used for the whole-cell catalysts was slightly adjusted to the requirements of purified enzymes. The initial activity of the variants with single mutations was determined in this assay (Figure 36). Wild-type OxdB showed a specific activity of 14.0 U·mg⁻¹. Small changes original preparation of OxdB^[163] such as different aeration rates during protein expression, the protein purification method and the oxygen saturation in the activity assay cause a significant deviation of the determined Oxd activity. Therefore, this value was not compared to literature known activities of purified wild-type OxdB. As for the constructed variants all procedures including expression, purification and activity assay are carried out under the same conditions compared to the wild-type enzyme, the determined activity was a suitable reference for evaluation of the mutations.

A majority of 60 % of the variants showed an improved specific activity compared to the wild-type enzyme. A few issues have to be considered in order to compare activities determined with a whole-cell catalyst and a purified enzyme. The expression level of the protein is one factor important for the whole-cell catalyst activity. Therefore, some variants showing a high activity for the whole-cell catalyst does not necessarily have to be superior to other variants for the purified enzyme. Another factor which might have an influence on the whole-cell catalyst activity can be the other components of the cells, which could have an impact on the enzymatic activity. Mass transfer and substrate uptake and excretion can also vary from cell to cell. The specific activity of the purified enzyme is considered to be the most adequate value for comparison of enzymatic activities, however, this value gives no absolute information about applicability for synthetic purposes. Substrate and product inhibition and stability issues are important in this regard as well. Even though these variants were less active in the whole-cell screening, the highest specific activities observed were 24.7 U·mg⁻¹ and 24.0 U·mg⁻¹ for OxdB-M1 (I319E) and OxdB-M19 (Q250I), respectively. Five variants (OxdB-M5, M6, M10, M11, M13) showed activities lower than 11 U·mg⁻¹, corresponding to a relative activity below 79 % of the wild-type enzyme. The specific activity of OxdB-M5 (I105R) was with 13 % relative to the wild-type enzyme particularly low. Also OxdB-M13 (D135L) was less active than the wild-type, even though a slight improve was observed with the whole-cell catalyst. For this mutant, a different migration behaviour (slightly faster than the other proteins) was observed in the SDS-PAGE analysis as well. Seven variants (OxdB-M2, M7, M8, M12, M15 and M16, M17) exhibited a slightly improved activity between 17.4 and 18.2 U·mg⁻¹, which corresponds to a relative increase of up to 30 % compared to the wild-type enzyme. OxdB-M4 (V149E) and OxdB-M9 showed an activity increase of 36 and 44 %, respectively. The other variants (OxdB-

6 Improvement of heme incorporation by a protein sequence based enzyme engineering approach

M3, M14, M18, and M20) showed specific activities in the same range as the wild-type enzyme ($\pm 10\%$). It was decided to not investigate reaction kinetics, as the K_m -value for the substrate Z-PAOx is in sub-millimolar range, thus, a change might alter the applicability in synthetic transformations only minorly.^[162] Furthermore, the mutations are not located in the active site.

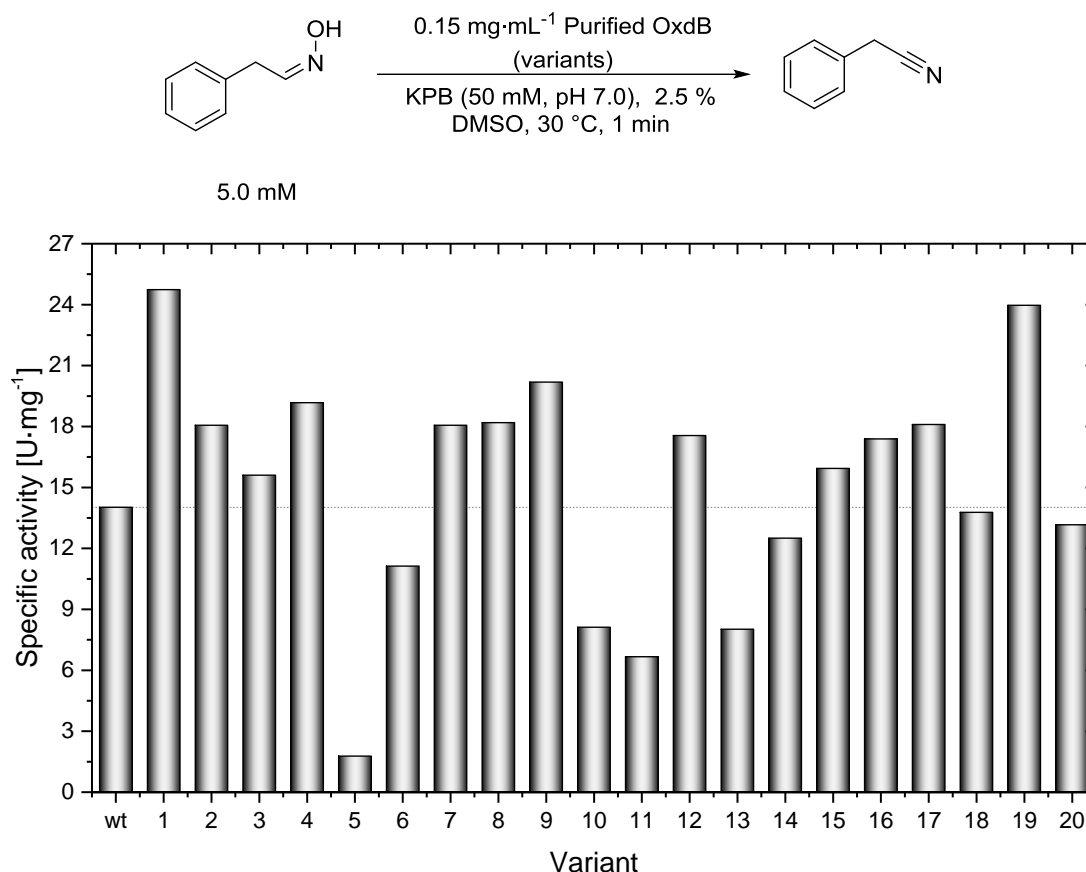


Figure 36. Specific activities of wild-type OxdB and its variants (purified enzyme) for the standard substrate Z-PAOx.

For the variants with two point mutations, activities outperforming their parents were observed (Table 28). OxdB-D1 (L65H_I180A) and OxdB-D3 (L65H_K190R) showed a specific activity of 26.4 U·mg⁻¹ and 28.4 U·mg⁻¹, respectively (Entries 1 and 3). This corresponds to a 1.9- and 2.0-fold increase compared to the wild-type. The specific activities were even exceeding the best single mutations OxdB-M1 and OxdB-M19. OxdB-D2 (I180A_K190R) shows an activity improvement below 10% compared to its parents (Entry 2).

6 Improvement of heme incorporation by a protein sequence based enzyme engineering approach

Table 28. The specific activities of the variants OxdB-D1 to OxdB-D3 and the relative activities compare to the wild-type protein and the corresponding parent variants.

Entry	Specific activity [U·mg ⁻¹]	Activity relative to wt [%]	Activity relative to parent 1 [%]	Activity relative to parent 2 [%]
1	26.4	189	+31	+51
2	19.1	136	+5.1	+8.8
3	28.4	203	+41	+62

6.4.2 Protein mass-spectrometry

In contrast to the results from *Matsui et al.*, huge deviations of the specific activity of the wild-type enzyme and its variants were observed. Static nanoESI-MS measurements under denaturing conditions were used for the determination of the protein masses. The following constructs were analyzed: The wild-type enzyme, the most active variants (OxdB-M1, M2, M4, M8, M9, M12, M17, and M19) and OxdB-M13 because of its different gel electrophoresis behaviour. The results for all analyzed variants can be found in Table 29. Besides the charge state envelope of the protein ions, protoheme IX was identified with a high mass accuracy (m/z 616.1773, m/z_{theo} 616.1774, $\Delta mass$ 0.1 mmu; deviation: 0.17 ppm). This indicated, that the heme cofactor is bound non-covalently to the enzyme as reported by previous publications.^[162,174] Under native conditions, the static nanoESI-MS spectra contained a charge state envelope at significantly higher m/z values with a lower amount of charge states. In most variants, each charge state consisted of two peaks with a typical mass shift of 615 ± 40 Da (after charge state clean up). This is in good agreement for two enzyme species, one with and the other without the cofactor protoheme IX.

6 Improvement of heme incorporation by a protein sequence based enzyme engineering approach

Table 29. Protein masses determined with static nanoESI-MS for wild-type OxdB and selected variants. The charge state adjusted protein masses in the denatured state and the native state are given in Da. For the native state, two masses were determined, only the result with the higher molecular mass is displayed in this table. The other values are available in the appendix (Table 61).

Variant	M _{sequence} [Da]	M _{Denatured} [Da]	ΔMass to sequence [Da]	M _{Native} [Da]	ΔMass to denatured protein [Da]
Wild-type	41216.78	41255.8 ± 9.0	+39.02	41901.8±6.0	646.0
M1 (I319E)	41232.73	41248.21±1.97	+15.45	41863.76±0.37	615.55
M2 (I226Q)	4231.75	41236.9±4.8	+5.15	41844.5±2.6	607.6
M4 (V149E)	41246.76	41302.7±6.4	+55.94	41862.4±2.1	559.7
M8 (I180A)	41174.69	41208.0±6.8	+33.51	41824.1±6.7	615.9
M9 (L65H)	41240.76	41218.7±4.8	-22.06	41829.4±12.4	610.7
M12 (K190R)	41244.79	41291.3±4.6	+46.51	41863.8±0.4	572.5
M13 (D135L)	41214.85	41216.4±0.7	+1.55	41830.60±0.04	615.0
M17 (H296L)	41192.79	41229.0±8.0	+36.21	41791.2±3.3	562.2
M19 (Q250I)	41201.80	41182.9±7.8	-18.9	41801.6±1.0	618.7
D1 (L65H_ I180A)	41198.68	41215.9±2.6	+17.22	41829.9±0.4	614.0
D2 (I180A_ K190R)	41202.71	41217.82±0.16	+15.09	41824.02±0.91	606.2
D3 (L65H_ K190R)	41268.77	41298.9±1.1	+30.13	41889.8±18.8	590.8

The determined molecular masses of wild-type OxdB and its variants exhibit deviations compared to the theoretical molecular weight from the sequence which exceeded the usual error range of such an analysis. This is probably caused by residual amounts of salt, which lead to broad signals in the mass spectrum, causing the inaccuracy of the molecular masses. This is quite common in measurements under native conditions, as ions of the buffer (here: ammonium acetate) form salt adducts with the protein, however, in the case of denaturing conditions protein clean-up might not be sufficient. Interestingly, the variants OxdB-M9 and OxdB-M19 yielded a lower protein mass compared to the theoretical mass derived from the sequence. An explanation for this finding is difficult without further data. Nevertheless, by overlaying both spectra of the denatured and the native protein (or an excerpt of a few charge states) the protein species with bound heme (w) can be easily differentiated from the protein species without heme (w/o). An example for this approach is visualized in Figure 37.

6 Improvement of heme incorporation by a protein sequence based enzyme engineering approach

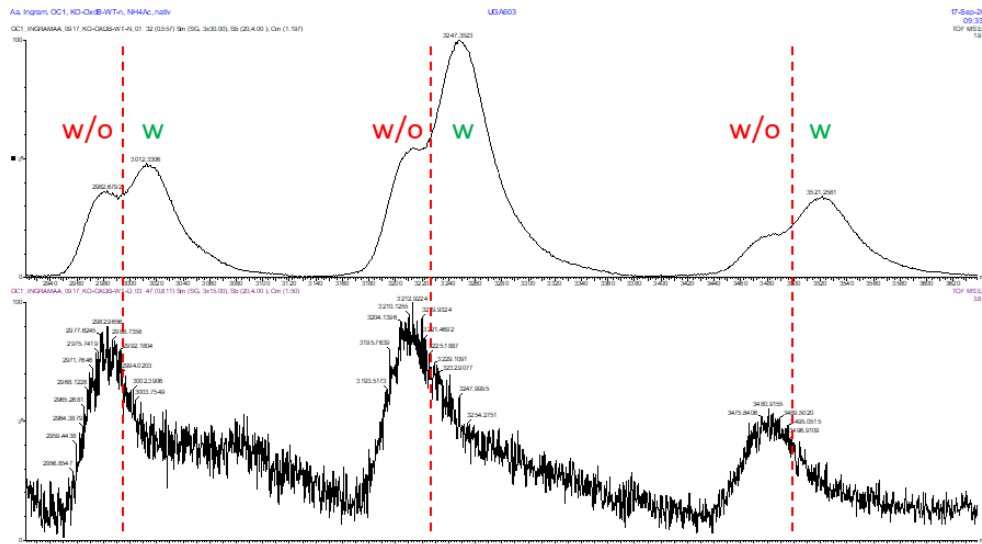


Figure 37. Overlay of excerpts of native (upper) and denatured (lower) wild-type OxdB mass spectra. The shown region refers to 2930 and 3520 m/z , in which the peaks referring to the charge states +11 to +13 are visible.

By comparing the peak intensities of the protein signals with and without heme in the native mass spectra, a rough estimate about the relative heme content can be made (Figure 38). For the wild-type enzyme, the ratio of the integrals of the peaks of apoprotein to heme-containing enzyme was estimated to be 30:70. However, a heme content of 33 % was reported for wild-type OxdB expressed in *E. coli* JM109 harboring pUC18-OxdB.^[163] In contrast to this expression system, a different expression vector and host cell was used in this approach (*E. coli* BL21(DE3) harboring pET22b(+)-OxdB). In addition, a C-terminal hexahistidine-tag was fused to the protein. Alterations of the expression system have an effect on the heme incorporation of OxdRE. For example, the fusion of a hexahistidine-tag caused a deviation of the heme content between 32 and 43 %.^[166] There are mainly two issues which have to be considered regarding the heme incorporations observed in the native mass spectra. On one hand, the heme content of the protein originally produced in the host cell might be higher than determined because some cofactor is lost during the purification process. The cofactor leaching might be different depending on the performed procedures. More complex purification protocols probably cause a higher cofactor leaching. On the other hand, the ratio of 30:70 (apoprotein / holoprotein) for wild-type OxdB can also indicate that the relative ionization efficiency of the apoprotein is lower compared to the holoprotein. Therefore, the absolute value of heme incorporation of wild-type OxdB remains unknown. A determination of this value by an orthogonal method such as the extraction of heme by treatment with hydrochloric acid / acetone would be suitable to verify the MS results regarding the ionization efficiency.^[250] For comparing the heme incorporation of the wild-type and the constructed variants to each other, it was sufficient to make the realistic assuming that the introduction of the mutations does not alter the ionization efficiency of the protein. For all variants investigated *via* native MS

6 Improvement of heme incorporation by a protein sequence based enzyme engineering approach

measurements, a change in the ratio of the relative peak integrals of a selected charge state was observed (e.g. Figure 38). For all mutants, it was assumed that the amount of heme incorporated during the expression has been increased.

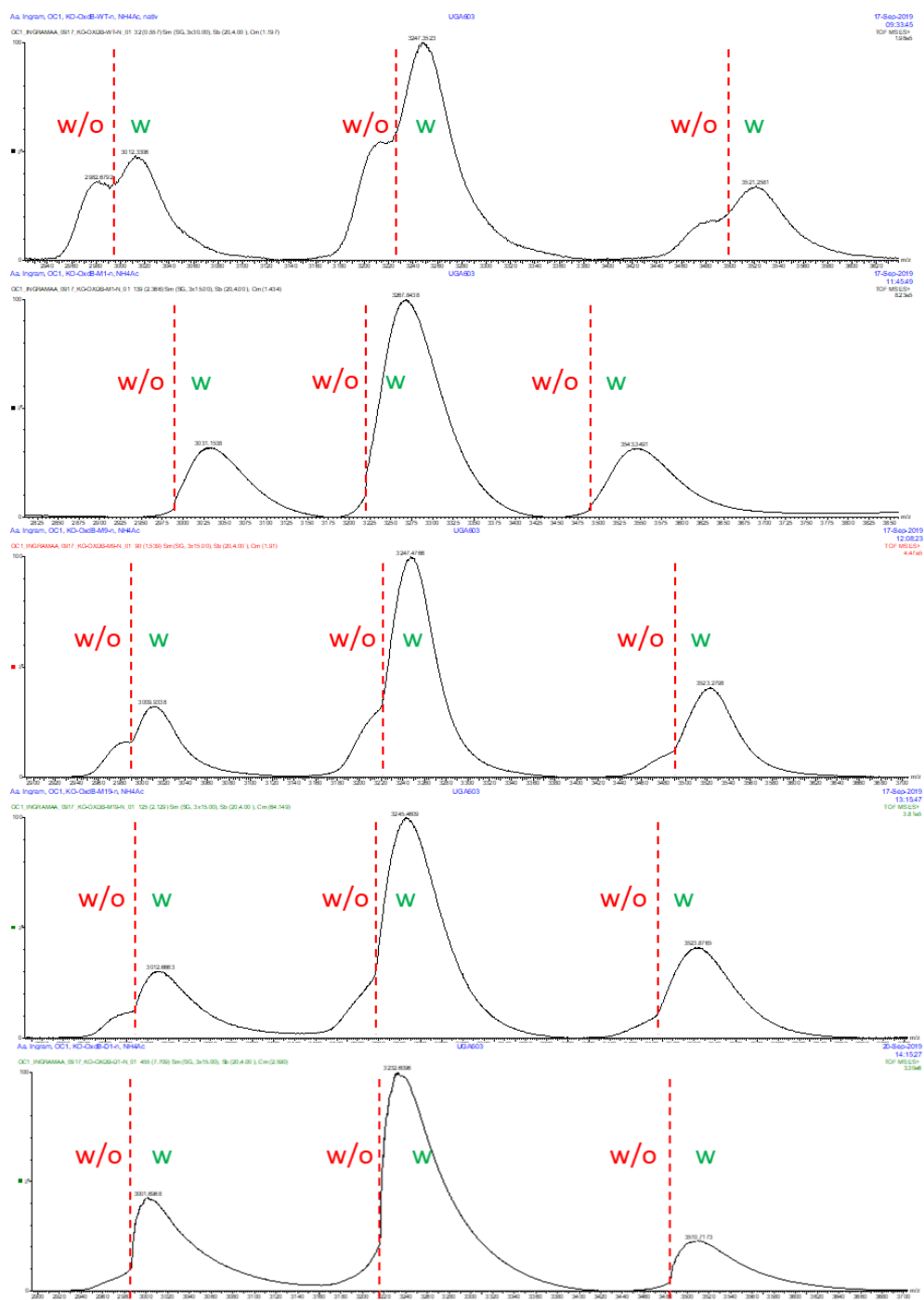


Figure 38. Excerpt of native mass spectra of wild-type OxdB and selected variants (from top to bottom: Wild-type OxdB, OxdB-M1, OxdB-M9, OxdB-M19, OxdB-D1).

6 Improvement of heme incorporation by a protein sequence based enzyme engineering approach

If the relative heme content estimated by the described method is compared to the specific activity of the enzyme, a correlation between enzymatic activity and heme incorporation could have been found (Table 30). This effect has also been previously observed with OxdB.^[162] Nearly all tested variants which exhibited higher activity compared to the wild-type also contained a higher amount of the cofactor. The variant OxdB-M13 is an exception to this finding. For example, the single mutation variants OxdB-M1, OxdB-M2, OxdB-M8, OxdB-M12, and OxdB-M13, and all double mutation variants exhibited heme contents above 90 %; the apoprotein was barely present in these analysis. For OxdB-M9, a ratio of 17:83 was observed, which correlated to its relative activity 44 % higher than the wild-type. For OxdB-M19, a ratio of 12:88 was found, while the activity was even higher with 24.0 U·mg⁻¹. The variant with the highest activity amongst the single mutants (OxdB-M1) also exhibited almost no apoprotein. The double mutants OxdB-D1 and OxdB-D3 showed even higher catalytic efficiency than all single mutations, their heme content compared to their parents was in a comparable range. As the purified variants showed heme contents of up to 98 % (OxdB-M1), it is unlikely that cofactor leaching occurred during the protein purification. The procedures from the cell disruption by sonification until the desalting were performed according to the same protocol for all variants (also same incubation times between all steps). This underlines that cofactor leaching observed only in the wild-type enzyme is unlikely. In addition, the incubation time between the activity determination and the MS measurements was kept short (between 4 and 14 days). A precipitation of the heme cofactor reducing the absolute heme content of OxdB by ~20 % is known for longer incubation times (~4 months).^[162] However, this effect is assumed to be not relevant for shorter incubation times. Moreover, the incubation time of the protein between expression and MS measurement with the highest heme content (OxdB-M1) and the lowest heme content (wild-type OxdB) was equal. This results serve as an evidence that the heme content of wild-type OxdB is below 100 % when originally produced in the cells, at least when produced with a C-terminal hexahistidine-tag in *E. coli* BL21(DE3). The introduction of the designed mutations led to a higher heme incorporation during expression, especially for OxdB-M1.

6 Improvement of heme incorporation by a protein sequence based enzyme engineering approach

Table 30. Specific activities and ratios of the integrals of non-heme containing and heme containing OxdB (mutants) estimated for a selected number of charge states.

Variant	Specific activity [U·mg ⁻¹]	Ratio w/o:w heme
Wild-type	14.0	30:70
M1	24.7	2:98
M2	18.1	4:96
M4	19.2	10:90
M8	18.2	3:97
M9	20.2	17:83
M12	17.6	5:95
M13	12.0	9:91
M17	18.1	22:78
M19	24.0	12:88
D1	26.4	6:94
D2	19.1	7:93
D13	28.4	7:93

The specific enzymatic activity is of course not only related to the heme content but also many other factors. Additionally, the natural errors of this estimation have to be considered. Furthermore, several other factors such as steric and electronic effects in the second sphere of the active site and changes of the secondary and tertiary structure of the protein induced by the mutation can have a tremendous effect on the enzymatic activity. This explains why some variants with a higher estimated cofactor content (e.g. OxdB-M2 and M12) are less catalytically efficient than other mutants with a lower estimated heme content such as OxdB-M9. Another example for a less active mutant despite of its high heme content is OxdB-M13, which additionally shows faster migration in the gel electrophoresis under denatured conditions (SDS). The activity was still even lower compared to the wild-type enzyme. In comparison to the mass spectra of the other variants, the peaks of OxdB-M13 were very sharp lacking almost completely the peak broadening caused by adduct formation with the buffer. The reason for this finding is unclear.

6.5 Conclusion and outlook

Utilizing INTMSAlign_HiSol, hydrophathy mismatches in the structure of OxdB were identified and corrected. Therefore, 23 variants were constructed only based on sequential data. Aldoxime dehydration activity of Z-PAOx was tested with OxdB and all generated variants confirming that only active protein was obtained. The observed specific activity of the majority of the variants was significantly higher (up to 1.8 fold with a single mutation) compared to the wild-type enzyme, even though the mutations were not located in the active site. Combination of the mutations led to a further increase of the specific enzymatic activity. An improvement of whole-cell catalyst activity was observed for a few variants as well. The expression level was not altered majorly by the mutations. For a few variants, even a lower amount of protein was produced during expression.

In contrast, previous investigations showed that mutations calculated with INTMSAlign_HiSol led to active enzymes and solubilized them during expression in *E. coli*. However, an increase of the specific enzymatic activity was not observed.^[237] The reason for the increased specific activity of OxdB was analyzed with static nanoESI-MS measurements of the purified wild-type enzyme and selected variants under native and denaturing conditions. By comparing the integrals of the peaks of a selected charge state of OxdB with and without bound protoheme IX, an improved cofactor incorporation during expression was observed for all tested variants with a higher specific activity. For OxdB-M1 (I319E), the heme incorporation was nearly quantitative. It is impressive that such an improvement of cofactor incorporation was achieved by means of a single mutation designed with a rational method requiring only the amino acid sequence of the enzyme. A correlation between the heme incorporation and the specific activity of the variants was found. However, the increase of specific activity for enzymes with higher heme content was not linear and did not apply to all variants. When the crystal structure of OxdB will be determined, the impact of the mutations could be discussed more in detail. Nevertheless, the chosen method proved suitable to increase the heme content and the specific activity of OxdB by means of a single mutation and without further alteration of the expression system.

6 Improvement of heme incorporation by a protein sequence based enzyme engineering approach

It would be interesting to test if other Oxds or heme-dependent proteins such as CYP enzymes can also be optimized with INTMSAlign_HiSol. In this regard, the developed protein engineering strategy might be an easy tool to improve functional heme protein expression which does not require co-expression of other proteins, the addition of expensive heme precursors or heme itself. This method might be also advantageous for the production of whole-cell catalyst for synthetic purposes. Furthermore, if the promising variants will be expressed in the established system (*E. coli* BL21(DE3)-RIL harboring pUC18-OxdB), their synthetic potential, especially regarding stability and productivity, can be evaluated for interesting substrates such as fatty aliphatic nitriles. These engineered variants might also facilitate the expression of soluble OxdB regarding the heme incorporation in the fed-batch fermentations.

6.6 The effect of the cofactor flavin mononucleotide on aldoxime dehydration activity

Kato and Asano reported in their initial studies that OxdB requires the cofactor FMN for being active. On one hand, FMN is assumed to have a function related to electron transfer processes. Depending on the purification protocol, especially when longer dialysis is implied, OxdB is not active without addition of FMN or is inactivated fast. Other redox agents such as sodium thionite or sulphite or other flavin cofactors can restore the activity. On the other hand, OxdA does not require the cofactor FMN.^[162,165,166] In this work, the measurements of the specific activity of OxdB was carried out in absence of this cofactor. Nevertheless, consistent results were observed. Shorter purification protocols are reported to reduce the inactivating effect of long dialysis procedures, especially when affinity chromatography is used as the only purification method.^[166,178] Furthermore, the MS measurements proved the absence of the cofactor FMN both in native and denaturated OxdB and its variants. If the cofactor FMN was added to the activity assay, the variants corresponded differently (Figure 39). Even though all variants were active in absence of the cofactor (also after longer incubation times with an activity loss), most of the variants showed an increased activity, with a maximum increase of 289 % (3.9 fold) for OxdB-M10 (V262G). In particular, variants with a rather low activity measured in absence of FMN showed an increase over 2.8 fold in its presence (OxdB-M6, M10, M13, M16, and M18), but this is not exclusive to those (OxdB-M7). Surprisingly, wild-type OxdB, OxdB-M12 and OxdB-M14 showed a slightly lower activity (~0.8 fold) in the presence of FMN compared to when measured in absence of FMN. The activity increased between 1.1 fold to 2.3 fold for the other variants.

6 Improvement of heme incorporation by a protein sequence based enzyme engineering approach

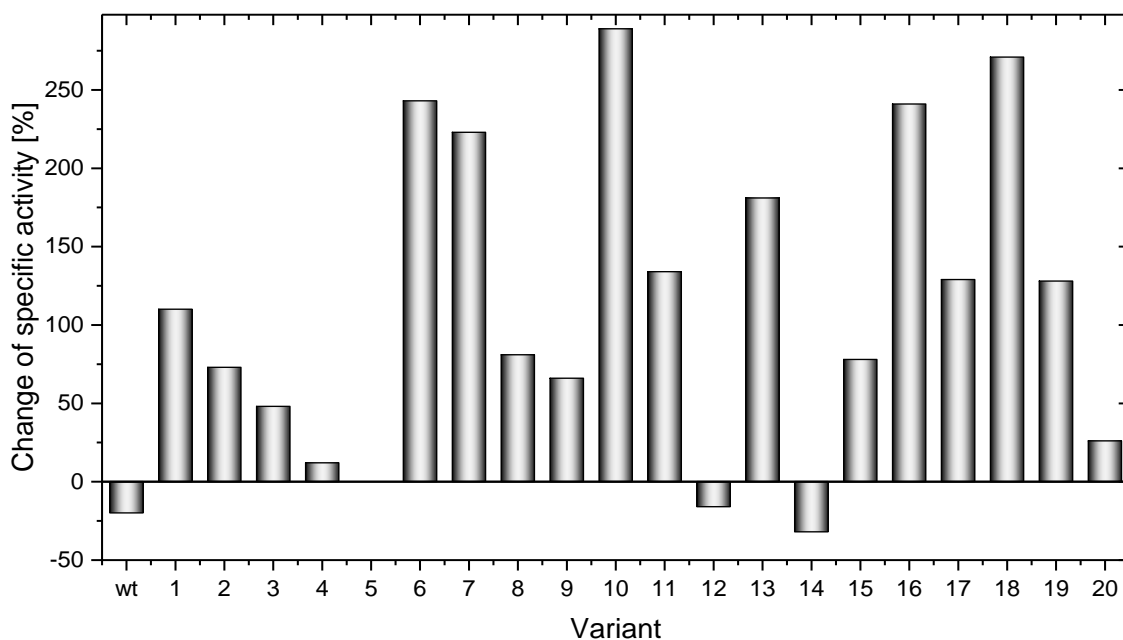
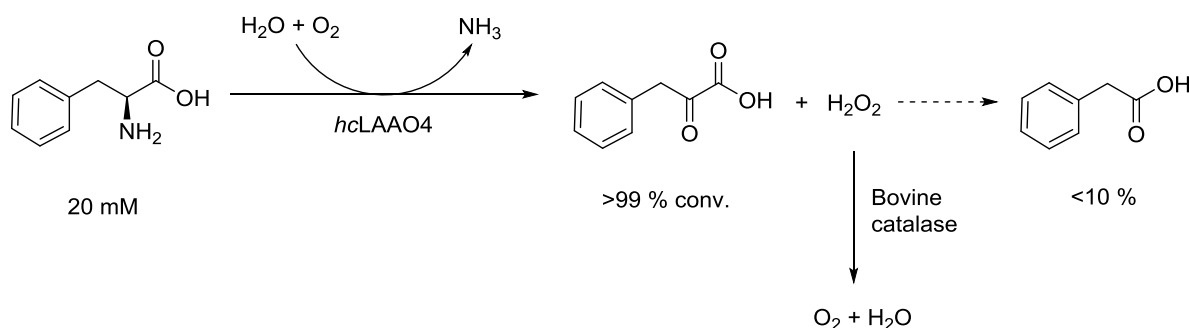


Figure 39. Change of the specific activity of purified wild-type OxdB and its variants for Z-PAOx in the standard assay in presence of 250 nmol FMN compared to the activities measured in absence of FMN.

This might be caused by different occupation of the oxidation states of the heme iron in OxdB and its variants (ferrous and ferric). The addition of FMN might reduce the iron atoms in the inactive ferric state back to the active ferrous state, thus, improving the dehydration activity. As all procedures were performed similarly also with the same incubation times between the step, the different oxidation of the heme cofactor is less likely. Especially the affinity chromatography was carried out very fast, thus, avoiding longer air contact of the protein. Another reason might be that the introduced mutations change the electronic properties of the enzyme, thus, affecting the function of FMN. The effect of the cofactor FMN observed in the activity assay could also be related to the heme-content of the enzymes, which was different for each variant. Besides the above-mentioned hypotheses, other components in the assay solution could have an effect on the activity and electron transfer processes mediated by FMN. Residual amounts of Tris-salt and imidazole (μM scale), which were not totally removed by the desalting after purification, are contained in the protein solutions used in the assay. On one hand, Tris is a well-known quencher for especially hydroxyl-radicals,^[251] an accepting ligand in charge-transfer complexes,^[252] and is moreover involved in uncoupling processes in chloroplasts.^[253] On the other hand, imidazole can be involved in electron transfer processes.^[254] This is only a speculation as the precise role of FMN in the catalytic mechanism of OxdB is not known yet.^[162,172] Other Oxds are also active in the absence of FMN or other reducing agents.^[166] Nevertheless, if all procedures from purification, dialysis, and the activity assay could be carried out under strict anaerobic conditions (e.g. in a glove box under nitrogen atmosphere), a better comparability of the conditions might help to get further insights in these processes.

7 Summary and outlook

In this thesis, two different enzyme classes were utilized for the synthesis of α -keto acids and nitriles, respectively. First, a newly discovered L-AAO from *H. cylindrosporium* which accepts a broad range of α -amino acid derivatives as well as unnatural amino acids was utilized in biotransformations targeting α -keto acid synthesis requiring only air as oxidant. Despite the challenging expression of this enzyme class, an efficient expression protocol and activation method is known for this enzyme.^[184] For a model substrate, L-phenylalanine, important characteristics regarding initial process development for the synthesis of phenylpyruvate were investigated (Scheme 63). The formation of the naturally occurring byproduct formed by oxidative decarboxylation of phenylpyruvate, phenylacetic acid, was suppressed effectively by addition of a commercially available bovine catalase. The purified enzyme and the reaction product were robust against the reaction conditions. Alternatively, the activated cell lysate is a suitable catalyst as well. A substrate concentration of 20 mM was converted smoothly in four hours reaction time. The great potential of this enzyme is underlined by the absence of inhibitory effects of buffer salt, substrate and product in concentrations close to the solubility limits. Moreover, the turnover rate of the enzyme increased at higher substrate loadings. If this reaction system can be successfully transferred to the oxidative deamination of an α -amino acid ester, this synthetically interesting product class might be accessible using *hcLAAO4*.



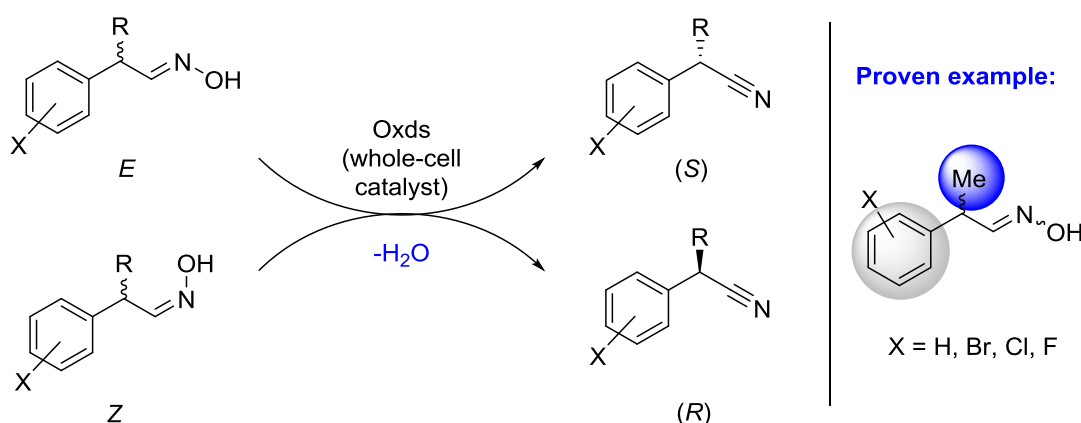
Scheme 63. Overview about the process for production of phenylpyruvate from L-phenylalanine using *hcLAAO4*.

Second, the scope of chiral nitrile synthesis with Oxds was investigated (Scheme 64). Together with the coworkers *Betke* and *Rommelmann*,^[189,190] an initial study on enantioselective aldoxime dehydration by *Metzner et al.* on this topic^[180] was expanded and regularities in the enantioselective aldoxime dehydration were observed. Therefore, a broad variety of chiral aldoximes was synthesized and the enantioselectivity of the reactions was investigated with five Oxds available as recombinant whole-cell catalysts. Amongst these substrates, a “privileged” substrate structure applying for all tested enzymes was identified and verified for several substrates. The relevant features of this structure are a stereocenter in α -position to the aldoxime moiety, strong differentiation between the substituents regarding their size in this

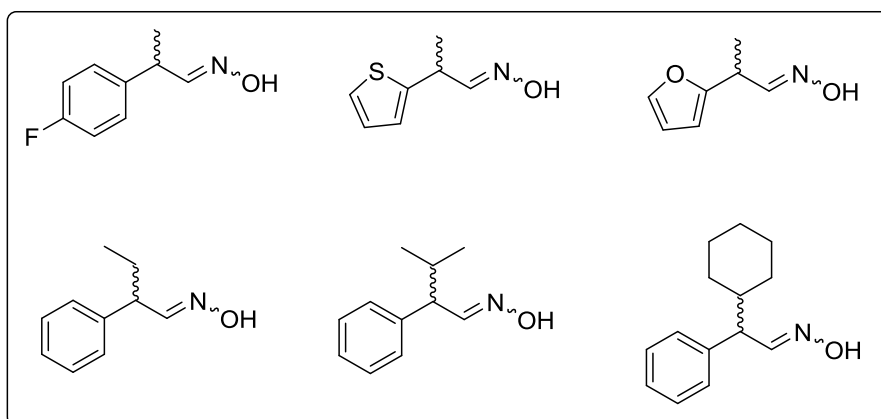
7 Summary and outlook

position and a specific rotational flexibility of these substituents. In particular, Oxds are found to be especially enantioselective for 2-PPOx and its halogenated derivatives.

For the large majority of the substrates corresponding to this “privileged” substrate structure, a switch in the enantioselectivity was observed when the *E*- or *Z*-isomer is given as substrate. (*S*)-Nitriles are preferably formed from *E*-aldoximes and (*R*)-nitriles *vice versa* from the *Z*-aldoximes. This is a very rare example in which both enantiomers of the product are accessible with the same enzymes. Furthermore, excellent enantiopurities of the nitriles of up to 99 % *ee* were achieved in the kinetic resolutions of isomerically pure racemic aldoximes even at elevated conversions close to the theoretical maximum of 50 %. This study was expanded to bulky derivatives of 2-PPOx with a decreased size difference of the substituents, which led to reduced enantioselectivity in accordance to the expectations. With the developed system, a new cyanide-free biocatalytic approach for the production of chiral nitriles has been presented. With the methods of enzyme engineering and chemical reaction engineering, higher selectivities and productivities might be achieved bringing this reaction closer to an application in organic chemistry.



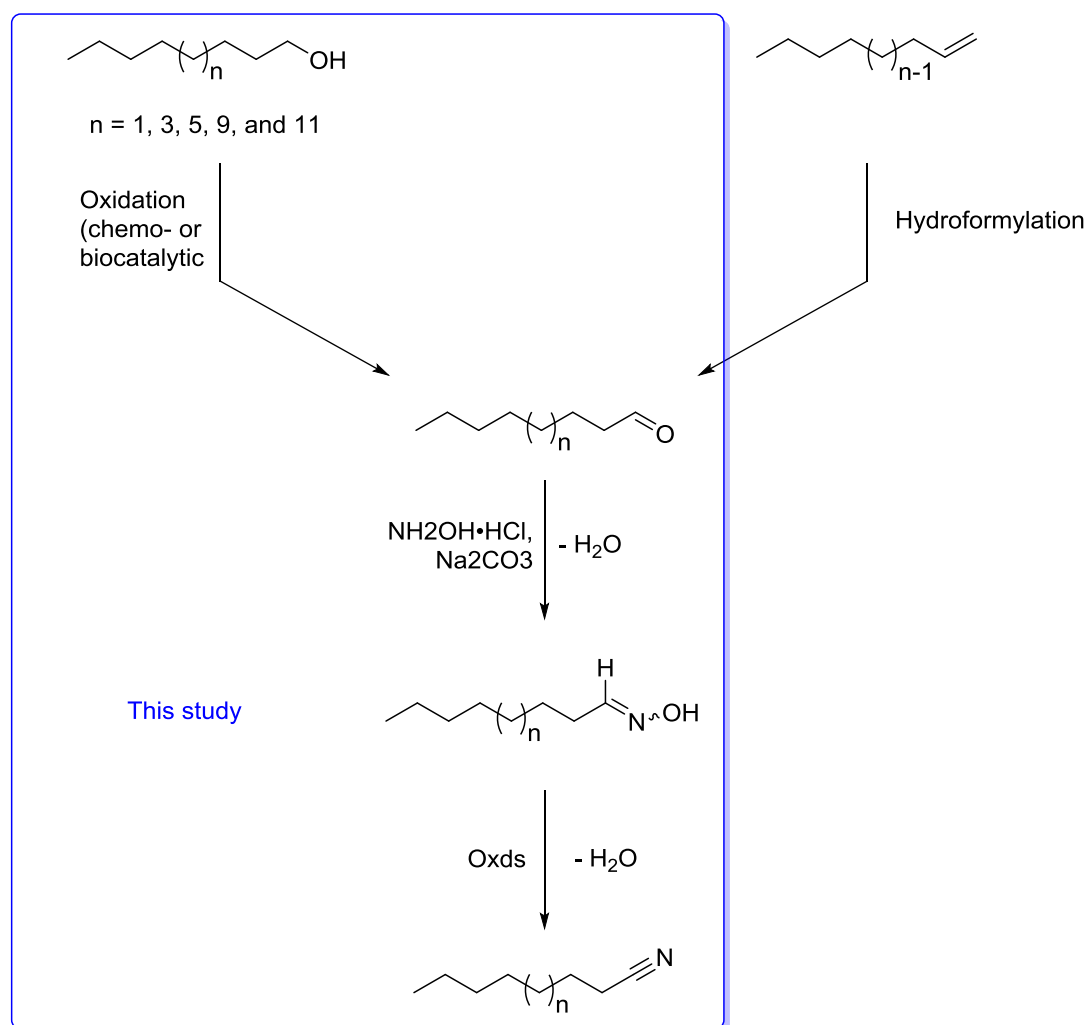
Tested substrates:



Scheme 64. Overview about the enantioselective aldoxime dehydration, the privileged substrate structure and all tested substrates in this thesis.

7 Summary and outlook

Oxds were not only used as biocatalysts for the synthesis of chiral nitriles, but also integrated in a reaction sequence forming aliphatic fatty nitriles from the corresponding fatty alcohols or alternatively terminal alkenes. Thus, a new approach towards the production of chemicals from the bulk chemistry segment was developed (Scheme 65). Initial studies on the feasibility of such a synthetic approach were carried out. In particular, the oxidation of fatty alcohols to the corresponding aldehydes, the condensation of fatty aldehydes with hydroxylamine forming the aldoximes and their dehydration with Oxds were investigated. The results indicated that such a cascade is possible in principle as the aldoxime dehydration catalyzed by Oxds as the key step is promising. The project of fatty nitrile synthesis was continued by the coworkers *Busch*, *Hinzmann* and *Plass*, who further investigated the reactions individually and established *inter alia* a cascade reaction for the synthesis of nonanenitrile starting from 1-octene featuring hydroformylation, condensation with hydroxylamine and biocatalytic aldoxime dehydration without intermediate workup procedures.^[205,215,219]



Scheme 65. Project overview about the synthesis of fatty nitriles in reaction sequences employing Oxd-catalyzed aldoxime dehydration.

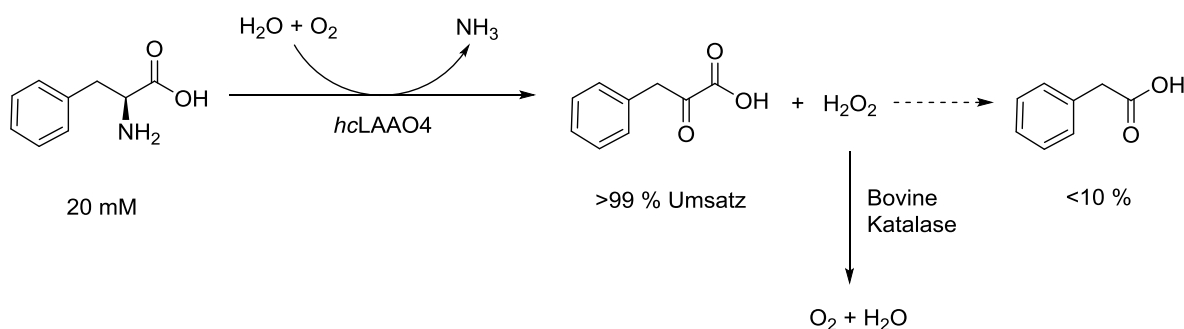
7 Summary and outlook

Addressing another important issue of the application of enzymes in bulk chemistry, high cell-density fermentation of OxdB was investigated in collaboration with the *Friebs* group. Despite the difficulty of functional heme protein expression in larger bioreactors, promising results regarding the enzymatic activity of the produced whole-cell catalyst were observed. Valuable information on the effect of oxygen saturation as a cause for lower catalyst activity was obtained. However, optimization of this process especially regarding the oxygen saturation, was not successful with the established expression system. *Inter alia* challenging points such as insufficient plasmid stability require the establishment of a novel expression system.

Another observation in the fermentations of OxdB was the formation of high amounts of insoluble protein. Incorrect protein folding or the insufficient incorporation of the cofactor heme b were proposed as possible reasons. In order to address this issue, a method of enzyme engineering was applied to OxdB. Based on a method for solubilization of proteins in recombinant expression in *E. coli* using the software INTMSAlign_HiSol,^[237] 23 variants of OxdB were constructed. This software utilizes only primary structure data (if the α -helix rule is neglected). Even though the expression level did not improve for the variants under the same culture conditions, an increased specific activity was observed. No mutation was located in the proposed active site of the protein, nonetheless the best single mutant showed a specific activity improved by 76 % compared to the wild-type OxdB. Double mutants led to an even higher improvement. nanoESI MS measurements of OxdB and its variants under native conditions revealed an increased cofactor incorporation for several variants in comparison to the wild-type enzyme. One variant (OxdB_I319E) showed nearly quantitative heme incorporation. A correlation between the relative heme content and the enzymatic activity of the mutants was figured out. Besides, this strategy represents the first protein engineering-based approach for increasing the heme incorporation during heterologous expression of hemoproteins. An increased soluble expression in shaking flask cultures for an already solubly expressed protein was not observed. However, the effect of the mutations on expression at a higher temperature or in a larger bioreactor has to be evaluated yet.

8 Zusammenfassung und Ausblick

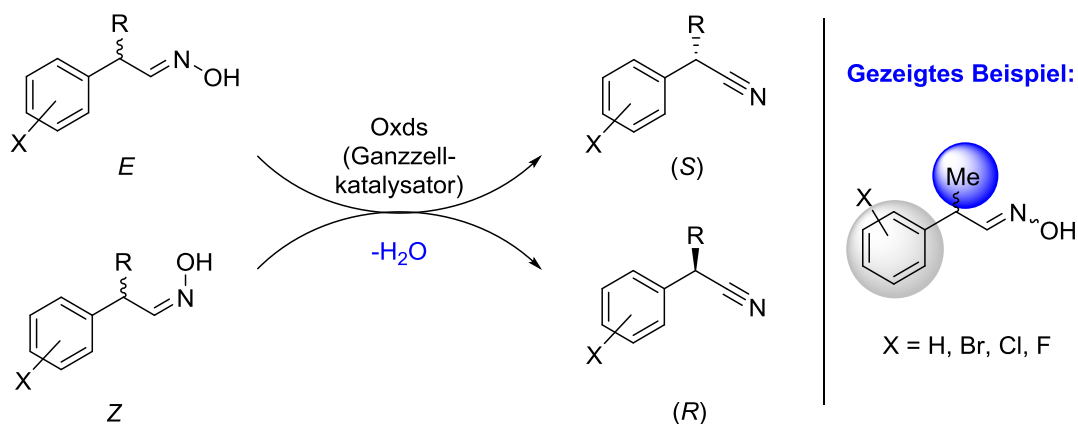
In dieser Arbeit wurden zwei verschiedene Enzymklassen zur Synthese von α -Ketosäuren und Nitrilen untersucht. Zunächst wurde eine L-AAO aus dem Fungus *H. cylindrosporum* in Biotransformationen mit dem Ziel der Synthese von α -Ketosäuren eingesetzt. Dieses Enzym zeichnet weiterhin aus, dass neben vieler proteinogener Aminosäuren auch deren Derivate wie Ester und zusätzlich eine Reihe an unnatürlichen α -Aminosäuren umgesetzt werden. Trotz der schwierigen Überexpression dieser Proteinfamilie in heterologen Expressionssystemen ist ein effizientes Protokoll zur Produktion von aktivem Protein für dieses Enzym bekannt. Anhand eines Modellsystems mit dem Substrat L-Phenylalanin wurden wichtige Parameter bezüglich initialer Prozessentwicklung zur Synthese von Phenylpyruvat mit diesem Enzym untersucht (Scheme 66). Die Bildung des natürlichen Nebenproduktes Phenylelessigsäure, welche durch eine oxidative Decarboxylierung von Phenylpyruvat mit Wasserstoffperoxid hervorgerufen wird, konnte erfolgreich durch Zugabe einer kommerziell erhältlichen Katalase aus der Schweineleber unterdrückt werden. Sowohl das aufreinihte Protein und das säuraktivierte Zelllysate als auch das Reaktionsprodukt waren stabil unter den Reaktionsbedingungen. Bei einer Substratbeladung von 20 mM wurde vollständiger Umsatz nach vier Stunden Reaktionszeit erreicht. Die Abwesenheit von inhibitorischen Effekten von Puffersalz, Substrat und Produkt selbst an deren Löslichkeitsgrenzen unterstreichen das vielversprechende Potenzial dieses Enzyms. Ferner wurde eine höhere katalytische Effizienz des Enzyms bei höheren Substratbeladungen beobachtet. Sofern dieses Reaktionssystem erfolgreich auf die Anforderungen der Synthese von α -Ketoestern zugeschnitten werden kann, würde dies einen neuen möglichen synthetischen Zugang zu dieser Produktklasse eröffnen.



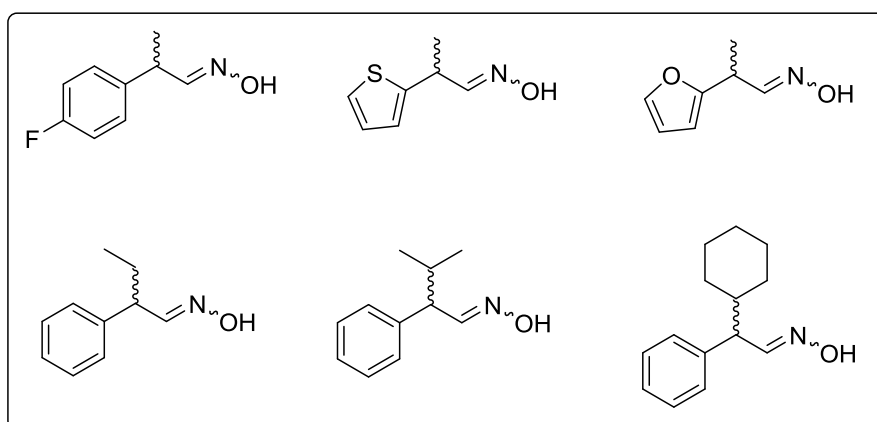
Scheme 66. Überblick über den Prozess zur Produktion von Phenylpyruvat von L-Phenylalanin mit hcLAAO4.

Zweitens wurde der Anwendungsbereich von Aldoximdehydratasen (Oxds) bezüglich der Synthese von chiralen Nitrilen untersucht. Gemeinsam mit *Betke* und *Rommelmann*^[189,190] wurde die initiale Studie von *Metzner et al.*^[180] ausgeweitet und Regelmäßigkeiten der enantioselektiven Dehydratisierung von Aldoximen beobachtet. Eine breitgefächerte Auswahl an chiralen Aldoximen wurde synthetisiert und die Enantioselektivität der Biotransformationen

mit fünf Oxds aus Mikroorganismen in Form von Ganzzellkatalysatoren untersucht (Scheme 67). Aus dieser Reihe an Substraten wurde eine privilegierte Substratstruktur ermittelt, welche mit allen getesteten Enzymen für mehrere Substrate bestätigt wurde. Ein Stereozentrum in α -Position zu der Aldoximfunktionalität, gute Differenzierung der Substituenten in dieser Position bezüglich ihrer Größe sowie eine spezifische rotatorische Flexibilität der Substituenten kennzeichnen diese Struktur. Allgemein gefasst, sind Oxd-katalysierte Reaktionen besonders für 2-PPOx und halogensubstituierte Derivate davon enantioselektiv.



Gestete Substrate (in dieser Arbeit):



Scheme 67. Überblick über die enantioselektive Aldoximdehydratisierung mit Oxds, der privilegierten Substratstruktur sowie allen in dieser Arbeit getesteten Substraten.

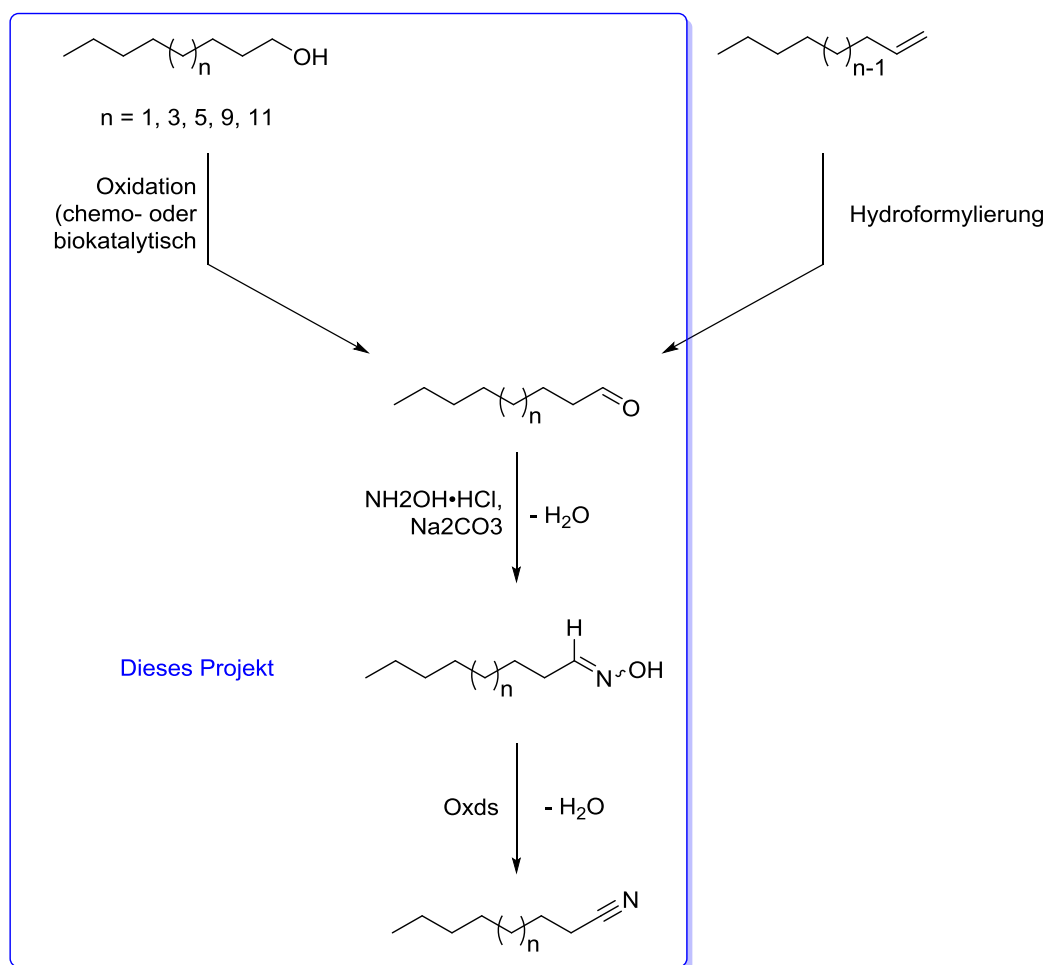
Für die große Mehrheit der Substrate, die dieser Struktur entsprechen, wurde ein Wechsel der Enantiopräferenz beobachtet abhängig davon ob das *E*- oder *Z*-Isomer des Aldoxims als Substrat vorlag. Bevorzugt wurden (*S*)-konfigurierte Nitrile aus *E*-Aldoximen und (*R*)-konfigurierte Nitrile umgekehrt aus *Z*-Aldoximen gebildet. Dies ist ein sehr ungewöhnliches Phänomen in der Enzymkatalyse. In diesem Fall sind prinzipiell beide Enantiomere einer Verbindung mit demselben Enzym zugänglich sind. Weiterhin wurden sehr hohe Enantiomerenreinheiten der Nitrile von bis zu 99 % ee in kinetischen Racematspaltungen ausgehend von isomerenreinen racemischen Aldoximen auch bei hohen Umsätzen nah dem

8 Zusammenfassung und Ausblick

theoretischen Maximum von 50 % Umsatz beobachtet. Diese Studie wurde außerdem auf Derivate von 2-PPOx mit sperrigeren Substituenten in α -Position erweitert, wodurch eine geringere Größendifferenz zwischen den beiden Substituenten erreicht wurde. Hier wurde entsprechend der aufgestellten Hypothese eine verringerte Enantioselektivität beobachtet. Mit dem hier entwickelten System wurde ein neuer Syntheseweg für chirale Nitrile in Reaktionen ohne das hochtoxische Cyanid präsentiert. Unter Anwendung der Methoden von „Enzyme Engineering“ und chemisch technischen Ansätzen könnte die Selektivität und Produktivität dieser Reaktion erhöht werden, was einen Einsatz in präparativer organischer Chemie wahrscheinlich machen würde.

Oxds wurden nicht nur als Biokatalysator zur Synthese von chiralen Nitrilen eingesetzt, sondern auch in eine Kaskade zur Synthese von Fettnitrilen aus den entsprechenden Fettsäuren oder terminalen Alkenen verwendet. Dabei sollte ein neuer Ansatz zur Synthese von Bulkchemikalien adressiert werden. Initiale Experimente zur Machbarkeit eines solchen Syntheseweges wurden untersucht. Genauer gefasst wurde die Oxidation von Fettalkoholen zu den Aldehyden, deren Kondensation mit Hydroxylamin zu Aldoximen und deren Dehydratisierung mit Oxds untersucht (Scheme 68). Die Ergebnisse legen nahe, dass die Aldoximdehydratisierung mit Oxds ein vielversprechender Ansatz ist. Das der Fettnitrilsynthese wurde von den Kollegen *Busch*, *Hinzmann* und *Plass* detaillierter untersucht und so unter anderem eine erfolgreiche Reaktionskaskade zur Synthese von Nonannitril ausgehend von 1-Octen *via* Hydroformylierung, Kondensation mit Hydroxylamin und der biokatalytische Aldoximdehydratisierung ohne Aufreinigungsschritte auf dem Syntheseweg etabliert.^[205,215,219]

8 Zusammenfassung und Ausblick



Scheme 68. Überblick über die Reaktionssequenz zur Synthese von Fettnitrilen mit biokatalytischer Aldoximedehydratisierung als Schlüsselschritt.

Um einen weiteren Aspekt von sehr großer Relevanz im Bereich der Enzymkatalyse im Bulkchemiesegment zu adressieren, wurde die Hochzelldichtefermentation von OxdB in Zusammenarbeit der Arbeitsgruppe *Friebs* untersucht. Trotz der erheblichen Schwierigkeiten der funktionalen Expression von Hämproteinen in größeren Bioreaktoren konnte vielversprechende Ergebnisse im Bezug auf die Proteinaktivität der hergestellten Ganzzellkatalysators erzielt werden. Relevante Informationen über den Effekt der Sauerstoffsättigung des Kulturmediums auf die Enzymaktivität konnten gewonnen werden. Eine Optimierung der Prozessbedingungen in dieser Hinsicht war jedoch nicht erfolgreich. Die ausschlaggebenden Aspekte wie unzureichende Plasmidstabilität erfordern die Etablierung eines neuartigen Expressionssystems.

Eine weitere Beobachtung in den Hochzelldichtefermentationen war die Bildung von größeren Mengen an unlöslichem Protein. Inkorrekte Faltungsmechanismen oder die unzureichende Präsenz bzw. Binding des Cofactors Häm b wurden dafür verantwortlich gemacht. Um diese Probleme zu lösen, wurde OxdB mit Methoden des Protein Engineerings modifiziert. Auf Grundlage einer Methode zur Solvatisierung von Proteinen bei heterologer Enzymexpression

8 Zusammenfassung und Ausblick

in *E. coli* mit dem Programm INTMSAlign_HiSol^[237] wurden verschiedene Varianten von OxdB hergestellt. Diese Software nutzt nur die Primärstruktur des Proteins (da die α -Helixregel vernachlässigt wurde). Obwohl keine Verbesserung des Expressionslevels des Proteins unter gleichen Expressionsbedingungen in Schüttelkolbenexperimenten erreicht werden konnte, wurde eine erhöhte spezifische Aktivität des Proteins beobachtet. Die beste 1-Punkt-Mutante war um 76 % aktiver als das Wildtypenzym, dabei lag die mutierte Aminosäure nicht im aktiven Zentrum des Proteins. Doppelmутanten waren noch effizienter. Mit nanoESI MS Messungen unter nativen Bedingungen konnte gezeigt werden, dass die Varianten eine höhere Einbindung des Cofactors Häm b verglichen mit dem Wildtyp aufzeigten. Die Variante OxdB_I319 erreichte eine fast vollständige Einbindung des Cofactors. Eine Abhängigkeit der Proteinaktivität von der Cofactoreinbindung wurde gefunden. Dieser Ansatz repräsentiert die erste auf Protein Engineering basierte Methode zur Verbesserung der Häm-Einbindung während heterologer Proteinexpression. Es war annehmbar, dass diese Varianten in Schüttelkolbenexperimenten keine erhöhte lösliche Expression aufzeigten, da das System dies bereits für den Wildtyp schafft. Der Effekt der Mutationen auf die lösliche Expression bei höheren Temperaturen sowie im größeren Maßstab im Bioreaktor bei höheren Zelldichten wäre darüber hinaus interessant zu untersuchen.

9 Experimental section

9.1 General information and analytics

9.1.1 Chemicals

All chemicals used throughout this thesis were purchased from commercial sources such as Sigma Aldrich, VWR, AppliChem, Roth, Alfa Aesar, ACROS Organics, TCI Chemicals and used without further purification.

9.1.2 Devices

Table 31. List of devices used throughout this thesis and their manufacturer.

Device	Manufacturer
Autoclave	Tuttnauer 3850 ELV Systec DX-23
Heat dryer	Incu Line, VWR
Incubator	Sartorius Certomat Is Infors HT Mutitron Pro
pH-meter	Orion 4 Star, Thermo Scientific
Shaker	Eppendorf Thermomixer Comfort Thermoshaker Universal Laborotechnik
Gel electrophoresis	Power Pac 200, Bio-Rad
Sterile working bench	Mars Safety Class 2, Scanlaf
Sonotrode	Sonopuls hd 2070, Bandelin
UV/Vis-spectrometer	Thermo Scientific Multiskan GO Tecan Spark 10M
Micro volume spectral photometer	Thermo Scientific Nanodrop
Balance	Extend, Sartorius CPA225D, Sactorius
Centrifuges	Himac CT15RE, Hitachi Heraeus Multifuge X3R, Thermo Electron Corporation High-Speed Refrigerated Centrifuge CR 22N, Hitachi
Centrifugal filters	Amicon Ultra (Millipore)

9.1.3 Analytical methods

9.1.3.1 Nuclear magnetic resonance-spectroscopy

NMR-measurements were measured on a Bruker Avance III 500 or Bruker Avance III 500HD and were processed with the software MestreNova. ^1H -NMR measurements were performed at 500 MHz and ^{13}C -NMR at 126 MHz. The chemical shift δ is given in ppm and refers the corresponding solvent signal. Coupling constants are given in Hz. All measurements were conducted in chloroform-d, dichloromethane-d₂ (deuteron) or water-d₂ (Roth).

9.1.3.2 Mass spectrometry

Electron ionization

EI mass spectra were recorded using an Autospec X magnetic sector mass spectrometer with EBE geometry (Vacuum Generators, Manchester, UK) equipped with a standard EI source. Samples were dissolved in dichloromethane and aluminum crucibles were filled with this solution and the solvent was evaporated. The aluminum crucibles were introduced by push rod. Ions were accelerated by 8 kV in EI mode. The mass axis was externally calibrated with perfluorokerosine as calibration standard. The spectra shown were recorded and processed with the OPUS software (V3.6, Micromass 1998) by the accumulation and averaging of several single spectra.

Electron spray ionization

Nano-ESI mass spectra were recorded using an Esquire 3000 ion trap mass spectrometer (Bruker Daltonik, Bremen, Germany) equipped with a nano-ESI source. Samples were dissolved in acetonitrile containing sodium perchlorate and introduced by static nano-ESI using *in-house* pulled glass emitters. Nitrogen served as both the nebulizer and dry gas. Nitrogen was generated by a Bruker nitrogen generator NGM 11. Helium served as cooling gas for the ion trap. The mass axis was externally calibrated with ESI-L Tuning Mix (Agilent Technologies, Santa Clara, CA, USA) as a calibration standard. The spectra were recorded with the Bruker Daltonik esquireNT 5.2 esquireControl software by the accumulation and averaging of 20 single spectra. FlexAnalysis 3.4 (Bruker Daltonik, Bremen, Germany) was used for processing the spectra.

High resolution electron spray ionization (proteins)

Accurate nanoESI measurements of proteins were performed using a Q-IMS-TOF mass spectrometer Synapt G2Si (Waters GmbH, Manchester, UK) in resolution mode, interfaced to nano-ESI ion source. Nitrogen served as both the nebulizer gas and the dry gas for nanoESI.

9 Experimental section

Nitrogen is generated by a nitrogen generator NGM 11. Samples were dissolved in Ace containing 0.1 % formic acid for measurements under denaturing conditions. The samples were filled into *in-house* made ESI-emitters. The mass axis was internally calibrated with LeuEnk (Waters GmbH, Manchester, UK) as calibration standard. Scan accumulation and data processing (baseline subtraction, smoothing and centroidation) was performed with MassLynx 4.1 (Waters GmbH, Manchester, UK) on a PC Workstation. The spectra shown here were generated by the accumulation and averaging of several single spectra.

High resolution electron spray ionization (chemicals)

Accurate nanoESI measurements of proteins were performed using a Q-IMS-TOF mass spectrometer Synapt G2Si (Waters GmbH, Manchester, UK) in resolution mode, interfaced to nano-ESI ion source. Nitrogen served as both the nebulizer gas and the dry gas for nanoESI. Nitrogen is generated by a nitrogen generator NGM 11. Samples (10 μ M protein) were dissolved in 0.1 M ammonium acetate (pH 7.0) for native state measurements or 50 % acetonitrile containing 0.1 % formic acid for measurements under denaturing conditions. The samples were filled into *in-house* made ESI-emitters. The mass axis was externally calibrated with Agilent tune mix as calibration standard. Scan accumulation and data processing (baseline subtraction, smoothing and centroidation) was performed with MassLynx 4.1 (Waters GmbH, Manchester, UK) on a PC Workstation. The spectra shown here were generated by the accumulation and averaging of several single spectra. Determination of the accurate mass of protoheme IX and protein masses were performed using centroided data. The protein masses were determined using the software ESIprot from *Winkler*.^[255]

9.1.3.3 High-performance liquid chromatography

HPLC measurements were performed with systems from Jasco (Pumps PU-2080Plus) equipped with automatical back pressure regulator BP-2080Plus, Column oven CO-2060, multi wavelength detector MD-2010Plus, Autosampler AS.2059-SFPlus and Degasser DG-2080-53. Measurements in reversed-phase were conducted on the column Nucleodur C18Htec (Macherey-Nagel) with a solvent mixture of water/acetonitrile (isocratic) or a gradient of methanol and water supplemented with 0.1 % TFA as mobile phase. Normal-phase measurements were conducted on Chiracel columns with supercritical carbon dioxide and isopropanol as mobile phase. Further details about the temperature, solvent composition, detection, etc. are found in the respective sections.

9.1.3.4 Gas chromatography

Gas chromatographic analysis (Shimadzu GC 2010) was utilized for determining the conversions of biotransformations of alcohols to the corresponding aldehydes and aldoximes to the corresponding nitriles in comparison to calibration curves, respectively. Measurements were conducted on a Phenomenex ZB-5Msi (30 m × 0.25 mm × 0.25 μm). An injector temperature of 300 °C in a split injection mode (1:10) was used and a sample amount of 1 μL was injected in this method. A mixture of N₂/synthetic air was used as carrier gas in a pressure flow control mode (total flow: 13.9 mL·min⁻¹; column flow: 0.99 mL·min⁻¹). The methods and retention times are found in the respective sections.

9.1.3.5 Thin layer chromatography

TLC measurements were performed on Merck silica gel 60 F₂₅₄ plates. Products were visualized by UV light, potassium permanganate, phosphomolybdic acid or iodine staining.

9.1.3.6 Infrared spectroscopy

IR spectra were recorded on a Nicolet 380 FT/IR spectrometer. All measurements were carried out with the neat compounds.

9.1.3.7 CHN analysis

CHN analysis was performed by the CHN analysis service of Bielefeld University or by the Microanalytical laboratory Kolbe (Mülheim an der Ruhr).

9.1.4 Microorganisms and genes

9.1.4.1 Strains

Table 32. Strains of *E. coli* used throughout this thesis.

Entry	Organism	Strain
1	<i>E. coli</i>	JM109
2	<i>E. coli</i>	BL21(DE3)
3	<i>E. coli</i>	BL21(DE3)-RIL

9.1.4.2 Plasmids

Table 33. Plasmids transformed throughout this thesis.

Entry	Enzyme	Source organism	Vector	Supplier	Resistance
1	OxdA	<i>Pseudomonas chlororaphis</i> B23	pET28b _(C)6His	Asano laboratory	Kanamycin
2	OxdB	<i>Bacillus</i> sp. OxB-1	pUC18(-)	Asano laboratory	Ampicillin/Carbenicillin
3	OxdB	<i>Bacillus</i> sp. OxB-1	pET22b _(C)6His	Asano laboratory	Ampicillin/Carbenicillin
4	OxdFG	<i>Fusarium graminearum</i> MAFF305135	pET28a _(N)6His	Thermo Fischer Scientific	Kanamycin
5	OxdRE	<i>Rhodococcus</i> sp. N-771	pET28a _(N)6His	Thermo Fischer Scientific	Kanamycin
6	OxdRG	<i>Rhodococcus globerulus</i> A-4	pET28a _(N)6His	Thermo Fischer Scientific	Kanamycin

9.1.4.3 Enzymes

The enzyme 6His-*hcLAAO4* was obtained from the research group of *Fischer von Mollard* as whole cells or in form of the purified enzyme. The enzyme used in this thesis was used as an activated lysate (prepared according to GP1) or in the purified form. The enzyme was obtained from the working group of *Fischer von Mollard* in form of whole-cells or purified protein (Ni²⁺-NTA affinity chromatography). The preparation of the lysate from whole-cells is described below. The enzyme with its related gene sequence, the preparation of this enzyme linked with a hexahistidine-tag as well as its expression in *E. coli* and purification is described in literature (GenBank accession number MH751433).^[184] Alternatively, enzyme obtained from expression in *P. pastoris* was also utilized.^[185] Pp-ADH and Lk-ADH were obtained from previous experiments by *Daniel Bakonyi* as whole-cells containing the expressed proteins. All other proteins were expressed according to the methods described in this chapter.

9.1.5 Buffers and solutions

Table 34. Compositions of solutions and buffer used throughout this thesis.

Solution	Composition
KH ₂ PO ₄ (1.0 M)	136.1 g·L ⁻¹ in <i>dd</i> H ₂ O
K ₂ HPO ₄ (1.0 M)	174.2 g·L ⁻¹ in <i>dd</i> H ₂ O
NaCl (3.0 M)	175.3 g·L ⁻¹ in <i>dd</i> H ₂ O
Imidazole (5.0 M)	340.3 g·L ⁻¹ in <i>dd</i> H ₂ O
KPB (1.0 M)	pH-value adjusted to 7.0 by mixing KH ₂ PO ₄ (1.0 M) and K ₂ HPO ₄ (1.0 M) solutions
Laemmli-buffer (6x)	1.47 g Tris-HCl (pH 6.8; final concentration 375 mM) 1.50 g SDS (6.0 %, <i>m,v</i>) 1.20 mL Glycerol (4.8 %, <i>m,v</i>) 2.25 mL 2-Mercaptoethanol (9.0 %, <i>v,v</i>) 7.50 mg Bromophenyl blue (0.03 %, <i>m,v</i>) Filled up to 25 mL with <i>dd</i> H ₂ O
Urea (6.0 M)	360.4 g·L ⁻¹ in <i>dd</i> H ₂ O
Tris-HCl buffer (1.0 M)	121.1 g TRIS pH adjusted to desired value (HCl) Filled 1.0 L with <i>dd</i> H ₂ O
TEA-buffer (0.5)	74.6 g Triethanolamine pH adjusted to 7.0 with HCl
Equilibration buffer	20 mL TRIS (1.0 M, pH 8.0, final concentration: 50 mM) 2.0 mL Imidazole (5.0 M, final concentration: 10 mM) 100 mL NaCl (3.0 M, final concentration: 300 mM)
Elution buffer	20 mL TRIS (1.0 M, pH 8.0, final concentration: 20 mM) 30 mL Imidazole (5.0 M, final concentration: 150 mM) 100 mL NaCl (3.0 M, final concentration: 300 mM)

9.2 Computational methods

9.2.1 Determination of aggregation hotspots

The mutation sites were identified using the program INTMSAlign_HiSol in accordance to *Matsui et al.*^[237] applied to the amino acid sequence of OxdB (Table 35). The output file was used to calculate the HiSol score (as dimensionless value) by the following formula using the normalized hydrophathy indices (I_{hyp} , z-transformed) according to *Kyte and Doolittle*.^[245]

$$\text{HiSol score (j)} = (I_{hyp})_{j,\text{OxdB}(i)} - \sum_{i=1}^{20} (I_{hyp})_i \{(R_{cons})_{ij}/100\}$$

The variable “ i ” represents the amino acid residues numbered in alphabetical order of their one-letter abbreviations; e.g. the i values of Ala, Cys and Asp are 1, 2, and 3, respectively. Thus, $(I_{hyp})_{j,\text{OxdB}(i)}$ refers to the hydrophathy index of the amino acid residue “ i ” at the j th residue in the sequence of OxdB. $(R_{cons})_{ij}$ represents the appearance rate of that amino acid at the j th residue of OxdB in the library.

Table 35. Predicted aggregation hotspots and mutation of OxdB with appearance in the consensus protein and HiSol scores.

Entry	Position	Original	Changed	Similarity [%]	HiSol score
1	319	I	E	90.0	2.656
2	226	I	Q	26.5	2.411
3	220	L	E	39.7	2.281
4	149	V	E	65.6	2.278
5	105	I	R	32.6	2.252
6	267	L	R	40.0	2.226
7	316	I	Q	67.9	2.175
8	180	I	A	13.9	1.890
9	65	L	H	24.2	1.880
10	262	V	G	43.8	1.852
11	317	E	L	17.8	-1.452
12*	190	K	R	34.5	(-1.471)*
13	135	D	L	35.0	-1.496
14	67	Q	T	32.2	-1.533
15	49	K	V	24.2	-1.582
16	63	R	L	34.6	-1.882
17	296	H	L	56.7	-1.943
18	229	N	M	80.1	-1.974
19	250	Q	I	29.3	-2.153
20	283	K	L	57.8	-2.485

9 Experimental section

*For this variant, the hydrophilic arginine (appearance rate: 34.5 %) was introduced instead of the hydrophobic valine (appearance rate: 34.2 %) for its higher conservation. The HiSol score given refers to the calculated value for valine.

9.2.2 Secondary structure determination

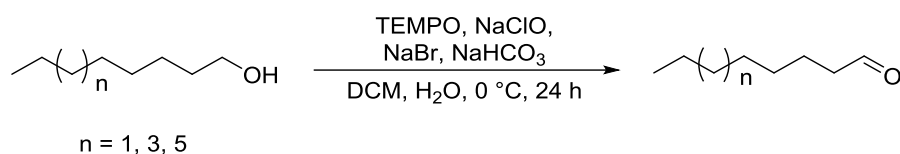
The secondary structure of OxdB was determined *via* position-specific scoring matrices *via* the PSIPRED software (Table 36).^[248] The PSIPRED server was utilized for calculations.^[249]

Table 36. Predicted secondary structures of OxdB at the identified aggregation hotspots.

Entry	Position	Amino acid	Secondary structure
1	319	I	Strand
2	226	I	Helix
3	220	L	Helix
4	149	V	Coil
5	105	I	Coil
6	267	L	Coil
7	316	I	Strand
8	180	I	Coil
9	65	L	Strand
10	262	V	Strand
11	317	E	Strand
12	190	K	Strand
13	135	D	Coil
14	67	Q	Strand
15	49	K	Helix
16	63	R	Strand
17	296	H	Coil
18	229	N	Helix
19	250	Q	Strand
20	283	K	Helix

9.3 Chemical methods

9.3.1 General procedure 1 (GP1): TEMPO-catalyzed oxidation of fatty alcohols



The fatty alcohol (1.0 eq.) was given into a flask and dissolved by dichloromethane. TEMPO (0.01 eq.) was added and the reaction solution was cooled to 0 °C. Sodium bromide (0.1 eq.) dissolved in water was added. An aqueous solution of sodium hypochlorite (13 wt%, 1.1 eq.) was slowly added to the solution under vigorous stirring. The pH of the reaction solution was checked with pH strips and adjusted to 9.5 by addition of aqueous sodium hydrogen carbonate solution if necessary. The progress of the reaction was followed by TLC (cyclohexane/ethyl acetate). After 24 hours, extraction with dichloromethane for three times (20 mL), washing with 2 M hydrochloric acid and potassium iodide (2 mol%, 0.6 mmol), 0.1 M sodium thiosulfate (20 mL), and 10% sodium hydrogen carbonate (20 mL), drying over magnesium sulfate. After filtration, all volatiles were removed *in vacuo* and the relative conversion of the fatty alcohol to the aldehyde was determined by ¹H-NMR spectroscopy.

9.3.1.1 Attempted synthesis of *n*-octanal

The reaction was carried out according to GP1. 1-Octanol (3.91 g, 30.0 mmol) was dissolved in 10 mL dichloromethane and cooled down to 0 °C. TEMPO (46.9 mg, 300 μmol) was added and the reaction solution was cooled down to 0 °C. Sodium bromide (309 mg, 3.00 mmol) dissolved in 1.0 mL water was added. Sodium hypochlorite (2.46 g, 33.0 mmol) dissolved in 17 mL water was added dropwise and the solution was stirred vigorously for 24 hours.

Conversion (¹H-NMR spectroscopy): 20 %.

9.3.1.2 Attempted synthesis of *n*-decanal

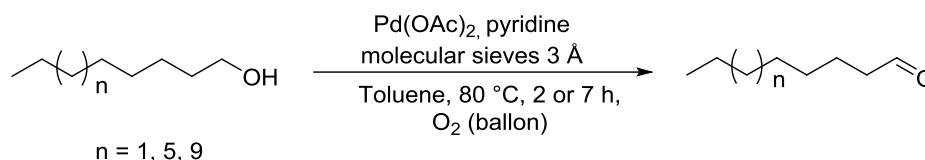
The reaction was carried out according to GP1. 1-Decanol (4.75 g, 30.0 mmol) was dissolved in 10 mL dichloromethane (10 mL) and cooled down to 0 °C. TEMPO (46.9 mg, 300 μmol) was added and the reaction solution was cooled down to 0 °C. Sodium bromide (309 mg, 3.00 mmol) dissolved in 1.0 mL water was added. Sodium hypochlorite (2.46 g, 33.0 mmol) dissolved in 17 mL water was added dropwise and the solution was stirred vigorously for 24 hours.

Conversion (¹H-NMR spectroscopy): 26 %.

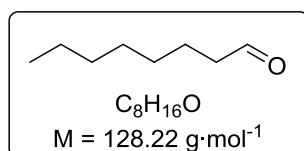
9.3.1.3 Attempted synthesis of *n*-dodecanal

The reaction was carried out according to GP1. 1-Dodecanol (5.59 g, 30.0 mmol) was dissolved in 10 mL dichloromethane and cooled down to 0 °C. TEMPO (46.9 mg, 300 μmol) was added and the reaction solution was cooled down to 0 °C. Sodium bromide (309 mg, 3.00 mmol) dissolved in 1.0 mL water was added. Sodium hypochlorite (2.46 g, 33.0 mmol) dissolved in 17 mL water was added dropwise and the solution was stirred vigorously for 24 hours.

Conversion (¹H-NMR spectroscopy): 23 %.

9.3.2 General procedure 2 (GP2): Palladium(II) acetate-catalyzed oxidation of fatty alcohols with molecular oxygen

The oxidation of fatty alcohols to fatty aldehydes was performed in analogy to the procedure by *Nishimura et al.*^[216] Palladium(II) acetate (0.05 eq.) was dissolved in toluene. Pyridine (0.20 eq) and molecular sieves (3 Å) were added. The flask was set under oxygen atmosphere (1 atm) and bubbled through the solution. After heating the solution at 80 °C for 10 minutes, the fatty alcohol dissolved in toluene was added. After stirring at 80 °C under oxygen atmosphere for 2 or 7 hours, reaction progress was monitored *via* TLC with iodine stain (cyclohexane/ethyl acetate varying *v,v*). Subsequently, the reaction solution was filtered and the solvents were removed *in vacuo*. The crude was purified by automated flash column chromatography (cyclohexane/ethyl acetate) yielding the aldehydes as colorless oils.

9.3.2.1 Attempted synthesis of *n*-octanal

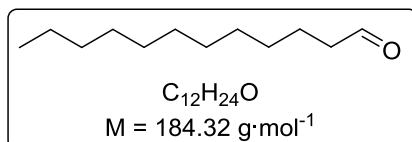
The synthesis was conducted according to GP2. Palladium(II) acetate (11 mg, 49 μmol), pyridine (15.8 μL, 204 μmol) and molecular sieves (3 Å, 500 mg) were added. The flask was set under oxygen atmosphere (1 atm) and bubbled through the solution. After heating the solution at 80 °C for 10 minutes, the 1-octanol (130 mg, 1.0 mmol) dissolved in 4 mL toluene

9 Experimental section

was added and stirred at 80 °C for 2 hours. Workup yielded a mixture of the product and non-converted educt as a colorless oil.

The analytical data corresponds to literature values.^[256]

9.3.2.2 Synthesis of *n*-dodecanal



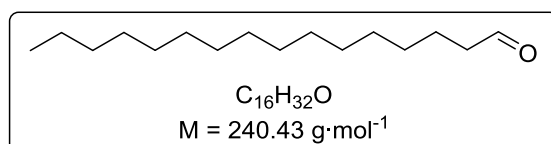
The synthesis was conducted according to GP2. Palladium(II) acetate (56.1 mg, 250 μmol), pyridine (80.9 μL , 1.00 mmol) and molecular sieves (3 Å, 1.5 g) were added. The flask was set under oxygen atmosphere (1 atm) and bubbled through the solution. After heating the solution at 80 °C for 10 minutes, 1-octanol (932 mg, 5.00 mmol) dissolved in 24 mL toluene was added and stirred at 80 °C for 7 hours. Workup yielded the product as a colorless oil.

Yield: 470 mg, 2.55 mmol, 51 %.

$^1\text{H-NMR}$ (500 MHz, CDCl_3): δ [ppm] = 9.76 (t, $^3J = 1.9$ Hz, 1H, $\text{CH}_2\text{-CHO}$), 2.42 (td, $^3J = 7.4$, 1.9 Hz, 2H, $\text{CH}_2\text{-CHO}$), 1.67 – 1.58 (m, 2H, $\text{CH}_2\text{-CH}_2\text{-CHO}$), 1.37 – 1.18 (m, 16H, $-\text{CH}_2-$), 0.88 (t, $^3J = 7.0$ Hz, 3H, $\text{CH}_2\text{-CH}_3$).

The analytical data corresponds to literature values.^[257]

9.3.2.3 Synthesis of *n*-hexadecanal



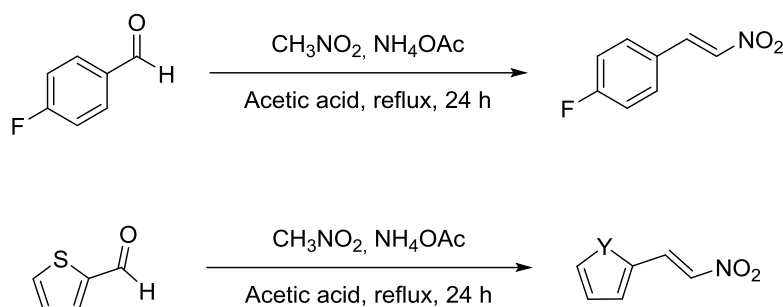
The synthesis was conducted according to GP2. Palladium(II) acetate (56.1 mg, 250 μmol), pyridine (80.9 μL , 1.00 mmol) and molecular sieves (3 Å, 1.5 g) were added. The flask was set under oxygen atmosphere (1 atm) and bubbled through the solution. After heating the solution at 80 °C for 10 minutes, 1-dodecanol (1.21 g, 5.00 mmol) dissolved in 24 mL toluene was added and stirred at 80 °C for 7 hours. Workup yielded the product as a colorless oil.

Yield: 370 mg, 1.53 g, 31 %.

$^1\text{H-NMR}$ (500 MHz, CDCl_3): δ [ppm] = δ 9.76 (t, $^3J = 1.9$ Hz, 1H, $\text{CH}_2\text{-CHO}$), 2.41 (td, $^3J = 7.4$, 1.9 Hz, 2H, $\text{CH}_2\text{-CHO}$), 1.67 – 1.58 (m, 2H, $\text{CH}_2\text{-CH}_2\text{-CHO}$), 1.38 – 1.16 (m, 24H, $-\text{CH}_2-$), 0.88 (t, $^3J = 7.0$ Hz, 3H, $\text{CH}_2\text{-CH}_3$).

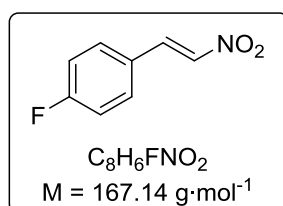
The analytical data corresponds to literature values.^[258]

9.3.3 General procedure 3 (GP3): Nitroaldol condensation of aromatic aldehydes with nitromethane



The synthesis was conducted in analogy to *Wong et al.*^[259] The corresponding benzaldehyde derivative (1.0 eq.), ammonium acetate (0.1 eq.) and nitromethane (6.5 eq.) were dissolved in acetic acid and heated to reflux for 24 hours. Afterwards, complete conversion was confirmed *via* TLC (cyclohexane/ethyl acetate). Water was added; the precipitate was filtered off and dried *in vacuo*. Recrystallization from ethanol yielded the corresponding *E*-nitroalkene as crystalline solid. The crude product could also be purified *via* column chromatography (cyclohexane/ethyl acetate).

9.3.3.1 Synthesis of (*E*)-1-fluoro-4-(2-nitrovinyl)benzene



The synthesis was conducted according to GP3. 4-Fluorobenzaldehyde (8.59 mL, 80.0 mmol), ammonium acetate (617 mg, 8.00 mmol) and nitromethane (27.8 mL, 527 mmol) were dissolved in 40 mL acetic acid and refluxed for 18 hours. Recrystallization yielded the product as yellow, crystalline solid.

Yield: 5.22 g, 31.2 mmol, 39 %.

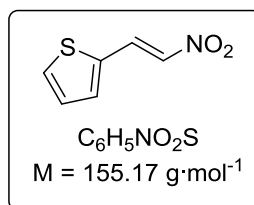
¹H-NMR (500 MHz, CDCl₃): δ [ppm] = 7.98 (d, 1H, ²*J* = 13.6 Hz, CH=CH-NO₂), 7.59-7.51 (m, 3H, Ar-H, CH=CH-NO₂), 7.19-7.12 (m, 2H, Ar-H).

¹³C-NMR (125 MHz, CDCl₃): δ [ppm] = 166.1, 164.1, 138.0, 137.0, 137.0, 131.5, 131.4, 126.5, 126.4, 117.0, 116.9.

9 Experimental section

The analytical data corresponds to literature values.^[260]

9.3.3.2 Synthesis of (*E*)-2-(2-nitrovinyl)thiophene



The synthesis was conducted according to GP3. Thiophen-2-carbaldehyde (7.46 mL, 80.0 mmol), ammonium acetate (616 mg, 8.00 mmol) and nitromethane (27.8 mL, 527 mmol) were dissolved in 40 mL acetic acid and refluxed for 18 hours. Recrystallization yielded the product as yellow, crystalline solid.

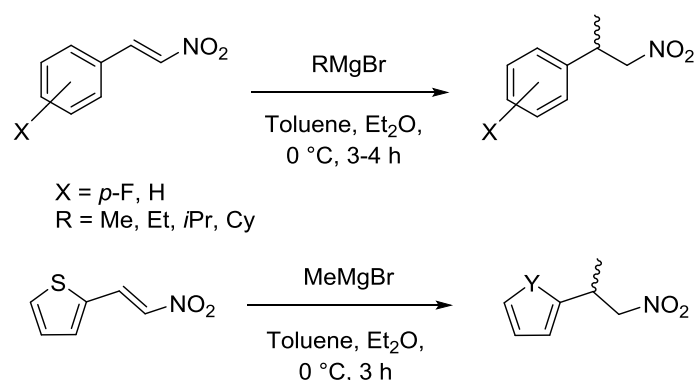
Yield: 7.40 g, 47.7 mmol, 60 %.

¹H-NMR (500 MHz, CDCl₃): δ [ppm] = 8.16 (d, 1H, ²*J* = 13.4 Hz, CH=CH-NO₂), 7.57 (dt, 1H, ³*J* = 5.3 Hz, ⁴*J* = 1.0 Hz, Ar-*H*), 7.48 (d, 1H, ²*J* = 13.4 Hz, CH=CH-NO₂), 7.47-7.44 (m, 1H, Ar-*H*), 7.15 (dd, 1H, ³*J* = 5.1 Hz, ⁴*J* = 3.7 Hz, Ar-*H*).

¹³C-NMR (125 MHz, CDCl₃): δ [ppm] = 135.4, 134.6, 133.8, 132.1, 131.6, 128.9.

The analytical data corresponds to literature values.^[261]

9.3.4 General procedure 4 (GP4): Synthesis of nitroalkanes by Michael-addition of magnesium halides to nitroalkenes

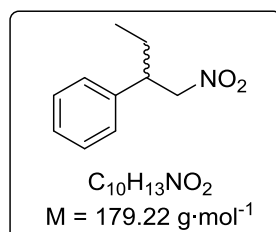


The synthesis was carried out in a heat dried Schlenk flask under argon atmosphere. Dry toluene was filled into the flask and cooled down to 0 °C. The nitroalkene (1.0 eq.) was dissolved and a solution of Grignard-reagent in diethyl ether or tetrahydrofuran (1.5 eq.) was slowly added to the solution under vigorous stirring. After stirring for three to four hours at 0 °C, complete conversion was achieved according to TLC (cyclohexane/ethyl acetate) and

9 Experimental section

saturated NH_4Cl -solution (1:1, v,v) was added. The phases were separated and the aqueous phase was extracted three times with ethyl acetate (1:1, v,v). After washing of the organic phase with brine (1:3, v,v), it was dried over magnesium sulfate and the solvent was removed *in vacuo*. Column chromatography (cyclohexane/ethyl acetate 9:1, v,v) yielded the racemic nitroalkanes as yellow oils or brown solid.

9.3.4.1 Synthesis of *rac*-(1-nitrobutan-2-yl)benzene



The synthesis was carried out according to GP4. *trans*- β -Nitrostyrene (2.22 g, 14.8 mmol) was dissolved in 100 mL freshly distilled toluene at 0 °C and ethylmagnesium bromide (1.0 M in Et_2O 22.5 mL, 22.5 mmol) was added. Workup (cyclohexane / ethyl acetate 9:1) yielded the product as a yellow oil.

Yield: 1.11 g, 6.2 mmol, 42 %.

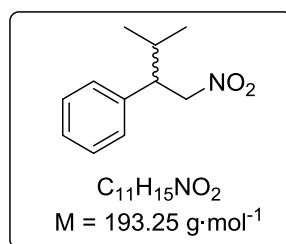
$^1\text{H-NMR}$ (500 MHz, CDCl_3): δ [ppm] = 7.37 – 7.31 (m, 2H, ArH), 7.30 – 7.25 (m, 1H, ArH), 7.21 – 7.16 (m, 1H, ArH), 4.62 – 4.50 (m, 2H, $\text{O}_2\text{N-CH}_2$), 3.36 (dtd, $^3J = 9.6, 7.8, 5.2$ Hz, 1H, Ph-CH), 1.82 – 1.64 (m, 2H, $\text{H}_3\text{C-CH}$), 0.84 (t, $^3J = 7.4$ Hz, 3H, CH_3).

$^{13}\text{C-NMR}$ (126 MHz, CDCl_3): δ [ppm] = 139.4, 129.0, 127.7, 80.9, 46.1, 26.3, 11.7.

IR (neat): $\tilde{\nu}$ [cm^{-1}] = 3084, 3064, 3030, 2966, 2932, 2976, 2746, 2361, 2342, 1604, 1546, 1494, 1454, 1430, 1378, 1332, 1280, 1196, 1157, 1121, 1076, 1157, 1121, 1076, 1030, 1002, 967, 910, 862, 810, 756, 699, 642, 538, 529, 482, 435, 418, 402.

MS (EI, 70 eV): $m/z = 179.1$ (100 %) $[\text{M}]^{+\bullet}$.

EA: calcd for $\text{C}_{10}\text{H}_{13}\text{NO}_2$: C, 67.02; H, 7.31; N, 7.82. Found: C, 67.73; H, 7.75; N, 7.58.

9.3.4.2 Synthesis of *rac*-(3-methyl-1-nitrobutan-2-yl)benzene

The synthesis was carried out according to GP4. *trans*- β -Nitrostyrene (2.21 g, 14.8 mmol) was dissolved in 100 mL freshly distilled toluene at 0 °C and *iso*-propylmagnesium bromide (0.75 M in Et₂O, 30.0 mL, 22.5 mmol) was added. Workup yielded the product as orange oil.

Yield: 1.21 g, 6.2 mmol, 42 %.

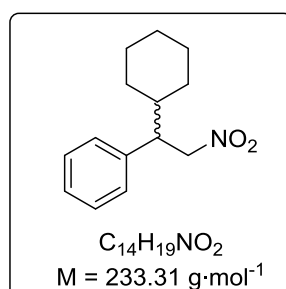
¹H-NMR (500 MHz, CDCl₃): δ [ppm] = 7.34 – 7.29 (m, 2H, ArH), 7.28 – 7.24 (m, 1H, ArH), 7.17 – 7.13 (m, 2H, ArH), 4.76 (dd, ²J = 12.3 Hz, ³J = 5.7 Hz, 1H, O₂N-CH₂), 4.64 (dd, ²J = 12.3 Hz, ³J = 9.9 Hz, 1H, O₂N-CH₂), 3.23 (ddd, ³J = 9.9, 8.0, 5.7 Hz, 1H, Ph-CH), 1.96 (dp, ³J = 7.9, 6.7 Hz, 1H, (CH₃)₂-CH), 1.01 (d, ³J = 6.7 Hz, 3H, CH₃), 0.81 (d, ³J = 6.8 Hz, 3H, CH₃).

¹³C-NMR (126 MHz, CDCl₃): δ [ppm] = 138.8, 128.7, 128.3, 127.6, 79.2, 51.2, 31.5, 20.8, 20.4.

IR (neat): $\tilde{\nu}$ [cm⁻¹] = 3084, 3063, 3030, 2961, 2929, 2872, 2361, 2342, 1602, 1549, 1494, 1467, 1554, 1433, 1379, 1288, 1250, 1202, 1166, 1130, 1093, 1075, 1032, 1004, 978, 937, 911, 854, 835, 777, 754, 700, 669, 649, 625, 544, 526, 456, 419, 410, 403.

MS (ESI, positive ions): m/z = 216.0 [M+Na]⁺, 238.1 [M+2Na-H]⁺.

EA: calcd for C₁₁H₁₅NO₂: C, 68.72; H, 7.82; N, 7.25. Found: C, 69.05; H, 8.28; N, 7.11.

9.3.4.3 Synthesis of *rac*-(1-cyclohexyl-2-nitroethyl)benzene

The synthesis was carried out according to GP4. *trans*- β -Nitrostyrene (2.22 g, 14.8 mmol) was dissolved in 100 mL freshly distilled toluene at 0 °C and cyclohexylmagnesium chloride (2.0 M in THF, 8.0 mL, 16.0 mmol) was added. Workup yielded the product as a brown solid.

Yield: 1.85 g, 7.90 mmol, 53 %.

9 Experimental section

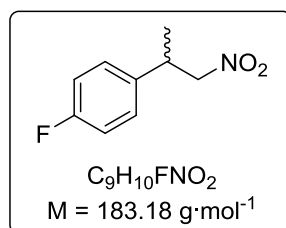
¹H-NMR (500 MHz, CDCl₃): δ [ppm] = 7.34 – 7.28 (m, 2H, ArH), 7.28 – 7.22 (m, 1H, ArH), 7.16 – 7.11 (m, 2H, ArH), 4.78 (dd, ²J = 12.3 Hz, ³J = 5.7 Hz, 1H, O₂N-CH₂), 4.62 (dd, ²J = 12.3 Hz, ³J = 10.0 Hz, 1H, O₂N-CH₂), 3.27 (ddd, ³J = 10.0, 8.1, 5.7 Hz, 1H, Ph-CH), 1.78 (ttd, J = 13.0, 3.5, 1.7 Hz, 2H, CyH), 1.73 – 1.56 (m, 3H, CyH), 1.53 – 1.44 (m, 1H, CyH), 1.32 – 1.20 (m, 1H), 1.20 – 0.95 (m, 3H, CyH), 0.87 (tdd, J = 12.6, 11.5, 3.6 Hz, 1H, CyH).

¹³C-NMR (126 MHz, CDCl₃): δ [ppm] = 139.1, 128.9, 128.4, 127.7, 79.2, 50.6, 41.3, 31.3, 30.9, 26.4.

IR (neat): $\tilde{\nu}$ [cm] = 3084, 3064, 3028, 2930, 2914, 2844, 2787, 2671, 2360, 2341, 2178, 2152, 2025, 1978, 1955, 1599, 1550, 1438, 1379, 1349, 1308, 1286, 1271, 1203, 978, 960, 911, 891, 845, 803, 754, 720, 698, 669, 632, 618, 598, 526, 487, 457, 435, 420, 402.

HRMS (ESI, positive ions): calcd for C₁₄H₁₉NO₂Na⁺ [M+Na]⁺: 256.1308, found: 256.1299.

9.3.4.4 Synthesis of *rac*-1-fluoro-4-(1-nitropropan-2-yl)benzene



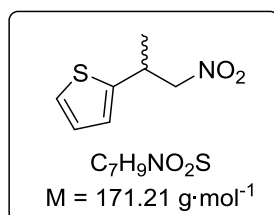
The synthesis was carried out according to GP4. (*E*)-1-Fluoro-4-(2-nitrovinyl)benzene (5.01 g, 30 mmol) was dissolved in 150 mL dry toluene at 0 °C and methylmagnesium bromide (5.18 mL, 45 mmol) was added. Workup yielded the product as yellow oil.

Yield: 2.74 g, 15.0 mmol, 50 %.

¹H-NMR (500 MHz, CDCl₃): δ [ppm] = 7.23-7.17 (m, 2H, Ar-H), 7.07-7.00 (m, 2H, Ar-H), 4.51 (dd, 1H, ²J = 12.1 Hz, ³J = 7.6 Hz, CHH-NO₂), 4.47 (dd, 1H, ²J = 12.1 Hz, ³J = 7.9 Hz, CHH-NO₂), 3.63 (h, 1H, ³J = 7.3 Hz, CH-CH₂-NO₂), 1.37 (d, 3H, ³J = 7.0 Hz, CH₃).

¹³C-NMR (125 MHz, CDCl₃): δ [ppm] = 163.2, 161.2, 136.7, 128.6, 116.1, 116.0, 82.0, 38.1, 19.0.

The analytical data corresponds with literature data.^[262,263]

9.3.4.5 Synthesis of *rac*-2-(1-nitropropan-2-yl)thiophene

The synthesis was carried out according to GP4. (*E*)-2-(2-Nitrovinyl)thiophene (6.20 g, 40 mmol) was dissolved in 150 mL dry toluene at 0 °C and methylmagnesium bromide (6.91 mL, 60 mmol) was added. Workup yielded the product as orange oil.

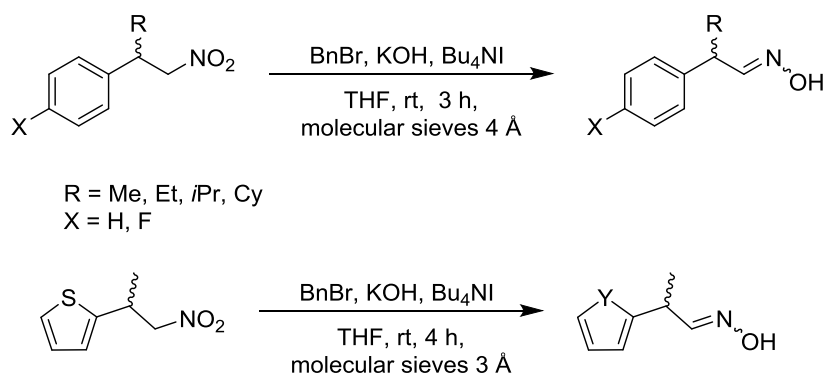
Yield: 1.98 g, 11.6 mmol, 29 %.

¹H-NMR (500 MHz, CDCl₃): δ [ppm] = 7.22 (dd, 1H, ³J = 5.1 Hz, ⁴J = 1.2 Hz, Ar-*H*), 6.96 (dd, 1H, ³J = 5.1 Hz, ⁴J = 3.5 Hz, Ar-*H*), 6.90 (dt, 1H, ⁴J = 3.6, 0.9 Hz, Ar-*H*), 4.58 (dd, 1H, ²J = 12.2 Hz, ³J = 7.0 Hz, CHH-NO₂), 4.48 (dd, 1H, ²J = 12.2 Hz, ³J = 8.1 Hz, CHH-NO₂), 3.96 (dpd, 1H, ³J = 7.8, 6.9 Hz, ⁴J = 0.8 Hz, CH-CH₂-NO₂), 1.47 (d, 3H, ³J = 7.0 Hz, CH₃).

¹³C-NMR (125 MHz, CDCl₃): δ [ppm] = 144.1, 127.2, 124.6, 124.5, 82.3, 34.3, 19.9.

The analytical data corresponds with literature data.^[191]

9.3.5 General procedure 5 (GP5): Synthesis of aldoximes by disproportionation of nitroalkanes with benzyl bromide

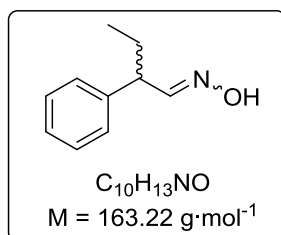


The syntheses were carried out in a heat dried Schlenk flask under argon atmosphere in analogy to *Czekelius et al.*^[191] Freshly distilled tetrahydrofuran (or alternatively dried over molecular sieves) was given into the flask. KOH (85 wt% pellets, 1.05 eq.) and molecular sieves 4 Å were added and the suspension was stirred for one hour. Afterwards, benzyl bromide (1.1 eq.) and tetrabutylammonium iodide (TBAI, 0.05 eq.) were added. Lastly, the nitroalkane (1.0 eq.) was added over 5 minutes. The resulting suspension was stirred overnight at room temperature and conversion was checked *via* TLC (cyclohexane/ethyl acetate). Water

9 Experimental section

(1:1, v,v) was added, the phases were separated and the aqueous phase was extracted three times with ethyl acetate. Drying over magnesium sulfate and removal of the solvent *in vacuo* yielded an oily crude product. Purification *via* automated column chromatography (cyclohexane/ethyl acetate) yielded the *E*- and *Z*- isomers as colorless solids or oils depending on percentage of isomeric excess.

9.3.5.1 Synthesis of *rac*-2-phenylbutanal oxime



The synthesis was carried out according to GP5. 20 mL Tetrahydrofuran were given into a schlenk flask, Potassium hydroxide (343 mg, 6.11 mmol) and molecular sieves 4 Å (296 mg) were added. Benzyl bromide (649 μL , 5.46 mmol) and TBAI (95.1 mg, 295 μmol) were added after an hour. (1-Nitrobutan-2-yl)benzene (900 mg, 5.02 mmol) was added and the reaction mixture was stirred overnight. Workup and purification *via* automated column chromatography (cyclohexane/ethyl acetate 10:1, 4:1, v,v) yielded the *E*-isomer (96:4 *E/Z*) as a yellow oil and the *Z*-isomer (3:97 *E/Z*) as a colorless oil which crystallized at -20°C .

Combined yield: 306 mg, 1.87 mmol, 37 %.

rac-E-2-Phenylbutanal oxime

$^1\text{H-NMR}$ (500 MHz, CD_2Cl_2): δ [ppm] = 8.18 (s, 1H, HC=NOH), 7.36 – 7.28 (m, 2H, ArH), 7.28 – 7.19 (m, 3H, ArH), 6.38 (d, $^3J = 7.7$ Hz, 1H, HC=NOH), 4.17 (q, $^3J = 7.6$ Hz, 1H, CH-CH=NOH), 1.86 – 1.75 (m, 2H, $\text{CH}_2\text{-CH}_3$), 0.90 (t, $^3J = 7.4$ Hz, 3H, $\text{CH}_2\text{-CH}_3$).

$^{13}\text{C-NMR}$ (126 MHz, CD_2Cl_2): δ [ppm] = 155.1, 141.8, 129.1, 128.3, 127.2, 43.0, 27.5, 12.2.

IR (neat): $\tilde{\nu}$ [cm^{-1}] = 3197, 3085, 3026, 2961, 2930, 2873, 2360, 2341, 1743, 1717, 1683, 1636, 1599, 1583, 1558, 1541, 1521, 1506, 1494, 1473, 1451, 1382, 1325, 1260, 1230, 1217, 1191, 1138, 1116, 1067, 1047, 1031, 984, 935, 906, 886, 851, 829, 791, 748, 694, 677, 628, 529, 500, 545, 443, 435, 420, 411.

RP-HPLC: *Macherey-Nagel* Nucleodur C_{18} HTec, water/acetonitrile 60:40, 1.0 $\text{mL}\cdot\text{min}^{-1}$, 40 $^\circ\text{C}$, 210 nm, $R_{t1} = 9.65$ min.

NP-HPLC: *Daicel Chiracel* OB-H, CO_2 /isopropanol = 99.5:0.5, 0.8 $\text{mL}\cdot\text{min}^{-1}$, 20 $^\circ\text{C}$, 210 nm, $R_{t1} = 45.8$ min, $R_{t2} = 50.9$ min.

9 Experimental section

rac-Z-2-Phenylbutanal oxime

¹H-NMR (500 MHz, CD₂Cl₂): δ = 8.19 (s, 1H, HC=NOH), 7.51 (d, ³J = 7.0 Hz, 1H, HC=NOH), 7.33 (m, 2H, ArH), 7.28 – 7.18 (m, 3H, ArH), 3.38 (q, ³J = 7.4, 1H, CH-CH=NOH), 1.96 – 1.86 (m, 1H, CH₂-CH₃), 1.86 – 1.75 (m, 1H, CH₂-CH₃), 0.90 (t, ³J = 7.4 Hz, 3H, CH₂-CH₃).

¹³C-NMR (126 MHz, CD₂Cl₂): δ [ppm] = 154.8, 141.5, 129.2, 128.4, 127.4, 48.5, 27.2, 12.2.

IR (neat): $\tilde{\nu}$ [cm⁻¹] = 3254, 3085, 3028, 2963, 2930, 2874, 2360, 2341, 1740, 1717, 1683, 1647, 1601, 1558, 1541, 1491, 1453, 1379, 1340, 1294, 1157, 1134, 1098, 1074, 1030, 996, 947, 827, 787, 757, 696, 623, 615, 577, 524, 457, 442, 418, 410.

RP-HPLC: *Macherey-Nagel* Nucleodur C₁₈ HTec, water/acetonitrile 60:40, 1.0 mL·min⁻¹, 40 °C, 210 nm, R_{t1} = 9.00 min,

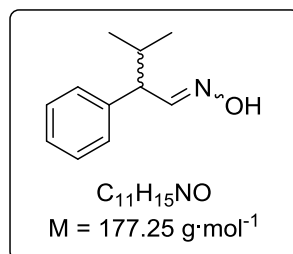
NP-HPLC: *Daicel Chiracel* OB-H, CO₂/isopropanol = 99.5:0.5, 0.8 mL·min⁻¹, 20 °C, 210 nm, R_{t1} = 34.2 min, R_{t2} = 38.7 min.

rac-E/Z-2-Phenylbutanal oxime

MS (ESI, positive ions): *m/z* = 164.0 [M+H]⁺, 186.0 [M+Na]⁺.

EA: calcd. for C₁₀H₁₃NO: C, 73.59; H, 8.03, N, 8.58, found: C, 73.67; H, 7.84; N, 8.64.

9.3.5.2 Synthesis of rac-3-methyl-2-phenylbutanal oxime



The synthesis was carried out according to GP5. 20 mL tetrahydrofuran were given into a Schlenk flask, Potassium hydroxide (327 mg, 5.83 mmol) and molecular sieves 4 Å (286 mg) were added. Benzyl bromide (609 μL, 5.13 mmol) and TBAI (75.0 mg, 233 μmol) were added after an hour. (3-Methyl-1-nitrobutan-2-yl)benzene (902 mg, 4.67 mmol) was added and the reaction mixture was stirred overnight. Workup and purification *via* automated column chromatography (cyclohexane/ethyl acetate 10:1, 4:1, *v,v*) yielded the *E*-isomer (97:3 *E/Z*) and the *Z*-isomer (2:98 *E/Z*) as a colorless oils which crystallized at -20 °C.

Combined yield: 309 mg, 1.74 mmol, 37 %.

rac-E-3-Methyl-2-phenylbutanal oxime

¹H-NMR (500 MHz, CD₂Cl₂): δ [ppm] = 8.19 (s, 1H, HC=NOH), 7.36 – 7.27 (m, 2H, Ar-H), 7.25 – 7.19 (m, 3H, Ar-H), 6.91 (d, ³J = 8.2 Hz, 1H, HC=NOH), 3.94 (t, ³J = 8.9 Hz, 1H, CH-

9 Experimental section

CH=NOH), 2.09 – 1.99 (m, 1H, CH-(CH₃)₂), 1.01 (d, ³J = 6.7 Hz, 3H, CH-(CH₃)₂), 0.79 (d, ³J = 6.7 Hz, 3H, CH-(CH₃)₂).

¹³C-NMR (126 MHz, CD₂Cl₂): δ [ppm] = 154.5, 141.2, 129.1, 128.8, 127.1, 48.7, 32.5, 20.9, 20.7.

IR (neat): $\tilde{\nu}$ [cm⁻¹] = 3734, 3226, 3086, 3028, 2956, 2928, 2869, 2360, 2341, 1792, 1739, 1717, 1698, 1683, 1653, 1647, 1636, 1599, 1584, 1576, 1558, 1533, 1521, 1506, 1491, 1464, 1449, 1387, 1350, 1319, 1229, 1217, 1164, 1140, 1109, 1076, 1051, 1031, 1015, 1002, 964, 943, 916, 901, 846, 824, 747, 696, 670, 619, 592, 549, 531, 485, 478, 456, 443, 435, 420, 411.

RP-HPLC: *Macherey-Nagel* Nucleodur C₁₈ HTec, water/acetonitrile 60:40, 1.0 mL·min⁻¹, 40 °C, 210 nm, R_{t1} = 12.5 min.

NP-HPLC: *Daicel Chiracel* OB-H, CO₂/isopropanol = 99.5:0.5, 0.8 mL·min⁻¹, 20 °C, 210 nm, R_{t1} = 43.6 min, R_{t2} = 49.0 min.

rac-Z-3-Methyl-2-phenylbutanal oxime

¹H-NMR (500 MHz, CD₂Cl₂): δ [ppm] = 7.70 (s, 1H, HC=NOH), 7.57 (d, ³J = 8.4 Hz, 1H, HC=NOH), 7.36 – 7.29 (m, 2H, Ar-H), 7.27 – 7.21 (m, 1H, Ar-H), 7.20 – 7.15 (m, 2H, Ar-H), 3.11 (t, ³J = 8.9 Hz, 1H, CH-CH=NOH), 2.16 – 2.07 (m, 1H, CH-(CH₃)₂), 1.00 (d, ³J = 6.7 Hz, 3H, CH-(CH₃)₂), 0.78 (d, ³J = 6.7 Hz, 3H, CH-(CH₃)₂).

¹³C-NMR (126 MHz, CD₂Cl₂): δ [ppm] = 154.6, 141.3, 129.2, 128.8, 127.3, 54.3, 32.2, 21.2, 21.0.

IR (neat): $\tilde{\nu}$ [cm⁻¹] = 3239, 3086, 3028, 2958, 2930, 2871, 2360, 2341, 1866, 1792, 1740, 1717, 1683, 1669, 1653, 1647, 1636, 1600, 1576, 1558, 1541, 1521, 1506, 1490, 1465, 1455, 1386, 1331, 1298, 1230, 1217, 1166, 1143, 1118, 1078, 1030, 1002, 952, 924, 823, 757, 698, 669, 626, 611, 543, 523, 486, 473, 452, 442, 434, 520, 412.

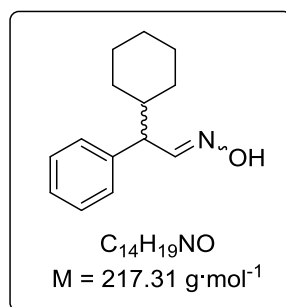
RP-HPLC: *Macherey-Nagel* Nucleodur C₁₈ HTec, water/acetonitrile 60:40, mL·min⁻¹, 40 °C, 210 nm, R_{t1} = 11.3 min.

NP-HPLC: *Daicel Chiracel* OB-H, CO₂/isopropanol = 99.5:0.5, 0.8 mL·min⁻¹, 20 °C, 210 nm, R_{t1} = 30.0 min, R_{t2} = 34.8 min.

rac-E/Z-3-Methyl-2-phenylbutanal oxime

MS (ESI, positive ions): *m/z* = 178.0 [M+H]⁺, 200.0 [M+Na]⁺.

EA: calcd. for C₁₀H₁₃NO: C, 74.54; H, 8.53, N, 7.90, found: C, 74.62; H, 8.81; N, 7.81.

9.3.5.3 Synthesis of *rac-E/Z*-2-cyclohexyl-2-phenylacetaldoxime

The synthesis was carried out according to GP5. 20 mL tetrahydrofuran was given into a Schlenk flask, Potassium hydroxide (324 mg, 5.49 mmol) and molecular sieves 4 Å (232 mg) were added. Benzyl bromide (652 μL , 5.49 mmol) and TBAI (85.0 mg, 264 μmol) were added after an hour. (2-Cyclohexyl-1-nitroethyl)-benzene (1.17 g, 5.00 mmol) was added and the reaction mixture was stirred overnight. Workup and purification *via* automated column chromatography (cyclohexane/ethyl acetate 9:1, *v,v*) yielded the *E/Z*-mixture (15:85 *E/Z*) as a brown solid.

Yield: 520 mg, 2.39 mmol, 48 %.

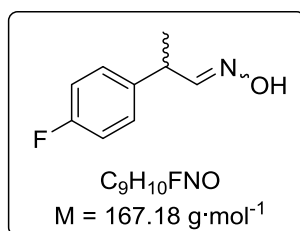
$^1\text{H-NMR}$ (500 MHz, CD_2Cl_2): δ = 8.00 (s, 1H, HC=NOH, minor, *E*), 7.71 (s, 1H, HC=NOH, major, *Z*), 7.55 (d, $^3J = 8.6$ Hz, 1H, HC=NOH, major, *Z*), 7.37 – 7.26 (m, 2H, Ar-*H*), 7.26 – 7.20 (m, 1H, Ar-*H*), 7.19 – 7.14 (m, 2H, Ar-*H*), 6.90 (d, $^3J = 8.2$ Hz, 1H, HC=NOH, minor, *E*), 4.07 – 3.95 (m, 1H, CH-CH=NOH, minor, *E*), 3.21 – 3.10 (m, 1H, CH-CH=NOH, major, *Z*), 1.88 – 1.57 (m, 5H, Cy-*H*_{eq}), 1.41 (m, 1H, Cy-*H*), 1.31 – 0.76 (m, 5H, Cy-*H*_{ax}).

$^{13}\text{C-NMR}$ (126 MHz, CD_2Cl_2): δ [ppm] = 154.6 (major, *Z*), 154.5 (minor, *E*), 141.0 (major, *Z*), 140.8 (minor, *E*), 129.2 (major, *Z*), 129.1 (minor, *E*), 128.9 (minor, *E*), 128.8 (major, *Z*), 127.3 (major, *Z*), 127.1 (minor, *E*), 53.2 (major, *Z*), 47.6 (minor, *E*), 41.8 (minor, *E*), 41.5 (major, *Z*), 32.0 (major, *Z*), 31.7 (minor, *E*), 31.5 (major, *Z*), 31.2 (minor, *E*), 26.9 (minor, *E*), 26.9 (major, *Z*), 26.8 (minor, *E*), 26.7 (major, *Z*), 26.7 (major, *Z*), 26.7 (minor, *E*).

IR (neat): $\tilde{\nu}$ [cm^{-1}] = 3226, 3087, 3061, 3027, 2920, 287, 2669, 2369, 2338, 1869, 1801, 1772, 1749, 1716, 1698, 1653, 1600, 1584, 1542, 1490, 1448, 1367, 1348, 1319, 1297, 1274, 1209, 1183, 1155, 1135, 1100, 1090, 1074, 1047, 1032, 1002, 961, 930, 887, 847, 822, 798, 757, 697, 627, 617, 574, 511, 473, 448, 434, 418.

RP-HPLC: *Macherey-Nagel* Nucleodur C₁₈ HTec, water/acetonitrile 60:40, 1.0 mL·min⁻¹, 40 °C, 210 nm, R_{t1} = 36.7 min (major, *Z*), R_{t2} = 41.1 min (minor, *E*).

HRMS (ESI, positive ions): calcd for C₁₄H₁₉NONa⁺ [M+Na]⁺: 240.13588, found: 240.1359.

9.3.5.4 Synthesis of *rac*-4-fluorophenyl-propanal oxime

The synthesis was carried out according to GP5. 20 mL tetrahydrofuran were given into a Schlenk flask, 85 wt% KOH (177 mg, 3.15 mmol) and molecular sieves 4 Å (150 mg) were added. Benzyl bromide (393 μL , 3.30 mmol) and TBAI (55.4 mg, 150 μmol) were added after an hour. *rac*-1-Fluoro-4-(1-nitropropan-2-yl)benzene (550 mg, 3.00 mmol) was added and the reaction mixture was stirred for three hours. Workup and purification *via* automated column chromatography (cyclohexane/ethyl acetate 6:1, *v,v*) yielded the *E*-isomer (92 % *E*) as pale yellow oil and the *Z*-isomer (97 % *Z*) as crystalline colorless solid.

Combined yield: 482 mg, 2.88 mmol, 96 %.

rac-E-2-(4-Fluorophenyl)propanal oxime:

$^1\text{H-NMR}$ (500 MHz, CDCl_3): δ [ppm] = 7.47 (d, 1H, $^3J = 6.1$ Hz, $\text{HC}=\text{NOH}$), 7.21 (m, 2H, Ar-*H*), 7.07 (m, 2H, Ar-*H*), 3.66 (qi, 1H, $^3J = 6.9$ Hz, $\text{CH-CH}=\text{NOH}$), 1.41 (d, 3H, $^3J = 7.1$ Hz, CH_3).

$^{13}\text{C-NMR}$ (125 MHz, CD_2Cl_2): δ [ppm] = 163.3, 161.3, 155.1, 138.6, 129.6, 129.5, 116.0, 115.9, 40.2, 19.3.

IR (neat): $\tilde{\nu}$ [cm^{-1}] = 3256, 3101, 2971, 2933, 2875, 2363, 2337, 1889, 1737, 1650, 1602, 1506, 1450, 1413, 1375, 1297, 1221, 1159, 1098, 1065, 1014, 930, 832, 722, 668, 625, 576, 544, 529, 466, 413.

RP-HPLC: *Macherey-Nagel* Nucleodur C_{18} HTec, water/acetonitrile 70:30, 1.5 $\text{mL}\cdot\text{min}^{-1}$, 40 $^\circ\text{C}$, 210 nm, $R_{t1} = 13.6$ min.

NP-HPLC: *Daicel Chiracel* OB-H, CO_2 /isopropanol 98:2, 0.8 $\text{mL}\cdot\text{min}^{-1}$, 20 $^\circ\text{C}$, 210 nm, $R_{t1} = 19.4$ min, $R_{t2} = 21.6$ min.

rac-Z-2-(4-Fluorophenyl)propanal oxime:

$^1\text{H-NMR}$ (500 MHz, CDCl_3): δ [ppm] = 7.29 (m, 2H, Ar-*H*), 7.07 (m, 2H, Ar-*H*), 6.76 (d, 1H, $^3J = 7.3$ Hz, $\text{HC}=\text{NOH}$), 4.41 (p, 1H, $^3J = 7.2$ Hz, $\text{CH-CH}=\text{NOH}$), 1.39 (d, 3H, $^3J = 7.1$ Hz, CH_3).

$^{13}\text{C-NMR}$ (125 MHz, CD_2Cl_2): δ [ppm] = 163.1, 161.2, 155.6, 138.8, 129.3, 115.9, 115.8, 34.7, 19.0.

9 Experimental section

IR (neat): $\tilde{\nu}$ [cm⁻¹] = 3256, 3101, 2971, 2933, 2875, 2363, 2337, 1889, 1737, 1650, 1602, 1506, 1450, 1413, 1375, 1297, 1221, 1159, 1098, 1065, 1014, 930, 832, 722, 668, 625, 576, 544, 529, 466, 413.

RP-HPLC: *Macherey-Nagel* Nucleodur C₁₈ HTec, water/acetonitrile 70:30, 1.5 mL·min⁻¹, 40 °C, 210 nm, R_t = 15.6 min.

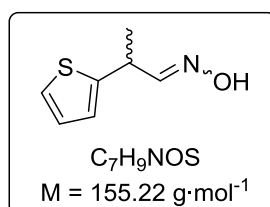
NP-HPLC: *Daicel Chiracel* OB-H, CO₂/isopropanol 98:2, 0.8 mL·min⁻¹, 20 °C, 210 nm, R_{t1} = 21.1 min, R_{t2} = 22.0 min.

rac-E/Z-2-(4-Fluorophenyl)propanal oxime:

MS (ESI): *m/z* = 168.0 [M+H]⁺, 190.0 [M+Na]⁺.

EA: calcd for C₉H₁₀FNO: C, 64.66; H, 6.03; N, 8.38. Found: C, 64.77; H, 6.26; N, 7.98.

9.3.5.5 Synthesis of *rac-E/Z-2-(thiophen-2-yl)propanal oxime*



The synthesis was carried out according to GP5. 60 mL tetrahydrofuran were given into a Schlenk flask, 85 wt% KOH (619 mg, 11.0 mmol) and molecular sieves 4 Å (150 mg) were added. Benzyl bromide (1.37 mL, 11.6 mmol) and TBAI (194 mg, 525 μmol) were added after an hour. *rac-2-(1-Nitropropan-2-yl)thiophene* (1.80 g, 10.5 mmol) was added and the reaction mixture was stirred for three hours. Workup and purification *via* automated column chromatography (cyclohexane/ethyl acetate 6:1, *v,v*) yielded the *E/Z*-mixture (70 % *E*, 30 % *Z*) as pale orange oil.

Combined yield: 850 mg, 5.48 mmol, 52 %.

rac-E/Z-2-(thiophen-2-yl)propanal oxime:

¹H-NMR (500 MHz, CDCl₃): δ [ppm] = 7.49 (dd, 0.63H, ³*J* = 6.6 Hz, ⁴*J* = 1.6 Hz, HC=NOH, major, *E*), 7.21 (ddd, 1H, ²*J* = 10.1 Hz, ³*J* = 5.1 Hz, ⁴*J* = 1.2 Hz, Ar-*H*), 6.97 (dt, 1H, ³*J* = 5.2 Hz, ⁴*J* = 3.4 Hz, Ar-*H*), 6.90 (ddt, 1H, ⁴*J* = 14.5 Hz, ⁴*J* = 3.5, 1.1 Hz, Ar-*H*), 6.76 (d, 0.33H, ³*J* = 7.4 Hz, HC=NOH, minor, *Z*), 4.69 (m, 0.35H, CH-CH=NOH, major, *Z*), 3.94 (m, 0.69H, CH-CH=NOH, major, *E*), 1.51 (d, 2.23H, ³*J* = 7.0 Hz, CH₃, major, *E*), 1.48 (d, 1.12H, ³*J* = 7.1 Hz, CH₃, minor, *Z*).

9 Experimental section

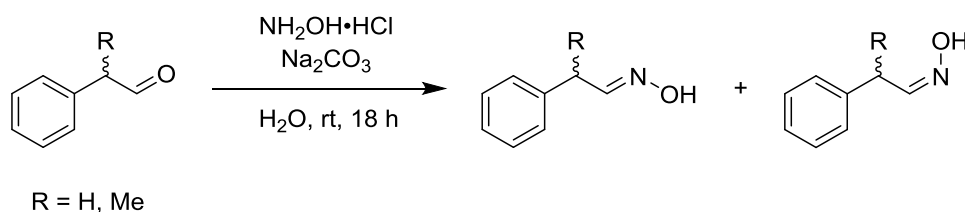
¹³C-NMR (125 MHz, CD₂Cl₂): δ [ppm] = 154.9, 154.6, 146.1, 127.5, 127.4, 124.7, 124.6, 124.4, 124.3, 36.3, 31.0, 20.1, 19.6.

The analytical data corresponds with literature data.^[191]

RP-HPLC: *Macherey-Nagel* Nucleodur C₁₈ HTec, water/acetonitrile 70:30, 1.0 mL·min⁻¹, 40 °C, 220 nm, R_{t1} = 9.52 min, R_{t2} = 11.1 min.

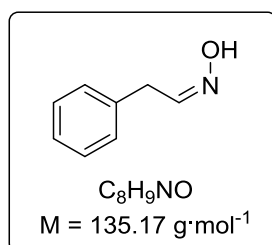
NP-HPLC: *Daicel Chiracel* OJ-H, CO₂/isopropanol 95:5, 1.0 mL·min⁻¹, 20 °C, 210 nm, R_{t1} = 16.3 min, R_{t2} = 18.9 min, R_{t3} = 19.4 min, R_{t4} = 20.6 min.

9.3.6 General procedure 6 (GP6): Synthesis of aldoximes by condensation of aldehydes with hydroxyl amine salts



Hydroxylamine hydrochloride (1.5 eq.) and sodium carbonate (1.5 eq.) were dissolved in H₂O at room temperature. Aldehyde was added to this solution and stirred vigorously until complete conversion according to TLC analysis (cyclohexane/ethyl acetate in different volumetric percentages) was achieved. The solution was extracted three times with ethyl acetate (1:1 v, v) and the combined organic phases were washed with H₂O (1:3 v, v). Drying over magnesium sulfate and evaporation of the solvent gave a crude product, which was purified by column chromatography or recrystallized. The *E/Z*-ratio of the product was determined by ¹H-NMR spectroscopy.

9.3.6.1 Synthesis of *Z*-phenylacetaldoxime



The synthesis was carried out according to GP6. Hydroxylamine hydrochloride (10.3 g, 148 mmol) and sodium carbonate (17.3 g, 163 mmol) were dissolved in 100 mL water at room temperature. After the addition of phenyl acetaldehyde (12.04 g, 100 mmol) the colorless suspension was stirred overnight, upon which complete conversion was achieved according

9 Experimental section

to TLC analysis (cyclohexane/ethyl acetate 1:1, v,v). Workup and recrystallization from a mixture of diethyl ether and di-isopropyl ether (-80 °C) yielded the product (*E/Z* 1:>99) as colorless crystals.

Yield: 5.6 g, 41.4 mmol, 41 %.

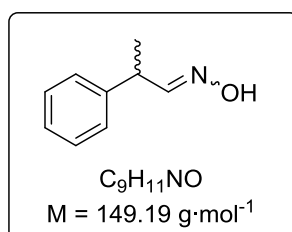
¹H-NMR (500 MHz, CD₂Cl₂): δ [ppm] = 8.88 (s, 1H, CH=NOH), 7.37-7.30 (m, 2H, *E/Z*- PhH), 7.29 – 7.22 (m, 3H, PhH), 6.91 (t, ³J = 5.4 Hz, 1H, CH=NOH), 3.74 (d, ³J = 5.3 Hz, 2H, Ph-CH₂).

¹³C-NMR (500 MHz, CD₂Cl₂): δ [ppm] = 151.2, 129.1, 129.1, 129.0, 126.9, 31.9.

RP-HPLC: *Macherey-Nagel* Nucleodur C₁₈ HTec, water/acetonitrile 70:30, 1.0 mL·min⁻¹, 40 °C, 210 nm, R_{t1} = 7.54 min, R_{t2} = 8.82 min.

The analytical data corresponds with literature.^[264]

9.3.6.2 Synthesis of *rac-E/Z*-2-phenylpropionaldoxime



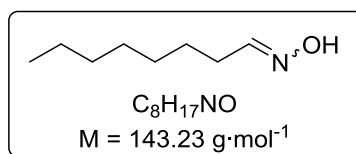
The synthesis was carried out according to GP6. Hydroxylamine hydrochloride (4.34 g, 62.4 mmol) and sodium carbonate (6.61 g, 62.4 mmol) were dissolved in 50 mL water at room temperature. After the addition of 2-phenylpropionaldehyde (6.90 mL, 41.6 mmol) the colorless suspension was stirred overnight, upon which complete conversion was achieved according to TLC analysis (cyclohexane/ethyl acetate 6:1, v,v). Workup and column chromatography yielded *E/Z*-mixture (70:30) as a colorless oil.

Yield: 2.53 g, 41.4 mmol, 41 %.

¹H-NMR (500 MHz, CD₂Cl₂): δ [ppm] = 8.27 (s, 1H, CH=NOH, minor, *Z*), 7.89 (s, 1H, CH=NOH, major, *E*), 7.51 (d, ³J = 6.1 Hz, 1H, CH=NOH, major, *E*), 7.36-7.31 (m, 4H, PhH, *E/Z*), 7.30-7.27 (m, 2H, PhH, *E/Z*), 7.27– 7.21 (m, 4H, PhH, *E/Z*), 6.82 (d, ³J = 7.4 Hz, 1H, CH=NOH, minor, *Z*), 4.42 (dq, ³J = 7.2 Hz, 7.2 Hz, 1H, Ph-CH, minor, *Z*), 3.68 (p, ³J = 6.9 Hz, 6.9 Hz 1H, Ph-CH, major, *E*), 1.44 (d, ³J = 7.2 Hz, 3H, CH-CH₃, major, *E*), 1.42 (d, ³J = 7.3 Hz, 3H, CH-CH₃, minor, *Z*).

RP-HPLC: *Macherey-Nagel* Nucleodur C₁₈ HTec, water/acetonitrile 70:30, 1.0 mL·min⁻¹, 40 °C, 210 nm, R_{t1} = 12.1 min, R_{t2} = 13.7 min.

The analytical data corresponds with literature.^[180]

9.3.6.3 Synthesis of *n*-octanal oxime

The synthesis was carried out according to GP6. Hydroxylamine hydrochloride (7.80 g, 112 mmol) and sodium carbonate (11.9 g, 112 mmol) were dissolved in 150 mL water at room temperature. After the addition of octanal (9.60 g, 74.9 mmol) the colorless suspension was stirred overnight, upon which complete conversion was achieved according to TLC analysis (cyclohexane/ethyl acetate). Workup and recrystallization from ethanol (reflux) yielded the *E/Z*-mixture (70:30) as colorless crystals.

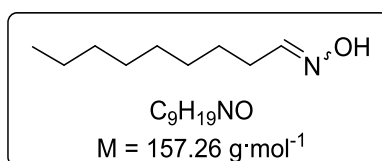
Yield: 2.62 g, 18.3 mmol, 24 %

$^1\text{H-NMR}$ (500 MHz, CD_2Cl_2): δ [ppm] = 8.68 (s, 1H, CHNOH), 7.42 (t, $^3J = 6.2$ Hz, 1H, CHNOH , major), 6.73 (t, $^3J = 5.4$ Hz, 1H, CHNOH , minor), 2.38 (td, $^3J = 7.6, 5.4$ Hz, 1H, CH_2CHNOH , minor), 2.19 (m, 1H, CH_2CHNOH , major), 1.49 (ddt, $^3J = 11.0, 7.6$ Hz 2H, $\text{CH}_3(\text{CH}_2)_3(\text{CH}_2)_2$), 1.38–1.19 (m, 8H, $\text{CH}_3(\text{CH}_2)_3(\text{CH}_2)_2$), 0.87 (td, $^3J = 7.0, 2.1$ Hz, 3H, CH_3CH).

$^{13}\text{C-NMR}$ (125 MHz, CD_2Cl_2): δ [ppm] = 152.0, 151.5, 30.8, 28.6, 28.5, 28.2, 28.1, 25.7, 25.1, 24.1, 21.7, 13.2.

The analytical data corresponds with literature.^[217]

GC: *Phenomenex* ZB-5MSi, 110 °C (0 min), 140 °C (6.0 min), 240 °C (8.0 min), $R_{t1} = 4.5$ min, (Nitrile: $R_{t2} = 3.4$ min).

9.3.6.4 Synthesis of *n*-nonanal oxime

The synthesis was carried out according to GP6. Hydroxylamine hydrochloride (7.80 g, 112 mmol) and sodium carbonate (11.9 g, 112 mmol) were dissolved in 150 mL water at room temperature. After the addition of nonanal (10.7 g, 75.2 mmol) the colorless suspension was stirred overnight, upon which complete conversion was achieved according to TLC analysis (cyclohexane/ethyl acetate). Workup and recrystallization from ethanol (reflux) yielded *E/Z*-mixture (70:30) as colorless crystals.

Yield: 3.81 g, 24.2 mmol, 32 %

9 Experimental section

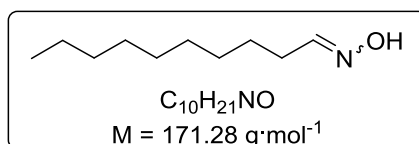
¹H-NMR (500 MHz, CD₂Cl₂): δ [ppm] = 8.44 (s, 1H, CHNOH), 7.42 (t, ³J = 6.2 Hz, 1H, CHNOH, major), 6.73 (t, ³J = 5.5 Hz, 1H, CHNOH, minor), 2.38 (td, ³J = 7.6, 5.4 Hz, 1H, CH₂CHNOH, minor), 2.19 (m, 1H, CH₂CHNOH, major), 1.48 (ddq, ³J = 11.2, 7.4, 3.6 Hz, 2H, CH₃(CH₂)₃(CH₂)₂), 1.39–1.17 (m, 10H, CH₃(CH₂)₃(CH₂)₂), 0.87 (m, 3H, CH₃CH).

¹³C-NMR (125 MHz, CD₂Cl₂): δ [ppm] = 153.1, 152.5, 32.0, 29.6, 29.5, 29.4, 29.3, 26.7, 26.1, 25.2, 22.8, 14.2.

The analytical data corresponds with literature.^[218]

GC: Phenomenex ZB-5MSi, 110 °C (0 min), 140 °C (6.0 min), 240 °C (8.0 min), R_{t1} = 5.9 min, (Nitrile: R_{t2} = 4.3 min).

9.3.6.5 Synthesis of *n*-decanal oxime



The synthesis was carried out according to GP6. Hydroxylamine hydrochloride (7.80 g, 112 mmol) and sodium carbonate (11.9 g, 112 mmol) were dissolved in 150 mL water at room temperature. After the addition of decanal (11.7 g, 74.9 mmol) the colorless suspension was stirred overnight, upon which complete conversion was achieved according to TLC analysis (cyclohexane/ethyl acetate). Workup and recrystallization from ethanol (reflux) yielded *E/Z*-mixture (70:30) as colorless crystals.

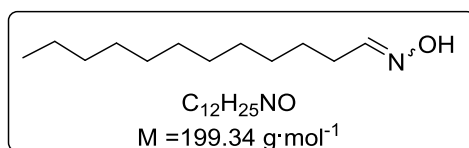
Yield: 5.14 g, 30 mmol, 40 %

¹H-NMR (500 MHz, CD₂Cl₂): δ [p] = 8.26 (s, 1H, CHNOH), 7.42 (t, ³J = 6.1 Hz, 1H, CHNOH, major), 6.74 (t, ³J = 5.5 Hz, 1H, CHNOH, minor), 2.38 (td, ³J = 7.6, 5.4 Hz, 1H, CH₂CHNOH, minor), 2.19 (q, ³J = 7.1 Hz, 1H, CH₂CHNOH, major), 1.48 (m, 2H, CH₃(CH₂)₃(CH₂)₂), 1.39–1.16 (m, 12H, CH₃(CH₂)₃(CH₂)₂), 0.87 (t, ³J = 6.8 Hz, 3H, CH₃CH).

¹³C-NMR (125 MHz, CD₂Cl₂): δ [ppm] = 153.1, 152.5, 32.0, 29.6, 29.5, 29.5, 29.4, 29.2, 26.7, 26.1, 25.2, 22.8, 14.2.

The analytical data corresponds with literature.^[217]

GC: Phenomenex ZB-5MSi, 110 °C (0 min), 140 °C (6.0 min), 240 °C (8.0 min), R_{t1} = 7.0 min, (Nitrile: R_{t2} = 5.6 min).

9.3.6.6 Synthesis of *n*-dodecanal oxime

The synthesis was carried out according to GP6. Hydroxylamine hydrochloride (7.80 g, 112 mmol) and sodium carbonate (11.9 g, 112 mmol) were dissolved in 150 mL water at room temperature. After the addition of dodecanal (13.8 g, 74.9 mmol) the colorless suspension was stirred overnight, upon which complete conversion was achieved according to TLC analysis (cyclohexane/ethyl acetate). Workup and recrystallization from ethanol (reflux) yielded *E/Z*-mixture (70:30) as colorless crystals.

Yield: 6.08 g, 30.5 mmol, 39 %

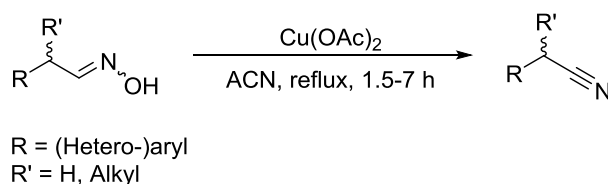
¹H-NMR (500 MHz, CD₂Cl₂): δ [ppm] = 7.50 (s, 1H, CHNOH), 7.42 (t, ³J = 6.1 Hz, 1H, CHNOH, major), 6.77 (t, ³J = 5.5 Hz, 1H, CHNOH, minor), 2.40 (td, ³J = 7.6, 5.5 Hz, 1H, CH₂CHNOH, minor), 2.20 (m, 1H, CH₂CHNOH, major), 1.48 (p, ³J = 7.2 Hz, 2H, CH₃(CH₂)₃(CH₂)₂), 1.39–1.17 (m, 16H, CH₃(CH₂)₃(CH₂)₂), 0.88 (t, ³J = 6.9 Hz, 3H, CH₃CH).

¹³C-NMR (125 MHz, CD₂Cl₂): δ [ppm] = 153.1, 152.5, 32.0, 29.6, 29.5, 29.3, 29.1, 26.5, 26.0, 25.0, 22.7, 14.1.

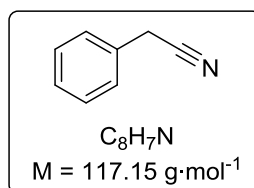
The analytical data corresponds with literature.^[217]

GC: Phenomenex ZB-5MSi, 140 °C (0 min), 180 °C (8.0 min), 280 °C (11.0 min), R_{t1} = 7.0 min, (Nitrile: R_{t2} = 5.5 min).

9.3.7 General procedure 7 (GP7): Synthesis of racemic nitriles by copper(II) catalyzed dehydration of aldoximes



The syntheses were carried out in analogy to *Ma et al.*^[89] Copper(II) acetate (0.06 – 0.11 eq) was dissolved in acetonitrile at room temperature. The corresponding aldoxime (1.0 eq.) was added and the solution was heated to reflux for 90 minutes to 7 hours. Complete conversion was determined *via* TLC (cyclohexane/ethyl acetate) and the solvent was removed *in vacuo*. The crude product was suspended in cyclohexane/ethyl acetate and filtered over a short plug of silica to yield the product as oil.

9.3.7.1 Synthesis of *rac*-2-phenylacetonitrile

The synthesis was carried out according to GP7. Copper(II) acetate (8.0 mg, 44 μmol) was dissolved in 1.5 mL acetonitrile. *rac*-*E/Z*-Phenylacetoxime (51 mg, 375 μmol) was added to the solution. After refluxing for 90 minutes, workup was conducted (cyclohexane/ethyl acetate 2:1, *v,v*) and yielded the product as a brown oil.

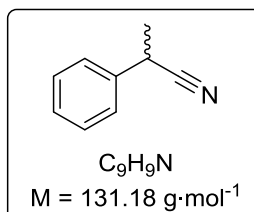
Yield: 29.7 mg, 253 μmol, 68 %.

¹H-NMR (500 MHz, CDCl₃): δ [ppm] = 7.40 – 7.37 (m, 2H, ArH), 7.35 – 7.33 (m, 3H, ArH), 3.76 (s, 2H, N≡C-CH₂).

¹³C-NMR (126 MHz, CDCl₃): δ [ppm] = 130.1, 129.3, 128.2, 128.1, 118.0, 23.8.

RP-HPLC: *Macherey-Nagel* Nucleodur C₁₈ HTec, Wasser/Acetonitril 70:30, 1.0 mL·min⁻¹, 40 °C, 210 nm, R_t = 11.7 min.

The analytical data corresponds with the literature.^[180]

9.3.7.2 Synthesis of *rac*-2-phenylpropane nitrile

The synthesis was carried out according to GP7. Copper(II) acetate (11.2 mg, 61.6 μmol) was dissolved in 4.0 mL acetonitrile. *rac*-*E/Z*-2-Phenylpropanal oxime (155.2 mg, 1.04 mmol) was added to the solution. After heating to reflux for 90 minutes, workup was conducted (MTBE) and yielded the product as a pale orange oil.

Yield: 86 mg, 655 μmol, 63 %.

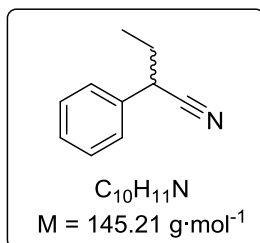
¹H-NMR (500 MHz, CDCl₃): 7.43-7.29 (m, 5H), 3.90 (q, ³J = 7.3 Hz, 1H, N≡C-CH), 1.65 (d, ³J = 7.3 Hz, 3H, CH₃).

¹³C-NMR (126 MHz, CDCl₃): δ [ppm] = 137.4, 129.5, 128.4, 127.0, 31.6, 21.8.

The analytical data corresponds with literature.^[180]

RP-HPLC: *Macherey-Nagel* Nucleodur C₁₈ HTec, water/acetonitrile 70:30, 1.0 mL·min⁻¹, 40 °C, 210 nm, R_t = 20.5 min.

9.3.7.3 Synthesis of *rac*-2-phenylbutane nitrile



The synthesis was carried out according to GP7. Copper(II) acetate (5.5 mg, 30 μmol) was dissolved in 5.0 mL acetonitrile. 2-Phenylbutanal oxime (67.2 mg, 412 μmol) was added to the solution. After heating to reflux for 7 hours, workup was conducted (MTBE) and yielded the product as a yellow oil.

Yield: 59.3 mg, 408 μmol, 99 %.

¹H-NMR (500 MHz, CDCl₃): δ [ppm] = 7.41 – 7.35 (m, 2H, Ar-*H*), 7.35 – 7.29 (m, 3H, Ar-*H*), 3.74 (t, ³J = 7.2 Hz, 1H, CH-C≡N), 1.99 – 1.90 (m, 2H, CH₂-CH₃), 1.08 (t, ³J = 7.3 Hz, 3H, CH₂-CH₃).

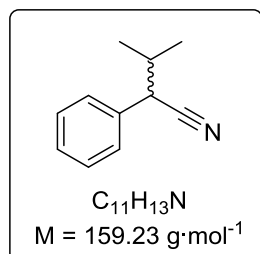
¹³C-NMR (126 MHz, CDCl₃): δ [ppm] = 135.9, 129.2, 128.1, 127.4, 120.9, 39.1, 29.4, 11.6.

The analytical data corresponds with literature.^[265]

RP-HPLC: *Macherey-Nagel* Nucleodur C₁₈ HTec, water/acetonitrile 60:40, 1.0 mL·min⁻¹, 40 °C, 210 nm, R_{t1} = 15.5 min.

NP-HPLC: *Daicel Chiracel* OB-H, CO₂/isopropanol = 99.5:0.5, 0.8 mL·min⁻¹, 20 °C, 210 nm, R_{t1} = 14.9 min, R_{t2} = 19.4 min.

9.3.7.4 Synthesis of *rac*-3-methyl-2-phenylbutane nitrile



The synthesis was carried out according to GP7. Copper(II) acetate (6.1 mg, 34 μmol) was dissolved in 5.0 mL acetonitrile. *E/Z*-3-Methyl-2-phenylbutanal oxime (65.0 mg, 367 μmol) was

9 Experimental section

added to the solution. After heating to reflux for 7 hours, workup was conducted (MTBE) and yielded the product as a yellow oil.

Yield: 46.8 mg, 294 μmol , 80 %.

$^1\text{H-NMR}$ (500 MHz, CDCl_3): δ [ppm] = 7.40 – 7.35 (m, 2H, Ar-*H*), 7.35 – 7.28 (m, 3H, Ar-*H*), 3.66 (d, $^3J = 6.2$ Hz, 1H, CH-C \equiv N), 2.13 (dq, $^3J = 6.8, 6.7$ Hz, 1H, CH-(CH $_3$) $_2$), 1.06 (d, $^3J = 6.7$ Hz, 3H, CH-(CH $_3$) $_2$), 1.04 (d, $^3J = 6.6$ Hz, 3H, CH-(CH $_3$) $_2$).

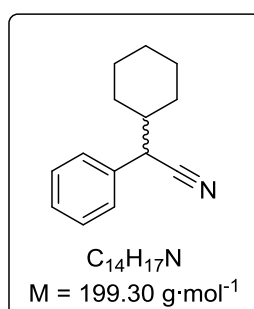
$^{13}\text{C-NMR}$ (126 MHz, CDCl_3): δ [ppm] = 135.1, 129.0, 128.1, 128.0, 45.3, 33.9, 21.0, 19.0.

The analytical data corresponds with literature.^[266]

RP-HPLC: *Macherey-Nagel* Nucleodur C $_{18}$ HTec, water/acetonitrile 60:40, 1.0 mL \cdot min $^{-1}$, 40 $^\circ\text{C}$, 210 nm, R $_{t1}$ = 24.1 min.

NP-HPLC: *Daicel Chiracel* OB-H, CO $_2$ /isopropanol = 99.5:0.5, 0.8 mL \cdot min $^{-1}$, 20 $^\circ\text{C}$, 210 nm, R $_{t1}$ = 11.1 min, R $_{t2}$ = 14.9 min.

9.3.7.5 Synthesis of *rac*-2-cyclohexyl-2-phenylacetonitrile



The synthesis was carried out according to GP7. Copper(II) acetate (7.8 mg, 43 μmol) was dissolved in 5.0 mL acetonitrile. 2-Cyclohexyl-2-phenylacetaldehyde oxime (83.9 mg, 386 μmol) was added to the solution. After heating to reflux for 7 hours, workup was conducted (MTBE) and yielded the product as a brown oil.

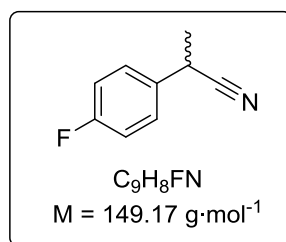
Yield: 71.3 mg, 358 μmol , 93 %.

$^1\text{H-NMR}$ (500 MHz, CDCl_3): δ [ppm] = 7.48 – 7.41 (m, 2H, Ar-*H*), 7.41 – 7.31 (m, 3H, Ar-*H*), 3.70 (d, $^3J = 6.6$ Hz, 1H, CH-C \equiv N), 1.96 – 1.68 (m, 6H, Cy-*H* $_{eq}$ / CH-CH), 1.32 – 1.18 (m, 5H, Cy-*H* $_{ax}$).

$^{13}\text{C-NMR}$ (126 MHz, CDCl_3): δ [ppm] = 134.8, 128.9, 128.1, 128.0, 120.3, 44.5, 42.9, 31.4, 29.7, 26.1, 26.0, 25.9.

The analytical data corresponds with literature.^[266]

RP-HPLC: *Macherey-Nagel* Nucleodur C $_{18}$ HTec, water/acetonitrile 60:40, 1.0 mL \cdot min $^{-1}$, 40 $^\circ\text{C}$, 210 nm, R $_{t1}$ = 76.5 min.

9.3.7.6 Synthesis of *rac*-4-fluorophenyl-propane nitrile

The synthesis was carried out according to GP7. Copper(II) acetate (14.6 mg, 80 μmol) was dissolved in 10 mL acetonitrile. *rac*-*E/Z*-2-(4-Fluorophenyl)propanal oxime (66.9 mg, 400 μmol) was added to the solution. After heating to reflux for 60 minutes, workup was conducted (cyclohexane/ethyl acetate 2:1, v,v) and yielded the product as pale yellow oil.

Yield: 30 mg, 201 μmol, 50 %.

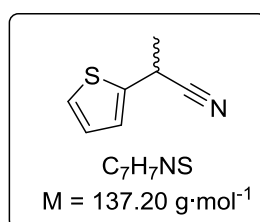
¹H-NMR (500 MHz, CDCl₃): δ [ppm] = 7.36-7.30 (m, 2H, Ar-*H*), 7.11-7.04 (m, 2H, Ar-*H*), 3.89 (q, 1H, ³*J*=7.3 Hz, CH-CN), 1.64 (d, 3H, ³*J*=7.3 Hz, CH₃).

¹³C-NMR (125 MHz, CDCl₃): δ [ppm] = 163.5, 161.5, 133.0, 128.6, 121.5, 116.4, 30.8, 21.7.

The analytical data corresponds with the literature.^[267]

RP-HPLC: *Macherey-Nagel* Nucleodur C₁₈ HTec, water/acetonitrile 70:30, 1.0 mL·min⁻¹, 40 °C, 210 nm, R_{t1} = 21.8 min.

NP-HPLC: *Daicel Chiracel* OB-H, CO₂/isopropanol = 98:2, 0.8 mL·min⁻¹, 20 °C, 210 nm, R_{t1} = 10.2 min, R_{t2} = 11.4 min.

9.3.7.7 Synthesis of *rac*-2-(thiophen-2-yl)propionitrile

The synthesis was carried out according to GP7. Copper(II) acetate (25.4 mg, 140 μmol) was dissolved in 10 mL acetonitrile. *rac*-*E/Z*-2-(Thiophen-2-yl)propanal oxime (109 mg, 700 μmol) was added to the solution. After heating to for 60 minutes, workup was conducted (cyclohexane/ethyl acetate 2:1, v,v) and yielded the product as pale orange oil.

Yield: 60 mg, 437 μmol, 68 %.

9 Experimental section

¹H-NMR (500 MHz, CDCl₃): δ [ppm] = 7.27 (dd, 1H, ³J = 5.1, ⁴J = 1.2 Hz, Ar-H), 7.08 (dt, 1H, ⁴J = 3.6, 1.1 Hz, Ar-H), 6.99 (dd, 1H, ³J = 5.1, ⁴J = 3.5 Hz, Ar-H), 4.18 (qd, 1H, ³J = 7.3, ⁴J = 1.0 Hz, CH-CN), 1.74 (d, 3H, ³J = 7.2 Hz, CH₃).

¹³C-NMR (125 MHz, CDCl₃): δ [ppm] = 139.3, 127.3, 125.7, 125.6, 120.8, 26.8, 21.6.

The analytical data corresponds with the literature.^[263]

RP-HPLC: *Macherey-Nagel* Nucleodur C₁₈ HTec, water/acetonitrile 70:30, 1.0 mL·min⁻¹, 40 °C, 220 nm, R_{t1} = 15.1 min.

NP-HPLC: *Daicel Chiracel* OD-H, a linear gradient CO₂/isopropanol 99:1 over 15 minutes followed by a linear gradient CO₂/isopropanol 90:10 over 45 minutes, 1.0 mL·min⁻¹, 20 °C, 240 nm, R_{t1} = 10.9 min, R_{t2} = 11.3 min.

9.4 Microbiological methods

9.4.1 General procedure 8 (GP8): Preparation of chemo-competent cells

E. coli BL21(DE3) (or alternatively *E. coli* JM109) was precultured at 37 °C for 12 hours in 5.0 mL of LB medium. 1.0 mL of the preculture was then transferred to 100 mL of SOB⁺⁺ medium consisted of 2.0 % of tryptone, 0.5 % of yeast extract, 0.0585 % of sodium chloride, 0.0186 % of potassium chloride and 1.0 M magnesium chloride. After cultivation at 30 °C for 4 hours, the cells were chilled for 15 minutes on ice before they are collected by centrifugation (3,000 rpm, 10 min, 4 °C). After removal of the supernant, the cells were suspended gently in 20 mL of ice cold TB buffer consisted of 10 mM piperazine–1,4-bis(2-ethanesulfonic acid), 15 mM calcium chloride, 250 mM potassium chloride and 55 mM manganese(II) chloride. After chilling on ice for 10 minutes, the cells were collected by centrifugation (3,000 rpm, 10 minutes, 4 °C) and suspended gently in 3.72 mL of TB buffer. 280 µL of DMSO was added, gently mixed and incubated on ice for further 10 minutes. The cell suspension was dispended into Eppendorf tubes® and frozen immediately at –198 °C by liquid nitrogen. The cells were kept at –80 °C until use.

9.4.2 General procedure 9 (GP9): Site-directed mutagenesis *via* polymerase chain reaction

Site-directed mutagenesis of the plasmid pET22b-OxdB(C)6His were carried out with QuikChange Lightning Site-directed Mutagenesis Kit (Stratagene, California, USA). pET22b-OxdB(C)6His was used as a dsDNA template in site-directed mutagenesis. The reaction mixture comprised of 0.5 µL of 10x reaction buffer, 0.2 µL of Quick Solution reagent, 0.2 µL of dNTP mix, 0.2 µL of QuikChange Lightning Enzyme, 125 ng of each the forward and reverse primers (see supplementary information), 20-30 ng of the plasmid as template DNA, and sterilized water to a final volume of 5.0 µL. After initial denaturation at 95 °C for 2 minutes, 18 cycles were repeated as follows: A denaturing step at 95 °C for 20 seconds, an annealing step at 50 °C for 10 seconds, and an elongation step at 68 °C for 3.5 minutes. The product was treated with 0.2 µL of DpnI at 37 °C for 2 hours, and then transformed to competent cells of *E. coli* BL21(DE3).

9.4.3 General procedure 10 (GP10): Photometric determination of DNA concentration

Measurements were conducted on a micro volume spectral photometer *via* absorption measurements at 260 nm wavelength.

9.4.4 General procedure 11 (GP11): Transformation of plasmids

2.5 μL of site-directed mutagenesis product and 50 μL of competent cells of *E. coli* BL21(DE3) (pET22b) or *E. coli* JM109 were gently mixed and placed on ice for 30 minutes. After that, the mixture was heated at 42 °C for one minute and placed on ice for two minutes. After adding 500 μL of LB medium, the mixture was cultured at 37 °C for one hour with shaking and centrifuged at 16,100 $\times g$ at 4 °C for 5 minutes. The supernatant was removed, and the cell pellet was resuspended with 100 μL of the medium. The suspension was spreaded onto an LB-agar plate containing the selective antibiotics. Plasmids from each colony were subjected to DNA sequencing to select a mutated plasmid.

9.4.5 General procedure 12 (GP12): Protein expression in shaking flasks

9.4.5.1 Auto-induction medium

A preculture of *E. coli* BL21(DE3)-RIL harbouring pET28a/b- or pUC18-Oxd was inoculated from a LB-agar-plate and grown for 18 hours in test-tubes containing 5.0 mL LB-medium (Roth) 34 $\mu\text{g}\cdot\text{mL}^{-1}$ Chloramphenicol (all Oxds) and 100 $\mu\text{g}\cdot\text{mL}^{-1}$ Carbenicillin (pUC18-OxdB) or 50 $\mu\text{g}\cdot\text{mL}^{-1}$ Kanamycin (other Oxds) at 37 °C at 160 rpm rotary shaking. Subsequently, a main culture of 100 mL Terrific-broth medium (Roth) containing 34 $\mu\text{g}\cdot\text{mL}^{-1}$ Chloramphenicol (all Oxds) and 100 $\mu\text{g}\cdot\text{mL}^{-1}$ Carbenicillin (OxdB) or 50 $\mu\text{g}\cdot\text{mL}^{-1}$ Kanamycin (other Oxds) in a 100 mL Erlenmeyer flask was inoculated with 1.0 mL of the pre-culture. The culture was incubated for approximately 2 hours at 37 °C and 160 rpm rotary shaking until the incubation temperature was changed to 30 °C (OxdB) or 15 °C (other Oxds). After 72 hours, the cells were harvested by centrifugation (4,000 $\times g$, 4 °C, 15 min) and washed twice with KPB buffer (50 mM, pH 7.0). After repeated centrifugation (4,000 $\times g$, 4 °C, 15 min), the cells were resuspended in 5 vol% of the initial medium volume KPB (50 mM, pH 7.0), overlaid with argon and stored at 4 °C as a resting cell suspension.

9.4.5.2 TB-medium pUC18-OxdB

A preculture of *E. coli* BL21(DE3)-RIL or *E. coli* JM109 harbouring pUC18-OxdB was inoculated from a LB-agar-plate and grown for 18 hours in test-tubes containing 5.0 mL LB-medium (Roth) 34 $\mu\text{g}\cdot\text{mL}^{-1}$ Chloramphenicol and 50 $\mu\text{g}\cdot\text{mL}^{-1}$ Carbenicillin. After incubation at 37 °C and 180 rpm for 18 hours, a main culture of 250 mL TB-medium in a 500 mL Erlenmeyer flask was inoculated with 0.1 vol% of the pre-culture, followed by addition of 34 $\mu\text{g}\cdot\text{mL}^{-1}$ Chloramphenicol and 50 $\mu\text{g}\cdot\text{mL}^{-1}$ Carbenicillin or 100 $\mu\text{g}\cdot\text{mL}^{-1}$ Ampicillin. The culture was incubated at 30 °C and 160 rpm until an OD_{600} of 0.6 – 0.8 was reached, induced with Isopropyl- β -D-thiogalactopyranosid (IPTG, final concentration 1.0 mM) followed by incubation at 30 °C

9 Experimental section

for 48 hours. The cells were harvested by centrifugation ($4,000 \times g$, $4\text{ }^{\circ}\text{C}$, 15 min). The supernatant was discarded and the pellets were washed twice with KPB (50 mM, pH 7.0). After repeated centrifugation ($4,000 \times g$, $4\text{ }^{\circ}\text{C}$, 15 min), the cells were resuspended in 5.0 vol% of the initial medium volume KPB (50 mM, pH 7.0), overlaid with argon and stored at $4\text{ }^{\circ}\text{C}$ as a resting cells suspension.

9.4.5.3 TB-medium pET22b-OxdB

Expression and purification were performed according to a slightly modified literature known protocol.^[178] A preculture of *E. coli* BL21(DE3) harbouring pET22b-OxdB(C)6His or its variants was inoculated from a LB-agar-plate and grown for 13 hours in test-tubes containing 5.0 mL LB-medium and $50\text{ }\mu\text{g}\cdot\text{mL}^{-1}$ Carbenicillin at $37\text{ }^{\circ}\text{C}$ at 160 rpm rotary shaking. Subsequently, a main culture of 350 mL Terrific-broth medium containing $50\text{ }\mu\text{g}\cdot\text{mL}^{-1}$ Carbenicillin in a 500 mL Erlenmeyer flask (for whole-cell activity screening: 70 mL medium in 100 mL flask) was inoculated with 1.0 mL of the pre-culture. The culture was incubated for approximately 7 hours at $30\text{ }^{\circ}\text{C}$ and 150 rpm rotary shaking until the OD_{600} reached approximately 0.8 and induced with IPTG (1.0 mM final concentration). After induction, the incubation conditions were changed to $26\text{ }^{\circ}\text{C}$ and 120 rpm rotary shaking. After 21 hours, the cells were harvested by centrifugation ($4,000 \times g$, $4\text{ }^{\circ}\text{C}$, 15 min) and washed twice with equilibration buffer comprising of Tris-HCl buffer (20 mM, pH 8.0) containing 300 mM sodium chloride and 10 mM imidazole. For the whole-cell activity screening the washing processes were performed with KPB (50 mM, pH 7.0), After repeated centrifugation ($4,000 \times g$, $4\text{ }^{\circ}\text{C}$, 15 min), the cells were resuspended in 5.0 vol% of the initial medium volume KPB (50 mM, pH 7.0), overlaid with argon and stored at $4\text{ }^{\circ}\text{C}$ as a resting cells suspension.

9.4.6 Fermentative production of aldoxime dehydratase from *Bacillus* sp. OxdB-1

(Fed-) Batch fermentations were conducted in a 3.4 L bioreactor with an operation volume of 2.0 L. These experiments were conducted in collaboration with the workgroup “AG Fermentationstechnik” led by *Friehs* (Bielefeld University).

9.4.6.1 Media

2.0 L of the medium was filled in the reactor and sterilized at 121 °C. Afterwards, the sterile filtered antibiotics (final concentration: 100 µg·mL⁻¹) were inserted into the bioreactor *via* a syringe. The composition of the batch-phase medium (Table 37) and the feed-medium is described in the table below. The feed-medium was prepared from two solutions, where the magnesium sulfate solution was added *via* syringe filtration after sterilization (at 121 °C) of the glycerol-containing solution.

Table 37. Composition of the media used for (fed-)batch fermentations.

Compound	AI-medium	HSG-medium	TB-medium	Feed-medium
Trypton	24.0 g	13.5 g	24.0 g	-
Yeast extract	12.0 g	7.00 g	12.0 g	90.0 g
NaCl	-	2.50 g	-	-
K ₂ HPO ₄	12.5 g	23.6 g	12.5 g	-
KH ₂ PO ₄	2.40 g	1.50 g	2.40 g	-
Glycerol	5.0 g	29.8 g	5.00 g	527 g
Glucose	50.0 g	-	-	-
Lactose	20.0 g	-	-	(20.0 g)*
MgSO ₄	-	0.14 g	-	20.0 g
Water	Filled up to 1.00 L		Filled up to 1.00 L	Filled up to 1.00 L

*Lactose was only added in the feed-medium when the batch-phase was run with AI-medium.

9.4.6.2 Process control

A preculture of an *E. coli* BL21(DE3) transformant harboring the pET22b(+)-OxdB plasmid was grown in 100 mL TB medium in a 300 mL shaking flask at 37 °C for 18 hours. The culture was centrifuged (4,000 × *g*, 4 °C, 15 min) and resuspended in the same amount of TB-media. 20 mL of the media were pulled into a syringe and transferred into the bioreactor. This point was defined as the start of the fermentation (*t* = 0). From this point the automatic control of the fermentation was started. The temperature was kept constant at 30 °C. The pH-value was set at 7.0. Therefore, ammonia water and 0.1 M phosphoric acid were used. In order to avoid foam formation, Pluronic was used as an anti-foam detergent. The stirrer was set to 200 rpm. For the first phase until induction, when the amount of dissolved oxygen (DO-value) reached a value under 30 % (or alternatively 0 or 10 %), the stirrer speed was increased gradually. After reaching an OD₆₀₀ of approximately 50, a 1.0 M IPTG-solution (final concentration: 1.0 mM) was added. The process was conducted for approximately 28 hours after induction. For fed-batch fermentations, the stirrer speed was increased gradually after the DO-value dropped under 30 % (or other setups). If the DO-value raised over 60 % (or other setpoint), feed-

9 Experimental section

medium was added over the feed-pump. The process was carried out for a total time of approximately 3 or 6 days.

9.4.6.3 Sampling

Every 2 hours samples of 20 mL were taken with an auto sampler, where only the last 2.0 mL of the samples were kept for further analysis. The OD₆₀₀ was measured at a Shimadzu UV-1202 spectrometer against tap water as a standard. For this measurement, the samples were diluted with tap water into the linear area of the spectrometer (absorbance in the range of 0.1 to 0.9). In addition to the measurement of the OD₆₀₀, the activity of the cells was measured with an activity assay based on the dehydration of *E/Z*-phenylacetaldoxime (PAOx, see GP24). For this assay, the cells from 100 µL of the samples were harvested by centrifugation (6,000 × *g*, 4 °C, 10 min) and the supernatant was discarded. The pellets were washed twice with 1 mL KPB (50 mM, pH 7.0), repeatedly centrifuged (6,000 × *g*, 4 °C, 10 min) and the residue was resuspended in 500 µL KPB (50 mM, pH 7.0). In addition to the measurement of the OD₆₀₀ and the activity of the whole cells, the dry biomass was calculated. Therefore, samples of 1.0 or 5.0 mL were taken from the bioreactor and the cell dry weight (CDW) was determined according to GP 5. The amount of glycerol was determined according to the following procedure.

9.4.6.3 Determination of the glycerol concentration

1.0 mL of the samples from the fermenter were transferred into Eppendorf Tubes® and centrifuged (16,000 × *g*, 20 °C, 15 min). Approximately 600 µL of the supernatant was removed and transferred into a HPLC-vial. The content of glycerol was determined *via* RP-HPLC chromatography in comparison to a calibration curve. The measurements were conducted on a Macherey-Nagel SUGAR 810 H column at 72 °C with 2.5 mM sulfuric acid as mobile phase and detection of the refractive index.

9.4.7 General procedure 13 (GP13): Determination of the cell dry weight

Samples from the fed-batch fermentations (usually 10 mL) were centrifuged (6,000 × *g*, 20 °C, 10 min). The supernatant was discarded and the pellets were washed twice with tap water. After repeated centrifugation (6,000 × *g*, 20 °C, 10 min), the cells were dried overnight under vacuum at 60 °C in an oven from Heraeus. The cell dry weight was determined as the difference between the empty Falcon tube® (dried before use) and the vessel containing the dried cells.

9.5 Biochemical methods

9.5.1 General procedure 14 (GP14): Preparation of protein fractions

1.0 mL from the fermentation samples or 1.0 mL of the cell suspension from the shaking flask overexpression was taken and the cells were disrupted by sonification (varying times, 5 cycles, 20 %) at 4 °C. After centrifugation (5,000 rpm, 5 min, 4 °C) the supernatant was taken and the residue kept (**membrane fraction**). The supernatant was centrifuged again (21,500 rpm, 4 °C, 45 min) and the supernatant was taken (**soluble fraction**). 50 or 100 μL of a 6.0 M urea solution was added to the residue left for incubation for 24 hours. Afterwards, the suspension was mixed rigorously to receive a solution, the **insoluble fraction**.

9.5.2 General procedure 15 (GP15): Acidic cell lysate activation

The cells were defrosted on ice and resuspended in approximately 10 mL of sodium phosphate buffer (pH 7.0, 50 mM) containing 300 mM sodium chloride per gram of cell wet weight. After adding of aprotinin (final concentration 3.0 μM), 100 μL of a protease inhibitor mix containing 50 μL phenylmethylsulfonylfluorid (Sigma Aldrich; 17.4 $\text{mg}\cdot\text{mL}^{-1}$ in methanol), 10 μL Pepstatin A (Roth; 1.0 $\text{mg}\cdot\text{mL}^{-1}$ in methanol), 1.0 μL Leupeptin (Roth; 10 $\text{mg}\cdot\text{mL}^{-1}$ in $dd\text{H}_2\text{O}$) and 39 μL methanol per gram of cell wet weight as well as 75 μL DnaseI (2.0 $\text{mg}\cdot\text{mL}^{-1}$ in $dd\text{H}_2\text{O}$) was added. The cells were lysed in a high-pressure homogenizer and the same amount of the protease inhibitor mix and the DNaseI solution were added repeatedly. The followed centrifugation at 27,000 $\times g$ for 30 minutes yielded the lysate as the supernatant. To the supernatant, 4 times of the volume of a citric acid buffer (pH 3.0) was added and the suspension was centrifuged at 4,200 $\times g$ for 5 minutes. The pellet was resuspended thoroughly with sodium phosphate buffer (50 mM, pH 7.0) containing 300 mM sodium chloride in the desired output volume and repeatedly centrifuged at 4,200 $\times g$ for 5 minutes. The supernatant is further used as the activated lysate.

9.5.3 General procedure 16 (GP16): Protein purification

The cells from two cultures (~1.0 g) were resuspended with equilibration buffer (1:5 *m,v*) disrupted with sonotrode (varying times, 5 cycles at 20 %), and the cell debris and insoluble protein was removed *via* centrifugation (18,000 $\times g$, 4 °C, 60 min). The obtained cell-free extract was applied to a column containing TALON® Metal Affinity Resin (Takara Biotechnology (DALIAN) Co., LTD., Dalian, PR China) (4.0 mL) equilibrated with wash buffer. After the column had been washed thoroughly (10 *cv*) with the same buffer, the enzyme was eluted with equilibration buffer (Tris-HCl buffer (20 mM, pH 8.0) containing 300 mM sodium

9 Experimental section

chloride and 150 mM imidazole). The purification step was performed at <20 °C. The combined active fractions were dialyzed in Amicon® Ultra centrifugal filters (Merck KGaA, Darmstadt, Germany) towards Tris-HCl buffer (20 mM, pH 7.0).

9.5.4 General procedure 17 (GP17): Determination of the protein concentration

The protein concentration was determined *via* a literature known protocol.^[268] The soluble fraction was diluted with millipore water to three different concentrations. The choice of dilution was empirical. 250 µL of the Bradford-assay solution (Table 38) were added to 5.0 µL of the diluted solutions in a 96-well plate. After incubation at 25 °C for 15 minutes and double shaking, the absorption at a wavelength of 595 nm were measured. Solutions of known bovine serum albumin concentration were measured as reference. All concentrations were determined thrice.

Table 38. Composition of the Bradford-assay solution.

Chemical	Amount
Coomassie Blue G 250	50 mg·mL ⁻¹
Methanol	50 mL
o-Phosphoric acid (wt = 85 %)	100 mL
Millipore water	1000 mL

For purified proteins, the protein concentration was determined alternatively by absorption measurements at a wavelength of 280 nm using a micro volume spectral photometer (1.0 Abs. unit \cong 1.0 mg·mL⁻¹ protein concentration).

9.5.5 General procedure 18 (GP18): Sodium dodecylsulfate acrylamide gel electrophoresis

Protein crude extract (obtained *via* GP 14) was diluted to a concentration of 1.2 mg·mL⁻¹ protein. The samples were denaturized for 5 minutes at 95 °C after addition of Laemmli-buffer (6x) (5:1 v,v).^[269] 10 µL of the samples or 5.0 µL of the marker were loaded onto the polyacrylamide gels (Table 39) and separated *via* gel electrophoresis at 200 V and 12.5 mA (per gel). When the samples reached the segregation gel, the current was raised to 25 mA (per gel). The gel was stained with a Cyclodextrin (Table 41) or Coomassie blue staining solution (Table 42) after finishing the separation of the proteins. The gel was washed afterwards with unstaining solution (Table 43) and dH₂O in case of the Coomassie stain.

9 Experimental section

Table 39. Composition of the gels used for electrophoresis, recipes are for 2 gels.

Chemical	Volume for segregation gel (12 %) [mL]	Volume for collecting gel (5 %) [mL]
Acrylamide	4.00	0.83
Tris-HCl	2.50 (1.5 M, pH 8.8)	1.30 (0.5 M, pH 6.8)
<i>d</i> H ₂ O	2.70	2.80
SDS (10 %)	0.10	0.05
TEMED	0.01	0.01
APS (10 %)	0.10	0.05

Table 40. Composition of the running buffer for SDS-PAGE (10x concentrated).

Chemical	Amount
TRIS	30.3 g
Glycine	144 g
SDS	10.0 g
<i>d</i> H ₂ O	Filled up to 1.00 L

Table 41. Composition of the α -cyclodextrine staining solution.

Chemical	Amount
α -Cyclodextrin	1.0 %
Bradford reagent	94 %
<i>ortho</i> -Phosphoric acid (wt = 85 %)	5.0 %

Table 42. Composition of the Coomassie Blue staining solution.

Chemical	Amount
Acetic acid	100 mL
Ethanol	300 mL
<i>d</i> H ₂ O	600 mL
Coomassie Blue G250	1.00 g

Table 43. Composition of the unstaining solution for the Coomassie stain.

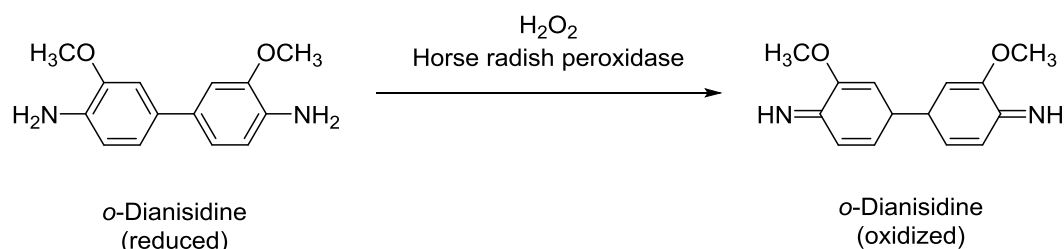
Chemical	Amount
Acetic acid	100 mL
Ethanol	300 mL
<i>d</i> H ₂ O	600 mL

9.5.6 General procedure 19 (GP19): Determination of the plasmid stability

The medium containing growing cells was diluted over single several steps (1:9 dilution) to three final dilutions depending on the optical density (e.g. for an OD₆₀₀ of 8.0, total dilution of 10⁻⁷ to 10⁻⁹). 1.0 mL of the diluted solutions was spread out on three LB-Agar plates containing Ampicillin (100 µg·mL⁻¹) and three LB-Agar plates containing no antibiotics. The plates were incubated for 18 hours at 37 °C and the number of colonies was determined with a colony counter. The plasmid stability is the average of the ratio of colonies on the LB-Agar plates containing antibiotics and those containing no antibiotics.

9.5.7 Protein activity assays

9.5.7.1 General procedure 20 (GP20): L-Amino acid oxidase assay



The activity of the activated lysate or the purified enzyme (obtained from the *Fischer von Mollard* group) was determined in analogy to literature known methods with a recently published adjustment.^[185] Enzymatic activities were determined by measuring the initial rate of hydrogen peroxide formation by a coupled peroxidase/*o*-dianisidine assay with 10 mM L-phenylalanine as described (*Hahn et al.* 2017). The standard assay mixture contained 10 mM L-glutamine, 50 mM TEA/HCl buffer (pH 7.0), 0.2 mg·mL⁻¹ of *o*-dianisidine, 5.0 U·mL⁻¹ peroxidase, and *hc*LAAO4 as activated lysate or in purified *via* affinity chromatography in limiting amounts. Reactions were carried out in 96-well plates at 30 °C in a Tecan Infinite 200 microplate reader at 436 nm. One unit was defined as the amount of enzyme that catalyzes the conversion of 1.0 µmol L-phenylalanine per minute. After preincubation for 10 minutes at 25 °C, 5.0 µL of activated enzyme were used per assay (200 µL).

9.5.7.2 General procedure 21 (GP21): ADH-assay

The reaction solution of the activity assay comprised 700 to 790 µL KPB (50 mM, pH 7.0), 100 µL of a NADPH (reductive) or NADP⁺ solution (2.5 mM, final concentration: 0.25 mM), 100 µL of the substrate solution in DMSO (50 mM, final concentration: 5.0 mM) and 10 to 100 µL of the enzyme crude extract in 1.0 mL cuvette. The time-dependent absorption at

340 nm was measured in a spectral photometer. One unit was defined as the amount of enzyme that catalysis the conversion of 1.0 μmol acetophenone per minute.

9.5.8 General procedure 22 (GP22): Biocatalytic deamination of amino acids to α -keto acids

The reaction solution contained 50 mM triethanolamine buffer (TEA buffer, pH 7.0), 5.0 mM (or higher) L-phenylalanine, 25 U (50 U·mL⁻¹), bovine catalase (Sigma Aldrich), and 0.05 to 0.30 U (0.10 – 0.60 U·mL⁻¹, according to GP20) activated lysate or purified *hcLAAO4* (expressed in *E. coli*, if mentioned in *P. pastoris*) in a total volume of 500 μL . The reaction was carried out for 30 minutes to 7 hours at 30 °C with shaking and terminated by boiling for 5 minutes at 95 °C. After centrifugation (16,100 $\times g$, 10 min, 4 °C), 900 μL of the supernatant were transferred to another Eppendorf tube® and again centrifuged under the same conditions. The supernatant (850 μL) was analyzed by HPLC with a Nucleodur C18 HTec (5.0 μm , 4.6 mm ID, 150 mm, Macherey-Nagel) at 25 °C using eluent A (water 0.1 % (v,v) trifluoroacetic acid (TFA)) and eluent B (methanol 0.1 % (v,v) TFA). Separation was carried out at a flow rate of 1.0 mL·min⁻¹ by a linear gradient from 60 to 30 % eluent A over 8 minutes followed by a linear gradient from 30 to 60 % eluent A over 4 minutes. Effluent fractions were monitored at 220 nm and the area was compared to a calibration curve.

9.5.8.1 Byproduct determination via ¹H-NMR-spectrometry

The reaction solution contained 50 mM TEA buffer (pH 7.0), 2.5 mM L-phenylalanine, and 0.05 U purified *hcLAAO4* in a total volume of 5.0 mL. The reaction was carried out for 4 hours with shaking and was terminated by extraction with ethyl acetate and dried *in vacuo*. ¹H-NMR spectra were measured of the obtained crude product. Full conversion was verified *via* RP-HPLC. The crude product was dissolved in water-d₂. ¹H-NMR spectra of the crude product and additionally with phenylacetic acid or phenylacetaldehyde were measured at 500 MHz.

9.5.8.2 Comparison of different catalase enzymes

The reaction solution contained 50 mM TEA buffer (pH 7.0), 5.0 mM L-phenylalanine, and 0.3 U purified *hcLAAO4*, 32.5 U catalase from bovine or human in a total volume of 4.0 mL. The reaction was carried out for 15 to 240 minutes and stopped by boiling at 95 °C.

Table 44. Relative amounts of L-phenylalanine, phenylpyruvate and phenylacetic acid in the reaction solution for the time course with lysate and purified enzyme of *hcLAAO4* expressed in *E. coli* and *P. pastoris*.

Time [min]	Catalase	L-Phenylalanine [%]	Phenylpyruvate [%]	Phenylacetic acid [%]	Specific product formation [%]
15	Human	94	4	3	57
30		90	7	3	70
60		87	12	1	82
120		74	26	0	100
180		48	48	4	92
240		38	59	3	95
30	Bovine	90	8	2	80
60		76	22	2	92
120		61	35	4	90
180		48	49	3	94
240		36	62	2	97

9.5.8.3 Time course

The reaction was carried out according to GP22 with 0.05 U *hcLAAO4* (lysate and purified enzyme expressed in *E. coli* or *P. pastoris*) at 5.0 mM substrate concentration. The reactions were terminated after varying reaction times.

Table 45. Relative amounts of L-phenylalanine, phenylpyruvate and phenylacetic acid in the reaction solution for the time course with lysate and purified enzyme of *hcLAAO4* expressed in *E. coli* and *P. pastoris*.

Time [h]	Form of enzyme	L-Phenylalanine [%]	Phenylpyruvate [%]	Phenylacetic acid [%]
0.5		65	31	5
2	Lysate (<i>E. coli</i>)	13	84	4
3		0	97	3
6		0	96	4
0.5		59	37	4
1	Purified (<i>E. coli</i>)	31	69	7
2		0	96	4
3		0	97	3
6		0	96	4
1	Lysate (<i>P. pastoris</i>)	20	71	8
3		0	98	2
6		0	98	2
1	Purified (<i>P. pastoris</i>)	41	53	6
2		18	73	9
3		2	92	6
6		0	80	20

9.5.8.4 Determination of the enzyme stability

For determination of the enzyme stability under the reaction conditions, samples containing all components except the substrate were stored for one week at $-20\text{ }^{\circ}\text{C}$ before usage. Reactions were carried out according to GP22 with purified enzyme from *E. coli* and *P. pastoris* and terminated by boiling after varying reaction times.

Table 46. Relative amounts of L-phenylalanine, phenylpyruvate and phenylacetic acid in the reaction solution for the time course purified enzyme of *hcLAAO4* expressed in *E. coli* and *P. pastoris* stored one week at $-20\text{ }^{\circ}\text{C}$ before reaction start.

Time [h]	Form of enzyme	L-Phenylalanine [%]	Phenylpyruvate [%]	Phenylacetic acid [%]
0		100	0	0
2	Purified (<i>E. coli</i>)	42	55	3
4		11	86	4
5		0	95	5
0		100	0	0
2	Purified (<i>P. pastoris</i>)	30	63	6
4		4	90	6
5		0	95	5

9.5.8.5 Variation of the substrate and catalyst loading

The reaction was carried out according to GP22 with 0.05, 0.10, 0.20 and 0.30 U purified *hcLAAO4* at 5.0, 10, 15 and 20 mM substrate concentration. Each reaction was terminated by boiling after 7 hours reaction time (only the reaction with 0.30 U *hcLAAO4* at 20 mM substrate concentration was stopped after 4 hours reaction time).

Table 47. Relative amounts of L-phenylalanine, phenylpyruvate and phenylacetic acid in the reaction solution after 7 hours reaction time for varying amounts of *hcLAAO4* at varying substrate concentrations.

Amount of enzyme [U]	Substrate conc. [mM]	L-Phenylalanine [%]	Phenylpyruvate [%]	Phenylacetic acid [%]
0.05	5.0	2	94	4
	10	46	49	5
	15	58	39	4
	20	54	40	6
0.10	5.0	0	97	3
	10	0	95	5
	15	0	94	6
	20	9	82	9
0.20	5.0	2	93	5
	10	0	92	8
	15	0	91	9
	20	0	91	9
0.30*	20	0	91	9

* This reaction was terminated after 4 hours reaction time.

9.5.8.6 Investigation of substrate and product inhibition

The reaction was carried out according to GP22 with 0.05 U purified *hcLAAO4* at 5.0, 10, 20, 30 and 40 mM substrate concentration. Each reaction was terminated by boiling after 1 and 7 hours reaction time. For investigating product inhibitions, 1.0 or 5.0 mM phenylpyruvate was additionally given to the reaction solution at 5.0 mM substrate concentration.

Table 48. Overall conversions and relative concentrations of phenylpyruvate and phenylacetic acid in the reaction solutions of the biotransformation of varying amount of L-phenylalanine after 1 and 7 hours with 0.05 U *hcLAAO4*.

Entry	Conc. L-phenyl-alanine [mM]	Time [h]	Conv. [%]	Conc. phenyl-pyruvate [mM]	Conc. phenyl-acetic acid [mM]
1	5.0	1	73	3.4	0.3
2		7	100	4.6	0.3
3	10	1	46	4.1	0.5
4		7	100	9.3	0.7
5	20	1	25	4.5	0.5
6		7	60	10.5	1.3
7	30	1	23	6.0	0.8
8		7	47	12.3	1.5
9	40	1	20	6.7	1.3
10		7	38	13.5	1.8

*The addition of phenylpyruvate had no effect on the conversion.

9.5.8.7 Investigation of different buffer systems

The reaction was carried out according to GP22 with 0.05 U purified *hcLAAO4* at 5.0 mM substrate concentration. TEA buffers with varying concentrations were compared. The reactions were terminated by boiling after 6 hours reaction time.

Table 49. Relative amounts of L-phenylalanine, phenylpyruvate and phenylacetic acid in the reaction solution after 6 hours reaction time with 0.05 U of *hcLAAO4* at varying TEA buffer concentrations.

Entry	Buffer concentration [mM]	L-Phenylalanine [%]	Phenylpyruvate [%]	Phenylacetic acid [%]
1	50	0	100	0
2	100	0	100	0
3	200	0	100	0
4	300	0	100	0
5	400	0	98	2
6	500	0	95	5

9.5.9 General procedure 23 (GP23): Biocatalytic oxidation of fatty alcohols to fatty aldehydes

Aliquoted cells ($-20\text{ }^{\circ}\text{C}$) with expressed LkADH and PpADH from previous experiments of the working group were used in the experiments. Each cell aliquot (1.0 g) was suspended in 3.0 mL KPB (50 mM, pH 7.0) and disrupted by sonification. The supernatant obtained from centrifugation ($10,000 \times g$, $4\text{ }^{\circ}\text{C}$, 15 min) was transferred to a new tube and used for the reaction as cell-free extract.

The standard assay solution contained the fatty alcohol (0.10 mmol, 20 mM), NADP⁺ (5.0 μmol , 5.0 mol%, 3.8 mg), the ADH crude extract (LkADH or PpADH, 1.0 mL), KPB buffer (50 mM, pH 7.0, 3500 mL), and acetone (10 %, 500 μL) in a total volume of 5.0 mL. The reaction was carried out for 24 hours at room temperature with shaking and terminated by the addition of 500 μL of 0.5 M hydrochloric acid. The reaction solution was extracted with methyl-*tert*-butylether (MTBE, 5.0 mL) under vigorous mixing for 15 seconds and centrifuged ($8,000 \times g$, 5 min, $4\text{ }^{\circ}\text{C}$) afterwards. 1.0 mL of the organic phase was transferred to vial and analyzed *via* GC equipped with a Phenomenex ZB-5MSi non-chiral column in comparison to a calibration curve (C_8 : alcohol: 3.3 min, aldehyde: 2.9 min, C_{10} : alcohol: 5.3 min, aldehyde: 4.5 min, C_{12} : alcohol: 5.3 min, aldehyde: 4.6 min).

9.5.10 General procedure 24 (GP24): Biocatalytic dehydration of aldoximes to nitriles

The standard assay solution contained 387.5 μL of KPB (50 mM, pH 7.0), 12.5 μL of an aldoxime solution in DMSO (200 mM, final concentration: 5.0 mM) and 100 μL of diluted resting cells suspension (2.0 μL resting cells suspension and 98 μL water) or 100 μL of a sample prepared from the fermentations in a total volume of 500 μL . The reaction was carried out for different times at 30 $^{\circ}\text{C}$ (or alternatively 8 $^{\circ}\text{C}$) with shaking at 800 rpm and terminated by the addition of 400 μL of acetonitrile and 100 μL of 0.1 M HCl. After centrifugation (21,500 $\times g$, 15 min, 4 $^{\circ}\text{C}$), the supernatant was transferred into HPLC vials and the conversion of the reaction was measured with RP-HPLC in comparison to a calibration curve. Measurements were conducted on a Macherey-Nagel Nucleodur C18 HTec column at 40 $^{\circ}\text{C}$ with acetonitrile/water (30:70 *v,v*) as mobile phase and UV detection at 210 nm.

9.5.10.1 Arylaliphatic aldoximes

The assay was conducted according to GP24. 387.5 μL of KPB (50 mM, pH 7.0), and 100 μL of a diluted resting cells suspension (2.0 μL resting cells suspension and 98 μL water) was given in an Eppendorf Tube. The reaction was started by addition of 12.5 μL of a solution of *Z*-PAOx, *E/Z*-2-PPOx, *E/Z*-EtPAOx, *E/Z*-*i*PrPAOX or *E/Z*-CyPAOx in DMSO (200 mM, final concentration: 5.0 mM). The reaction was terminated after 1, 10, and 180 minutes shaking at 30 $^{\circ}\text{C}$.

9 Experimental section

Table 50. Conversions, ee-values and specific activities of the biotransformations of bulky arylaliphatic aldoximes at 30 °C after different reaction times.

Entry	Substrate	Reaction time [min]	Oxd	Conv. [%]	ee [%]	Specific activity [U·mg _{bww} ⁻¹]
1	Z-PAOx (1:99 <i>E/Z</i>)	1	A	47	N.D.	1790
			B	40	N.D.	1900
			FG	33	N.D.	1210
			RE	51	N.D.	1540
			RG	45	N.D.	1440
2	<i>E/Z</i> -2-PPOx (50:50 <i>E/Z</i>)	10	A	65	N.D.	250
			B	28	N.D.	135
			FG	61	N.D.	226
			RE	70	N.D.	212
			RG	65	N.D.	210
3	<i>E/Z</i> -EtPAOx (30:70 <i>E/Z</i>)	180	A	38	24 (+)	8.23
			B	28	64 (-)	8.15
			FG	58	14 (-)	10.3
			RE	37	20 (+)	6.44
			RG	33	36 (+)	6.00
4	<i>E/Z</i> -iPrPAOx (50:50 <i>E/Z</i>)	180	A	4	38 (+)	0.80
			B	-	-	-
			FG	3	12 (+)	0.59
			RE	2	22 (+)	0.29
			RG	1	35 (-)	0.21
5	<i>E/Z</i> -CyPAOx (15:85 <i>E/Z</i>)	180	A	-	-	-
			B	-	-	-
			FG	-	-	-
			RE	-	-	-
			RG	-	-	-

N.D. not determined

The assay was conducted according to GP24. 387.5 µL of KPB (50 mM, pH 7.0), and 100 µL of diluted resting cells suspension (2.0 µL resting cells suspension and 98 µL water) were given in an Eppendorf Tube®. The reaction was started by addition of 12.5 µL of a solution of Z-PAOx, *E/Z*-TPOx, *E*- or *Z*-EtPAOx, *E*- or *Z*-iPrPAOX in DMSO (200 mM, final concentration: 5.0 mM). The reaction was terminated after 3, 4 and 24 hours shaking at 30 °C.

9 Experimental section

Table 51. Conversions, ee-values and specific activities of the biotransformations of arylaliphatic aldoximes at 8 °C after different reaction times.

Entry	Substrate	Reaction time [h]	Oxd	Conv. [%]	ee [%]	Specific activity [U·mg _{bw} ⁻¹]
1	<i>E/Z</i> -TPOx (70:30 <i>E/Z</i>)	3	A	18	34 (-)	0.01
			B	10	23 (+)	<0.01
			FG	7	90 (+)	<0.01
			RE	28	27 (-)	0.02
			RG	45	32 (-)	0.04
2	<i>E</i> -4-FPPOx (92:8 <i>E/Z</i>)	4	A	14	97 (+)	0.01
			B	7	73 (+)	<0.01
			FG	41	83 (+)	0.03
			RE	5	64 (+)	<0.01
			RG	6	67 (+)	<0.01
3	<i>Z</i> -4-FPPOx (3:97 <i>E/Z</i>)	4	A	6	52 (-)	<0.01
			B	10	93 (-)	<0.01
			FG	46	94 (-)	0.03
			RE	3	71 (-)	<0.01
			RG	3	60 (-)	<0.01
4	<i>E</i> -EtPAOx (96:4 <i>E/Z</i>)	24	A	24	73 (-)	0.68
			B	58	71 (-)	2.24
			FG	51	94 (-)	1.52
			RE	16	64 (-)	0.35
			RG	13	59 (-)	0.29
5	<i>Z</i> -EtPAOx (3:97 <i>E/Z</i>)	24	A	57	75 (+)	1.86
			B	29	82 (+)	1.11
			FG	44	74 (+)	1.36
			RE	58	72 (+)	1.51
			RG	58	72 (+)	1.61
6	<i>E</i> - <i>i</i> PrPAOx (97:3 <i>E/Z</i>)	24	A	-	-	-
			B	-	-	-
			FG	2	56 (-)	0.05
			RE	-	-	-
			RG	-	-	-
7	<i>Z</i> - <i>i</i> PrPAOx (2:98 <i>E/Z</i>)	24	A	9	29 (+)	0.24
			B	-	-	-
			FG	5	40 (+)	0.14
			RE	6	22 (+)	0.13
			RG	4	0	0.09

9.5.10.2 Linear fatty aldoximes

The assay was conducted according to GP24. 387.5 μL of KPB (50 mM, pH 7.0), and 100 μL of diluted resting cells suspension (2.0 μL resting cells suspension and 98 μL water) were given in an Eppendorf Tube®. The reaction was started by addition of 12.5 μL of a octanal oxime, nonanal oxime, decanal oxime or dodecanal oxime (isomeric mixtures) in DMSO (200 mM, final concentration: 5.0 mM). The reaction was terminated after 10, 30 and 60 minutes shaking at 30 °C. Another biotransformation of nonanal with 10 % ethanol as cosolvent (10 mM substrate) concentration was carried out for 120 minutes.

Table 52. Conversions of the biotransformations of linear fatty aldoximes at 30 °C after different reaction times.

Entry	Substrate	Reaction time [min]	Oxd	Conv. [%]	Specific activity [$\text{U}\cdot\text{mg}_{\text{bww}}^{-1}$]
1	Octanal oxime	10	A	22	N.D.
			B	23	N.D.
			FG	24	N.D.
			RE	21	N.D.
			RG	25	N.D.
2	Nonanal oxime	30	A	18	N.D.
			B	20	N.D.
			FG	15	N.D.
			RE	18	N.D.
			RG	18	N.D.
3	Nonanal oxime	120	A	82	N.D.
			B	100	N.D.
			FG	19	N.D.
			RE	9	N.D.
			RG	35	N.D.
4	Decanal oxime	60	A	15	N.D.
			B	28	N.D.
			FG	15	N.D.
			RE	13	N.D.
			RG	14	N.D.
5	Dodecanal oxime	60	A	2.7	N.D.
			B	1.1	N.D.
			FG	0.9	N.D.
			RE	3.1	N.D.
			RG	3.6	N.D.

N.D. not determined

9.5.10.3 Activity determination of whole-cells obtained in high cell-density fermentation

The assay was conducted according to GP24. 387.5 μL of KPB (50 mM, pH 7.0), and 100 μL of diluted resting cells suspension (according to 9.4.6.3) were given in an Eppendorf Tube®. The reaction was started by addition of 12.5 μL of a solution of Z-PAOx DMSO (200 mM, final concentration: 5.0 mM). The reaction was terminated after one minute shaking at 30 °C.

Table 53. Conversions, volumetric and specific activities of the whole-cells obtained in the fermentation experiments with AI-medium in the batch-phase depending on the process time.

Entry	Process time [h]	Conv. [%]	Volumetric activity [$\text{U}\cdot\text{L}^{-1}$]	Specific activity [$\text{U}\cdot\text{mg}_{\text{cdw}}^{-1}$]
1	12	2.8	3,500	1.78
2	18	4.5	5,600	1.88
3	24	6.6	8,200	2.28
4	28	10.8	13,500	2.88
5	32	15.9	19,900	2.98
6	36	24.8	31,000	3.92
7	40	26.0	32,500	3.53
8	44	25.7	32,100	2.93
9	48	27.4	34,200	2.79
10	52	22.1	27,600	2.31
11	56	21.2	26,500	2.04
12	60	17.9	22,400	1.74
13	64	17.0	21,300	1.54
14	68	19.3	24,200	1.57
15	72	19.1	23,800	1.51
16	82	2.9	3,600	0.21

9 Experimental section

Table 54. Conversions, volumetric and specific activities of the whole-cells obtained in the fermentation experiments with HSG-medium in the batch-phase depending on the process time.

Entry	Process time [h]	Conv. [%]	Volumetric activity [U·L ⁻¹]	Specific activity [U·mg _{cdw} ⁻¹]
1	10	0.5	600	0.08
2	20	3.3	4,100	0.19
3	24	2.9	3,600	0.18
4	28	2.7	3,400	0.16
5	32	3.8	4,800	0.20
6	40	5.9	7,300	0.23
7	44	9.3	11,600	0.43
8	50	9.5	11,900	0.41
9	58	14.6	18,200	0.65
10	62	19.3	24,100	0.81
11	66	22.4	27,900	0.88
12	70	31.0	38,800	1.26

Table 55. Conversions, volumetric and specific activities of the whole-cells obtained in the fermentation experiments with TB-medium in the batch-phase depending on the process time.

Entry	Process time [h]	Conv. [%]	Volumetric activity [U·L ⁻¹]	Specific activity [U·mg _{cdw} ⁻¹]
1	10	-	-	-
2	20	3.9	4,900	0.23
3	24	6.2	7,800	0.44
4	32	9.5	11,900	0.44
5	36	6.9	8,600	0.28
6	44	9.6	12,000	0.36
7	50	9.3	11,600	0.61
8	54	11.1	13,800	0.73
9	58	9.8	12,300	0.64
10	62	11.0	13,700	0.75
11	66	15.3	19,100	1.01
12	70	17.6	22,000	1.24

9.5.10.4 Activity determination of OxdB variants whole-cell catalysts via biotransformation of Z-phenylacetaldoxime

The assay was conducted according to GP24. 387.5 μ L of KPB (50 mM, pH 7.0), and 100 μ L of diluted resting cells suspension of the OxdB variants were given in an Eppendorf Tube®. The reaction was started by addition of 12.5 μ L of a solution of Z-PAOx in DMSO (200 mM, final concentration: 5.0 mM). The reaction was terminated after 1 minute shaking at 30 °C.

Table 56. Conversions and specific activities of the activity assay with purified OxdB (variants) for Z-PAOx as standard substrate.

Entry	Variant	Conv. [%]	Specific activity [U·mg _{bww} ⁻¹]
0	wt	34.9	0.82
1	I319E	30.2	0.75
2	I226Q	28.4	0.73
3	L220E	21.9	0.53
4	V149E	26.0	0.68
5*	I105R	1.9	0.06
6	L267R	22.2	0.55
7	I316Q	25.1	0.69
8	I180A	34.0	0.92
9	L65H	39.3	1.32
10	V262G	10.2	0.28
11**	E317L	8.8	0.24
12	K190R	36.6	1.09
13	D135L	36.9	0.99
14	Q67T	0	0
15	K49V	35.3	0.98
16	R63L	27.2	0.69
17	H296L	15.7	0.36
18	N229M	33.7	0.94
19	Q250I	18.0	0.47
20	K283L	37.2	0.98

9.5.10.5 Activity determination purified OxdB variants *via* biotransformation of Z-phenylacetaldoxime

The activity of the purified enzyme was determined in modified protocol according to literature known methods.^[178] The assay solution contained 437.5 μL KPB (50 mM, pH 7.0), 12.5 μL of PAOx (200 mM solution in DMSO), 50.0 μL of purified OxdB(C)6His or its variants (0.15 $\text{mg}\cdot\text{mL}^{-1}$; 3.75 μM), and optionally Flavin mononucleotide (250 nmol) in a total volume of 500 μL . The reaction was carried out for 1 minute at 30 °C with shaking at 900 rpm. Simultaneous addition of 400 μL of acetonitrile and 100 μL of hydrochloric acid (0.1 M) stopped the reaction. After centrifugation (21,500 $\times g$, 10 min, 4 °C), the supernatant was transferred into HPLC vials and the conversion to PAN was measured by reverse phase-HPLC (Jasco, Nova Scotia, Canada) in comparison to a calibration curve. Measurements were conducted on a Nucleodur C18 HTec column (Macherey-Nagel, Düren, Germany) at 40 °C isocratic with water/acetonitrile (70:30 *v,v*) as mobile phase and UV detection at 210 nm.

Table 57. Conversions and specific activities of the activity assay with purified OxdB (variants) for Z-PAOx as standard substrate.

Entry	Variant	Conv. [%]	Specific activity [$\text{U}\cdot\text{mg}_{\text{cdw}}^{-1}$]
0	wt	42.1	14.0
1	I319E	74.2	24.7
2	I226Q	54.2	18.1
3	L220E	46.8	15.6
4	V149E	57.5	19.2
5*	I105R	1.6	1.77
6	L267R	33.4	11.1
7	I316Q	54.2	18.1
8	I180A	54.6	18.2
9	L65H	60.6	20.2
10	V262G	24.3	8.10
11**	E317L	7.3	6.66
12	K190R	52.7	17.6
13	D135L	24.1	8.02
14	Q67T	37.5	12.5
15	K49V	47.8	15.9
16	R63L	52.2	17.4
17	H296L	54.3	18.1

9 Experimental section

18	N229M	41.3	13.8
19	Q250I	71.9	24.0
20	K283L	39.5	13.2
21	L65H_I180A	79.3	26.4
22	I180A_K190R	57.3	19.1
23	L65H_K190R	85.3	28.4

*Experiment carried out with 0.045 mg·mL⁻¹ protein concentration in the assay, **Experiment carried out with 0.055 mg·mL⁻¹ protein concentration in the assay.

Table 58. Storage time before use, Conversions of Z-PAOx with purified OxdB (variants) in the absence (w/o) and presence of FMN (w).

Entry	Variant	Storage time [d]	Conv. w/o FMN [%]	Conv. w FMN [%]
0	wt	19	8.10	6.40
1	I319E	11	53.9	>99
2	I226Q	2	55.0	95.2
3	L220E	0	46.8	69.4
4	V149E	0	57.5	54.5
5	I105R	N.D.	N.D.	N.D.
6	L267R	11	24.2	82.9
7	I316Q	11	37.3	>99
8	I180A	2	49.7	90.0
9	L65H	10	31.7	52.7
10	V262G	11	16.5	64.1
11*	E317L	0	7.3	17.0
12	K190R	0	52.7	44.4
13	D135L	4	17.8	49.8
14	Q67T	2	33.9	27.3
15	K49V	4	30.1	53.5
16	R63L	11	37.3	>99
17	H296L	11	27.3	62.7
18	N229M	11	34.5	>99
19	Q250I	11	45.3	>99
20	K283L	0	33.5	42.3
21	L65H_I180A	11	52.7	>99
22	I180A_K190R	2	61.4	>99
23	L65H_K190R	11	47.7	>99

*N.D. not determined * Experiment carried with 0.055 mg·mL⁻¹ protein concentration in the assay.

10 Register of illustrations

10.1 Figures

Figure 1. Overview of total numbers of granted patents in the years from 2014 to 2019 related to the application of the most prominent enzyme classes. Less relevant classes are neglected in the circle diagram (Adapted from P. Domínguez de María, G. de Gonzalo, A. R. Alcántara, <i>Catalysts</i> 2019, 9, 802. Creative Common CC BY license). ^[29]	5
Figure 2. Basic structure of L- α -amino acids, D- α -amino acids, and α -keto acids.....	11
Figure 3. Application of α -keto acids as acylating agents in organic chemistry (Adapted with permission from F. Penteado, E. F. Lopes, D. Alves, G. Perin, R. G. Jacob, E. J. Lenardão, <i>Chem. Rev.</i> 2019, 119, 7113–7278, Copyright © 2019, American Chemical Society). ^[55]	16
Figure 4. Structures of the drugs Saxagliptin and Vildagliptin bearing chiral nitrile moieties (marked in red). ^[72,73]	20
Figure 5. Crystallized chiral guest nitriles in a host framework consistent of an L-phenylalanine derivative and 4-hydroxybenzoic acid. ^[100]	26
Figure 6. Structures of isoalloxazine (red), riboflavin (blue), FMN (green) and FAD (light red). ^[102]	27
Figure 7. Examples for alkaloids with the β -carboline backbone. A) Harmicine, B) reserpine, C) ajmalicine, d) stimulant yohimbine. ^[152]	38
Figure 8. Structure of protoheme IX (heme b). ^[171]	43
Figure 9. Structure of the active site of the Michaelis-complex of OxdRE with bound <i>n</i> -propionaldoxime from the distal heme side. Oxygen, nitrogen and sulfur atoms are colored in red, blue and yellow, respectively. The dashed lines show possible hydrogen bonds. This figure was originally published in the Journal of Biological Chemistry. H. Sawai, H. Sugimoto, Y. Kato, Y. Asano, Y. Shiro, S. Aono, <i>J. Biol. Chem.</i> 2009, 284: 32089-32096, Copyright © 2009, the American Society for Biochemistry and Molecular Biology. ^[176]	45
Figure 10. Substrate spectrum of recombinant, acidic activated <i>hcLAAO4</i> . ^[184]	57
Figure 11. Verification of the purification of <i>hcLAAO4</i> (~67.5 kDa) via SDS-PAGE by <i>Bloess</i> . M: Marker, Lane 1: Crude extract, lane 2: Activated lysate, lane 3: Activated lysate after filtering, Lane 4: Ni-NTA purified enzyme. ^[185]	59
Figure 12. RP-HPLC chromatograms of the reaction mixtures with the addition of 50 U·mL ⁻¹ catalase (upper) and without addition (lower).	62
Figure 13. Time course of the standard biotransformation of L-phenylalanine with 0.05 U <i>hcLAAO4</i> given as lysate or purified enzyme obtained from expression in <i>E. coli</i> or <i>P. pastoris</i>	63

Figure 14. Results of the biotransformations with purified <i>hcLAAO4</i> (0.05 U, 0.10 U, and 0.20 U) obtained through expression in <i>E. coli</i> for substrate concentrations ranging from 5.0 to 20 mM.	66
Figure 15. Molecular model of OxdB showing the positions of a) <i>E</i> -(<i>S</i>)-2-PPOx and b) <i>E</i> -(<i>R</i>)-2-PPOx in the active site and comparison of the Fe–N and Fe–O distances for all isomers and enantiomers of PAOx and 2-PPOx (Adapted with permission from R. Metzner, S. Okazaki, Y. Asano, H. Gröger, <i>ChemCatChem</i> , 6, 3105-3109. Copyright © 2014, John Wiley & Sons, Inc.). ^[180]	71
Figure 16. Structures of target substrates for the investigation of the enantioselectivity of the Oxd catalyzed dehydration.	74
Figure 17. Visualization of the automated column chromatography of the crude product of 4-FPPOx synthesis (detection wavelength between 200 and 800 nm). <i>E</i> -4-FPPOx elutes before <i>Z</i> -4-FPPOx.	78
Figure 18. Expression analysis of Oxds <i>via</i> SDS-PAGE. M: Marker, Lane I: OxdA (soluble fraction), Lane II: OxdA (insoluble fraction), Lane III: OxdB (soluble fraction), Lane IV: OxdB (insoluble fraction), Lane V: OxdFG (soluble fraction), Lane VI: OxdFG (insoluble fraction), Lane VII: OxdRE (soluble fraction), Lane VIII: OxdRE (insoluble fraction), Lane IX: OxdRG (soluble fraction), Lane X: OxdRG (insoluble fraction).	81
Figure 19. Proposed lead structure of substrate for which Oxds exhibit enantioselectivity (Adapted from T. Betker, P. Rommelmann, K. Oike, Y. Asano, H. Gröger, <i>Angew. Chem. Int. Ed.</i> 2017, 56, 12361-12366. Copyright © 2017, John Wiley & Sons, Inc.). ^[196]	84
Figure 20. Activities of Oxds towards PAOx, racemic <i>E/Z</i> -mixtures of 2-PPOx and bulky derivatives thereof measured in biotransformations at 30 °C.	90
Figure 21. Conversions of biocatalytic oxidations of fatty alcohols (C ₈ to C ₁₂) to their corresponding aldehydes catalyzed by LkADH or PpADH.	100
Figure 22. Conversions of biocatalytic aldoxime dehydration of fatty aldoximes with five Oxds after 10 (C ₈), 30 (C ₉), and 60 minutes (C ₁₀ , C ₁₂).	104
Figure 23. Conversions of 10 mM nonanal oxime to nonane nitrile with five Oxds after three hours reaction time.	105
Figure 24. Dehydration of octanal oxime to octane nitrile catalyzed by Oxds and reaction solution while and after the stirring. Phase separation between the organic phase consisted of only the desired nitrile after the reaction is shown above (Adapted with permission from A. Hinzmann, S. Glinski, M. Worm, H. Gröger, <i>J. Org. Chem.</i> 2019, 84, 4867–4872. Copyright © 2019, American Chemical Society). ^[217]	106
Figure 25. Process parameters such as DO, OD ₅₇₈ and acetate formation for the fed-batch fermentation (5.0 L scale) of <i>E. coli</i> BL21(DE3) expressing CYP102A1 (Reprinted from <i>J. Biotechnol.</i> , 129, Development of a fed-batch process for the production of the cytochrome	

10 Register of illustrations

P450 monooxygenase CYP102A1 from <i>Bacillus megaterium</i> , S. Pflug, S. M. Richter, V. B. Urlacher, 481-488. Copyright © 2007, with permission from Elsevier). ^[223]	109
Figure 26. Selected process parameters for the fed-batch fermentations of <i>E. coli</i> BL21(DE3)-RIL harboring pUC18-OxdB with different media in the batch phase (AI-medium: upper, HSG-medium: middle, TB-medium: lower). Blue line: DO-level, green line: stirrer speed, red squares: OD ₆₀₀	113
Figure 27. Specific (upper) and volumetric activities (lower) observed in the fed-batch fermentations of <i>E. coli</i> BL21(DE3)-RIL harboring pUC18-OxdB comparing different medias used in the batch-phase. Black: AI-medium, red: TB-medium, blue: HSG-medium.	115
Figure 28. SDS-PAGE analysis of the fed-batch fermentation of <i>E. coli</i> BL21(DE3)-RIL harboring pUC18-OxdB with AI-medium in the batch phase. M: Marker, Lane 1: Soluble fraction (0.83 d), Lane 2: Insoluble fraction (0.83 d), Lane 3: Membrane fraction (0.83 d), Lane 4: Soluble fraction (1.83 d), Lane 5: Insoluble fraction (1.83 d), Lane 6: Membrane fraction (1.83 d), Lane 7: Soluble fraction (2.83 d), Lane 8: Insoluble fraction (2.83 d), Lane 9: Membrane fraction (2.83 d).	116
Figure 29. SDS-PAGE analysis of the fed-batch fermentation of <i>E. coli</i> BL21(DE3)-RIL harboring pUC18-OxdB with HSG-medium in the batch phase. M: Marker, Lane 1: Soluble fraction (0.83 d), Lane 2: Insoluble fraction (0.83 d), Lane 3: Membrane fraction (0.83 d), Lane 4: Soluble fraction (1.83 d), Lane 5: Insoluble fraction (1.83 d), Lane 6: Membrane fraction (1.83 d), Lane 7: Soluble fraction (2.83 d), Lane 8: Insoluble fraction (2.83 d), Lane 9: Membrane fraction (2.83 d).	116
Figure 30. SDS-PAGE analysis of the fed-batch fermentation of <i>E. coli</i> BL21(DE3)-RIL harboring pUC18-OxdB with TB-medium in the batch phase. M: Marker, Lane 1: Soluble fraction (0.83 d), Lane 2: Insoluble fraction (0.83 d), Lane 3: Membrane fraction (0.83 d), Lane 4: Soluble fraction (1.83 d), Lane 5: Insoluble fraction (1.83 d), Lane 6: Membrane fraction (1.83 d), Lane 7: Soluble fraction (2.83 d), Lane 8: Insoluble fraction (2.83 d), Lane 9: Membrane fraction (2.83 d).	117
Figure 31. DO-level (blue) and stirrer speed (green) monitored for attempts of fed-batch fermentation of <i>E. coli</i> BL21(DE3)-RIL harboring pUC18-OxdB with HSG-medium given in the batch phase. Upper: DO <10 % controlled by DO-spike strategy, lower: Constant stirrer speed after induction.....	118
Figure 32. Flowchart of the development of primary and secondary structure based approach to identify aggregation hotspots in proteins using the software INTMSAlign_HiSol (Reprinted from D. Matsui, S. Nakano, M. Dadashipour, Y. Asano, <i>Sci. Rep.</i> 2017, 7, 9558. Creative Common CC BY license). ^[237]	122
Figure 33. z-Transformed values of the normalized hydropathy indices of the 20 naturally occurring amino acids according to the scale of <i>Kyte</i> and <i>Doolittle</i> (Adapted from D. Matsui, S.	

Nakano, M. Dadashipour, Y. Asano, <i>Sci. Rep.</i> 2017, 7, 9558, Creative Common CC BY license). ^[237,245]	126
Figure 34. Relative activities of the whole-cell catalysts expressing OxdB variants compared to the wild-type enzyme.....	129
Figure 35. SDS-PAGE visualizing the successful purification of OxdB (here OxdB-M18) via affinity chromatography. M: Marker, C: Crude-extract, FT: Flowthrough, W: Wash fraction, P: Eluted protein.	130
Figure 36. Specific activities of wild-type OxdB and its variants (purified enzyme) for the standard substrate Z-PAOx.	132
Figure 37. Overlay of excerpts of native (upper) and denatured (lower) wild-type OxdB mass spectra. The shown region refers to 2930 and 3520 <i>m/z</i> , in which the peaks referring to the charge states +11 to +13 are visible.	135
Figure 38. Excerpt of native mass spectra of wild-type OxdB and selected variants (from top to bottom: Wild-type OxdB, OxdB-M1, OxdB-M9, OxdB-M19, OxdB-D1).....	136
Figure 39. Change of the specific activity of purified wild-type OxdB and its variants for Z-PAOx in the standard assay in presence of 250 nmol FMN compared to the activities measured in absence of FMN.	142
Figure 40. ¹ H-NMR spectra of the crude reaction product of the biotransformation of L-phenylalanine with <i>hcLAAO4</i> without addition of catalase (in D ₂ O; violet: with addition of phenylacetaldehyde, dark blue: with addition of phenylacetic acid, light blue: without additives) and reference compounds (in chloroform-d ₃ ; green: phenylacetic acid, yellow: phenylacetaldehyde, red: L-phenylalanine).....	256
Figure 41. ESI-mass spectrum of native (upper) and denatured (lower) purified wild-type-OxdB.	258
Figure 42. ESI-mass spectrum of native (upper) and denatured (lower) purified OxdB-M1.	258
Figure 43. ESI-mass spectrum of native (upper) and denatured (lower) purified OxdB-M2.	259
Figure 44. ESI-mass spectrum of native (upper) and denatured (lower) purified OxdB-M4.	259
Figure 45. ESI-mass spectrum of native (upper) and denatured (lower) purified OxdB-M8.	260
Figure 46. ESI-mass spectrum of native (upper) and denatured (lower) purified OxdB-M9.	260
Figure 47. ESI-mass spectrum of native (upper) and denatured (lower) purified OxdB-M12.	261
Figure 48. ESI-mass spectrum of native (upper) and denatured (lower) purified OxdB-M13.	261
Figure 49. ESI-mass spectrum of native (upper) and denatured (lower) purified OxdB-M17.	262
Figure 50. ESI-mass spectrum of native (upper) and denatured (lower) purified OxdB-M19.	262

10 Register of illustrations

Figure 51. ESI-mass spectrum of native (upper) and denatured (lower) purified OxdB-D1.	263
Figure 52. ESI-mass spectrum of native (upper) and denatured (lower) purified OxdB-D2.	263
Figure 53. ESI-mass spectrum of native (upper) and denatured (lower) purified OxdB-D3.	264
Figure 54. SDS-PAGE of OxdB mutants purified <i>via</i> TALON® affinity chromatography. The lanes refer to the corresponding variants (see Table 35).	265
Figure 55. SDS-PAGE of OxdB mutants purified <i>via</i> TALON® affinity chromatography. The lanes refer to the corresponding variants (see Table 35).	265
Figure 56. SDS-PAGE of OxdB mutants purified <i>via</i> TALON® affinity chromatography. The lanes refer to the corresponding variants (see Table 35).	266

10.2 Schemes

Scheme 1. Nitrile hydratase-catalyzed acrylamide production from acrylonitrile. ^[10,24]	3
Scheme 2. Synthesis of glycolic acid from formaldehyde, hydrogen cyanide, and sodium hydroxide <i>via</i> cyanhydrine formation (99 % yield), subsequent nitrilase-catalyzed hydrolysis (99 % yield) and IEC. ^[13,25]	4
Scheme 3. Synthesis of (<i>R</i>)-epichlorohydrine from 1,3-dichloro-2-propanol by dehalogenation with a halohydrin dehalogenase followed by the kinetic resolution of the epoxide with a (<i>S</i>)-selective epoxide hydrolase. ^[13,26]	4
Scheme 4. Isomerization of D-glucose to D-fructose catalyzed by glucose isomerase. ^[13,27,28]	5
Scheme 5. Kinetic resolution of 1-phenylethylamine by a lipase-catalyzed amidation with ethyl methoxyacetate as acyl-donor. ^[31–33]	6
Scheme 6. Synthesis of the antibiotic amoxicillin from 6-APA by amide formation catalyzed by pen G amidase CLEAs. ^[16,38]	6
Scheme 7. Comparison of the chemocatalytic (left side) and a novel biocatalytic route for the synthesis of Sitagliptin from its precursor Prositagliptin. ^[37]	7
Scheme 8. Biocatalytic ketone reduction with an engineered ketone reductase as a key step in the synthesis of the drug Montelukast-sodium. ^[12]	9
Scheme 9. Cyclopropanation of (heteroatom-substituted) olefins with azoesters catalyzed by engineered CYP monooxygenases. ^[41,42]	10
Scheme 10. Schematic procedure of the production of α -amino acids by the Strecker-reaction. An aldehyde gets transformed into an α -aminonitrile by ammonia and hydrogen cyanide, which is acidly hydrolyzed to the amino acid. ^[46]	12
Scheme 11. Synthesis of amino acids by the Bucherer-Bergs-synthesis forming hydanthoiones and subsequent hydrolysis or resolution with hydanthoionases. ^[46]	12
Scheme 12. Synthesis of halogenated derivatives of L-phenylalanine from <i>trans</i> -cinnamic acid with whole-cell catalysts expressing phenylalanine-ammonia lyases. ^[53]	13
Scheme 13. Enzymatic cascade implying hydroxylation with a peroxygenase, alcohol oxidation with HIC and reductive amination with AADH forming (unnatural) L-amino acids from carboxylic acids. ^[54]	14
Scheme 14. Oxidation of acetophenone (upper) or styrene (lower) with potassium permanganate under basic conditions yielding phenylglyoxylic acid. ^[61,62]	17
Scheme 15. Synthesis of phenylglyoxylic acid from benzoyl cyanide, which is prepared from benzoyl chloride by substitution with cyanide salts. ^[63,64]	17
Scheme 16. Hydrolysis of saturated (upper) and unsaturated (lower) oxazolones yielding α -keto acids, ammonia and aldehydes (upper) or carboxylic acids (lower). ^[44,65]	17

10 Register of illustrations

Scheme 17. Oxidation of acetophenone derivatives with selenium(IV) oxide in dry pyridine yielding phenylglyoxylic acid derivatives. ^[66]	18
Scheme 18. AZADO (structure on top of the arrow)-catalyzed oxidation of 2-hydroxycarboxylic acids under air forming α -keto acids. ^[68]	18
Scheme 19. Non-oxidative deamination of L-amino acids to α -keto acids catalyzed by membrane-bound AADs. ^[56]	19
Scheme 20. Ammoxidation of propylene (upper) and 3-picoline (lower) forming acrylonitrile and nicotinonitrile. ^[74]	20
Scheme 21. Synthesis of nitriles by substitution or addition reactions. ^[46,71,75,76,80]	21
Scheme 22. Oxidative pathways for nitrile synthesis from alcohols, carbonyl-compounds, azides and amines. ^[81-84]	21
Scheme 23. Selected methods of aldoxime dehydration for the synthesis of racemic nitriles. ^[85-90]	22
Scheme 24. Transformation of CDG to PreQ ₀ catalyzed by the nitrile sythetase ToyM. ^[91]	23
Scheme 25. Hydrocyanation of alkenes (here styrene) by avoiding hydrogen cyanide. The reaction proceeds by an asymmetric hydroformylation followed by enamine formation and an aza-Cope-elimination induced by MMPP. ^[80]	24
Scheme 26. Negishi-cross-coupling of α -brominated nitriles with diaryl or dialkenylzinc forming enantiomerically enriched nitriles in presence of a chiral nickel catalyst. ^[97]	24
Scheme 27. Enantioselective Bayer-Villiger oxidation of nitriloketones catalyzed by BVMOs forming normal and abnormal nitrilolactones. ^[98]	25
Scheme 28. Iridium(II)-catalyzed allylation of cyanoacetate methylester followed by a Krapcho demethoxycarbonylation forming allylic nitriles. ^[99]	25
Scheme 29. Catalytic mechanism of the α -keto acid synthesis by L-AAOs. ^[109]	28
Scheme 30. Deracemization of chiral amines or amino acids by oxidases. A cyclic sequence of enantioselective oxidation coupled with a non-selective reduction enriches the non-converted enantiomer. ^[113]	29
Scheme 31. Synthesis of β -methyl-arylphenylalanine derivatives by L-AAO or D-AAO implying stereoinversion. ^[115]	30
Scheme 32. Formation of Cbz-N _ε -L-oxylysine from Cbz-N _ε -L-lysine in a four enzyme system. ^[125]	31
Scheme 33. The reaction from aminopropylcystein to [1,4]-thiazepane-3-carboxylic acid by the combination of LO from <i>T. viride</i> and NMAADH from <i>P. putida</i> ATCC12633. ^[134]	32
Scheme 34. The conversion of CPC into 7-ACA with an enzymatic system comprising of D-AAO, catalase, and glutaryl acylase. ^[144]	34
Scheme 35. The two step (left) or one step (right) conversion of CPC into 7-ACA. ^[146]	35

Scheme 36. The conversion of racemic ATPPA into (S)-ATPPA A) using (R)-selective D-AAO and (S)-aminotransferase, B) using (R)-selective D-AAO and (S)-selective AADH, and C) by dynamic kinetic resolution using (R)-selective D-AAO combined with unselective chemical imine reduction. ^[147]	36
Scheme 37. The conversion of an amine (here <i>n</i> -pentylamine) to the corresponding aldehyde by oxidation with MAO-N and subsequent hydrolysis of the formed imine. ^[133]	37
Scheme 38. The dynamic kinetic resolution of racemic 2-methyl-THQ forming (R)-2-methyl-THQ using a CHAO variant (T198F_L199S_M226F) from <i>Brevibacterium oxidans</i> IH-35A expressed in <i>E. coli</i> . ^[155]	40
Scheme 39. Oxds are special heme containing lyases involved in the “aldoxime-nitrile-pathway” of microbes. These enzymes catalyze the dehydration of aldoximes to nitriles, which are metabolized by nitrile hydratases and amidases or by nitrilases. ^[159–161]	41
Scheme 40. Proposed mechanism of the dehydration of aldoximes catalyzed by Oxds (active site of OxdA shown). The ovals refer to the heme b unit in the active site of the Oxds with different oxidation state of the iron atom: Brown (+II), yellow: (+III), green: (+IV) (Reprinted with permission from T. Betke, J. Higuchi, P. Rommelmann, K. Oike, T. Nomura, Y. Kato, Y. Asano, H. Gröger, <i>ChemBioChem</i> 2018, 19, 769-778, Copyright © 2018, John Wiley & Sons, Inc.). ^[175]	46
Scheme 41. Oxidation of 1-methoxynapthalene catalyzed by wild-type OxdA and OxdA_H320D mutant forming Russig-blue or 2-hydroxy-1-methoxynapthalene. ^[177]	47
Scheme 42. Kemp-elimination of (5-nitro-)benzoxazole catalyzed by Oxds and subsequent protonation forming 2-cyano-(5-nitro-)phenol. ^[178]	47
Scheme 43. Bioengineered pathway for the synthesis of PAN from L-phenylalanine by oxidation with CYP79A2 and dehydration of the <i>in situ</i> produced aldoxime with OxdB. ^[182] ...	50
Scheme 44. K_m - and v_{max} -values for PAOx derivatives with OxdB, OxdFG and OxdRG. ^[162,164,167]	50
Scheme 45. Dehydration of <i>E</i> -furfuryl-2-aldoxime and <i>E</i> -pyridine-3-aldoxime to 2-furonitrile and 3-cyanopyridine catalyzed by recombinant OxdYH3-3 in <i>E. coli</i> BL21(DE3). ^[170]	53
Scheme 46. Overview about a process for production of phenylpyruvate from L-phenylalanine with <i>hcLAAO4</i>	58
Scheme 47. Oxidation of <i>o</i> -dianisidine with hydrogen peroxide as oxidant catalyzed by horseradish peroxidase.	60
Scheme 48. Possible decomposition pathways of phenylpyruvate produced in biotransformations catalyzed by L-AAO. The oxidative decarboxylation to phenylacetic acid is observed while no evidence was found for the formation of phenylacetaldehyde <i>via</i> non-oxidative decarboxylation.	60

10 Register of illustrations

Scheme 49. Standard biotransformation of L-phenylalanine to phenylpyruvate catalyzed by <i>hcLAAO4</i>	61
Scheme 50. Proposed mechanism for the aldoxime dehydration to nitriles catalyzed by copper(II)-ions by transfer of water to acetonitrile forming acetamide. The mechanism is shown for the dehydration of 2-PPOx to 2-PPN in analogy to the proposed mechanism of the dehydration of benzaldoxime. ^[88]	69
Scheme 51. Dehydration of a racemic mixture of <i>E/Z</i> -2-PPOx forming both enantiomers of 2-PPN catalyzed by OxdB. ^[180]	70
Scheme 52. Enantioselective dehydrations of racemic mixtures of 3-hexen-1-aldoxime, tetrahydrofuran-3-aldoxime, and 3-phenylbutanal oxime with OxdB. ^[180]	72
Scheme 53. Synthesis routes chosen for obtaining the racemic chiral aldoximes starting from aryl aldehydes or <i>trans</i> - β -nitrostyrene.	75
Scheme 54. Principle of the identification of the absolute configuration of FPN by resolution with the highly selective (<i>R</i>)-selective nitrilase from <i>Bacillus</i> sp. OxB-1.	82
Scheme 55. Synthesis of aliphatic dinitriles from dialdehydes <i>via</i> condensation of dialdehydes with hydroxylamine hydrochloride and subsequent biocatalytic dehydration with OxdA or OxdB. ^[197]	95
Scheme 56. Hypothetical reaction sequence for the formation of fatty nitriles starting from fatty alcohols (blue) or alkenes.	97
Scheme 57. Principle of the cofactor regeneration for ADH-catalyzed oxidation of primary alcohols <i>via</i> coupling the reduction of the co-substrate acetone with the same enzyme. ^[211] .	99
Scheme 58. Biotransformation of fatty aldoximes with Oxds.....	103
Scheme 59. Reaction sequence for synthesis of nonane nitrile from 1-octene without workup steps. ^[218]	107
Scheme 60. PIPO-catalyzed oxidation of primary (di)alcohols with sodium hypochlorite pentahydrate as oxidant. ^[221]	107
Scheme 61. Dehydration of <i>Z</i> -PAOx to PAN as the standard activity assay for the determination of OxdB activity in whole-cells.	111
Scheme 62. Activity assay of the determination the whole-cell catalyst activity of OxdB and its variants.....	128
Scheme 63. Overview about the process for production of phenylpyruvate from L-phenylalanine using <i>hcLAAO4</i>	143
Scheme 64. Overview about the enantioselective aldoxime dehydration, the privileged substrate structure and all tested substrates in this thesis.	144
Scheme 65. Project overview about the synthesis of fatty nitriles in reaction sequences employing Oxd-catalyzed aldoxime dehydration.....	145

10 Register of illustrations

Scheme 66. Überblick über den Prozess zur Produktion von Phenylpyruvat von L-Phenylalanin mit <i>hcLAAO4</i>	147
Scheme 67. Überblick über die enantioselektive Aldoximdehydratisierung mit Oxds, der privilegierten Substratstruktur sowie allen in dieser Arbeit getesteten Substraten.....	148
Scheme 68. Überblick über die Reaktionssequenz zur Synthese von Fettnitrilen mit biokatalytischer Aldoximdehydratisierung als Schlüsselschritt.	150

10.3 Tables

Table 1. Principles of green chemistry and how biocatalysis as a method addresses them. ^[1]	1
Table 2. Annual production scale and <i>E</i> -factors in the different segments of the chemical industry. ^[7-9]	2
Table 3. Application of selected α -keto acids. ^[57]	15
Table 4. Enantioselectivity of MAO-N variants D9 and D11 with various racemic alkaloids containing the β -carboline backbone. ^[152]	39
Table 5. Properties of selected Oxds expressed recombinantly in <i>E. coli</i> . ^[162,164-169]	44
Table 6. Kinetic data, conversions and isolated yields for biotransformations of arylaliphatic aldoximes with Oxds.	49
Table 7. Kinetic data and conversions for chiral derivatives of PAOx with various Oxds.	51
Table 8. Conversions or yields of biotransformations of (hetero-)aromatic aldoximes with whole-cells of <i>Rhodococcus</i> sp. YH3-3. ^[181]	52
Table 9. Kinetic data, conversions and isolated yields for biotransformations of linear aliphatic aldoximes with Oxds.	54
Table 10. Kinetic data, conversions and isolated yields of biotransformations of branched linear aliphatic aldoximes with Oxds.	55
Table 11. Conversions and (by-)product formation in the biotransformations after one hour reaction time at higher substrate concentrations with 0.05 U <i>hcLAAO4</i> from <i>E. coli</i> .	65
Table 12. Conversions and <i>ee</i> -values of the biotransformation of racemic <i>E/Z</i> -2-PPOx mixtures of varying <i>E/Z</i> -ratios towards 2-PPN with OxdB. ^[180]	70
Table 13. Reaction conditions and isolated yields of the Nitroaldol-condensation of (hetero-)arylic aldehydes.	76
Table 14. Reaction conditions and isolated yields of the addition of the aliphatic Grignard-reagents to <i>E</i> -nitroalkenes.	76
Table 15. Reaction conditions and isolated yields of the disproportionation of nitroalkanes to aldoximes with benzylbromide.	77
Table 16. Isomeric ratios of the aldoximes separated with automated column chromatography.	79
Table 17. Reaction conditions and isolated yields of the copper(II) acetate-catalyzed dehydration of aldoximes to the corresponding racemic nitriles.	80
Table 18. Conversions and <i>ee</i> -values for the biotransformation of isomeric mixtures of heteroaromatic derivatives of 2-PPOx with Oxds performed at 8 °C.	83
Table 19. Conversions and <i>ee</i> -values for the biotransformation of halogen-substituted 2-PPOx derivatives with isomerically pure aldoximes with Oxds performed at 8 °C.	86

10 Register of illustrations

Table 20. Conversions and ee-values for the biotransformation of isomerically pure 2-PPOx and bulkier derivatives thereof with Oxds performed at 8 °C.....	92
Table 21. Reaction conditions of the TEMPO-catalyzed oxidation and conversions of the aldehydes according to ¹ H-NMR spectroscopy.....	101
Table 22. Reaction conditions of the palladium(II) acetate-catalyzed oxidation of alcohols to aldehydes and the isolated yields.	102
Table 23. Reaction conditions and yields of the condensation of fatty aldehydes with hydroxylamine hydrochloride forming the corresponding fatty aldoximes.....	103
Table 24. Expression systems and conditions for the expression of recombinant OxdB in <i>E. coli</i>	110
Table 25. Specific and volumetric activities of OxdB-whole-cell catalyst expression of under different conditions in <i>E. coli</i> BL21(DE3)-RIL harboring the pUC18-OxdB vector.....	112
Table 26. Hydropathy of the 20 proteinogene amino acids according to selected scales....	125
Table 27. Predicted aggregation hotspots for the sequence of OxdB by the program INTMSAlign_HiSol. ^[237] The structure elements were predicted by PSIPRED. ^[248,249]	127
Table 28. The specific activities of the variants OxdB-D1 to OxdB-D3 and the relative activities compare to the wild-type protein and the corresponding parent variants.	133
Table 29. Protein masses determined with static nanoESI-MS for wild-type OxdB and selected variants. The charge state adjusted protein masses in the denatured state and the native state are given in Da. For the native state, two masses were determined, only the result with the higher molecular mass is displayed in this table. The other values are available in the appendix (Table 61).....	134
Table 30. Specific activities and ratios of the integrals of non-heme containing and heme containing OxdB (mutants) estimated for a selected number of charge states.....	138
Table 31. List of devices used throughout this thesis and their manufacturer.	152
Table 32. Strains of <i>E. coli</i> used throughout this thesis.....	156
Table 33. Plasmids transformed throughout this thesis.....	156
Table 34. Compositions of solutions and buffer used throughout this thesis.	157
Table 35. Predicted aggregation hotspots and mutation of OxdB with appearance in the consensus protein and HiSol scores.....	158
Table 36. Predicted secondary structures of OxdB at the identified aggregation hotspots. .	159
Table 37. Composition of the media used for (fed-)batch fermentations.	188
Table 38. Composition of the Bradford-assay solution.....	191
Table 39. Composition of the gels used for electrophoresis, recipes are for 2 gels.....	192
Table 40. Composition of the running buffer for SDS-PAGE (10x concentrated).	192
Table 41. Composition of the α -cyclodextrine staining solution.....	192
Table 42. Composition of the Coomassie Blue staining solution.....	192

Table 43. Composition of the unstaining solution for the Coomassie stain.....	192
Table 44. Relative amounts of L-phenylalanine, phenylpyruvate and phenylacetic acid in the reaction solution for the time course with lysate and purified enzyme of <i>hcLAAO4</i> expressed in <i>E. coli</i> and <i>P. pastoris</i>	195
Table 45. Relative amounts of L-phenylalanine, phenylpyruvate and phenylacetic acid in the reaction solution for the time course with lysate and purified enzyme of <i>hcLAAO4</i> expressed in <i>E. coli</i> and <i>P. pastoris</i>	196
Table 46. Relative amounts of L-phenylalanine, phenylpyruvate and phenylacetic acid in the reaction solution for the time course purified enzyme of <i>hcLAAO4</i> expressed in <i>E. coli</i> and <i>P. pastoris</i> stored one week at $-20\text{ }^{\circ}\text{C}$ before reaction start.....	197
Table 47. Relative amounts of L-phenylalanine, phenylpyruvate and phenylacetic acid in the reaction solution after 7 hours reaction time for varying amounts of <i>hcLAAO4</i> at varying substrate concentrations.	198
Table 48. Overall conversions and relative concentrations of phenylpyruvate and phenylacetic acid in the reaction solutions of the biotransformation of varying amount of L-phenylalanine after 1 and 7 hours with 0.05 U <i>hcLAAO4</i>	199
Table 49. Relative amounts of L-phenylalanine, phenylpyruvate and phenylacetic acid in the reaction solution after 6 hours reaction time with 0.05 U of <i>hcLAAO4</i> at varying TEA buffer concentrations.	200
Table 50. Conversions, ee-values and specific activities of the biotransformations of bulky arylaliphatic aldoximes at $30\text{ }^{\circ}\text{C}$ after different reaction times.	202
Table 51. Conversions, ee-values and specific activities of the biotransformations of arylaliphatic aldoximes at $8\text{ }^{\circ}\text{C}$ after different reaction times.	203
Table 52. Conversions of the biotransformations of linear fatty aldoximes at $30\text{ }^{\circ}\text{C}$ after different reaction times.	204
Table 53. Conversions, volumetric and specific activities of the whole-cells obtained in the fermentation experiments with AI-medium in the batch-phase depending on the process time.	205
Table 54. Conversions, volumetric and specific activities of the whole-cells obtained in the fermentation experiments with HSG-medium in the batch-phase depending on the process time.	206
Table 55. Conversions, volumetric and specific activities of the whole-cells obtained in the fermentation experiments with TB-medium in the batch-phase depending on the process time.	206
Table 56. Conversions and specific activities of the activity assay with purified OxdB (variants) for Z-PAOx as standard substrate.	207

Table 57. Conversions and specific activities of the activity assay with purified OxdB (variants) for Z-PAOx as standard substrate.	208
Table 58. Storage time before use, Conversions of Z-PAOx with purified OxdB (variants) in the absence (w/o) and presence of FMN (w).	209
Table 59. Primers used for the introduction of single mutations in the sequence of OxdB via PCR with wild-type or mutated pET22b-OxdB(C)6His as template DNA.....	242
Table 60. Output sheet of INTMSAlign_HiSol applied to the sequence of OxdB according to the formula given in chapter 9.2. Conservation (similarity) of all amino acid residues in the gene family for the positions, which exhibited the highest absolute HiSol. The suggested mutations are marked in yellow.....	257
Table 61. Molecular masses determined with static nanoESI-MS for selected OxdB variants and the wild-type enzyme. The charge state adjusted masses in the denatured state and the native state are given in Da. For the native state, two masses were determined.....	264

11 List of abbreviations

The one letter code and the three letter code for the proteinogenic amino acids was used throughout this thesis.

(Bio-)chemical terms

7-ACA – 7-Aminocephalosporanic acid

acac – Acetylacetonato

ACN – Acetonitrile

6-APA – 6-Aminopenicillanic acid

APS – Ammonium persulfate

ATP – Adenosine triphosphate

ATPPA – 2-Amino-3-(6-*o*-tolylpyridin-3-yl)propanoic acid

Bn – Benzyl

Bu – *n*-Butyl

Cbz – Benzyloxycarbonyl

CDG – 7-Carboxy-7-deazaguanine

CLEA – Cross-linked enzyme aggregate

Cy – Cyclohexyl

CyPAN – 2-Cyclohexyl-2-phenylacetonitrile

CyPAOx – 2-Cyclohexyl-2-phenylacetaldoxime

d – Doublet (nuclear magnetic resonance spectroscopy)

DCM – Dichloromethane

*dd*H₂O – Millipore water

*d*H₂O – Distilled water

DMSO – Dimethyl sulfoxide

DNA – Desoxyribonucleic acid

Et – Ethyl

Et₂O – Diethylether

EtPAN – 2-Phenylbutane nitrile

EtPAOx – 2-Phenylbutanal oxime

FAD – Flavin adenine dinucleotide

FAD_{ox} – Oxidized form of flavin adenine dinucleotide

11 List of abbreviations

FAD_{red} – Reduced form of flavin adenine dinucleotide

Fe₂O₃/NGr@C – Iron(III) oxide based nanocatalyst prepared by pyrolysis of nitrogen introduced graphene

FMN – Flavin mononucleotide

FPN – 2-(Furan-2-yl)propionitrile

FPOx – 2-(Furan-2-yl)propanal aldoxime

4-FPPN – 2-(4-Fluorophenyl)propionitrile

4-FPPOx – 2-(4-Fluorophenyl)propanal oxime

glyme – 1,2-Dimethoxyethane

HAP@AEPH₂-SO₃H – Sulfonated hydroxyapatite nanocatalyst functionalized with 2-amino-ethylidihydrogenphosphate

*i*Pr – *iso*-Propyl

*i*PrOH – 2-Propanol

*i*PrPAN – 3-Methyl-2-phenylbutane nitrile

*i*PrPAOx – 3-Methyl-2-phenylbutanal oxime

IPTG – *iso*-Propyl β-D-thiogalactopyranoside

KPB – Potassium phosphate buffer

LB-medium – Luria-Bertani medium

m – *meta*

m – Multiplet (nuclear magnetic resonance spectroscopy)

MMPP – Magnesiumperoxyphthalate

NAD(P)⁺ – Nicotinamide adenine dinucleotide (phosphate) oxidized form

NAD(P)H – Nicotinamide adenine dinucleotide (phosphate) reduced form

o – *ortho*

p – *para*

PAN – Phenylacetonitrile

PAOx – Phenylacetaldoxime

PCR – Polymerase chain reaction

Pen G – Penicillin G

Ph – Phenyl

PIPO – Polymer immobilized 2,2,6,6-tetramethylpiperidinyloxy

2-PPN – 2-Phenylpropionitrile

2-PPOx – 2-Phenylpropionaldoxime

11 List of abbreviations

PreQ₀ – 7-Cyano-7-deazaguanine
s – Singlet
SDS – Sodium dodecyl sulfate
t – Triplet
T3P – Propanephosphonic acid anhydride
TB-medium – Terrific broth medium
TBHP – *tert*-butylhydroperoxide
TEA buffer – Triethanolamine buffer
TEMED – Tetramethylethylenediamine
TEMPO – 2,2,6,6-Tetramethylpiperidinyloxy
TFA – Trifluoroacetic acid
TMEDA – Tetramethylethylenediamine
THBC – Tetrahydro- β -carboline
THQ – 1,2,3,4-Tetrahydroquinoline
THF – Tetrahydrofuran
TLC – Thin layer chromatography
TPN – 2-(Thiophen-2-yl)propionitrile
TPOx – 2-(Thiophen-2-yl)propanal oxime
TPPTS – 3',3''-Phosphanetriyltris(benzenesulfonic acid) trisodium salt
Tris – Tris(hydroxymethyl)-aminomethane

Enzymes

AAD – Amino acid deaminase
AADH – Amino acid dehydrogenase
AAO – Amino acid oxidase
D-AAO – D-Amino acid oxidase
L-AAO – L-Amino acid oxidase
ADH – Alcohol dehydrogenase
AO – Amine oxidase
BVMO – Bayer-Villiger monooxygenase
CHAO – Cyclohexylamine oxidase
CYP – Cytochrom P450

11 List of abbreviations

CYP102A1 – Monooxygenase from *Bacillus megaterium*
CYP79A2 – Phenylalanine N-monooxygenase from *Arabidopsis thaliana*
FDH – Formate dehydrogenase
GDH – Glucose dehydrogenase
hcLAAO4 – Putative L-amino acid oxidase from *Hebeloma cylindrosporum*
HIC – α -Hydroxyisocaproate dehydrogenase
LkADH – (*R*)-Alcohol dehydrogenase from *Lactobacillus kefir* DSM 20587
LO – L-Lysine oxidase
MAO – Monoamine oxidase
MAO-N – Monoamine oxidase N
PAL – Phenylammonia lyase
PpADH – Alcohol dehydrogenase from *Pichia pastoris* CBS 7435
ToyM – Nitrile synthetase from *Streptomyces rimosus*
Oxd – Aldoxime dehydratase
OxdA – Aldoxime dehydratase from *Pseudomonas chloraphis* B23
OxdB – Aldoxime dehydratase from *Bacillus* sp. OxB-1
OxdBr1 – Aldoxime dehydratase from *Bradirhizobium* sp. LTSPM299
OxdFG – Aldoxime dehydratase from *Fusarium graminearum* MAFF 305135
OxdK – Aldoxime dehydratase from *Pseudomonas* sp. K-9
OxdRE – Aldoxime dehydratase from *Rhodococcus* sp. N-771
OxdRG – Aldoxime dehydratase from *Rhodococcus globerula* A-4
L-PheDH – L-Phenylalanine dehydrogenase

General

a – year

Conc. – Concentration

Conv. – Conversion

d – day (unit)

de – Diastereomeric excess

ee – Enantiomeric excess

e.g. – For example

eq. – Molar equivalents

11 List of abbreviations

ESI – Electron spray ionization

FACS – Fluorescence-activated cell sorting

g – Gravity constant

GC – Gas chromatography

h – Hour

HPLC – High-performance liquid chromatography

IEC – Ion-exchange chromatography

Isol. yield – Isolated yield

kDa – Kilodalton

min – Minute

MS – Mass spectrometry

NMR – Nuclear magnetic resonance

NP-HPLC – Normal phase high-performance liquid chromatography

OD₆₀₀ – Optical density at a wavelength of 600 nm

pH – *Pondus hydrogenii*

RP-HPLC – Reverse phase high-performance liquid chromatography

rpm – Revolutions per minute

rt – Room temperature

SDS-PAGE – Sodium dodecyl sulfate polyacrylamide gel electrophoresis

UV/vis – Ultraviolet/visible

(Micro-)organisms

B. subtilis – *Bacillus subtilis*

C. adamanteus – *Crotalus adamanteus* (diamondback rattle snake)

C. glutamicum – *Corinebacterium glutamicum*

E. coli – *Escherichia coli*

H. cylindrosporum – *Hebeloma cylindrosporum*

P. alcalifaciens – *Providencia alcalifaciens*

P. pastoris – *Pichia pastoris*

P. putida – *Pseudomonas putida*

R. opacus – *Rhodococcus opacus*

T. viride – *Trichoderma viride*

11 List of abbreviations

T. variabilis – *Trigonopsis variabilis*

12 References

- [1] R. A. Sheldon, J. M. Woodley, *Chem. Rev.* **2018**, *118*, 801–838.
- [2] J. M. Woodley, *Curr. Opin. Green Sust. Chem.* **2020**, *21*, 22–26.
- [3] P. Anastas, J. C. Warner, *Green Chemistry: Theory and Practice*, Oxford University Press, Oxford, U.K., **1998**.
- [4] R. Noyori, *Chem. Commun. (Camb.)* **2005**, 1807–1811.
- [5] R. A. Sheldon, D. Brady, M. L. Bode, *Chem. Sci.* **2020**, *293*, 7880–7898.
- [6] M. Höning, P. Sondermann, N. J. Turner, E. M. Carreira, *Angew. Chem. Int. Ed.* **2017**, *56*, 8942–8973.
- [7] R. A. Sheldon, *Green Chem.* **2014**, *16*, 950–963.
- [8] R. A. Sheldon, *Green Chem.* **2017**, *19*, 18–43.
- [9] R. A. Sheldon, I. Arends, U. Hanefeld, *Green Chemistry and Catalysis*, Wiley-VCH, Weinheim, **2007**.
- [10] H. Gröger, Y. Asano, U. T. Bornscheuer, J. Ogawa, *Chem. Asian J.* **2012**, *7*, 1138–1153.
- [11] A. Schmid, F. Hollmann, J. B. Park, B. Bühler, *Curr. Opin. Biotechnol.* **2002**, *13*, 359–366.
- [12] G. Hughes, J. C. Lewis, *Chem. Rev.* **2018**, *118*, 1–3.
- [13] E. M. M. Abdelraheem, H. Busch, U. Hanefeld, F. Tonin, *React. Chem. Eng.* **2019**, *4*, 1878–1894.
- [14] U. T. Bornscheuer, G. W. Huisman, R. J. Kazlauskas, S. Lutz, J. C. Moore, K. Robins, *Nature* **2012**, *485*, 185–194.
- [15] P. N. Devine, R. M. Howard, R. Kumar, M. P. Thompson, M. D. Truppo, N. J. Turner, *Nat. Rev. Chem.* **2018**, *2*, 409–421.
- [16] R. P. Elander, *Appl. Microbiol. Biotechnol.* **2003**, *61*, 385–392.
- [17] Q. M. Dudley, A. S. Karim, M. C. Jewett, *Biotechnol. J.* **2015**, *10*, 69–82.
- [18] a) M. Bilal, Y. Zhao, S. Noreen, S. Z. H. Shah, R. N. Bharagava, H. M. N. Iqbal, *Biocatal. Biotransfor.* **2019**, *37*, 159–182; b) R. H. Wijffels, R. M. Buitelaar, C. Bucke, J. Tramper (Eds.) *Progress in Biotechnology, Vol. 11*, Elsevier, Amsterdam, **1996**.
- [19] a) A. Dennig, A. Thiessenhusen, S. Gilch, T. Haas, M. Hall, *Biospektrum* **2016**, *22*, 614–616; b) E. M. Wittmann, T. Haas, S. Schaffer, M. Pötter, Y. Schiemann, N. Kirchner, WO 2014/198560 A2, **2014**.
- [20] M. Ayala, R. Vazques-Duhalt, "Enzymatic catalysis on petroleum products" in *Studies in Surface Science and Catalysis, Vol. 151* (Eds.: R. Vazques-Duhalt, R. Quintero-Ramirez), Elsevier, Amsterdam, **2004**, 67–111.
- [21] A. M. Azoddein, F. A. M. Azli, A. B. Bustary, M. H. Sulaiman, A. Z. M. Salehen, M. N. A. Seman, S. Nurdin, M. Sulaiman, *Int. J. Res. Eng. Sci.* **2016**, *4*, 6–20.

12 References

- [22] A. Machado de Castro, Cavalcanti da Silva, José André, "PETROBRAS: Efforts on Biocatalysis for Fuels and Chemicals Production" in *Catalysis Series, Vol. 29* (Eds.: G. de Gonzalo, P. Domínguez de María), Royal Society of Chemistry, Cambridge, **2017**, 276–297.
- [23] a) M. Bilal, M. Asgher, H. M. N. Iqbal, H. Hu, X. Zhang, *Int. J. Biol. Macromol.* **2017**, *98*, 447–458; b) S. Eker, M. Sarp, *Int. J. Hydrogen Energ.* **2017**, *42*, 2562–2568; c) F. A. Fiorda, G. V. de Melo Pereira, V. Thomaz-Soccol, S. K. Rakshit, M. G. B. Pagnoncelli, L. P. d. S. Vandenberghe, C. R. Soccol, *Food Microbiol.* **2017**, *66*, 86–95; d) Q. Liu, F. Lou, J. Geng, Y. Li, F. Gao, *IOP Conf. Ser.: Earth Environ. Sci.* **2019**, *330*, 32041; e) S. Mohapatra, C. Mishra, S. S. Behera, H. Thatoi, *Renew. Sust. Energ. Rev.* **2017**, *78*, 1007–1032; f) S. H. Mohd Azhar, R. Abdulla, S. A. Jambo, H. Marbawi, J. A. Gansau, A. A. Mohd Faik, K. F. Rodrigues, *Biochem. Biophys. Rep.* **2017**, *10*, 52–61; g) C. K. Phwan, H. C. Ong, W.-H. Chen, T. C. Ling, E. P. Ng, P. L. Show, *Energ. Conv. Man.* **2018**, *173*, 81–94; h) R. K. Salar, S. K. Gahlawat, P. Siwach, J. S. Duhan, *Biotechnology: Prospects and Applications*, Springer India, New Delhi, **2013**; i) K. R. Birikh, M. W. Heikkila, A. Michine, A. Mialon, T. Grönroos, P. Ihalainen, A. Varho, V. Hämäläinen, A. Suonpää, S.-P. Rantanen, "MetGen: Value from Wood - Enzymatic Solutions" in *Catalysis Series, Vol. 29* (Eds.: G. de Gonzalo, P. Domínguez de María), Royal Society of Chemistry, Cambridge, **2017**, 298–324.
- [24] J. Ogawa, S. Shimizu, *Curr. Opin. Biotechnol.* **2002**, *13*, 367–375.
- [25] A. Panova, L. J. Mersinger, Q. Liu, T. Foo, D. C. Roe, W. L. Spillan, A. E. Sigmund, A. Ben-Bassat, L. W. Wagner, D. P. O'Keefe et al., *Adv. Synth. Catal.* **2007**, *349*, 1462–1474.
- [26] H.-X. Jin, Z.-Q. Liu, Z.-C. Hu, Y.-G. Zheng, *Eng. Life Sci.* **2013**, *13*, 385–392.
- [27] S. H. Bhosale, M. B. Rao, V. V. Deshpand, *Microbiol. Rev.* **1996**, *60*, 280–300.
- [28] R. DiCosimo, J. McAuliffe, A. J. Poulouse, G. Bohlmann, *Chem. Soc. Rev.* **2013**, *42*, 6437–6474.
- [29] P. Domínguez de María, G. de Gonzalo, A. R. Alcántara, *Catalysts* **2019**, *9*, 802.
- [30] F. van Rantwijk, R. A. Sheldon, *Tetrahedron* **2004**, *60*, 501–519.
- [31] F. Balkenhohl, K. Ditrich, B. Hauer, W. Ladner, *J. prakt. Chem.* **1997**, *339*, 381–384.
- [32] M. Breuer, K. Ditrich, T. Habicher, B. Hauer, M. Kesseler, R. Stürmer, T. Zelinski, *Angew. Chem. Int. Ed.* **2004**, *43*, 788–824.
- [33] A. Bruggink, Eric C., E. de Vroom, *Org. Process Res. Dev.* **1998**, *2*, 128–133.
- [34] J. P. Adams, M. J. B. Brown, A. Diaz - Rodriguez, R. C. Lloyd, G. - D. Roiban, *Adv. Synth. Catal.* **2019**, *361*, 2421–2432.

12 References

- [35] J. Liang, J. Lalonde, B. Borup, V. Mitchell, E. Mundorff, N. Trinh, D. A. Kochrekar, R. Nair Cherat, G. G. Pai, *Org. Process Res. Dev.* **2010**, *14*, 193–198.
- [36] X.-M. Gong, Z. Qin, F.-L. Li, B.-B. Zeng, G.-W. Zheng, J.-H. Xu, *ACS Catal.* **2019**, *9*, 147–153.
- [37] C. K. Saville, J. M. Janey, E. C. Mundorff, J. C. Moore, S. Tam, W. R. Jarvis, J. C. Colbeck, A. Krebber, F. J. Fleitz, J. Brands et al., *Science* **2010**, *329*, 305–309.
- [38] S. Ospina, E. Barzana, O. T. Ramírez, A. López-Munguía, "Strategies in the design of an enzymatic process for the synthesis of ampicillin: A whole cell E. coli recombinant penicillin amidase biocatalyst" in *Progress in Biotechnology, Vol. 11* (Eds.: R. H. Wijffels, R. M. Buitelaar, C. Bucke, J. Tramper), Elsevier, Amsterdam, **1996**, 464–471.
- [39] T. Shibatani, "Industrial Application of Immobilized Biocatalysts in Japan" in *Progress in Biotechnology, Vol. 11* (Eds.: R. H. Wijffels, R. M. Buitelaar, C. Bucke, J. Tramper), Elsevier, Amsterdam, **1996**, 585–591.
- [40] F. H. Arnold, *Angew. Chem. Int. Ed.* **2019**, *58*, 14420–14426.
- [41] P. S. Coelho, E. M. Brustad, A. Kannan, F. H. Arnold, *Science* **2013**, *339*, 307–311.
- [42] O. F. Brandenburg, C. K. Prier, K. Chen, A. M. Knight, Z. Wu, F. H. Arnold, *ACS Catal.* **2018**, *8*, 2629–2634.
- [43] G. C. Barrett, D. T. Elmore, *Amino Acids and Peptides*, Cambridge University Press, Cambridge, **2012**.
- [44] A. J. L. Cooper, J. Z. Ginos, A. Meister, *Chem. Rev.* **1983**, *83*, 321–358.
- [45] M. D'Este, M. Alvarado-Morales, I. Angelidaki, *Biotechnol. Adv.* **2018**, *36*, 14–25.
- [46] M. Gruber-Khadjawi, M. H. Fechter, H. Griengl, "Cleavage and Formation of Cyanohydrins" in *Enzyme catalysis in organic synthesis* (Eds.: H. Gröger, K. Drauz, O. May), Wiley-VCH, Weinheim, New York, **2012**, 947-990.
- [47] R. P. Herrera, V. Sgarzani, L. Bernardi, F. Fini, D. Pettersen, A. Ricci, *J. Org. Chem.* **2006**, *71*, 9869–9872.
- [48] M. Ikeda, "Amino Acid Production Processes" in *Advances in Biochemical Engineering/Biotechnology, Vol. 79* (Eds.: T. Scheper, R. Faurie, J. Thommel), Springer, Berlin, Heidelberg, **2003**, 1–35.
- [49] V. F. Wendisch, J. M. P. Jorge, F. Pérez-García, E. Sgobba, *World J. Microbiol. Biotechnol.* **2016**, *32*, 105.
- [50] T. Fukushima, M. Yamauchi, *Chem. Commun. (Camb.)* **2019**, *55*, 14721–14724.
- [51] a) Y. Wang, X. Song, J. Wang, H. Moriwaki, V. A. Soloshonok, H. Liu, *Amino Acids* **2017**, *49*, 1487–1520; b) V. A. Larionov, N. V. Stoletova, V. I. Kovalev, A. F. Smol'yakov, T. F. Savel'yeva, V. I. Maleev, *Org. Chem. Front.* **2019**, *6*, 1094–1099.
- [52] M. Jiang, Y. Jin, H. Yang, H. Fu, *Sci. Rep.* **2016**, *6*, 26161.

12 References

- [53] A. Dreßen, T. Hilberath, U. Mackfeld, A. Billmeier, J. Rudat, M. Pohl, *J. Biotechnol.* **2017**, *258*, 148–157.
- [54] A. Dennig, F. Blaschke, S. Gandomkar, E. Tassano, B. Nidetzky, *Adv. Synth. Catal.* **2019**, *361*, 1348–1358.
- [55] F. Penteadó, E. F. Lopes, D. Alves, G. Perin, R. G. Jacob, E. J. Lenardão, *Chem. Rev.* **2019**, *119*, 7113–7278.
- [56] P. Nshimiyimana, L. Liu, G. Du, *Bioengineered* **2019**, *10*, 43–51.
- [57] Y. Song, J. Li, H.-d. Shin, L. Liu, G. Du, J. Chen, *Bioresour. Technol.* **2016**, *219*, 716–724.
- [58] P. Kelefiotis-Stratidakis, T. Tyrikos-Ergas, I. V. Pavlidis, *Org. Biomol. Chem.* **2019**, *17*, 1634–1642.
- [59] S. A. Kelly, S. Pohle, S. Wharry, S. Mix, C. C. R. Allen, T. S. Moody, B. F. Gilmore, *Chem. Rev.* **2018**, *118*, 349–367.
- [60] K. L. Waters, *Chem. Rev.* **1947**, *41*, 585–598.
- [61] A. Claus, W. Neukranz, *J. prakt. Chem.* **1891**, *44*, 77–85.
- [62] C. D. Hurd, R. W. McNamee, F. O. Green, *J. Am. Chem. Soc.* **1939**, *61*, 2979–2980.
- [63] T. S. Oakwood, C. A. Weisgerber, *Org. Synth.* **1944**, *24*, 16.
- [64] T. S. Oakwood, C. A. Weisgerber, *Org. Synth.* **1944**, *24*, 14–15.
- [65] F. Weygand, W. Steglich, H. Tanner, *Liebigs Ann. Chem.* **1962**, *658*, 128–150.
- [66] K. Wadhwa, C. Yang, P. R. West, K. C. Deming, S. R. Chemburkar, R. E. Reddy, *Synth. Commun.* **2008**, *38*, 4434–4444.
- [67] D. Crich, Y. Zou, *J. Org. Chem.* **2005**, *70*, 3309–3311.
- [68] K. Furukawa, H. Inada, M. Shibuya, Y. Yamamoto, *Org. Lett.* **2016**, *18*, 4230–4233.
- [69] H. B. Coban, A. Demirci, "Applied Research Perspectives of Alpha-Keto Acids: From Production to Applications" in *Handbook of Food Bioengineering* (Eds.: A. M. Grumezescu, A. M. Holban), Elsevier, Amsterdam, **2017**, 427–447.
- [70] V. M. Luque-Almagro, R. Blasco, M. Martínez-Luque, C. Moreno-Vivián, F. Castillo, M. D. Roldán, *Biochem. Soc. Trans.* **2011**, *39*, 269–274.
- [71] S.-I. Murahashi (Ed.) *Science of Synthesis*, Georg Thieme Verlag, Stuttgart, **2004**.
- [72] S. A. Savage, G. S. Jones, S. Kolotuchin, S. A. Ramrattan, T. Vu, R. E. Waltermire, *Org. Process Res. Dev.* **2009**, *13*, 1169–1176.
- [73] L. Pellegatti, J. Sedelmeier, *Org. Process Res. Dev.* **2015**, *19*, 551–554.
- [74] K. V. Raghavan, B. M. Reddy (Eds.) *Industrial Catalysis and Separations: Innovations for Process Intensification*, Apple Academic Press, New Jersey, **2014**.
- [75] H. Gröger, *Chem. Rev.* **2003**, *103*, 2795–2828.
- [76] E. N. Jacobsen, A. Pfaltz, H. Yamamoto, *Comprehensive Asymmetric Catalysis*, Springer, Berlin, **2004**.

12 References

- [77] A. Martin, V. N. Kalevaru, *ChemCatChem* **2010**, *2*, 1504–1522.
- [78] F. Trifirò, *Catal. Today* **2020**, in press, DOI:10.1016/j.cattod.2019.09.012.
- [79] Z. Wang, *Comprehensive Organic Name Reactions and Reagents*, John Wiley & Sons Ltd., Hoboken, NJ, **2010**.
- [80] X. Li, C. You, J. Yang, S. Li, D. Zhang, H. Lv, X. Zhang, *Angew. Chem. Int. Ed.* **2019**, *58*, 10928–10931.
- [81] L. M. Dornan, Q. Cao, J. C. A. Flanagan, J. J. Crawford, M. J. Cook, M. J. Muldoon, *Chem. Commun. (Camb.)* **2013**, *49*, 6030–6032.
- [82] J.-J. Ge, C.-Z. Yao, M.-M. Wang, H.-X. Zheng, Y.-B. Kang, Y. Li, *Org. Lett.* **2016**, *18*, 228–231.
- [83] R. V. Jagadeesh, H. Junge, M. Beller, *ChemSusChem* **2015**, *8*, 92–96.
- [84] M. Lamani, K. R. Prabhu, *Angew. Chem. Int. Ed.* **2010**, *49*, 6622–6625.
- [85] R. M. Denton, J. An, P. Lindovska, W. Lewis, *Tetrahedron* **2012**, *68*, 2899–2905.
- [86] Basavaprabhu, T. M. Vishwanatha, N. Rao Panguluri, V. V. Sureshbabu, *Synthesis* **2013**, *45*, 1569–1601.
- [87] S. M. Masjed, B. Akhlaghinia, M. Zarghani, N. Razavi, *Aust. J. Chem.* **2017**, *70*, 33.
- [88] Á. Kiss, Z. Hell, *Synth. Commun.* **2013**, *43*, 1778–1786.
- [89] X.-Y. Ma, Y. He, T.-T. Lu, M. Lu, *Tetrahedron* **2013**, *69*, 2560–2564.
- [90] K. Hyodo, S. Kitagawa, M. Yamazaki, K. Uchida, *Chem. Asian J.* **2016**, *11*, 1348–1352.
- [91] M. T. Nelp, V. Bandarian, *Angew. Chem. Int. Ed.* **2015**, *54*, 10627–10629.
- [92] R. Hernández, E. I. León, P. Moreno, C. Riesco-Fagundo, E. Suárez, *J. Org. Chem.* **2004**, *69*, 8437–8444.
- [93] A. Sadhukhan, M. C. Hobbs, A. J. H. M. Meijer, I. Coldham, *Chem. Sci.* **2017**, *8*, 1436–1441.
- [94] J. Scharfbier, H. Hazrati, E. Irran, M. Oestreich, *Org. Lett.* **2017**, *19*, 6562–6565.
- [95] J. Liu, H.-X. Zheng, C.-Z. Yao, B.-F. Sun, Y.-B. Kang, *J. Am. Chem. Soc.* **2016**, *138*, 3294–3297.
- [96] D. Kong, M. Li, R. Wang, G. Zi, G. Hou, *Org. Lett.* **2016**, *18*, 4916–4919.
- [97] J. Choi, G. C. Fu, *J. Am. Chem. Soc.* **2012**, *134*, 9102–9105.
- [98] M. J. Fink, R. Snajdrova, A. Winninger, M. D. Mihovilovic, *Tetrahedron* **2016**, *72*, 7241–7248.
- [99] A. Matsunami, K. Takizawa, S. Sugano, Y. Yano, H. Sato, R. Takeuchi, *J. Org. Chem.* **2018**, *83*, 12239–12246.
- [100] K. Kodama, H. Kanai, Y. Shimomura, T. Hirose, *Eur. J. Org. Chem.* **2018**, *2018*, 1726–1729.

12 References

- [101] S. Wedde, M. Biermann, J. E. Choi, K. Oike, N. Zumbrägel, H. Gröger, "The Recent Developments of Enzymatic Oxidation" in *Green Oxidation in Organic Synthesis* (Eds.: N. Jiao, S. S. Stahl), John Wiley & Sons Ltd., Hoboken, NJ, **2019**, 439–496.
- [102] M. H. Hefti, J. Vervoort, W. J. H. van Berkel, *Eur. J. Biochem.* **2003**, *270*, 4227–4242.
- [103] V. Joosten, W. J. H. van Berkel, *Curr. Opin. Chem. Biol.* **2007**, *11*, 195–202.
- [104] I. P. Fotheringham, I. Arcer, R. Carr, N. J. Turner, *Biochem. Soc. Trans.* **2006**, *34*, 287–290.
- [105] Du, Xiao-Yan; Clementson, Kenneth J., *Toxicol.* **2002**, *40*, 659–665.
- [106] Z. Yu, H. Qiao, *Appl. Biochem. Biotechnol.* **2012**, *167*, 1–13.
- [107] A. Faust, K. Niefind, W. Hummel, D. Schomburg, *J. Mol. Biol.* **2007**, *367*, 234–248.
- [108] I. M. Moustafa, S. Foster, A. Y. Lyubimov, A. Vrieling, *J. Mol. Biol.* **2006**, *364*, 991–1002.
- [109] P. Bhattacharjee, J. Mitra, D. Bhattacharyya, "L-Amino Acid Oxidase from Venoms" in *Toxins and Drug Discovery* (Ed.: P. Gopalakrishnakone), Springer, Dordrecht, **2017**, 295–320.
- [110] Hafner, Edmund, W., D. Wellner, *Proc. Natl. Acad. Sci. U.S.A.* **1971**, *68*, 987–991.
- [111] E. Romero, J. R. Gómez Castellanos, G. Gadda, M. W. Fraaije, A. Mattevi, *Chem. Rev.* **2018**, *118*, 1742–1769.
- [112] P. F. Fitzpatrick, *Bioorg. Chem.* **2004**, *32*, 125–139.
- [113] F.-R. Alexandre, D. P. Pantaleone, P. P. Taylor, I. G. Fotheringham, D. J. Ager, N. J. Turner, *Tetrahedron Lett.* **2002**, *43*, 707–710.
- [114] T. M. Beard, N. J. Turner, *Chem. Commun. (Camb.)* **2002**, 246–247.
- [115] G. J. Roff, R. C. Lloyd, N. J. Turner, *J. Am. Chem. Soc.* **2004**, *126*, 4098–4099.
- [116] a) M. Y. Ahn, B. M. Lee, Y. S. Kim, *Int. J. Biochem. Cell Biol.* **1997**, *29*, 911–919; b) D. H. F. Souza, L. M. Eugenio, J. E. Fletcher, M.-S. Jiang, R. C. Garratt, Oliva, Glaucius, H. S. Selistre-de-Araujo, *Arch. Biochem. Biophys.* **1999**, *368*, 285–290.
- [117] M. Y. Ahn, K. S. Ryu, Y. W. Lee, Y. S. Kim, *Arch. Pharm. Res.* **2000**, *23*, 477–481.
- [118] a) H. Kusakabe, K. Kodama, A. Kuninaka, H. Yoshino, *J. Biol. Chem.* **1980**, *255*, 976–981; b) J. T. Nuutinen, S. Timonen, *Mycol. Res.* **2008**, *112*, 1453–1464.
- [119] K. Hahn, K. Neumeister, A. Mix, T. Kottke, H. Gröger, G. Fischer von Mollard, *Appl. Microbiol. Biotechnol.* **2017**, *101*, 2853–2864.
- [120] J. T. Nuutinen, E. Marttinen, R. Soliymani, K. Hildén, S. Timonen, *Microbiology (Reading, Engl.)* **2012**, *158*, 272–283.
- [121] H. Koyama, H. Suzuki, *J. Biochem.* **1986**, *100*, 859–866.
- [122] B. Geueke, W. Hummel, *Enzyme Microb. Technol.* **2002**, *31*, 77–87.
- [123] a) O. Vallon, L. Bulté, R. Kuras, J. Olive, F.-A. Wollman, *Eur. J. Biochem.* **1993**, *215*, 351–360; b) P. Piedras, M. Pineda, J. Muñoz, J. Cárdenas, *Planta* **1992**, *188*, 13–18.

12 References

- [124] A. Meister, *J. Biol. Chem.* **1954**, *206*, 577–585.
- [125] R. L. Hanson, K. S. Bembenek, R. N. Patel, L. J. Szarka, *Appl. Microbiol. Biotechnol.* **1992**, *37*, 599–603.
- [126] S. Singh, B. K. Gogoi, R. L. Bezbaruah, *Can. J. Microbiol.* **2009**, *55*, 1096–1102.
- [127] S. Singh, B. K. Gogoi, R. L. Bezbaruah, *Curr. Microbiol.* **2011**, *63*, 94–99.
- [128] B. Geueke, W. Hummel, *Prof. Expr. Purif.* **2003**, *28*, 303–309.
- [129] Z. Findrik, B. Geueke, W. Hummel, Đ. Vasić-Rački, *Biochem. Eng. J.* **2006**, *27*, 275–286.
- [130] K. Isobe, H. Tamauchi, K.-I. Fuhshuku, S. Nagasawa, Y. Asano, *Enzyme Res.* **2010**, *2010*, 567210.
- [131] K. Isobe, S. Nagasawa, *J. Biosci. Bioeng.* **2007**, *104*, 218–223.
- [132] D. Bifulco, L. Pollegioni, D. Tessaro, S. Servi, G. Molla, *Appl. Microbiol. Biotechnol.* **2013**, *97*, 7285–7295.
- [133] N. J. Turner, *Chem. Rev.* **2011**, *111*, 4073–4087.
- [134] M. Yasuda, M. Ueda, H. Muramatsu, H. Mihara, N. Esaki, *Tetrahedron: Asymmetry* **2006**, *17*, 1775–1779.
- [135] L. Pollegioni, P. Motta, G. Molla, *Appl. Microbiol. Biotechnol.* **2013**, *97*, 9323–9341.
- [136] L. Pollegioni, G. Molla, *Trends Biotechnol.* **2011**, *29*, 276–283.
- [137] S. Takahashi, M. Furukawara, K. Omae, N. Tadokoro, Y. Saito, K. Abe, Y. Kera, *Appl. Environ. Microbiol.* **2014**, *80*, 7219–7229.
- [138] S. Yano, H. Ozaki, S. Matsuo, M. Ito, M. Wakayama, *Adv. Biosci. Biotechnol.* **2012**, *3*, 7–13.
- [139] M. F. Gisby, E. A. Mudd, A. Day, *Plant Physiol.* **2012**, *160*, 2219–2226.
- [140] G. Molla, S. Sacchi, M. Bernasconi, M. S. Pilone, K. Fukui, L. Pollegioni, *FEBS Lett.* **2006**, *580*, 2358–2364.
- [141] J. C. Campillo-Brocal, P. Lucas-Elío, A. Sanchez-Amat, *Mar. Drugs* **2015**, *13*, 7403–7418.
- [142] M. S. Pilone, L. Pollegioni, *Biocatal. Biotransfor.* **2002**, *20*, 145–159.
- [143] a) A. Matsuda, K. Toma, K.-I. Komatsu, *J. Bacteriol.* **1987**, *169*, 5821–5826; b) A. Nikolov, B. Danielsson, *Enzyme Microb. Technol.* **1994**, *16*, 1031–1036.
- [144] F. López-Gallego, L. Batencor, A. Hidalgo, C. Mateo, R. Fernandez-Lafuente, J. M. Guisan, *Adv. Synth. Catal.* **2005**, *347*, 1804–1810.
- [145] F. López-Gallego, L. Batencor, C. F. Sio, C. R. Reis, P. N. Jimenez, J. M. Guisan, W. J. Quax, R. Fernandez-Lafuente, *Adv. Synth. Catal.* **2008**, *350*, 343–348.
- [146] L. Pollegioni, E. Rosini, G. Molla, *Appl. Microbiol. Biotechnol.* **2013**, *97*, 2341–2355.
- [147] Y. Chen, S. L. Goldberg, R. L. Hanson, W. L. Parker, I. Gill, T. P. Tully, M. A. Montana, A. Goswami, R. N. Patel, *Org. Process Res. Dev.* **2011**, *15*, 241–248.

12 References

- [148] P. L. Dostert, M. Strolin Benedetti, K. F. Tipton, *Med. Res. Rev.* **1989**, *9*, 45–89.
- [149] B. Schilling, K. Lerch, *Biochim. Biophys. Acta* **1995**, *1243*, 529–537.
- [150] S. O. Sablin, V. Yankovskaya, S. Bernard, C. N. Cronin, T. P. Singer, *Eur. J. Biochem.* **1998**, *253*, 270–279.
- [151] a) M. Alexeeva, A. Enright, M. J. Dawson, M. Mahmoudian, N. J. Turner, *Angew. Chem. Int. Ed.* **2002**, *41*, 3177–3180; b) K. R. Bailey, A. J. Ellis, R. Reiss, T. J. Snape, N. J. Turner, *Chem. Commun. (Camb.)* **2007**, 3640–3642; c) R. Carr, M. Alexeeva, M. J. Dawson, V. Gotor-Fernández, C. E. Humphrey, N. J. Turner, *ChemBioChem* **2005**, *6*, 637–639; d) R. Carr, M. Alexeeva, A. Enright, T. S. C. Eve, M. J. Dawson, N. J. Turner, *Angew. Chem. Int. Ed.* **2003**, *42*, 4807–4810; e) C. J. Dunsmore, R. Carr, T. Fleming, N. J. Turner, *J. Am. Chem. Soc.* **2006**, *128*, 2224–2225; f) T. S. C. Eve, A. Wells, N. J. Turner, *Chem. Commun. (Camb.)* **2007**, 1530–1531.
- [152] D. Ghislieri, D. Houghton, A. P. Green, S. C. Willies, N. J. Turner, *ACS Catal.* **2013**, *3*, 2869–2872.
- [153] D. Ghislieri, A. P. Green, M. Pontini, S. C. Willies, I. Rowles, A. Frank, G. Grogan, N. J. Turner, *J. Am. Chem. Soc.* **2013**, *135*, 10863–10869.
- [154] T. Wang, L.-G. Zhuo, Z. Li, F. Chen, Z. Ding, Y. He, Q.-H. Fan, J. Xiang, Z.-X. Yu, A. S. C. Chan, *J. Am. Chem. Soc.* **2011**, *133*, 9878–9891.
- [155] G. Li, J. Ren, P. Yao, Y. Duan, H. Zhang, Q. Wu, J. Feng, P. C. K. Lau, D. Zhu, *ACS Catal.* **2014**, *4*, 903–908.
- [156] T. Betke, J. Higuchi, P. Rommelmann, K. Oike, T. Nomura, Y. Kato, Y. Asano, H. Gröger, *ChemBioChem* **2018**, *19*, 768–779.
- [157] Y. Asano, Y. Kato, *FEMS Microbiol. Lett.* **1998**, *158*, 185–190.
- [158] Y. Asano, *J. Biotechnol.* **2002**, *94*, 65–72.
- [159] Y. Kato, R. Ooi, Y. Asano, *Arch. Microbiol.* **1998**, *170*, 85–90.
- [160] Y. Kato, R. Ooi, Y. Asano, *Appl. Environ. Microbiol.* **2000**, *66*, 2290–2296.
- [161] Y. Kato, S. Yoshida, Y. Asano, *FEMS Microbiol. Lett.* **2005**, *246*, 243–249.
- [162] Y. Kato, K. Nakamura, H. Sakiyama, S. G. Mayhew, Y. Asano, *Biochemistry* **2000**, *39*, 800–809.
- [163] Y. Kato, Y. Asano, *Prof. Expr. Purif.* **2003**, *28*, 131–139.
- [164] S.-X. Xie, Y. Kato, H. Komeda, S. Yoshida, Y. Asano, *Biochemistry* **2003**, *42*, 12056–12066.
- [165] K.-I. Oinuma, Y. Hashimoto, K. Konishi, M. Goda, T. Noguchi, H. Higashibata, M. Kobayashi, *J. Biol. Chem.* **2003**, *278*, 29600–29608.
- [166] Y. Kato, S. Yoshida, S.-X. Xie, Y. Asano, *J. Biosci. Bioeng.* **2004**, *97*, 250–259.
- [167] Y. Kato, Y. Asano, *Biosci. Biotechnol. Biochem.* **2005**, *69*, 2254–2257.
- [168] Y. Kato, Y. Asano, *Appl. Microbiol. Biotechnol.* **2006**, *70*, 92–101.

12 References

- [169] R. Rädisch, M. Chmátal, L. Rucká, P. Novotný, L. Petrásková, P. Halada, M. Kotik, M. Pátek, L. Martínková, *Int. J. Biol. Macromol.* **2018**, *115*, 746–753.
- [170] J. E. Choi, S. Shinoda, R. Inoue, D. Zheng, H. Gröger, Y. Asano, *Biocatal. Biotransfor.* **2019**, *37*, 414–420.
- [171] J. Zhang, Z. Kang, J. Chen, G. Du, *Sci. Rep.* **2015**, *5*, 8584.
- [172] K. Kobayashi, S. Yoshioka, Y. Kato, Y. Asano, S. Aono, *J. Biol. Chem.* **2005**, *280*, 5486–5490.
- [173] K. Konishi, T. Ohta, K.-I. Oinuma, Y. Hashimoto, T. Kitagawa, M. Kobayashi, *Proc. Natl. Acad. Sci. U.S.A.* **2006**, *103*, 564–568.
- [174] K. Konishi, K. Ishida, K.-I. Oinuma, T. Ohta, Y. Hashimoto, H. Higashibata, T. Kitagawa, M. Kobayashi, *J. Biol. Chem.* **2004**, *279*, 47619–47625.
- [175] J. Nomura, H. Hashimoto, T. Ohta, Y. Hashimoto, K. Wada, Y. Naruta, K.-I. Oinuma, M. Kobayashi, *Proc. Natl. Acad. Sci. U.S.A.* **2013**, *110*, 2810–2815.
- [176] H. Sawai, H. Sugimoto, Y. Kato, Y. Asano, Y. Shiro, S. Aono, *J. Biol. Chem.* **2009**, *284*, 32089–32096.
- [177] M. Yamada, Y. Hashimoto, T. Kumano, S. Tsujimura, M. Kobayashi, *PLoS ONE* **2017**, *12*, e0175846.
- [178] Y. Miao, R. Metzner, Y. Asano, *ChemBioChem* **2017**, *18*, 451–454.
- [179] S.-X. Xie, Y. Kato, Y. Asano, *Biosci. Biotechnol. Biochem.* **2001**, *65*, 2666–2672.
- [180] R. Metzner, S. Okazaki, Y. Asano, H. Gröger, *ChemCatChem* **2014**, *6*, 3105–3109.
- [181] Y. Kato, R. Ooi, Y. Asano, *J. Mol. Catal., B Enzym.* **1999**, *6*, 249–256.
- [182] Y. Miki, Y. Asano, *Appl. Environ. Microbiol.* **2014**, *80*, 6828–6836.
- [183] A. Piatasi, W. Siegel, K.-U. Baldenius, US9080191, **2015**.
- [184] S. Bloess, T. Beuel, T. Krüger, N. Sewald, T. Dierks, G. Fischer von Mollard, *Appl. Microbiol. Biotechnol.* **2019**, *103*, 2229–2241.
- [185] S. Bloess, G. Fischer von Mollard, *Unpublished results*.
- [186] A. van Boven, P. S. T. Tan, W. N. Konings, *Appl. Environ. Microbiol.* **1988**, *54*, 43–49.
- [187] T. Krüger, N. Sewald, *unpublished results*.
- [188] M. A. Metrick, J. E. Temple, G. MacDonald, *Biophys. Chem.* **2013**, *184*, 29–36.
- [189] P. Rommelmann, *Dissertation*, Bielefeld University, Bielefeld, **2018**.
- [190] T. Betke, *Dissertation*, Bielefeld University, Bielefeld, **2018**.
- [191] C. Czekelius, E. M. Carreira, *Angew. Chem. Int. Ed.* **2005**, *44*, 612–615.
- [192] K. Oike, Toyama Prefectural University, Toyama, Japan, **2016**.
- [193] F. A. Luzzio, *Tetrahedron* **2001**, *57*, 915–945.
- [194] B. M. Trost, J. Hitce, *J. Am. Chem. Soc.* **2009**, *131*, 4572–4573.

12 References

- [195] a) D. Enders, L. Tedeschi, J. W. Bats, *Angew. Chem. Int. Ed.* **2000**, *39*, 4605–4607; b) M. S. Rasalkar, M. K. Potdar, S. S. Mohile, M. M. Salunkhe, *J. Mol. Catal., A Chem.* **2005**, *235*, 267–270.
- [196] T. Betke, P. Rommelmann, K. Oike, Y. Asano, H. Gröger, *Angew. Chem. Int. Ed.* **2017**, *56*, 12361–12366.
- [197] T. Betke, M. Maier, H. Gruber-Wölfler, H. Gröger, *Nat. Commun.* **2018**, *9*, 5112.
- [198] D. Riesenberg, R. Guthke, *Appl. Microbiol. Biotechnol.* **1999**, *51*, 422–430.
- [199] S. Y. Lee, *Trends Biotechnol.* **1996**, *14*, 98–105.
- [200] a) R. A. Reck, *J. Am. Oil Chem. Soc.* **1985**, *62*, 355–365; b) A. Hinzmann, H. Gröger, *Eur. J. Lipid Sci. Technol.* **2020**, *122*, 1900163; c) Z. S. Breitbach, C. A. Weatherly, R. M. Woods, C. Xu, G. Vale, A. Berthod, D. W. Armstrong, *J. Sep. Sci.* **2014**, *37*, 558–565.
- [201] L. R. Subramanian, "Introduction of the Cyano Group by Substitution of a Halogen" in *Science of Synthesis* (Ed.: S.-I. Murahashi), Georg Thieme Verlag, Stuttgart, **2004**.
- [202] A. Enferadi Kerenkan, F. Béland, T.-O. Do, *Catal. Sci. Technol.* **2016**, *6*, 971–987.
- [203] T. Voeste, H. Buchold, *J. Am. Oil Chem. Soc.* **1984**, *61*, 350–352.
- [204] M. Whittaker, D. Bergmann, D. Arciero, A. B. Hooper, *Biochim. Biophys. Acta* **2000**, *1459*, 346–355.
- [205] C. Plass, *Dissertation*, Bielefeld University, Bielefeld, **not published**.
- [206] a) D. Romano, R. Villa, F. Molinari, *ChemCatChem* **2012**, *4*, 739–749; b) W. Kroutil, H. Mang, K. Edegger, K. Faber, *Adv. Synth. Catal.* **2004**, *346*, 125–142.
- [207] M. Biermann, *Dissertation*, Bielefeld University, Bielefeld, **2016**.
- [208] R. L. Perlman, J. Wolff, *Science* **1968**, *160*, 317–319.
- [209] A. Weckbecker, W. Hummel, *Biocatal. Biotransfor.* **2006**, *24*, 380–389.
- [210] D. Bulut, N. Duangdee, H. Gröger, A. Berkessel, W. Hummel, *ChemBioChem* **2016**, *17*, 1349–1358.
- [211] B. Geueke, B. Riebel, W. Hummel, *Enzyme Microb. Technol.* **2003**, *32*, 205–211.
- [212] J. B. Jones, K. E. Taylor, *J. Chem. Soc., Chem. Commun.* **1973**, *2*, 205–206.
- [213] T. Okada, T. Asawa, Y. Sugiyama, T. Iwai, M. Kirihaara, Y. Kimura, *Tetrahedron* **2016**, *72*, 2818–2827.
- [214] M. Zhao, J. Li, E. Mano, Z. Song, D. M. Tschaen, E. J. J. Grabowski, P. J. Reider, *J. Org. Chem.* **1999**, *64*, 2564–2566.
- [215] J. Busch, *Master thesis*, Universität Bielefeld, Bielefeld, **2018**.
- [216] T. Nishimura, T. Onue, K. Ohe, S. Uemura, *Tetrahedron Lett.* **1998**, *39*, 6011–6014.
- [217] A. Hinzmann, S. Glinski, M. Worm, H. Gröger, *J. Org. Chem.* **2019**, *84*, 4867–4872.
- [218] C. Plass, A. Hinzmann, M. Terhorst, W. Brauer, K. Oike, H. Yavuzer, Y. Asano, A. J. Vorholt, T. Betke, H. Gröger, *ACS Catal.* **2019**, *9*, 5198–5203.
- [219] A. Hinzmann, *Dissertation*, Bielefeld University, Bielefeld, **not published**.

12 References

- [220] M. Stricker, *Dissertation*, Bielefeld University, Bielefeld, **not published**.
- [221] A. Hinzmann, M. Stricker, J. Busch, S. Glinski, K. Oike, H. Gröger, *Eur. J. Org. Chem.* **2020**, 2020, 2399–2408.
- [222] F. J. Gonzalez, K. R. Korzekwa, *Annu. Rev. Pharmacol. Toxicol.* **1995**, 35, 369–390.
- [223] S. Pflug, S. M. Richter, V. B. Urlacher, *J. Biotechnol.* **2007**, 129, 481–488.
- [224] J. H. Choi, S. J. Lee, S. J. Lee, S. Y. Lee, *Appl. Environ. Microbiol.* **2003**, 69, 4737–4742.
- [225] J.-D. Zhang, A.-T. Li, J.-H. Xu, *Bioprocess Biosyst. Eng.* **2010**, 33, 1043–1049.
- [226] T. Omura, R. Sato, *J. Biol. Chem.* **1964**, 239, 2370–2378.
- [227] R. S. Velur Selvamani, M. Telaar, K. Friehs, E. Flaschel, *Microb. Cell Fact.* **2014**, 13, 58.
- [228] N. Brechmann, V. Kaiser, *Internship report*, Bielefeld University, Bielefeld, **2017**.
- [229] a) T. H. Grossmann, E. S. Kawasaki, S. R. Punreddy, M. S. Osburne, *Gene* **1998**, 209, 95–103; b) S.-h. Pan, B. A. Malcolm, *Biotechniques* **2018**, 29, 1234–1237.
- [230] N. Mertens, E. Remaut, W. Fiers, *Nat. Biotechnol.* **1995**, 13, 175–179.
- [231] Kumar, P. K. R., Maschke, H.-E., K. Friehs, K. Schügerl, *Trends Biotechnol.* **1991**, 9, 279–284.
- [232] B. L. Nielsen, C. van Willis, C.-Y. Lin, *Biochem. Mol. Biol. Educ.* **2007**, 35, 133–137.
- [233] F. H. Arnold, *Angew. Chem. Int. Ed.* **2018**, 57, 4143–4148.
- [234] Michael S. Packer, David R. Liu, *Nat. Rev. Genet.* **2015**, 16, 379–394.
- [235] D. P. Nannemann, W. R. Birmingham, R. A. Scism, B. O. Bachmann, *Future Med. Chem.* **2011**, 3, 803–819.
- [236] S. Nakano, Y. Asano, *Sci. Rep.* **2015**, 5, 8193.
- [237] D. Matsui, S. Nakano, M. Dadashpour, Y. Asano, *Sci. Rep.* **2017**, 7, 9558.
- [238] V. Kery, D. Elleder, J. P. Kraus, *Arch. Biochem. Biophys.* **1995**, 316, 24–29.
- [239] K. Fiege, C. J. Querebillo, P. Hildebrandt, N. Frankenberg-Dinkel, *Biochemistry* **2018**, 57, 2747–2755.
- [240] J. J. Woodward, N. I. Martin, M. A. Marletta, *Nat. Methods* **2007**, 4, 43–45.
- [241] J. Sudhamsu, M. Kabir, M. V. Airola, B. A. Patel, S.-R. Yeh, D. L. Rousseau, B. R. Crane, *Prof. Expr. Purif.* **2010**, 73, 78–82.
- [242] S. Simm, J. Einloft, O. Mirus, E. Schleiff, *Biol. Res.* **2016**, 49, 31.
- [243] D. Eisenberg, E. Schwarz, M. Komaromy, R. Wall, *J. Mol. Biol.* **1984**, 179, 125–142.
- [244] D. M. Engelman, T. A. Steitz, A. Goldman, *Annu. Rev. Biophys. Biophys. Chem.* **1986**, 15, 321–353.
- [245] J. Kyte, R. F. Doolittle, *J. Mol. Biol.* **1982**, 157, 105–132.
- [246] T. P. Hoop, K. R. Woods, *Mol. Immunol.* **1983**, 20, 483–489.
- [247] J. Janin, *Nature* **1979**, 277, 491–492.

12 References

- [248] D. T. Jones, *J. Mol. Biol.* **1999**, *292*, 195–202.
- [249] D. W. A. Buchan, D. T. Jones, *Nucleic Acids Res.* **2019**, *47*, 402–407.
- [250] L. M. Siegel, M. J. Murphy, H. Kamin, *J. Biol. Chem.* **1973**, *248*, 251–264.
- [251] a) H. Shiraishi, M. Kataoka, Y. Morita, J. Umemoto, *Free Radic. Res. Commun.* **1993**, *19*, 315–321; b) A. E. Roush, M. Riaz, S. K. Misra, S. R. Weinberger, J. S. Sharp, *J. Am. Soc. Mass Spectrom.* **2020**, *31*, 169–172.
- [252] a) M. Salman, A. A. Issa, I. Sarairah, A. A. Abu-Yamin, *Jordan J. Chem.* **2016**, *11*, 85–98; b) S. Çakır, E. Biçerb, M. Odabaşoğlub, Ç. Albayarakb, *J. Braz. Chem. Soc.* **2005**, *15*, 711–717.
- [253] N. Good, S. Izawa, G. Hind, "Uncoupling and Energy Transfer Inhibition in Photophosphorylation" in *Current Topics in Bioenergetics* (Ed.: D. R. Sanadi), Academic Press Inc., New York, London, **1966**, 76–112.
- [254] B. H. Kipp, C. Faraj, G. Li, D. Njus, *Bioelectrochemistry* **2004**, *64*, 7–13.
- [255] R. Winkler, *Rapid Commun. Mass Spectrom.* **2010**, *24*, 285–294.
- [256] A. Rolfe, D. A. Probst, K. A. Volp, I. Omar, D. L. Flynn, P. R. Hanson, *J. Org. Chem.* **2008**, *73*, 8785–8790.
- [257] D. M. Hodgson, M. J. Fleming, S. J. Stanway, *J. Org. Chem.* **2007**, *72*, 4763–4773.
- [258] C.-X. Miao, L.-N. He, J.-L. Wang, F. Wu, *J. Org. Chem.* **2010**, *75*, 257–260.
- [259] J. C. Wong, G. Tang, X. Wu, C. Liang, Z. Zhang, L. Guo, Z. Peng, W. Zhang, X. Lin, Z. Wang et al., *J. Med. Chem.* **2012**, *55*, 8903–8925.
- [260] R. W. Taft, E. Price, I. R. Fox, I. C. Lewis, K. K. Andersen, G. T. Davis, *J. Am. Chem. Soc.* **1963**, *86*, 3146–3156.
- [261] J. Bourguignon, G. Le Nard, G. Queguiner, *Can. J. Chem.* **1985**, *63*, 2354–2361.
- [262] J. F. Schneider, M. B. Lauber, V. Muhr, D. Kratzer, J. Paradies, *Org. Biomol. Chem.* **2011**, *9*, 4323–4327.
- [263] J. Guin, G. Varseev, B. List, *J. Am. Chem. Soc.* **2013**, *135*, 2100–2103.
- [264] B. Ferreira-Silva, I. Lavandera, A. Kern, K. Faber, W. Kroutil, *Tetrahedron* **2010**, *66*, 3410–3414.
- [265] B. Gaspar, E. M. Carreira, *Angew. Chem. Int. Ed.* **2007**, *46*, 4519–4522.
- [266] S. Hameed, N. H. Rama, H. Duddeck, *J. Chem. Soc. Pak.* **2005**, *27*, 667–674.
- [267] M. Selva, C. A. Marques, P. Tundo, *J. Chem. Soc. Perkin Trans.* **1994**, 1323–1328.
- [268] M. M. Bradford, *Anal. Biochem.* **1976**, *72*, 248–254.
- [269] U. K. Laemmli, *Nature* **1979**, *227*, 680–685.

13 Appendix

Primers for polymerase chain reaction

Table 59. Primers used for the introduction of single mutations in the sequence of OxdB *via* PCR with wild-type or mutated pET22b-OxdB(C)6His as template DNA.

Entry	Mutation	Sequence (5' to 3')
1	I319E	Forward: GATATCGAGCTT GAAT ATGTCAACTGCCATC Reverse: GATGGCAGTTGACATAT TTC AAGCTCGATATC
2	I226Q	Forward: GACCCTC CAA AAAGCGAATACGTTTC Reverse: GAAACGTATTCGCTTT TTG GAGGGTC
3	L220E	Forward: CGTATATAGG GAAG TGGAACCGACCCTC Reverse: GAGGGTCGGTCCACT TTC TCCTATATACG
4	V149E	Forward: GTACCGATCAAGCATACAGA AGAG CATGAATATTG Reverse: CAATATTCATG CTC TTCTGTATGCTTGATCGGTAC
5	I105R	Forward: GTCGGGTAAAA AGAG ATGAAAATAGTCCAATC Reverse: GATTGGACTATTTTCATC TCT TTTTTTTACCCGAC
6	L267R	Forward: GTGTCATCGGATATTAT CGCT CCATGG Reverse: CCATGG GCG ATAATATCCGATGACAC
7	I316Q	Forward: CAATCCAAAGAT CAG GAGCTTATCTATGTCAAC Reverse: GTTGACATAGATAAGCTC CTG ATCTTTGGATTG
8	I180A	Forward: CTTCAATTACCGGAACCC GCT GTCC Reverse: GGAC AGC GGGTCCGGTAATTGAAG
9	L65H	Forward: CATGTGGATCGAGCC CAC CATCAAG Reverse: CTTGAT GTG GGCTCGATCCACATG
10	V262G	Forward: CATGT GGC ATCGGATATTATCTCTCCATG Reverse: CATGGAGAGATAATATCCGAT GCC ACATG
11	E317L	Forward: CCAAAGATATC CTG CTTATCTATGTCAACTGCC Reverse: GGCAGTTGACATAGATAAG CAG GATATCTTTGG
12	K190R	Forward: CTTTCGGAAAACGGCTA AGA GTACAG Reverse: CGTGACT TCT TAGCCGTTTTCCGAAAG
13	D135L	Forward: GAGAAAATTAC CTA AATGGGGTTTCACACTTTGTAC Reverse: GTACAAAGTGTGAAACCCCAT TAG GTAATTTTCTC
14	Q67T	Forward: CTTGCAT ACA GGAGCCGATGGATAC Reverse: GTATCCATCGGCTC TGT ATGCAAGG
15	K49V	Forward: CATTGGGAATGATG GTA AAGAGTTTCGATTTG Reverse: CAAATCGAAACTCTT TACC ATCATTCCCAAATG

13 Appendix

16	R63L	Forward: CAAACATGTGGAT CTAG CCTTGCATCAAG Reverse: CTTGATGCAAGGCT TAG ATCCACATGTTTG
17	H296L	Forward: GTTGAAAAGG CTT GATTTTAAGACCGAACTTG Reverse: CAAGTTCGGTCTTAAAATC AAG CCTTTTCAAC
18	N229M	Forward: CTCATAAAAGCG ATG ACGTTTCTTCGTG Reverse: CACGAAGAAACGT CAT CGCTTTTATGAG
19	Q250I	Forward: CTATGAA ATC ACCCATGACGGCGAAATAG Reverse: CTATTTGCGCGTCATGGGT GAT TTTCATAG
20	K283L	Forward: GATCATCCAACACAT TTAG GCGATCTACGG Reverse: CCGTAGATCGCT TAA ATGTGTTGGATGATC

Gene and amino acid sequences

L-Amino acid oxidase

hcLAAO4(N)6His: L-Amino acid oxidase from *Hebeloma cylindrosporum* in pET22b with N-terminal hexahistidine-tag (codon optimized for expression in *P. pastoris*)^[184]

Gene

ATGGGCAGCAGCCATCATCATCATCACAGCAGCGGCCTGGTGCCGCGCGGCAGC
 CATATGGCTGACACTACTTCCGTTCCATTCGACGCTGAATCCAGAGATCAGATTTTCCAG
 CACCACGCTAGATCCGTTATCTCCGTTACACTAACACTTTGGGTGAGAAGAACATCTC
 TGTTCCATCTTCTCCACCAGGTGGTGAGAGAGTTGGTATTTTGGGAGCTGGTATCGGTG
 GTTTGTACTCCGCTTTGATCTTGACGCTTTGGACGTTCCCTTCGAGATCATCGAGGCTT
 CCAACAGAGTTGGTGGTAGATTGTTCACTCACAAGTTCCCAAACGGTGGTAAGTACGAC
 TACTACGACGTTGGTGCTATGAGATACCCATTGCCAAAGTCTGACGACAAGGGTAAC
 CCAGCCAGGTGTTATGCAAAGAGTTGGTCAGTTGTTCACTTACTTGGGTATGCACAAGC
 AGTTGATCCCTTACTACTTCAAGTCCAACAAGTCCCCAGGTTTCCAGTACTTCAACGGTG
 TTAGAGCTAGAATCGGTGAGGGTTCATCTTTCGATGCTCCAGCTTTGGGTATCAACTCC
 TCCTTGATTGACATCGGTGTTACTAAGATCGTTAATGACGCTGTTGGTCCATTCGCTCAG
 GCTTTGTTTGACGACTTGCAGAAGCACACTACTACTGGTTGGGACGACATGATGAAGAA
 CGACGCTTACTCCACTAGATCCTACTTCTCATTCAAGTATTTGCCATCCCCATCCTTCGG
 TTTGCCATCTGAACACTTCTCCACAAGAGTTATCAACTGGTTGGAGACTTTGACAAGTC
 CACTGGATGGTACGACAGAGGTTTACTGAGACTGTTTTGGAGGCTATCGCTTTCGGTG
 AAGTTGGTGATGGTGAGGTTGATTGGAGATGTATTGACGGTGGTTCCACGTTTTGCCA
 GACACTATTGCTGCTTCTTGCACAAGAAGGGTGGTAACGCTTTCGTTATGAACGCTTC
 CGTTACTGCTATCGGTTTGGAGAACCCAAACAAGAGGACTCCCCAATGGTTGTTGTTG
 CTGGTGGTCAGAAAAGAAAGTACTCCCACGTTATTTCCACTTTGCCATTGCCAGTTTTGA
 GAACAGTTGACTTGAAGAACTCCAAGTTGGACATCGTTCAGTCCAACGCTTTGAGAAAA
 TTGCAGTACGGTCCATCCATCAAGATCGGTATCTTGTTCAAAGAACCTTGGTGGACTACT
 GGTCAGGACAAGAACGGTGAAAAGTTCGACTTGGTTGGTGGACAGTCTACACTGACTT
 GCCAATCAGAACTGTTGTTTACCCATCCTACGGTGTTAACACTAACGCTCCATCCAATAC
 TTTGATCGCTTCTACTGTTGGACAAACGACGCTGAGAGAATGGGTTCCCTTGATCGGTA
 CTGGTAAGAAAACCTTACGAGGAACAGTTGGAGCACTTGGTTTTGTCTAACTTGGCTGCT
 GTTCAACAACACTGACTACCAGTACTTGAAGGACAGATTGGTTGACGTTCACTCCTGGGA
 TTGGAACCACAACCCATTGACTATGGGTGCTTTCGCTTTTTTTCGGTCCAGGTGACTTCCA
 GGACTTGTACACTTCTTGAACAGACCAGCTGCTAACGGAAAGTTGCACTTTGCTGGTG
 AAGCTTTGTCCGTTAGACACGCTTGGGTTGTTGGTGCTTTGGATTCTGCTTGGAGAGCT
 GTTTACAACACTTGTACGTTACTGACCCAGCTAAGTTGCCTAAGTTCTTCGAGTTGTGG
 GGTAAGAACGCTGAGTGGTTTGAACAACCAGGTGACGGTAAAGAGCCAAACTCTGACA
 ACTCCTTGTTGGAGAAATTCGTTAGAAGAACTCACGGTACTGTTTCCGTTTAA

Amino acids (629 AS, 69.6 kDa)

MGSSHHHHHHSSGLVPRGSHMADTTSPFDAESRDQIFQHHARSVISGYTNTLGEKNISVP
 SSPPGGERV GILGAGIGGLYSALILQSLDVPFEIIEASNRVGGRLFTHKFPNGGKYDYDVGA
 MRYPLPKSDDKGNYPGVMQRVGQLFTYLGMHKQLIPYYFKSNKSPGFQYFNGVRARIGE
 GSSFDAPALGINSSLIDIGVTKIVNDAVGPFAQALFDDLQKHTTTGWDDMMKNDAYSTRSYF
 SFKYLPSPSFGLPSEHFSTRVINWLETDFDKSTGWYDRGLTETVLEAIAFGEVGDGEVDWRCI
 DGGSHVLPDTIAAFLHKKGGNAFVMNASVTAIGLENPNKEDSPMVVVAGGQKRKYSHVIST
 LPLPVLRTVDLKNKSLDIVQSNALRKLQYGPSIKIGILFKEPWWTTGQDKNGEKFDLVGGQS
 YTDLPVRTVYPSYGVNTNAPSNTLIASYCWTNDAERMGLIGTGKKTYEEQLEHLVLSNLA
 AVHNTDYQYLKDRLDVHSDWNHNPLTMGAFAFFGPGDFQDLYTSLNRPAANGKLHFA
 GEALSVRHAWVVGALDSAWRAVYNYLYVTDPAKLPKFFELWGKNAEWFEQPGDGKEPNS
 DNSLLEKFVRRTHGTVSV

Aldoxime dehydratase

OxdA(C)6His: Aldoxime dehydratase from *Pseudomonas chloraphis* B23 in pET28b with a C-terminal hexahistidine-tag (based on GeneBank: AB093544.1, Uniprot: Q7WSJ4; codon optimized for expression in *E. coli*).

Gene

ATGGAAGCGCAATTGATACCCATCTGAAATGTCCGCGTACCCTGAGCCGTCGTGTTCC
 GGAAGAATATCAGCCTCCGTTTCCGATGTGGGTTGCACGTGCCGATGAACAGCTGCAG
 CAGGTTGTTATGGGTTATCTGGGTGTTGAGTATCGTGGTGAAGCACAGCGTGAAGCAGC
 ACTGCAGGCAATGCGTCATATTGTTAGCAGCTTTAGCCTGCCGGATGGTCCGCAGACC
 CATGATCTGACCCATCATAACCGATAGCAGCGGTTTTGATAATCTGATGGTTGTGGGTTAT
 TGAAAGATCCGGCAGCACATTGTCGTTGGCTGCGTAGTGCCGAAGTTAATGATTGGTG
 GACCAGCCAGGATCGTCTGGGTGAAGGTCTGGGTTATTTTCGTGAAATTAGCGCACCG
 CGTGCAGAACAGTTTGAACCCTGTATGCATTTTCAGGATAATCTGCCTGGTGTGGTGC
 AGTTATGGATAGCACCAGCGGTGAAATTGAAGAACATGGTTATTGGGGTAGCATGCGTG
 ATCGTTTTCCGATTAGCCAGACCGATTGGATGAAACCGACCAATGAACTGCAGGTTGTT
 GCCGGTGATCCGGCAAAGGTGGTCGTGTTGTTATTATGGGTCATGATAACATTGCACT
 GATTCGTAGCGGTCAGGATTGGGCAGATGCAGAAGCAGAAGAACGTAGCCTGTATCTG
 GATGAAATTCTGCCGACCCTGCAGGATGGTATGGATTTTCTGCGTGATAATGGTCAGCC
 GCTGGGTTGTTATAGCAATCGTTTTGTTGTAATATCGATCTGGATGGCAATTTTCTGGA
 TGTGAGCTATAACATTGGTCATTGGCGTAGCCTGGAAAACTGGAACGTTGGGCAGAAA
 GCCATCCGACCCATCTGCGTATTTTTGTTACCTTTTTTCGTGTTGCAGCCGGTCTGAAAA
 AACTGCGTCTGTATCATGAAGTTAGCGTGAGTGATGCAAAAAGCCAGGTGTTTGAATAT
 ATCAACTGTCATCCGCATACCGGCATGCTGCGTGATGCAGTTGTTGCACCGACCAAGCT
 TGCGGCCGCACTCGAGCACCACCACCACCACCTGACTCGAGCACCACCACCACCAC
 CACTGAGATCCGGCTGCTAACAAAGCCCGAAAGAAGTTTTTT

Amino acids (352 AS, 40.1 kDa)

MESAIDTHLKCPRTLSRRVPEEYQPPFPMWVARADEQLQQVVMGYLGVQYRGEAQREAL
 QAMRHIVSSFLPDGPQTHDLTHHTDSSGFDNLMVVGWYKDPAAHCRWLRSAEVNDWWT
 SQDRLGEGLYFREISAPRAEQFETLYAFQDNLPVGVAVMDSTSGEIEEHGYWGSMDRF
 PISQTDWMKPTNELQVVAGDPAKGRVIMGHDNIALIRSGQDWADAEAEERSLYLDEILPT
 LQDGMDFLRDNGQPLGCYSNRFVRNIDLGNFLDVSYNIGHWRSLEKLERWAESHPTHLRI
 FVTFFRVAAGLKKLRLYHEVSVSDAKSQVFYINCHPHTGMLRDAVVAPTLEHHHHHH

OxdB: Aldoxime dehydratase from *Bacillus* sp. OxB-1 in pUC18 (Gene Bank: AB028892.1, UniProt: P82604)^[162]

Gene (start codon changed from TTG to ATG)

ATGAAAAATATGCCGGAAAATCACAATCCACAAGCGAATGCCTGGACTGCCGAATTTCC
 TCCTGAAATGAGCTATGTAGTATTTGCGCAGATTGGGATTCAAAGCAAGTCTTTGGATCA
 CGCAGCGGAACATTTGGGAATGATGAAAAAGAGTTTCGATTTGCGGACAGGCCCCAAA
 CATGTGGATCGAGCCTTGCATCAAGGAGCCGATGGATACCAAGATTCCATCTTTTTAGC
 CTACTGGGATGAGCCTGAAACATTTAAATCATGGGTTGCGGATCCTGAAGTACAAAAGT
 GGTGGTCGGGTAAAAAATCGATGAAAATAGTCCAATCGGGTATTGGAGTGAGGTAACG
 ACCATTCCGATTGATCACTTTGAGACTCTTCATTCCGGAGAAAATTACGATAATGGGGTT
 TCACACTTTGTACCGATCAAGCATAACAGAAGTCCATGAATATTGGGGAGCAATGCCGGA
 CCGCATGCCGGTGTCTGCCAGTAGTGATTTGGAAAGCCCCCTTGGCCTTCAATTACCG
 GAACCCATTGTCCGGGAGTCTTTCCGAAAACGGCTAAAAGTCACGGCGCCGGATAATAT

TTGCTTGATTCTGAACCGCTCAAAATTGGTCTAAATGTGGTAGCGGGGAAAGGGAAACGT
 ATATAGGACTAGTGGAACCGACCCTCATAAAAGCGAATACGTTTCTTCGTGAAAATGCTA
 GTGAAACAGGCTGTATTAGTTCAAAATTAGTCTATGAACAGACCCATGACGGCGAAATA
 GTAGATAAATCATGTGTCATCGGATATTATCTCTCCATGGGGCATCTTGAACGCTGGAC
 GCATGATCATCCAACACATAAAGCGATCTACGGAACCTTTTATGAGATGTTGAAAAGGCA
 TGATTTTAAGACCGAACTTGCTTTATGGCACGAGGTTTCGGTGCTTCAATCCAAAGATAT
 CGAGCTTATCTATGTCAACTGCCATCCGAGTACTGGATTTCTTCCATTCTTTGAAGTGAC
 AGAAATTCAAGAGCCTTTACTGAAAAGCCCTAGCGTCAGGATCCAGTGA

Amino acids (351 AS, 40.2 kDa)

MKNMPENHNPQANAWTAEFPPEMSYVVFQAQIGIQSKSLDHAAEHLGMMKKSFDLRTGPKH
 VDRALHQGADGYQDSIFLAYWDEPETFKSWVADPEVQKWWSGKKIDENSPIGYWSEVTTI
 PIDHFETLHSGENYDNGVSHFVPIKHTEVHEYWGAMRDRMPVSASSDLESPLGLQLPEPIV
 RESFGKRLKVTAPDNI LIRTAQNWSKCGSGERETYIGLVEPTLIKANTFLRENASETGCISS
 KLVYEQTHDGEIVDKSCVIGYYLSMGHLERWTHDHPHKAIYGTIFYEMLKRHDFKTELALW
 HEVSVLQSKDIELIYVNCHPSTGFLPFFEVEIQEPLLKSPSVRIQ

OxdB(C)6His: Aldoxime dehydratase from *Bacillus* sp. OxB-1 in pET22b with a C-terminal hexahistidine-tag

Gene (359 AS, 41.2 kDa)

ATGAAAAATATGCCGGAAAATCACAATCCACAAGCGAATGCCTGGACTGCCGAATTTCC
 TCCTGAAATGAGCTATGTAGTATTTGCGCAGATTGGGATTCAAAGCAAGTCTTTGGATCA
 CGCAGCGGAACATTTGGGAATGATGAAAAAGAGTTTCGATTTGCGGACAGGCCCCAAA
 CATGTGGATCGAGCCTTGCATCAAGGAGCCGATGGATACCAAGATTCCATCTTTTTAGC
 CTACTGGGATGAGCCTGAAACATTTAAATCATGGGTTGCGGATCCTGAAGTACAAAAGT
 GGTGGTCGGGTAAAAAATCGATGAAAATAGTCCAATCGGGTATTGGAGTGAGGTAACG
 ACCATTCCGATTGATCACTTTGAGACTCTTCATTCCGGAGAAAATTACGATAATGGGGTT
 TCACACTTTGTACCGATCAAGCATAACAGAAGTCCATGAATATTGGGGAGCAATGCGCGA
 CCGCATGCCGGTGTCTGCCAGTAGTGATTTGGAAAGCCCCCTTGGCCTTCAATTACCG
 GAACCCATTGTCCGGGAGTCTTTTCGGAAAACGGCTAAAAGTCACGGCGCCGGATAATAT
 TTGCTTGATTCTGAACCGCTCAAAATTGGTCTAAATGTGGTAGCGGGGAAAGGGAAACGT
 ATATAGGACTAGTGGAACCGACCCTCATAAAAGCGAATACGTTTCTTCGTGAAAATGCTA
 GTGAAACAGGCTGTATTAGTTCAAAATTAGTCTATGAACAGACCCATGACGGCGAAATA
 GTAGATAAATCATGTGTCATCGGATATTATCTCTCCATGGGGCATCTTGAACGCTGGAC
 GCATGATCATCCAACACATAAAGCGATCTACGGAACCTTTTATGAGATGTTGAAAAGGCA
 TGATTTTAAGACCGAACTTGCTTTATGGCACGAGGTTTCGGTGCTTCAATCCAAAGATAT
 CGAGCTTATCTATGTCAACTGCCATCCGAGTACTGGATTTCTTCCATTCTTTGAAGTGAC
 AGAAATTCAAGAGCCTTTACTGAAAAGCCCTAGCGTCAGGATCCAGCTCGAGCACCACC
 ACCACCACCACTGAGATCCGGCTGCTAACAAAGCCCGAAAGAAGTTTTTT

Amino acids

MKNMPENHNPQANAWTAEFPPEMSYVVFQAQIGIQSKSLDHAAEHLGMMKKSFDLRTGPKH
 VDRALHQGADGYQDSIFLAYWDEPETFKSWVADPEVQKWWSGKKIDENSPIGYWSEVTTI
 PIDHFETLHSGENYDNGVSHFVPIKHTEVHEYWGAMRDRMPVSASSDLESPLGLQLPEPIV
 RESFGKRLKVTAPDNI LIRTAQNWSKCGSGERETYIGLVEPTLIKANTFLRENASETGCISS
 KLVYEQTHDGEIVDKSCVIGYYLSMGHLERWTHDHPHKAIYGTIFYEMLKRHDFKTELALW
 HEVSVLQSKDIELIYVNCHPSTGFLPFFEVEIQEPLLKSPSVRIQLEHHHHHH

OxdB(C)6His_I319E (M1):

Amino acids

MKNMPENHNPQANAWTAEFPPEMSYVVFAQIGIQSKSLDHAAEHLGMMKKSFDLRTGPKH
VDRALHQQADGYQDSIFLAYWDEPETFKSWVADPEVQKWWSGKKIDENSPIGYWSEVTTI
PIDHFETLHSGENYDNGVSHFVPIKHTEVHEYWGAMRDRMPVSASSDLESPLGLQLPEPIV
RESFGKRLKVTAPDNICLIRTAQNWSKCGSGERETYIGLVEPTLIKANTFLRENASETGCISS
KLVYEQTHDGEIVDKSCVIGYYLSMGHLERWTHDHPHKAHYGTFYEMLKRHDFKTELALW
HEVSVLQSKDIELEYVNCHPSTGFLPFFEVEIQEPLLKSPSVRIQLEHHHHHH

OxdB(C)6His_I226Q (M2):

Amino acids

MKNMPENHNPQANAWTAEFPPEMSYVVFAQIGIQSKSLDHAAEHLGMMKKSFDLRTGPKH
VDRALHQQADGYQDSIFLAYWDEPETFKSWVADPEVQKWWSGKKIDENSPIGYWSEVTTI
PIDHFETLHSGENYDNGVSHFVPIKHTEVHEYWGAMRDRMPVSASSDLESPLGLQLPEPIV
RESFGKRLKVTAPDNICLIRTAQNWSKCGSGERETYIGLVEPTLQKANTFLRENASETGCISS
KLVYEQTHDGEIVDKSCVIGYYLSMGHLERWTHDHPHKAHYGTFYEMLKRHDFKTELALW
HEVSVLQSKDIELIYVNCHPSTGFLPFFEVEIQEPLLKSPSVRIQLEHHHHHH

OxdB(C)6His_L220E (M3):

Amino acids

MKNMPENHNPQANAWTAEFPPEMSYVVFAQIGIQSKSLDHAAEHLGMMKKSFDLRTGPKH
VDRALHQQADGYQDSIFLAYWDEPETFKSWVADPEVQKWWSGKKIDENSPIGYWSEVTTI
PIDHFETLHSGENYDNGVSHFVPIKHTEVHEYWGAMRDRMPVSASSDLESPLGLQLPEPIV
RESFGKRLKVTAPDNICLIRTAQNWSKCGSGERETYIGEVEPTLIKANTFLRENASETGCISS
KLVYEQTHDGEIVDKSCVIGYYLSMGHLERWTHDHPHKAHYGTFYEMLKRHDFKTELALW
HEVSVLQSKDIELIYVNCHPSTGFLPFFEVEIQEPLLKSPSVRIQLEHHHHHH

OxdB(C)6His_V149E (M4):

Amino acids

MKNMPENHNPQANAWTAEFPPEMSYVVFAQIGIQSKSLDHAAEHLGMMKKSFDLRTGPKH
VDRALHQQADGYQDSIFLAYWDEPETFKSWVADPEVQKWWSGKKIDENSPIGYWSEVTTI
PIDHFETLHSGENYDNGVSHFVPIKHTEEHEYWGAMRDRMPVSASSDLESPLGLQLPEPIV
RESFGKRLKVTAPDNICLIRTAQNWSKCGSGERETYIGLVEPTLIKANTFLRENASETGCISS
KLVYEQTHDGEIVDKSCVIGYYLSMGHLERWTHDHPHKAHYGTFYEMLKRHDFKTELALW
HEVSVLQSKDIELIYVNCHPSTGFLPFFEVEIQEPLLKSPSVRIQLEHHHHHH

OxdB(C)6His_I105R (M5):

Amino acids

MKNMPENHNPQANAWTAEFPPEMSYVVFAQIGIQSKSLDHAAEHLGMMKKSFDLRTGPKH
VDRALHQQADGYQDSIFLAYWDEPETFKSWVADPEVQKWWSGKKRDENSPIGYWSEVTTI
PIDHFETLHSGENYDNGVSHFVPIKHTEVHEYWGAMRDRMPVSASSDLESPLGLQLPEPIV

RESFGKRLKVTAPDNICLIRTAQNWSKCGSGERETYIGLVEPTLIKANTFLRENASETGCISS
KLVYEQTHDGEIVDKSCVIGYYLSMGHLERWTHDHPHKAHYGTFYEMLKRHDFKTELALW
HEVSVLQSKDIELIYVNCHPSTGFLPFFEVEIQEPLLKSPSVRIQLEHHHHHH

OxdB(C)6His_L267R (M6):

Amino acids

MKNMPENHNPQANAWTAEFPPPEMSYVVFAQIGIQSKSLDHAAEHLGMMKKSFDLRTGPKH
VDRALHQGADGYQDSIFLAYWDEPETFKSWVADPEVQKWWSGKKIDENSPIGYWSEVTTI
PIDHFETLHSGENYDNGVSHFVPIKHTEVHEYWGAMRDRMPVSASSDLESPLGLQLPEPIV
RESFGKRLKVTAPDNICLIRTAQNWSKCGSGERETYIGLVEPTLIKANTFLRENASETGCISS
KLVYEQTHDGEIVDKSCVIGYYRSMGHLEWTHDHPHKAHYGTFYEMLKRHDFKTELALW
HEVSVLQSKDIELIYVNCHPSTGFLPFFEVEIQEPLLKSPSVRIQLEHHHHHH

OxdB(C)6His_I316Q (M7):

Amino acids

MKNMPENHNPQANAWTAEFPPPEMSYVVFAQIGIQSKSLDHAAEHLGMMKKSFDLRTGPKH
VDRALHQGADGYQDSIFLAYWDEPETFKSWVADPEVQKWWSGKKIDENSPIGYWSEVTTI
PIDHFETLHSGENYDNGVSHFVPIKHTEVHEYWGAMRDRMPVSASSDLESPLGLQLPEPIV
RESFGKRLKVTAPDNICLIRTAQNWSKCGSGERETYIGLVEPTLIKANTFLRENASETGCISS
KLVYEQTHDGEIVDKSCVIGYYLSMGHLERWTHDHPHKAHYGTFYEMLKRHDFKTELALW
HEVSVLQSKDQELIYVNCHPSTGFLPFFEVEIQEPLLKSPSVRIQLEHHHHHH

OxdB(C)6His_I180A (M8):

Amino acids

MKNMPENHNPQANAWTAEFPPPEMSYVVFAQIGIQSKSLDHAAEHLGMMKKSFDLRTGPKH
VDRALHQGADGYQDSIFLAYWDEPETFKSWVADPEVQKWWSGKKIDENSPIGYWSEVTTI
PIDHFETLHSGENYDNGVSHFVPIKHTEVHEYWGAMRDRMPVSASSDLESPLGLQLPEPAV
RESFGKRLKVTAPDNICLIRTAQNWSKCGSGERETYIGLVEPTLIKANTFLRENASETGCISS
KLVYEQTHDGEIVDKSCVIGYYLSMGHLERWTHDHPHKAHYGTFYEMLKRHDFKTELALW
HEVSVLQSKDIELIYVNCHPSTGFLPFFEVEIQEPLLKSPSVRIQLEHHHHHH

OxdB(C)6His_L65H (M9):

Amino acids

MKNMPENHNPQANAWTAEFPPPEMSYVVFAQIGIQSKSLDHAAEHLGMMKKSFDLRTGPKH
VDRAHHHQGADGYQDSIFLAYWDEPETFKSWVADPEVQKWWSGKKIDENSPIGYWSEVTTI
PIDHFETLHSGENYDNGVSHFVPIKHTEVHEYWGAMRDRMPVSASSDLESPLGLQLPEPIV
RESFGKRLKVTAPDNICLIRTAQNWSKCGSGERETYIGLVEPTLIKANTFLRENASETGCISS
KLVYEQTHDGEIVDKSCVIGYYLSMGHLERWTHDHPHKAHYGTFYEMLKRHDFKTELALW
HEVSVLQSKDIELIYVNCHPSTGFLPFFEVEIQEPLLKSPSVRIQLEHHHHHH

OxdB(C)6His_V262G (M10):

Amino acids

MKNMPENHNPQANAWTAEFPPEMSYVVFAQIGIQSKSLDHAAEHLGMMKKSFDLRTGPKH
VDRALHQGADGYQDSIFLAYWDEPETFKSWVADPEVQKWWWSGKKIDENSPIGYWSEVTTI
PIDHFETLHSGENYDNGVSHFVPIKHTEVHEYWGAMRDRMPVSASSDLESPLGLQLPEPIV
RESFGKRLKVTAPDNI^GLIRTAQNWSKCGSGERETYIGLVEPTLIKANTFLRENASETGCISS
KLVYEQTHDGEIVDKSCVIGYYLSMGHLERWTHDHP^GTHKAIYGTFYEMLKRHDFKTELALW
HEVSVLQSKDIELIYVNCHPSTGFLPFFEVEIQEPLLKSPSVRIQLEHHHHHH

OxdB(C)6His_E317L (M11):

Amino acids

MKNMPENHNPQANAWTAEFPPEMSYVVFAQIGIQSKSLDHAAEHLGMMKKSFDLRTGPKH
VDRALHQGADGYQDSIFLAYWDEPETFKSWVADPEVQKWWWSGKKIDENSPIGYWSEVTTI
PIDHFETLHSGENYDNGVSHFVPIKHTEVHEYWGAMRDRMPVSASSDLESPLGLQLPEPIV
RESFGKRLKVTAPDNI^LLIRTAQNWSKCGSGERETYIGLVEPTLIKANTFLRENASETGCISS
KLVYEQTHDGEIVDKSCVIGYYLSMGHLERWTHDHP^LTHKAIYGTFYEMLKRHDFKTELALW
HEVSVLQSKDIL^LLIYVNCHPSTGFLPFFEVEIQEPLLKSPSVRIQLEHHHHHH

OxdB(C)6His_K190R (M12):

Amino acids

MKNMPENHNPQANAWTAEFPPEMSYVVFAQIGIQSKSLDHAAEHLGMMKKSFDLRTGPKH
VDRALHQGADGYQDSIFLAYWDEPETFKSWVADPEVQKWWWSGKKIDENSPIGYWSEVTTI
PIDHFETLHSGENYDNGVSHFVPIKHTEVHEYWGAMRDRMPVSASSDLESPLGLQLPEPIV
RESFGKRL^RVTAPDNI^LLIRTAQNWSKCGSGERETYIGLVEPTLIKANTFLRENASETGCISS
KLVYEQTHDGEIVDKSCVIGYYLSMGHLERWTHDHP^RTHKAIYGTFYEMLKRHDFKTELALW
HEVSVLQSKDIELIYVNCHPSTGFLPFFEVEIQEPLLKSPSVRIQLEHHHHHH

OxdB(C)6His_D135L (M13):

Amino acids

MKNMPENHNPQANAWTAEFPPEMSYVVFAQIGIQSKSLDHAAEHLGMMKKSFDLRTGPKH
VDRALHQGADGYQDSIFLAYWDEPETFKSWVADPEVQKWWWSGKKIDENSPIGYWSEVTTI
PIDHFETLHSGENY^LNGVSHFVPIKHTEVHEYWGAMRDRMPVSASSDLESPLGLQLPEPIV
ESFGKRLKVTAPDNI^LLIRTAQNWSKCGSGERETYIGLVEPTLIKANTFLRENASETGCISSKL
VYEQTHDGEIVDKSCVIGYYLSMGHLERWTHDHP^LTHKAIYGTFYEMLKRHDFKTELALWHE
VSVLQSKDIELIYVNCHPSTGFLPFFEVEIQEPLLKSPSVRIQLEHHHHHH

OxdB(C)6His_Q67T (M14):

Amino acids

MKNMPENHNPQANAWTAEFPPEMSYVVFAQIGIQSKSLDHAAEHLGMMKKSFDLRTGPKH
VDRALH^TTGADGYQDSIFLAYWDEPETFKSWVADPEVQKWWWSGKKIDENSPIGYWSEVTTIP

IDHFETLHSGENYDNGVSHFVPIKHTEVHEYWGAMRDRMPVSASSDLESPLGLQLPEPIVR
ESFGKRLKVTAPDNI~~CLIR~~TAQNWSKCGSGERETYIGLVEPTLIKANTFLRENA~~SETGC~~ISSKL
VYEQTHDGEIVDKSCVIGYYLSMGHLERWTHDHP~~THKAI~~YGTFYEM~~LKR~~HDFKTELALWHE
VSVLQSKDIELIYVNCHPSTGFLPFFE~~VTEIQE~~PLLKSPSVRIQLEHHHHHH

OxdB(C)6His_K49V (M15):

Amino acids

MKNMPENHNPQANAWTAEFPP~~EMSY~~VVFAQIGIQSKSLDHAAEHLGMMVKSFDLRTGPKH
VDRALHQQGADGYQDSIFLAYWDEPETFKSWVADPEVQKWWSGKKIDENSPIGYWSEVTTI
PIDHFETLHSGENYDNGVSHFVPIKHTEVHEYWGAMRDRMPVSASSDLESPLGLQLPEPIV
RESFGKRLKVTAPDNI~~CLIR~~TAQNWSKCGSGERETYIGLVEPTLIKANTFLRENA~~SETGC~~ISS
KLVYEQTHDGEIVDKSCVIGYYLSMGHLERWTHDHP~~THKAI~~YGTFYEM~~LKR~~HDFKTELALW
HEVSVLQSKDIELIYVNCHPSTGFLPFFE~~VTEIQE~~PLLKSPSVRIQLEHHHHHH

OxdB(C)6His_R63L (M16):

Amino acids

MKNMPENHNPQANAWTAEFPP~~EMSY~~VVFAQIGIQSKSLDHAAEHLGMMKKSFDLRTGPKH
VDLALHQQGADGYQDSIFLAYWDEPETFKSWVADPEVQKWWSGKKIDENSPIGYWSEVTTIP
IDHFETLHSGENYDNGVSHFVPIKHTEVHEYWGAMRDRMPVSASSDLESPLGLQLPEPIVR
ESFGKRLKVTAPDNI~~CLIR~~TAQNWSKCGSGERETYIGLVEPTLIKANTFLRENA~~SETGC~~ISSKL
VYEQTHDGEIVDKSCVIGYYLSMGHLERWTHDHP~~THKAI~~YGTFYEM~~LKR~~HDFKTELALWHE
VSVLQSKDIELIYVNCHPSTGFLPFFE~~VTEIQE~~PLLKSPSVRIQLEHHHHHH

OxdB(C)6His_H296L (M17):

Amino acids

MKNMPENHNPQANAWTAEFPP~~EMSY~~VVFAQIGIQSKSLDHAAEHLGMMKKSFDLRTGPKH
VDRALHQQGADGYQDSIFLAYWDEPETFKSWVADPEVQKWWSGKKIDENSPIGYWSEVTTI
PIDHFETLHSGENYDNGVSHFVPIKHTEVHEYWGAMRDRMPVSASSDLESPLGLQLPEPIV
RESFGKRLKVTAPDNI~~CLIR~~TAQNWSKCGSGERETYIGLVEPTLIKANTFLRENA~~SETGC~~ISS
KLVYEQTHDGEIVDKSCVIGYYLSMGHLERWTHDHP~~THKAI~~YGTFYEM~~LKR~~LDFKTELALWH
EVSVLQSKDIELIYVNCHPSTGFLPFFE~~VTEIQE~~PLLKSPSVRIQLEHHHHHH

OxdB(C)6His_N229M (M18):

Amino acids

MKNMPENHNPQANAWTAEFPP~~EMSY~~VVFAQIGIQSKSLDHAAEHLGMMKKSFDLRTGPKH
VDRALHQQGADGYQDSIFLAYWDEPETFKSWVADPEVQKWWSGKKIDENSPIGYWSEVTTI
PIDHFETLHSGENYDNGVSHFVPIKHTEVHEYWGAMRDRMPVSASSDLESPLGLQLPEPIV
RESFGKRLKVTAPDNI~~CLIR~~TAQNWSKCGSGERETYIGLVEPTLIKAMTFLRENA~~SETGC~~ISS
KLVYEQTHDGEIVDKSCVIGYYLSMGHLERWTHDHP~~THKAI~~YGTFYEM~~LKR~~HDFKTELALW
HEVSVLQSKDIELIYVNCHPSTGFLPFFE~~VTEIQE~~PLLKSPSVRIQLEHHHHHH

OxdB(C)6His_Q250I (M19):

Amino acids

MKNMPENHNPQANAWTAEFPPEMSYVVFAQIGIQSKSLDHAAEHLGMMKKSFDLRTGPKH
VDRALHQGADGYQDSIFLAYWDEPETFKSWVADPEVQKWWSGKKIDENSPIGYWSEVTTI
PIDHFETLHSGENYDNGVSHFVPIKHTEVHEYWGAMRDRMPVSASSDLESPLGLQLPEPIV
RESFGKRLKVTAPDNI~~L~~IRTAQNWSKCGSGERETYIGLVEPTLIKANTFLRENASETGCISS
KLVYEI~~T~~HDGEIVDKSCVIGYYLSMGHLERWTHDHP~~T~~HKAIYGT~~F~~YEM~~L~~KRHDFKTELALWH
EVSVLQSKDIELIYVNCHPSTGFLPFFE~~V~~TEIQEPL~~L~~LKSPSVRIQLEHHHHHH

OxdB(C)6His_K283L (M20):

Amino acids

MKNMPENHNPQANAWTAEFPPEMSYVVFAQIGIQSKSLDHAAEHLGMMKKSFDLRTGPKH
VDRALHQGADGYQDSIFLAYWDEPETFKSWVADPEVQKWWSGKKIDENSPIGYWSEVTTI
PIDHFETLHSGENYDNGVSHFVPIKHTEVHEYWGAMRDRMPVSASSDLESPLGLQLPEPIV
RESFGKRLKVTAPDNI~~L~~IRTAQNWSKCGSGERETYIGLVEPTLIKANTFLRENASETGCISS
KLVYE~~Q~~THDGEIVDKSCVIGYYLSMGHLERWTHDHP~~T~~H~~L~~AIYGT~~F~~YEM~~L~~KRHDFKTELALWH
EVSVLQSKDIELIYVNCHPSTGFLPFFE~~V~~TEIQEPL~~L~~LKSPSVRIQLEHHHHHH

OxdB(C)6His_L65H_I180A (D1):

Amino acids

MKNMPENHNPQANAWTAEFPPEMSYVVFAQIGIQSKSLDHAAEHLGMMKKSFDLRTGPKH
VDRA~~H~~HQGADGYQDSIFLAYWDEPETFKSWVADPEVQKWWSGKKIDENSPIGYWSEVTTI
PIDHFETLHSGENYDNGVSHFVPIKHTEVHEYWGAMRDRMPVSASSDLESPLGLQLPE~~P~~~~A~~~~V~~
RESFGKRLKVTAPDNI~~L~~IRTAQNWSKCGSGERETYIGLVEPTLIKANTFLRENASETGCISS
KLVYE~~Q~~THDGEIVDKSCVIGYYLSMGHLERWTHDHP~~T~~HKAIYGT~~F~~YEM~~L~~KRHDFKTELALW
HEVSVLQSKDIELIYVNCHPSTGFLPFFE~~V~~TEIQEPL~~L~~LKSPSVRIQLEHHHHHH

OxdB(C)6His_I180A_K190R (D2):

Amino acids

MKNMPENHNPQANAWTAEFPPEMSYVVFAQIGIQSKSLDHAAEHLGMMKKSFDLRTGPKH
VDRALHQGADGYQDSIFLAYWDEPETFKSWVADPEVQKWWSGKKIDENSPIGYWSEVTTI
PIDHFETLHSGENYDNGVSHFVPIKHTEVHEYWGAMRDRMPVSASSDLESPLGLQLPE~~P~~~~A~~~~V~~
RESFGKRL~~R~~V~~T~~APDNI~~L~~IRTAQNWSKCGSGERETYIGLVEPTLIKANTFLRENASETGCISS
KLVYE~~Q~~THDGEIVDKSCVIGYYLSMGHLERWTHDHP~~T~~HKAIYGT~~F~~YEM~~L~~KRHDFKTELALW
HEVSVLQSKDIELIYVNCHPSTGFLPFFE~~V~~TEIQEPL~~L~~LKSPSVRIQLEHHHHHH

OxdB(C)6His_L65H_K190R (D3):

Amino acids

MKNMPENHNPQANAWTAEFPPEMSYVVFAQIGIQSKSLDHAAEHLGMMKKSFDLRTGPKH
VDRA~~H~~HQGADGYQDSIFLAYWDEPETFKSWVADPEVQKWWSGKKIDENSPIGYWSEVTTI

PIDHFETLHSGENYDNGVSHFVPIKHTEVHEYWGAMRDRMPVSASSDLESPLGLQLPEPIV
RESFGKRLRVTAPDNICLIRTAQNWSKCGSGERETYIGLVEPTLIKANTFLRENASETGCISS
KLVYEQTHDGEIVDKSCVIGYYLSMGHLERWTHDHPHKAHYGTFYEMLKRHDFKTELALW
HEVSVLQSKDIELIYVNCHPSTGFLPFFEVEIQQEPLLKSPSVRIQLEHHHHHH

OxdFG(N)6His: Aldoxime dehydratase from *Fusarium graminearum* MAFF 305135 in pET28a with a N-terminal hexahistidine-tag (based on GeneBank: AB214653.1, Uniprot: Q2WG72; codon optimized for expression in *E. coli*)

Gene (383 AS, 43.4 kDa)

ATGGGCAGCAGCCATCATCATCATCACAGCAGCGGCCTGGTGCCGCGCGGCAGC
CATATGCTGCGTAGCCGTTTTCCGGCAAGCCATCATTTACCGTTAGCGTTTTTGGTTGT
CAGTATCATAGCGAAGCACCGAGCGTTGAAAAACCGAACTGATTGGTCGTTTCGATAA
ACTGATTGATAGCGCAGCAATTCATGTGGAACATCTGGAACAGAATGATGTGCCGAGCA
AAATTTGGATGAGCTATTGGGAAAGTCCGCAGAAATCAAACAGTGGTGGGAAAAAGAT
GATACCGCAAGCTTTTTGGGCAAGCCTGCCGGATGATGCAGGTTTTTGGCGTGAAACCTT
TAGCCTGCCTGCAACCCGTGCAATGTATGAAGGCACCGGTAAGATGCCTATGGTTTTG
GTCATTGTGGTAGCCTGATTCCGCTGACCACAAAACCGGCTATTGGGGTGATATCGT
AGCCGTATGACACCGGATTTTGAAGGTGATACCTTTTCAAGCCCGATTCCGACCTATGC
AGATCAGAGCGTTCCGGCAGATAAAATTCGTCCGGGTCGTGTTTCGTATTACCGATTTTC
CGGATAATCTGTGCATGGTTGTTGAAGGTCAGCATTATGCAGATATGGGTGAACGTGAA
CGCGAATATTGGAACGAAAATTTTATGGTCTGACGAAACAGTGGGTTACCAATGTTGTT
ACCGCAGGTCATGAACAGGGTATGGTTATTGCACGTGCCTGTCATGGTTTTGCCGGTGA
AAAAAACTGGGTGCAACCAATGGTCCGGTGAATGGTATTTTTCCGGGTCTGGATTATG
TTCATCAGGCACAGATTCTGATTTGGCAGGATATTAGCAAAATGGAACATATCGGTGCTT
ATGATCAGACCCATGTTAAACTGCGTCCGATTTTTATGAAAGCCTATGGTCCGGGTGGT
GAAATGGAAGGTGGTGTCTGCTGCTGTGGGTTGATCTGGGTATTCTGAAAAAAGACGA
AATCGATGCCGAATATGTGGGTTGCTATGAAAGTACCGTTTTTCTGAAACTGGATAAAG
GCCAGTTTTTCAAAGTTGAAAGCACCGCAGGTAGCAAACCTGCCGAGCTTTTTTATGAA
CCGATTGAAAGCAAACCGATCGAATGGTAA

Amino acids

MGSSHHHHHHSSGLVPRGSHMLRSRFPASHHFTVSVFGCQYHSEAPSVEKTELIGRFDKLI
DSAAIHVEHLEQNDVPSKIWMSYWESPQKFKQWWEKDDTASFASLPDDAGFWRETFSL
PATRAMYEGTGKDAYGFGHCGSLIPLTTKTGYWGAYRSRMTPDFEGDTFSSPIPTYADQSV
PADKIRPGRVRITDFPDNLCMVVEGQHYADMGEREREYWNENFDGLTKQWVTNVVTAGH
EQGMVIARACHGFAGEKKGATNGPVNGIFPGLDYVHQAQILWQDISKMEHIGRYDQTHVK
LRRDFMKAYGPGGEMEGDLLLLWVDLILKKDEIDAAYVGCYESTGFLKLDKGQFFKVEST
AGSKLPSFFDEPIESKPIEW

OxdRE(N)6His: Aldoxime dehydratase from *Rhodococcus* sp. N-771 in pET28a with an additional N-terminal hexahistidine-tag (based on GeneBank: AB0942101.1, Uniprot: Q76K71; codon optimized for expression in *E. coli*)

Gene

ATGGGCAGCAGCCATCATCATCATCATCACAGCAGCGGCCTGGTGCCGCGCGGCAGC
CATATGGAAAGCGCAATTGGTGAACATCTGCAGTGTCCGCGTACCCTGACCCGTCGTGT
TCCGGATACCTATACCCCTCCGTTTTCCGATGTGGGTTGGTTCGTGCAGATGATGCACTGC

AGCAGGTTGTTATGGGTTATCTGGGTGTTTCAGTTTCGTGATGAAGATCAGCGTCCGGCA
 GCACTGCAGGCAATGCGTGATATTGTTGCAGGTTTTGATCTGCCGGATGGTCCGGCAC
 ATCATGATCTGACCCATCATATTGATAATCAGGGCTATGAAAACCTGATTGTGGTGGGTT
 ATTGAAAGATGTTAGCAGCCAGCATCGTTGGAGCACCAGCACCCCGATTGCAAGTTG
 GTGGGAAAGCGAAGATCGTCTGAGTGATGGTCTGGGTTTTTTTCGTGAAATTGTGGCAC
 CGCGTGCAGAACAGTTTCAAACCTGTATGCATTTCAAGAAGATCTGCCTGGCGTTGGT
 GCAGTTATGGATGGTATTAGCGGTGAAATTAACGAACATGGTTATTGGGGTAGCATGCG
 TGAACGTTTTCCGATTAGCCAGACCGATTGGATGCAGGCAAGCGGTGAACCTGCGTGTTA
 TTGCCGGTGATCCGGCAGTTGGTGGTCGTGTTGTTGTTTCGTGGTCATGATAACATTGCA
 CTGATTTCGTAGCGGTCAGGATTGGGCAGATGCCGAAGCAGATGAACGTAGCCTGTATC
 TGGATGAAATTCTGCCGACCCTGCAGAGCGGTATGGATTTTCTGCGTGATAATGGTCCT
 GCAGTTGGTTGTTATAGCAATCGTTTTGTGCGCAACATTGATATCGATGGCAATTTTCTG
 GATCTGAGCTATAACATTGGTCATTGGGCAAGCCTGGATCAGCTGGAACGTTGGAGCG
 AAAGCCATCCGACCCATCTGCGTATTTTTACCACCTTTTTTCGCGTTGCAGCCGGTCTGA
 GCAAACCTGCGTCTGTATCATGAAGTTAGCGTTTTTGTATGCAGCAGATCAGCTGTATGAAT
 ACATTAATTGTCATCCGGGTACAGGTATGCTGCGTGATGCAGTTACCATTGCAGAACATT
 AA

Amino acids (373 AS, 42.0 kDa)

MGSSHHHHHSSGLVPRGSHMESAIGEHLQCPRTLRRVDPDYTPPFPMWVGRADDALQ
 QVVMGYLGVQFRDEDQRPAALQAMRDIVAGFDLPDGPAAHDLTHHIDNQGYENLIVVGYW
 KDVSSQHRWSTSTPIASWWESEDRLSDGLGFFREIVAPRAEQFETLYAFQEDLPGVGAVM
 DGISGEINEHGYWGS MRERFPISQTDWMQASGELR VIAGDPAVGGRRVVRGHDNIALIRSG
 QDWADAEADERSLYLDEILPTLQSGMDFLRDNGPAVGCYSNRFVRNIDIDGNFLDLSYNIGH
 WASLDQLERWSESHPTHLRIFTTFFRVAAGLSKLRLYHEVSVFDAADQLYEYINCHPGTGML
 RDAVTIAEH

OxdRG(N)6His: Aldoxime dehydratase from *Rhodococcus globerulus* A-4 in pET28a with a N-terminal hexahistidine-tag (based on GeneBank: AM946017.1, Uniprot: B1GXZ8; codon optimized for expression in *E. coli*)

Gene

ATGGGCAGCAGCCATCATCATCATCACAGCAGCGGCCTGGTGCCGCGCGGCAGC
 CATATGGAAAGCGCAATTGGTGAACATCTGCAGTGCCGCGTACCCTGACCCGTCGTGT
 TCCGGATACCTATAACCCTCCGTTTCCGATGTGGGTTGGTTCGTGCAGATGATACCCTGC
 ATCAGGTTGTTATGGGTTATCTGGGTGTTTCAGTTTCGTGGTGAAGATCAGCGTCCGGCA
 GCACTGCGTGCAATGCGTGATATTGTTGCAGGTTTTGATCTGCCGGATGGTCCGGCACA
 TCATGATCTGACCCATCATATTGATAATCAGGGCTATGAAAACCTGATTGTGGTGGGTTA
 TTGAAAGATGTTAGCAGCCAGCATCGTTGGAGCACCAGCCCTCCGTTAGCAGTTGG
 TGGGAAAGCGAAGATCGTCTGAGTGATGGTCTGGGTTTTTTTCGTGAAATTGTGGCACC
 GCGTGCAGAACAGTTTCAAACCTGTATGCATTTCAAGGATGATCTGCCTGGTGTGGTG
 CAGTTATGGATGGTGTAGCGGTGAAATTAATGAACATGGTTATTGGGGTAGCATGCGT
 GAACGTTTTCCGATTAGCCAGACCGATTGGATGCAGGCAAGCGGTGAACCTGCGTGTTG
 TTGCCGGTGATCCGGCAGTTGGCGGTCGTGTTGTGGTTCGTGGTCATGATAACATTGCA
 CTGATTTCGTAGCGGTCAGGATTGGGCAGATGCCGAAGCAGATGAACGTAGCCTGTATC
 TGGATGAAATTCTGCCGACCCTGCAGAGCGGTATGGATTTTCTGCGTGATAATGGTCCT
 GCAGTTGGTTGTTATAGCAATCGTTTTGTGCGCAACATTGATATCGATGGCAATTTTCTG
 GATCTGAGCTATAACATTGGTCATTGGGCAAGCCTGGATCAGCTGGAACGTTGGAGCG
 AAAGCCATCCGACCCATCTGCGTATTTTTACCACCTTTTTTCGCGTTGCAGAAAGGTCTGA
 GCAAACCTGCGTCTGTATCATGAAGTTAGCGTTTTTGTATGCAGCAGATCAGCTGTATGAAT

ACATTAATTGTCATCCGGGTACAGGTATGCTGCGTGATGCAGTTATTACCGCAGAACATT
AA

Amino acids (373 AS, 42.1 kDa)

MGSSHHHHHSSGLVPRGSHMESAIGEHLQCPRTLTRRVPDITYPPFPMWVGRADDTLH
QVVMGYLGVQFRGEDQRPAALRAMRDIVAGFDLPDGPAAHDLTHHIDNQQYENLIVVGYW
KDVSSQHRWSTSPVSSWWESEDRLSDGLGFFREIVAPRAEQFETLYAFQDDLPGVGAVM
DGVSGEINEHGYWGS MRERFPISQTDWMQASGELRVVAGDPAVGGRVVVRGHDNIALIRS
GQDWADAEADERSLYLDEILPTLQSGMDFLRDNGPAVGCYSNRFVRNIDIDGNFLDLSYNIG
HWASLDQLERWSESHPTHLRIFTTFFRVAEGLSKLRLYHEVSVFDAADQLYEYINCHPGTG
MLRDAVITAEH

Alcohol dehydrogenase

LkADH: (*R*)-Alcohol dehydrogenase from *Lactobacillus kefir* DSM 20587 (Uniprot:
A0A0R1Z9F9.15)^[207]

Gene

ATGACTGACCGTTTCAAAGGTAAGGTAGCAATTGTAAGTGGCGGTACCTTGGGAATTGG
CTTGGCAATCGCTGATAAGTTTGTGAAGAAGGCGCAAAGGTTGTTATTACCGGCCGTC
ACGCTGATGTAGGTGAAAAAGCTGCCAAATCAATCGGCGGCACAGACGTTATCCGTTTT
GTCCAACACGATGCTTCTGATGAAGCCGGCTGGACTAAGTTGTTTGATACGACTGAAGA
AGCATTGGCCAGTTACCACGGTTGTCAACAATGCCGGAATTGCGGTCAGCAAGAGT
GTTGAAGATAACCACAAGTGAAGAATGGCGCAAGCTGCTCTCAGTTAACTTGGATGGTGT
CTTCTTCGGTACCCGTCTTGAATCCAACGTATGAAGAATAAAGGACTCGGAGCATCAA
TCATCAATATGTCATCTATCGAAGTTTTGTTGGTATCCAACCTCTGGGTGCATACAACG
CTTCAAAGGTGCTGTCAGAATTATGTCTAAATCAGCTGCCTTGGATTGCGCTTTGAAGG
ACTACGATGTTCCGGTTAACTGTTTCACTCCAGGTTATATCAAGACACCATTGGTTGACG
ATCTTGAAGGGGCGAGAAGAAATGATGTCACAGCGGACCAAGACACCAATGGGTATATC
GGTGAACCTAACGATATCGCTTGGATCTGTGTTTACCTGGCATCTGACGAATCTAAATTT
GCCACTGGTGCAGAATTCGTTGTCGACGGTGGCTACACTGCTCAATAG

Amino acids (232 AS, 26.8 kDa)

MTDRLKGVAVITGGTLGIGLAIADKFVEEGAKVVITGRHADVGEKAAKSIGGTDVIRFVQHD
ASDEAGWTKLFDTTTEAFGPVTTVVNNAGIAVSKSVEDTTTEEWKLLSVNLDGVFFGTRL
GIQRMKNKGLGASIIINMSSIEGFVGDPTLGAYNASKGAVRIMSKSAALDCALKDYDVRVNTV
HPGYIKTPLVDDLEGAEEMMSQRTKTPMGHIGEPNDIAWICVYLASDESKFATGAEFVVDG
GYTAQ

PpADH: Alcohol dehydrogenase from *Pichia pastoris* CBS 7435 (Uniprot: C4R4L0)^[207]

Gene

ATGTTTTCTAAGGTTTTATTGACAGGTGCTTCTGGTTACATCGCCCAACACATCACTAAT
GAATTACTTTCCACGGCTTTAAGGTCATTGGAAGTGTAAAGAAGACAGGAGCAGGCAGA
CCAATTGCATAAGCAATTTTCAGAGGAAAGTTCTGTTTTACAAAAAGATCCCTCCCTTCT
GACCTATGTCCTTGTCCCAGATATTGGTGCTTCGGATGCTTTTGATGAGGTATTGAAGTC
AACCCCGACATCACTTATGTCCTTCACACAGCTTCCCCATTTATTTTCAATGACGACAG
AGCTCTTGAGGACGTTTATTTGAAGCCTGCTGTTGAGGGTACCAGAAACATCTTAAGTG
CTATCAAGAAGTTTGCCAATGACAGTGTCAAGAACGTCGTGGTAACTTCCTCCTTTGCA
GCAATTTTGAACGCTGACAAGTTTGAAGACAAGAGTTTCATTCACACTGAGAAGGTGTG
GAATAACAACACCTGGGATCAAACCAAGAGTGGAGACAGAGGTGTTGCTTACATCGTTT
CCAAGAAGGAGGCTGAGAAAGCTGCCTGGGACTTCGTTGAGAAGGAGAAACCAAACCTT
TAAATTGACAACAGTAAACCCTCCTTATGTTTTTGGTCCTCAGAAATTCGATGCTTCGGC
TAAGAAGGAATCTTTGAACACCTCAGCTGAGATCGTTGGATCTCTGTTGCACACAAAGTA
TCCATCTGATGACAAGTTGTTTATGATGCCCTCAATTTATCCGTTGATGTTAGAGACGT
AGCTCTCTACCATGTTCTGCCACTTTTGAATGCTGATTTGGCTTCCAGGAGATTGCTTGT
TGTTCAATCCAAGTTCAGCGCTCAGAGAATCCTGAACATTATCAACGAGAATTTTCCTGA
ATTAAGGGCAAGATCGCAGTTGGAAAGCCCGAGGAAACGGCAAGAGTGGAAGCTATT
AAGGGCCCGGAGTATAACAACAGTGTACTGTAGGCCTAACTGGAGTTGACCCCATCCC
ACTGGAGAAAACGGTGTGGACTCTGTCAAACAGATATTGCGTGCTAATAAATAA

Amino acids (365 AS, 40.5 kDa)

MVSKVLLTGASGYIAQHITNELLSHGFKVIGTVRRREQADQLHKQFSEESSVLQKDPSLLTY
VLVPDIGASDAFDEVLKSTPDITYVLHTASPFIFNDDRALEDVYLKPAVEGTRNILSAIKKFAN
DSVKNVVVTSSFAAILNADKFEDKSFHTEKVVWNNNTWDQTKSGDRGVAYIVSKKEAEKAA
WDFVEKEKPNFKLTTVNPPYVFGPQKFDASAKKESLNTSAEIVGSLLHTKYPSDDKLFDDPL
NLSVDVRDVALYHVLPLLADLASRLLVVQSKFSAQRILNIINENFPELKGKIAVGVKPEETAR
VEAIKGPEYNNNSVTVGLTGVDPIPLEKTVVDSVKQILRANK

Nuclear magnetic resonance measurements

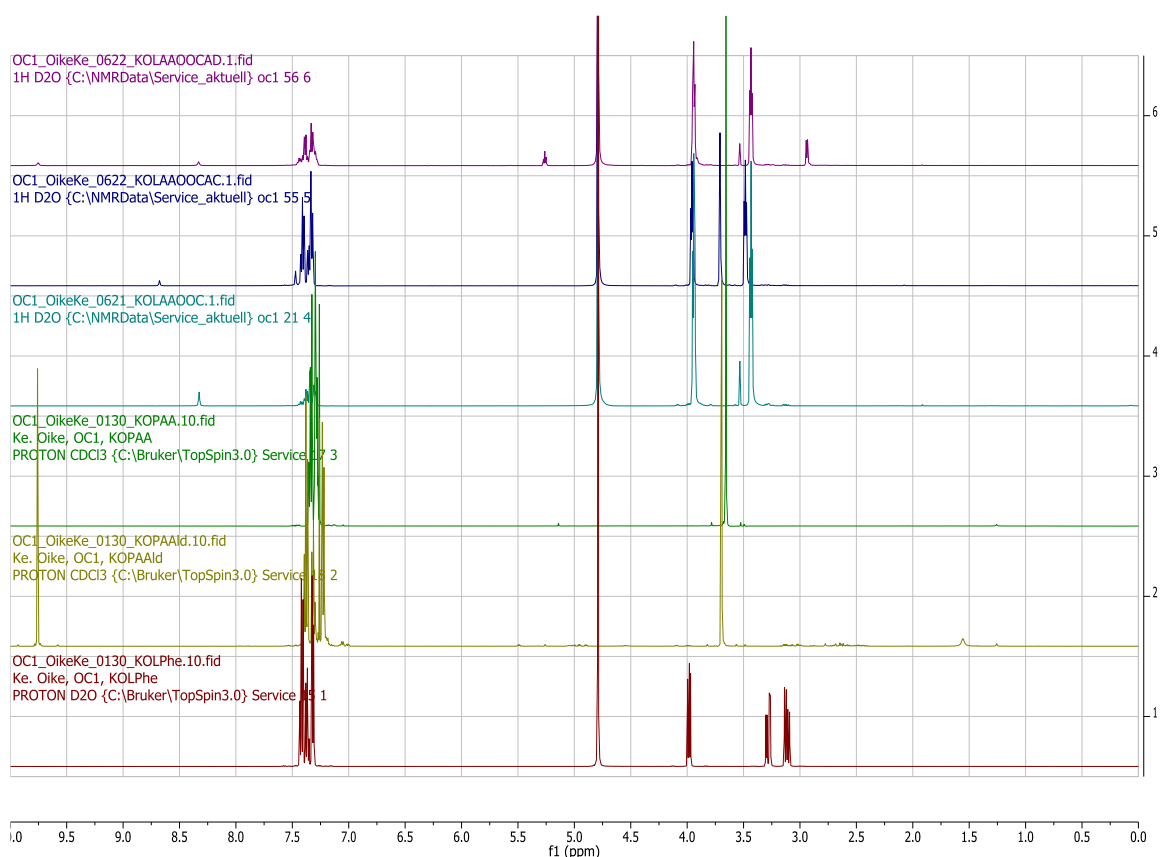


Figure 40. ¹H-NMR spectra of the crude reaction product of the biotransformation of L-phenylalanine with *h*cLAAO4 without addition of catalase (in D₂O; violet: with addition of phenylacetaldehyde, dark blue: with addition of phenylacetic acid, light blue: without additives) and reference compounds (in chloroform-d₃; green: phenylacetic acid, yellow: phenylacetaldehyde, red: L-phenylalanine).

13 Appendix

Output data of INTMSAlign_HiSol

Table 60. Output sheet of INTMSAlign_HiSol applied to the sequence of OxdB according to the formula given in chapter 9.2. Conservation (similarity) of all amino acid residues in the gene family for the positions, which exhibited the highest absolute HiSol. The suggested mutations are marked in yellow.

Position	Amino acid (OxdB)	Conservation [%]																					HiSol score
		A	C	D	E	F	G	H	I	K	L	M	N	P	Q	R	S	T	V	W	Y	none	
319	I	1.7	0.1	2.4	90.0	0.2	0.6	0.2	0	0.4	0.1	0.8	0	0.1	0.3	0.5	0.3	0.2	0.4	0.1	0.1	1.7	2.656
226	I	0.6	1.3	3.9	2.9	0.2	0.4	5.3	3.5	7.9	1.1	6.2	1.1	0.1	26.5	30.0	1.4	2.3	4.3	0	0	1.1	2.411
220	L	4.3	0	20.7	39.7	0	0.6	0.9	0.2	5.8	0	0.6	8.7	0.2	3.0	1.6	2.5	9.9	0.3	0	0	1.2	2.281
149	V	0.1	0	0.6	65.6	1.1	0.1	0.9	0.4	7	7.9	0.5	1.8	0.1	1.1	1.4	0	4.1	1.8	0.3	3.0	2.3	2.278
105	I	12.7	0.3	8.2	6.9	0.3	2.3	0.6	0	2.5	2.5	0.1	0.7	7.4	2.3	32.6	2.1	3.1	1.3	0	0	14.3	2.252
267	L	6.7	1.0	14.9	2.0	0	1.2	3.4	0.6	9.5	4.9	1.6	0.8	0.2	3.3	40.0	2.8	5.8	0.5	0	0.2	0.7	2.226
316	I	14.0	1.0	0.4	0.1	0.4	0.2	1.0	4.3	0	1.5	1.7	0.6	0.8	67.9	0.3	0.4	1.1	2.2	0	0	2.2	2.175
180	I	13.9	0.4	12.3	5.2	1.2	6.1	0.8	0.3	2.2	2.0	0.5	3.4	5.1	2.9	6.1	12.4	7.3	3.6	0	0.3	14.1	1.890
65	L	5.9	1.6	1.9	2.6	2.9	1.2	24.2	1.0	0.4	0	0.9	0.5	0.2	12	14.1	11.2	3.6	6.5	0.5	5.6	3.5	1.880
262	V	3.8	0.3	7.7	2.3	0.1	43.8	0	0.1	0.6	0.1	0.1	23.4	0	4.7	0.1	2.3	2.0	7.1	0	0.4	1.2	1.852
317	E	2.8	0.3	5.3	1.4	11.9	0.5	4.5	3.4	0.2	17.8	1.0	0.6	0.7	2.9	7.2	7.6	5.1	13.7	2.1	9.2	2.1	-1.452
190	K	0.7	0.7	0.1	0.7	2.3	1.0	0.7	8.0	0	4.7	1.6	0.1	0.1	1.1	34.5	1.5	5.3	34.2	0.4	0.3	2.0	-1.471
135	D	2.9	0.1	0.8	1.0	8.7	4.9	0.2	1.0	1.9	35.0	2.1	2.0	25.3	1.9	3.8	1.2	0.8	1.5	0.3	0.7	4.0	-1.496
67	Q	3.6	0.1	5.0	4.9	0.3	0.5	1.4	8.9	1.1	8.1	0.4	1.6	1.5	0	1.7	0.7	32.2	24.2	0	0.5	3.5	-1.533
49	K	15.0	0.3	4.5	3.2	1.5	1.7	1.6	5.0	0.9	6.9	1.1	1.8	0.7	4.2	9.7	3.7	7.1	24.2	1.1	0.1	5.6	-1.582
63	R	2.4	0.2	0.3	2.2	8.5	0.3	3.2	5.1	0.3	34.6	2.2	0.3	1.1	1.3	15.8	6.3	4.0	5.2	2.6	0.3	4.0	-1.882
296	H	0.8	0.1	0.2	0.6	13.5	5.3	0	0.7	0.4	56.7	4.3	0.4	0.1	1.2	0.3	0.4	0.5	1.5	0.7	7.4	5.0	-1.943
229	N	0.5	0	0	0	0.1	0	0.1	1.9	0	10.0	80.1	0	0	0	0	0	0.3	6.1	0	0	0.8	-1.974
250	Q	1.0	0.7	0.7	3.3	3.9	0.5	0.4	29.2	0.5	24.0	1.8	0.2	2.0	2.0	2.7	1.4	3.1	19.5	0	0.4	2.7	-2.153
283	K	2.7	0	0.3	0.7	0.3	0.1	1.5	2.4	1.9	57.8	0.3	0	0	0.5	1.3	0.3	0.2	28.8	0	0	1.0	-2.485

13 Appendix

Mass spectrometrical data of proteins

Spectra

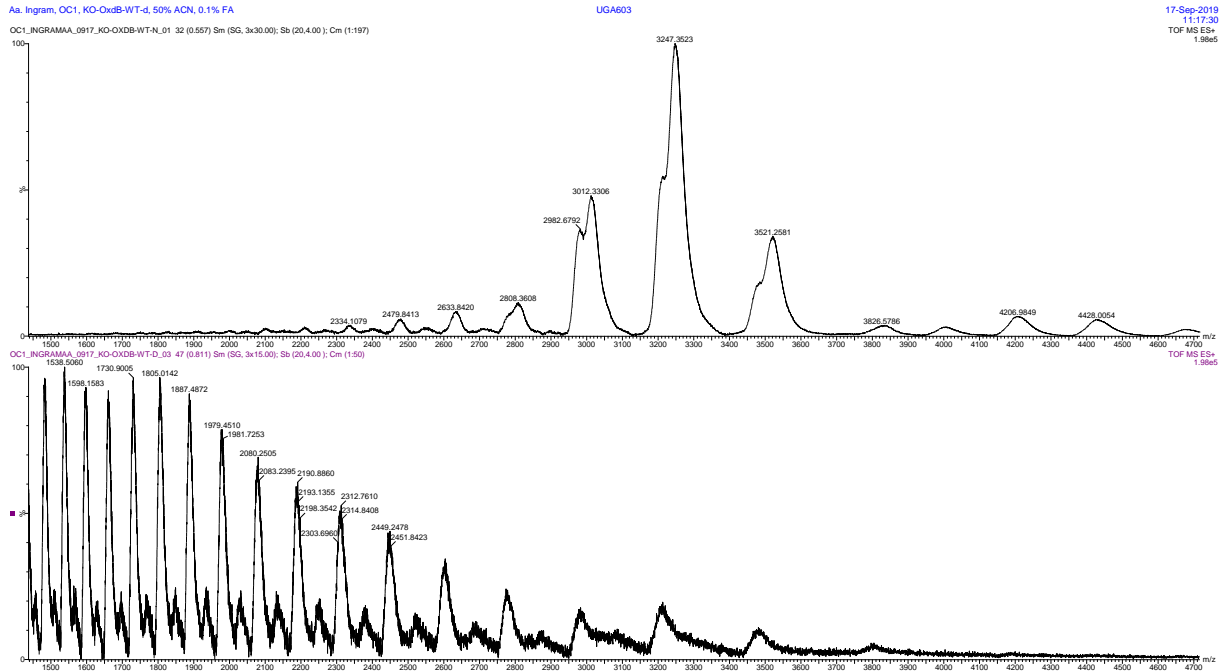


Figure 41. ESI-mass spectrum of native (upper) and denatured (lower) purified wild-type-OxdB.

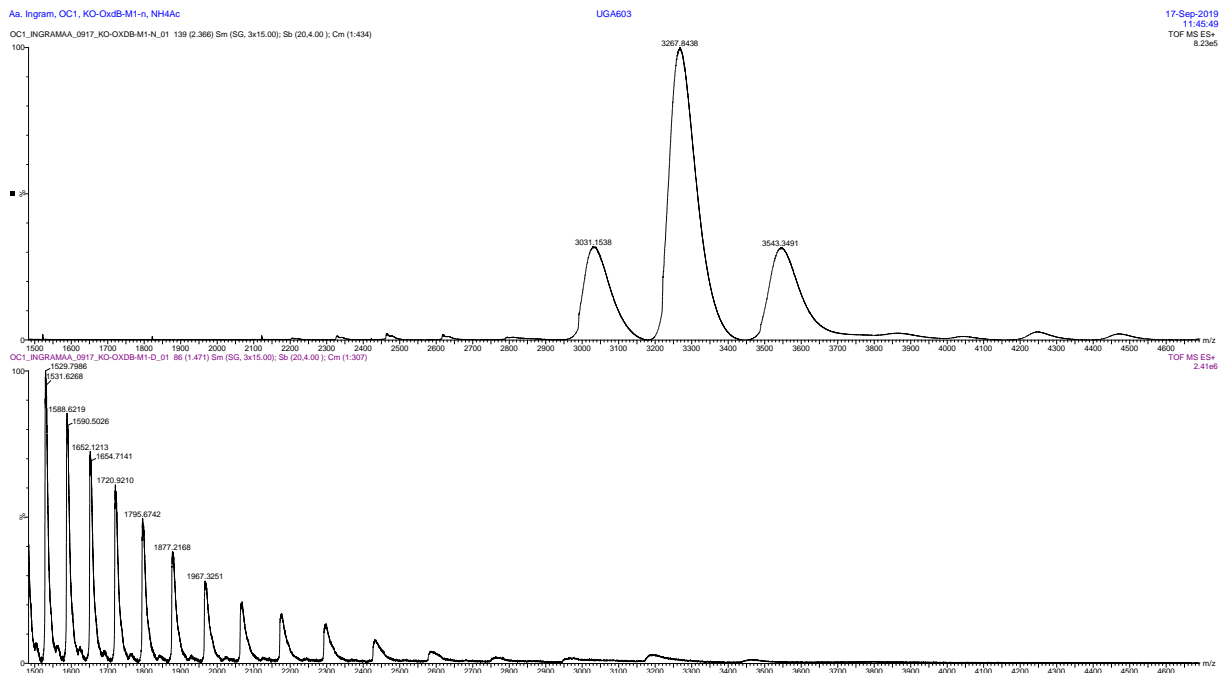


Figure 42. ESI-mass spectrum of native (upper) and denatured (lower) purified OxdB-M1.

13 Appendix

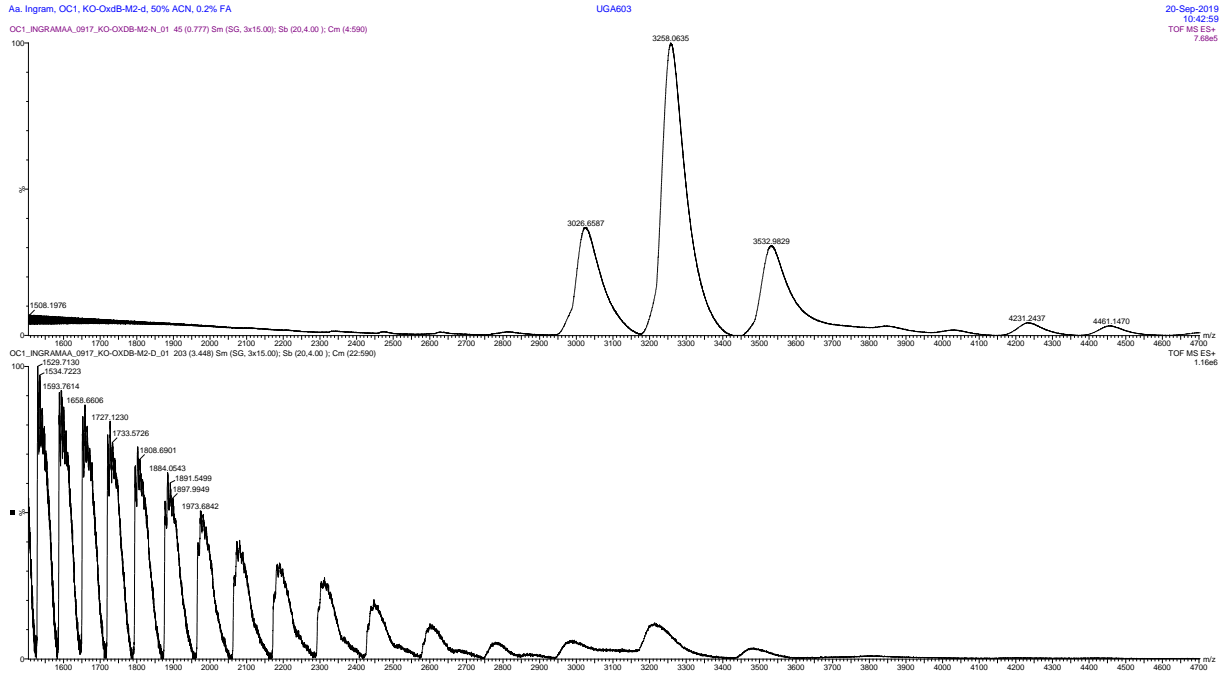


Figure 43. ESI-mass spectrum of native (upper) and denatured (lower) purified OxDb-M2.

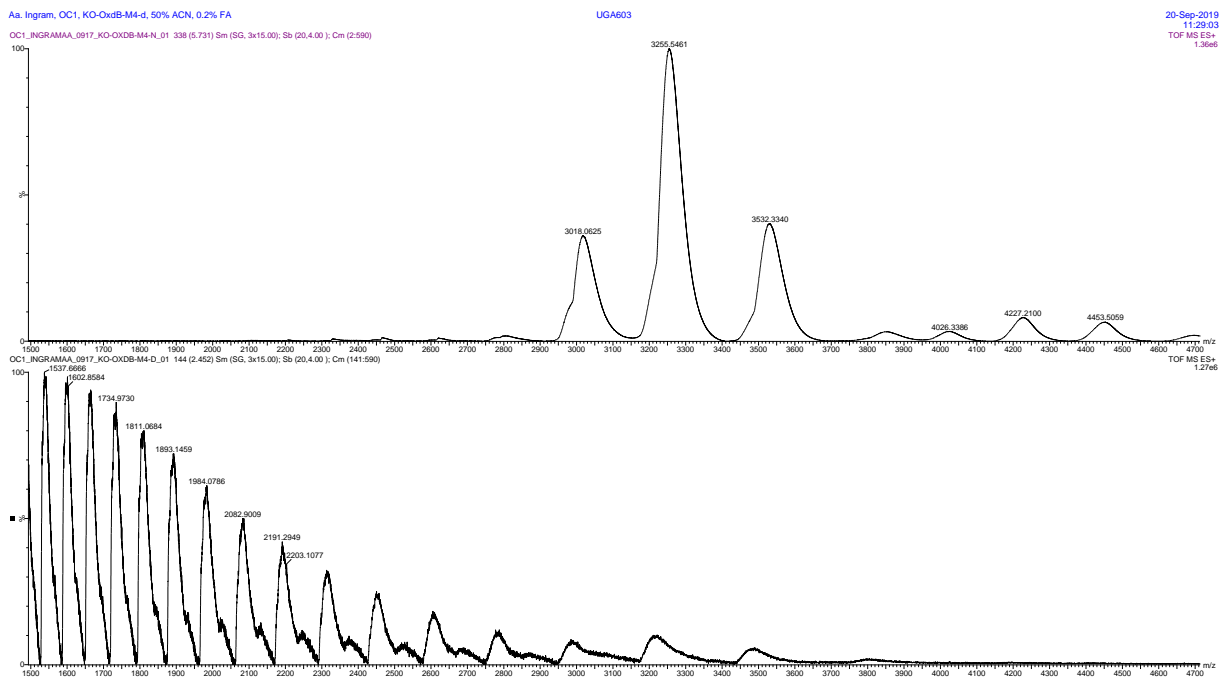


Figure 44. ESI-mass spectrum of native (upper) and denatured (lower) purified OxDb-M4.

13 Appendix

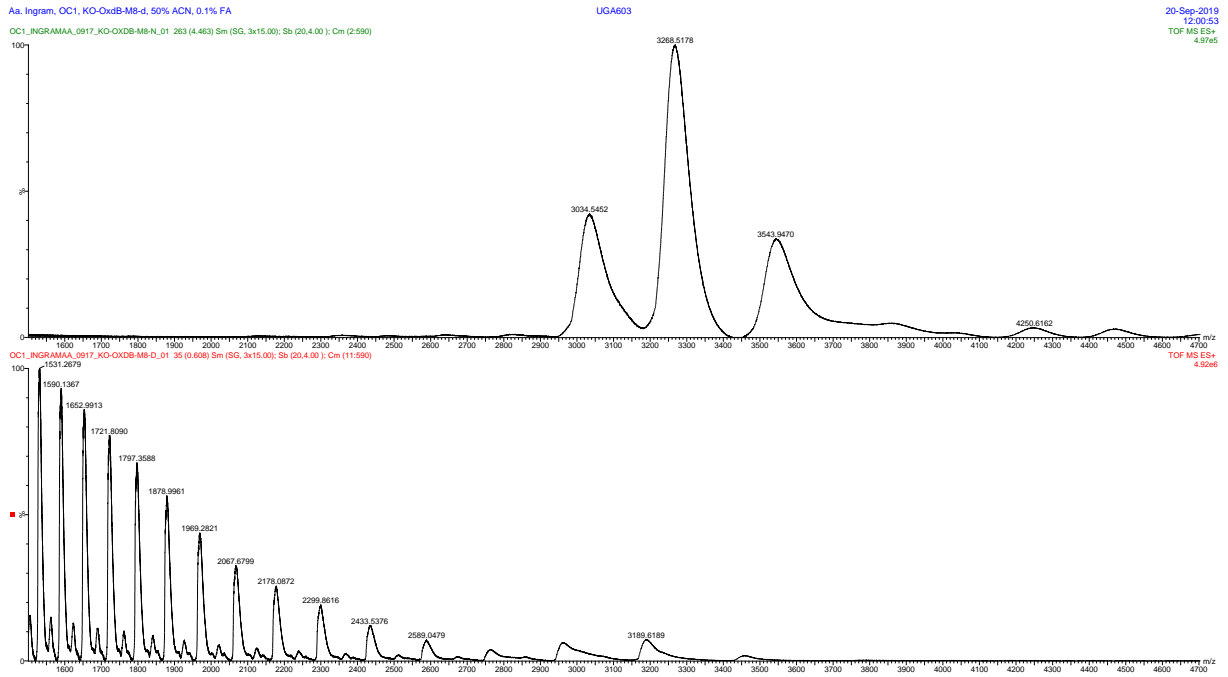


Figure 45. ESI-mass spectrum of native (upper) and denatured (lower) purified OxdB-M8.

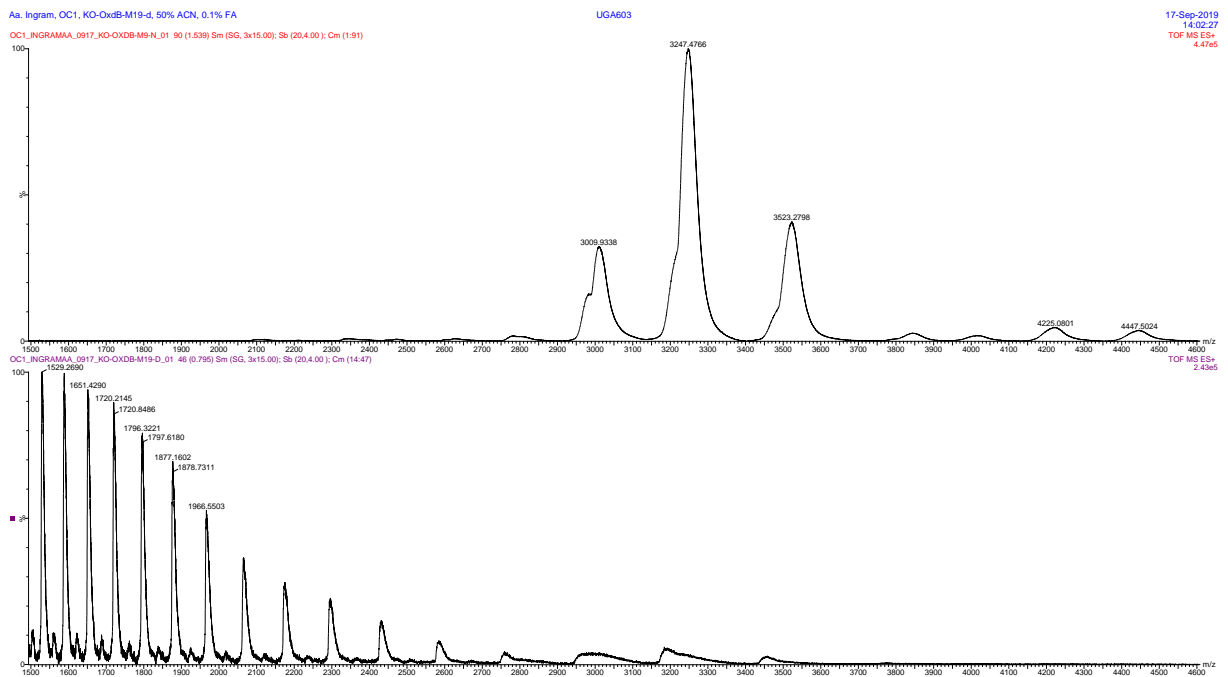


Figure 46. ESI-mass spectrum of native (upper) and denatured (lower) purified OxdB-M9.

13 Appendix

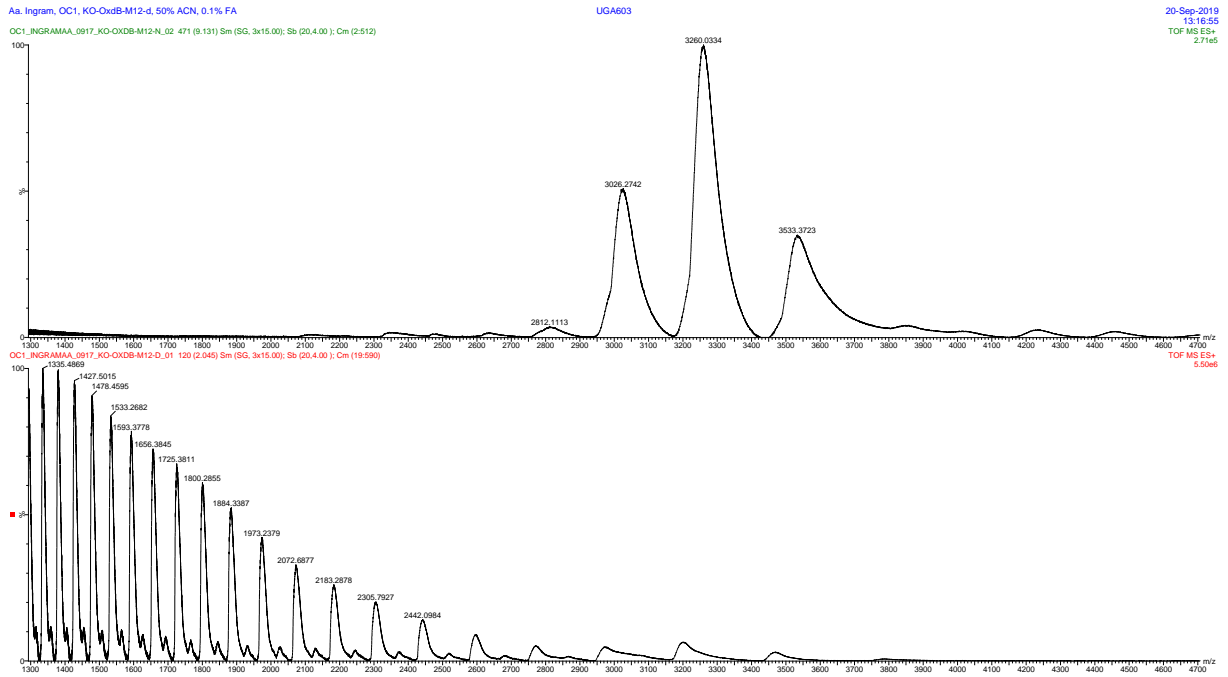


Figure 47. ESI-mass spectrum of native (upper) and denatured (lower) purified OxdB-M12.

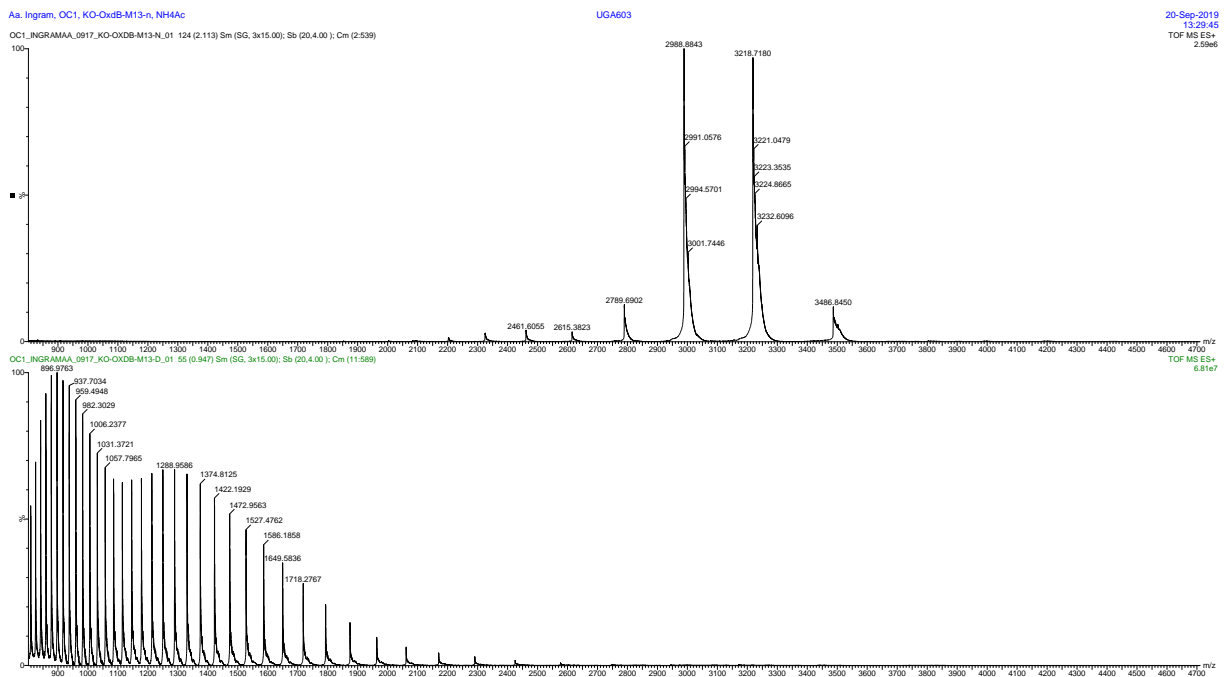


Figure 48. ESI-mass spectrum of native (upper) and denatured (lower) purified OxdB-M13.

13 Appendix

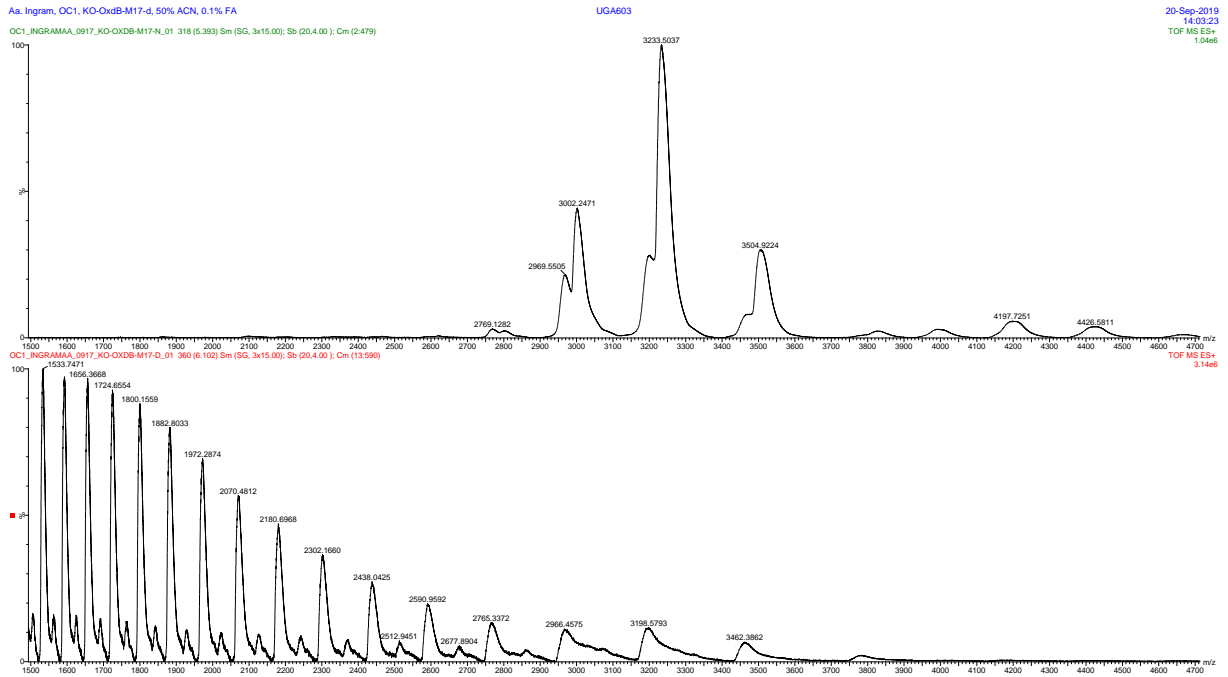


Figure 49. ESI-mass spectrum of native (upper) and denatured (lower) purified OxdB-M17.

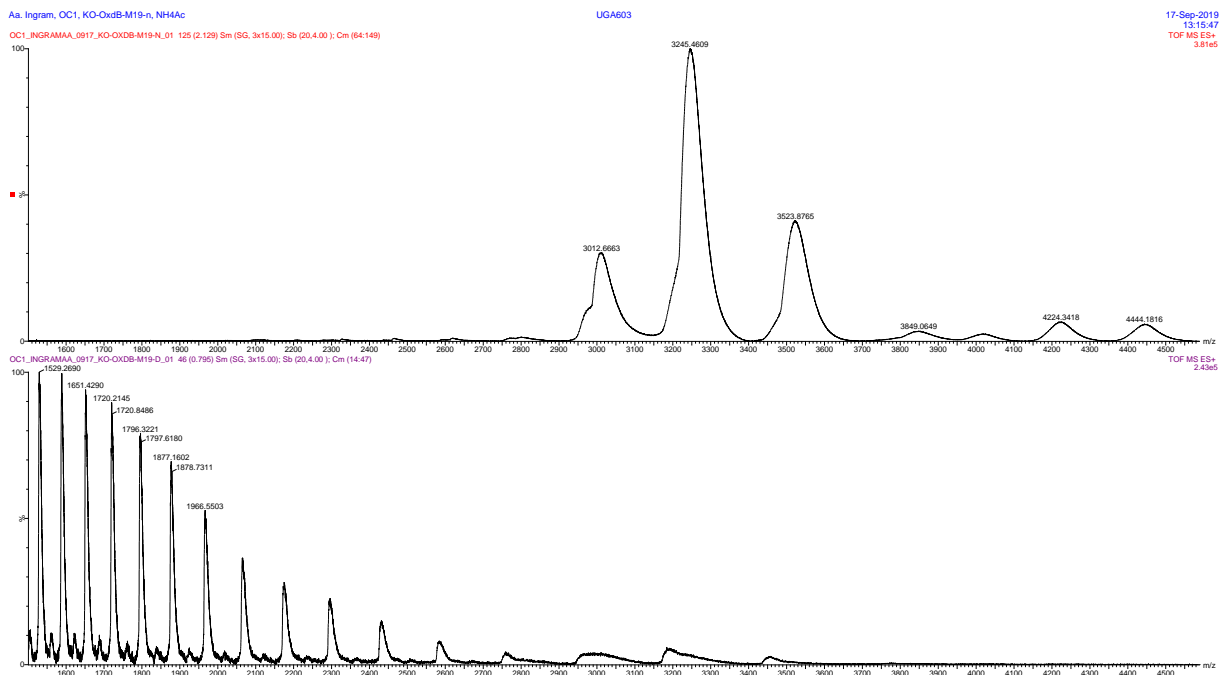


Figure 50. ESI-mass spectrum of native (upper) and denatured (lower) purified OxdB-M19.

13 Appendix

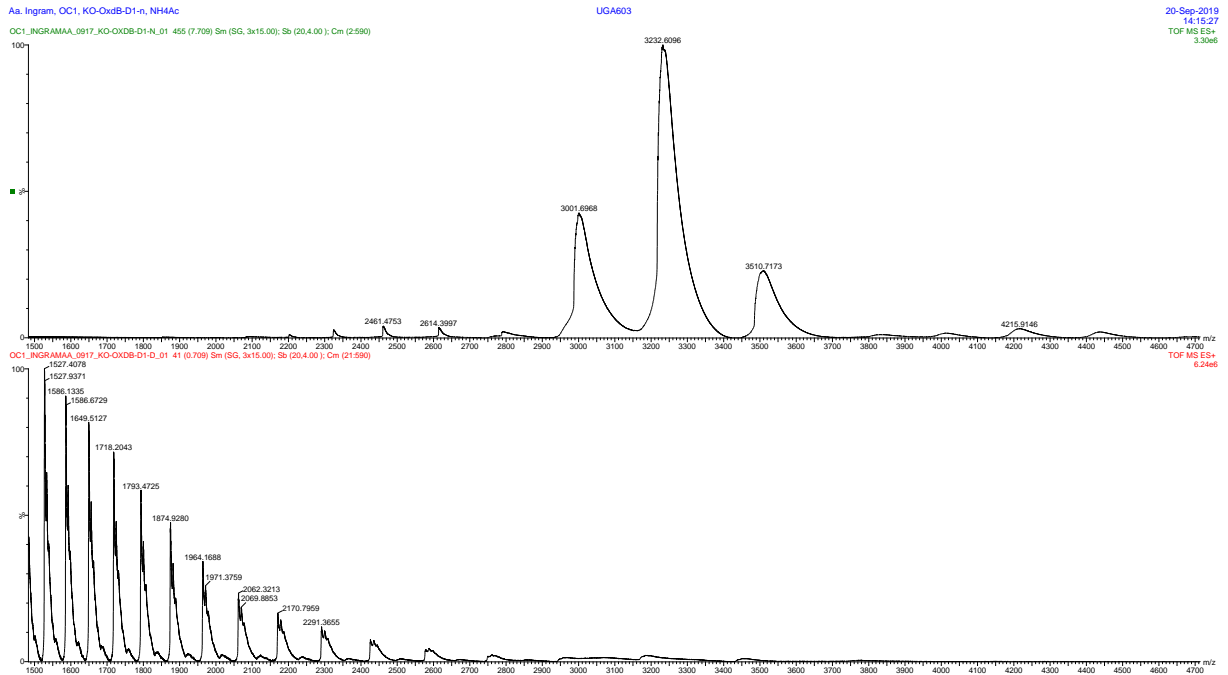


Figure 51. ESI-mass spectrum of native (upper) and denatured (lower) purified OxDb-D1.

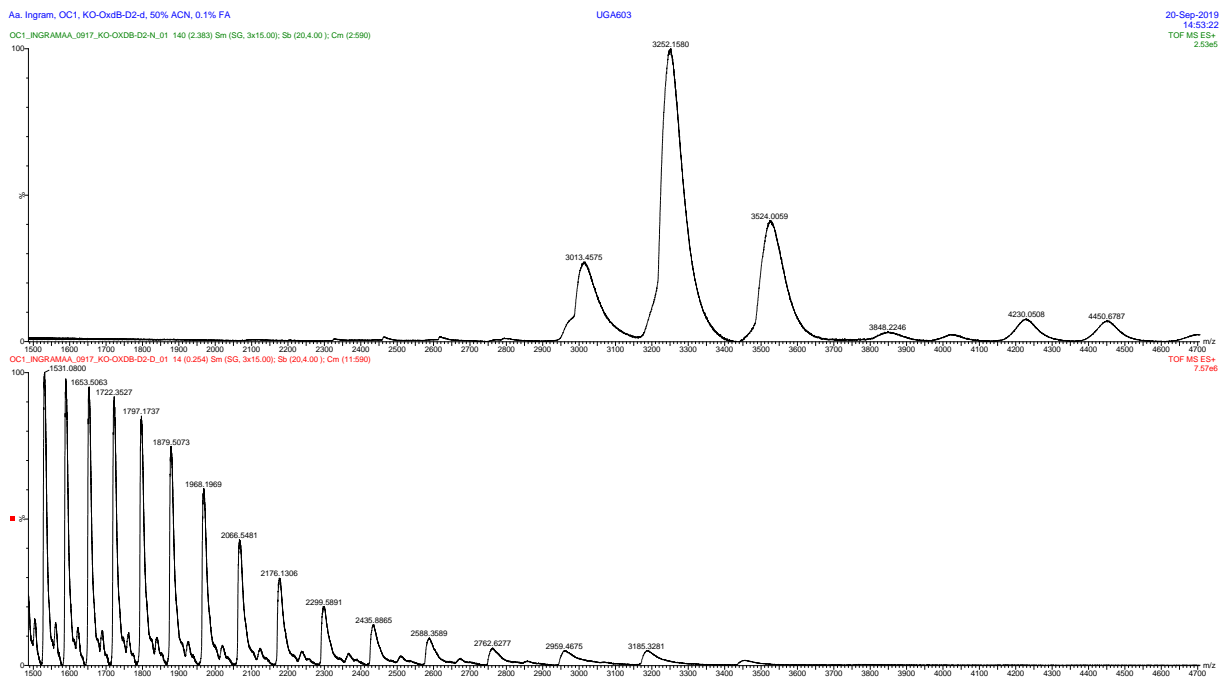


Figure 52. ESI-mass spectrum of native (upper) and denatured (lower) purified OxDb-D2.

13 Appendix

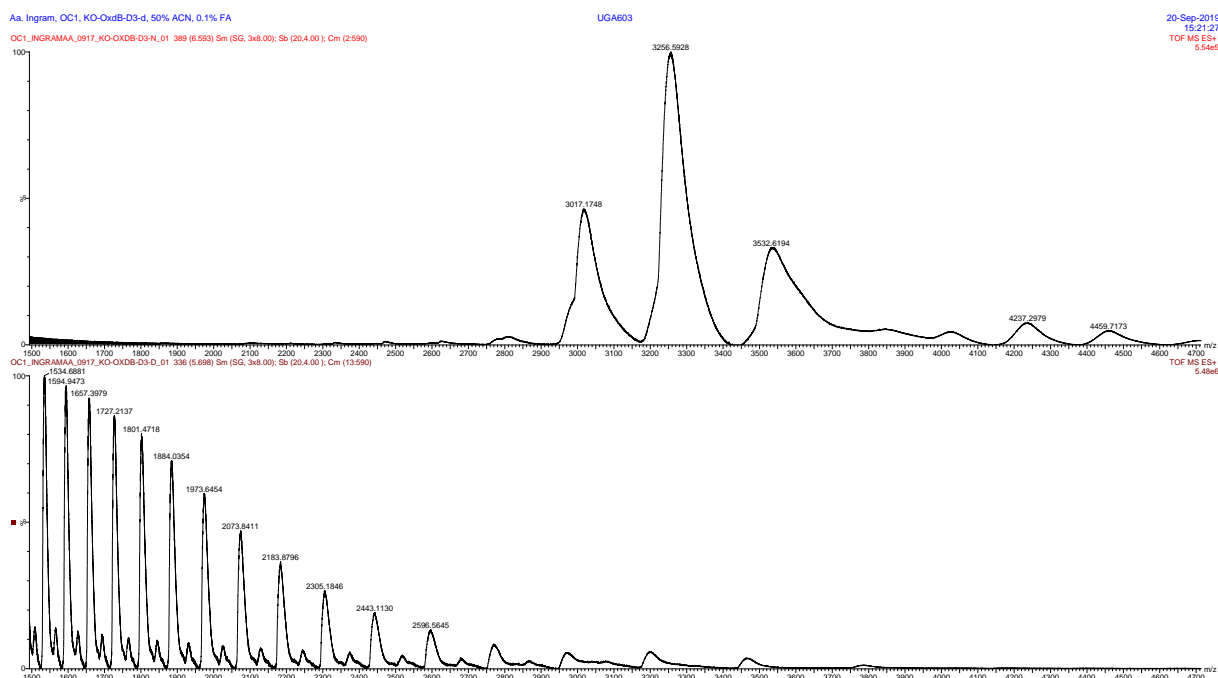


Figure 53. ESI-mass spectrum of native (upper) and denatured (lower) purified OxdB-D3.

Results

Table 61. Molecular masses determined with static nanoESI-MS for selected OxdB variants and the wild-type enzyme. The charge state adjusted masses in the denatured state and the native state are given in Da. For the native state, two masses were determined.

Variant	M_{sequence} [Da]	$M_{\text{Denatured}}$ [Da]	$M_{\text{Native,1}}$ [Da]	$M_{\text{Native,2}}$ [Da]
wt	41216.78	41255.8 ± 9.0	41901.8±6.0	41256.6±9.6
M1	41232.73	41248.21±1.97	41863.76±0.37	N.D.
M2	4231.75	41236.9±4.8	41844.5±2.6	41349.9±2.4*
M4	41246.76	41302.7±6.4	41862.4±2.1	41316.6±6.9
M8	41174.69	41208±6.8	41824.1±6.7	N.D.
M9	41240.76	21218.7±4.8	41829.4±12.4	41269.8±2.0
M12	41244.79	41291.3±4.6	41863.8±0.4	N.D.
M13	41214.85	41216.4±0.7	41830.60±0.04	N.D.
M17	41192.79	41229.0±8.0	41791.2±3.3	41190.0±12.3
M19	41201.80	41182.9±7.8	41801.6±1.0	41241.7±2.1
D1	41198.68	41215.9±2.6	41829.9±0.4	N.D.
D2	41202.71	41217.82±0.16	41824.02±0.91	N.D.
D13	41268.77	41298.9±1.1	41889.8±18.8	N.D.

N.D. not determined due to absence of spectral overlay of native and denatured form, *Na⁺ adducts observed due to high salt concentration in the sample.

SDS-PAGEs

Purified variants of aldoxime dehydratase from *Bacillus* sp. OxB-1

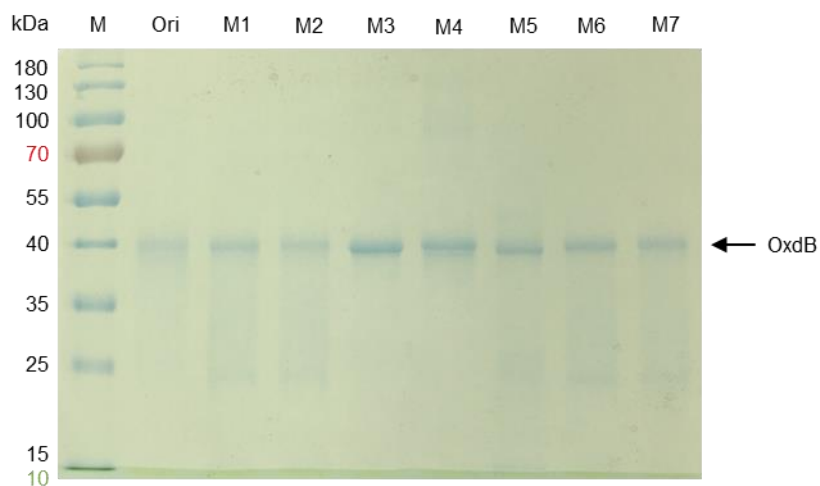


Figure 54. SDS-PAGE of OxdB mutants purified *via* TALON® affinity chromatography. The lanes refer to the corresponding variants (see Table 35).

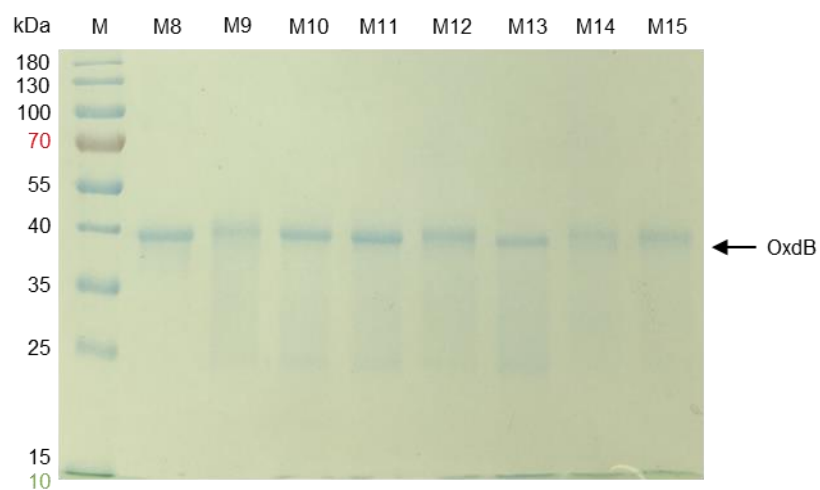


Figure 55. SDS-PAGE of OxdB mutants purified *via* TALON® affinity chromatography. The lanes refer to the corresponding variants (see Table 35).

13 Appendix

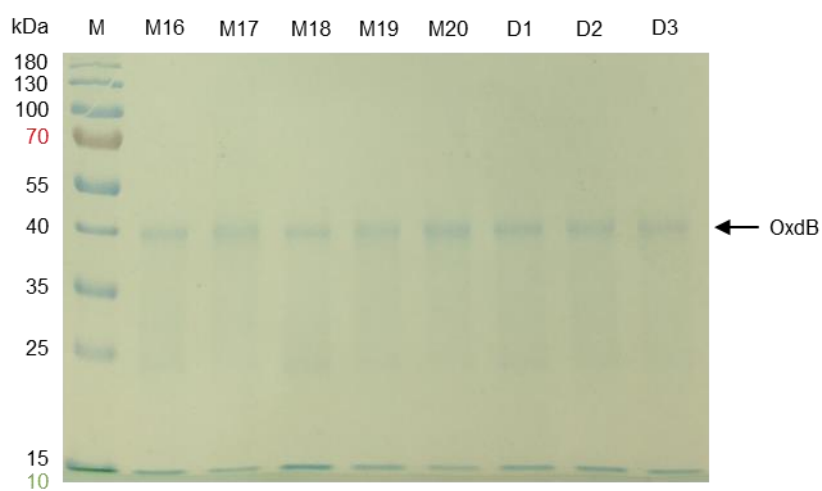


Figure 56. SDS-PAGE of OxdB mutants purified *via* TALON® affinity chromatography. The lanes refer to the corresponding variants (see Table 35).